The Response of Non-linear Structures by the Pseudo-Force Influence Method

Graham Stewart

Thesis submitted for the Degree of Doctor of Philosophy

Department of Naval Architecture and Ocean Engineering
University of Glasgow

May, 1995

ProQuest LLC.
789 East Eisenhower Parkway
P.O. Box 1346
Ann Arbor, MI 48106 – 1346

CONTENTS

Part III: A more formal treatment of the PFI-Method

Appendices

ACKNOWLEDGEMENTS

The research for this thesis was undertaken at Shell Research B.V. in Rijswijk, The Netherlands; my employer since 1986. I would like to thank the management of Shell Research Rijswijk, past and present, for granting me permission to publish my industrial work in this thesis. During the course of this study, I was a staff member of the Offshore Engineering Section. I would like to thank Dr. Gordon Edwards, head of this section, for allowing me sufficient continuity in my research tasks to complete this thesis. I am also grateful for the support offered by several of my colleagues. In particular, Dr. Frans Klever was always available for in-depth discussion and advice, and Dr. Paul Taylor read the completed manuscript.

As a graduate of the University of Glasgow, I very much appreciated being given the opportunity to submit my doctorate thesis to this university. For this I am indebted to my academic supervisor Professor D. Faulkner, Head of the Department of Naval Architecture and Ocean Engineering, who encouraged me to register as a part-time post-graduate student and provided support throughout. I would also like to thank Dr. A. Incecik and Dr. P.K. Das who were always very helpful on the occasions I visited the university.

Graham Stewart

DEDICATION

To my wife Isabel, for her patience and understanding.

DECLARATION

Except where reference is made to the work of others,
this thesis is believed to be original.

List of main symbols

Latin symbols

$\underline{a}$	self-equilibrating load-set
$\boldsymbol{B}$	infinitesimal strain deformation matrix
$\boldsymbol{C}$	damping matrix
$\boldsymbol{C}_r$, $\tilde{\boldsymbol{C}}$	modal damping matrices
$\boldsymbol{C}^E$, $\boldsymbol{C}^P$	matrices of elastic and plastic moduli
$\boldsymbol{C}^{EP}$	matrix of elastic-plastic moduli
$\boldsymbol{D}^{\alpha\beta}$	deformation influence matrices of the reduced system
$\underline{e}^*$	infinitesimal strains measured in co-rotational reference system
$\underline{e}_p^*$	infinitesimal plastic strains measured in co-rotational reference system
$\underline{f}_b$	boundary forces on statically restrained element
$\underline{f}^{ext}$	generalised applied 'load'
$\underline{f}^{int}$	generalised internal 'resistance'
f^{NL}, $\underline{f}_\eta^{NL}$	magnitude(s) of deformation dependent (material) pseudo-force
$\underline{f}_r$	generalised element resistance
F	applied force
F^D, $\underline{F}_U^D$	magnitude(s) of dynamic pseudo-force
$\underline{F}^{ext}$	force vector (including any dynamic forces)
$\underline{F}_U^{int}$	nodal resistance vector
$\underline{F}^W$	environmental load vector
F^W	measure of total environmental load (a scalar)
$\underline{F}_U^E$, $\underline{F}_U^{NL}$	elastic and inelastic contributions to nodal resistance vector
$\underline{F}^G$	gravity load vector
$\underline{F}^L$	applied loading vector
$\underline{g}(\underline{\eta},\lambda)$, $\underline{G}$	residual vector
h	wave-height; length scale; equation of constraining surface in arc length method
h_R	wave-height of return period, R
h_s	significant wave-height
$\boldsymbol{H}$	augmented (non-symmetric) iteration matrix
$\boldsymbol{H}^{\alpha\beta}$	displacement influence matrices of the reduced system
$\boldsymbol{I}$	identity matrix
$\boldsymbol{I}_r$, $\tilde{\boldsymbol{I}}$	modal mass matrices (unit matrices)
k	effective length factor, or member stiffness
$k_\phi = \tilde{k}_{\phi\phi}^{\sigma}$	rigid body stiffness of element

k^E	element elastic stiffness matrix
k^P	element inelastic (or plasticity) matrix
k^t	element tangent matrix
K	global stiffness matrix
K^t	global tangent stiffness matrix
K^E, K^P	linear-elastic and plastic global stiffness matrices
K^s	generalised global stiffness matrix (includes mass and damping effects)
$\overline{K}$	reduced nodal stiffness matrix
$\overline{K}^t_\eta$	tangent stiffness matrix of reduced system of deformation variables
$\overline{K}'$	modified reduced stiffness matrix = $\overline{K}^t_\eta D^{\eta\eta}$
m	mass
M	mass matrix
M, M_p	bending moment and fully plastic bending moment
N	matrix of shape functions
p, P_y	axial force and axial squash load of structural member
$P(x > y)$	probability that x exceeds y
$\underline{q}^{NL}$	local element pseudo-forces
$\underline{r}$	general response variable
$R^{s\eta}$	general rectangular response influence matrix
R_α, R_ϕ, R_θ	rotation matrices
$\underline{R}$	nodal resistance vector
s	distance along solution curve
t	time
T_r	period of vibration mode, r
$\underline{u}$	nodal displacements measured in fixed reference system (stored element by element)
$\underline{u}^*$	nodal displacement vector measured in co-rotational reference system
$\underline{r}$	nodal displacement vector (stored node by node)
$\dot{\underline{U}}$, $\ddot{\underline{U}}$	nodal velocity and acceleration vectors
V	volume
$\underline{v}$	element displacements w.r.t. a local fixed reference system
$\underline{v}_o$	translation of node 1 of finite element
$\underline{v}^*$, $\underline{w}^*$	absolute and relative displacements w.r.t. fixed reference frame momentarily coinciding with co-rotating reference frame
$\underline{w}$	element relative displacements
W	work
$\underline{x}_r$	generalised displacements in reduced basis
$\hat{\underline{X}}$	nodal co-ordinates measured in co-rotational reference frame
$\underline{X}^*$	material (co-rotating) co-ordinates of a point within an element

Greek symbols

$\underline{\beta}$	element generalised displacements (deformations and rotation)
$\underline{\beta}_o$	element generalised displacements (deformations and rotation) based on geometrically linear operators
δ	displacement at a location in the structure; variation in a quantity
$\underline{\varepsilon}$	strain tensor represented in vector form
$\underline{\varepsilon}^*$	strains measured in co-rotational reference system
ϕ	angle of rotation of edge joining nodes 1 and 2 of element
$\underline{\phi}, \underline{\Psi}$	eigenvectors
η	total deformation in element
η^c	control deformation
η^Y	yield deformation
λ	environmental load factor
λ_{ult}	value of λ at static collapse of structure
λ^D_{ult}	value of λ in a dynamic analysis when limiting ductility μ_{lim} is exceeded
μ_{lim}	limiting ductility
$\underline{\mu}$	re-ordering of element freedoms $\underline{\beta}$
$\underline{\sigma}$	stress tensor represented in vector form
$\underline{\sigma}^*$	Cauchy stresses measured in co-rotational reference system
ω^2, μ^2	eigenvalues
ω	(circular) frequency of applied force
ω_o	(circular) natural frequency of system
ξ_R	short-term variability factor associated with return period R
$\underline{\xi}$	generalised displacements in reduced basis
Ψ_{ult}	dynamic overload ratio, being $\lambda^D_{ult} / \lambda_{ult}$
$\underline{\zeta}$	non-zero element deformations
∂	partial derivative
Δ	incremental change; correction term; geometrical dependency
Φ_r, Ψ	modal transformation matrices
Φ_c, Φ_s	diagonal matrices of cosines and sines, respectively
Γ, Γ_o	equilibrium matrix; equilibrium matrix based on undeformed element geometry
Ω_o	skew-symmetric matrix
$\Omega_r^2, \tilde{\Omega}^2$	modal stiffness matrices

Kinematic transformation matrices

A	relates increments of $\underline{v}^*$ to increments of $\underline{\eta}$
$\tilde{A}$	relates increments of $\underline{w}^*$ to increments of $\underline{\eta}$
A_o, $\tilde{A}_o$	geometrically linear part of transformation matrices A and $\tilde{A}$
A_η, $\tilde{A}_\eta$	deformation dependent part of transformation matrices A and $\tilde{A}$
G_o	relates $\underline{\eta}$ and $\underline{\zeta}$
$\underline{h}^T$	relates increments of ϕ to increments of $\underline{v}^*$
$\underline{\tilde{h}}^T$	relates increments of ϕ to increments of $\underline{w}^*$
$\underline{h}_o^T$, $\underline{\tilde{h}}_o^T$	geometrically linear part of transformation matrices $\underline{h}^T$ and $\underline{\tilde{h}}^T$
$\underline{h}_\eta^T$, $\underline{\tilde{h}}_\eta^T$	deformation dependent part of transformation matrices $\underline{h}^T$ and $\underline{\tilde{h}}^T$
L	groups A and $\underline{h}^T$
$\tilde{L}$	groups $\tilde{A}$ and $\underline{\tilde{h}}^T$
M_o	relates increments of $\underline{w}^*$ to increments of $\underline{v}^*$
R_α	relates $\underline{v}$ and $\underline{u}$
S_o	boolean sorting matrix
S_G	matrix that identifies element displacements $\underline{u}$ from global freedoms, $\underline{U}$
S_μ	re-ordering operator
Z	general transformation matrix

Commonly used subscripts and superscripts

u, v, w,η	variable used indicates reference system that applies (list here non-exhaustive)
ϕ	rotation dependency
o	constant (vector or matrix) or dependency on geometrically linear quantities
D	dynamic
E	elastic
ext	external (force)
G	response caused by gravity force applied to the linear-elastic model
int	internal (force)
L	response caused by physical forces applied to the linear-elastic model
NL	inelastic
p	plastic
T	transpose
t	tangent (matrix)
W	response caused by environmental force applied to the linear-elastic model

SUMMARY

For any non-linearly responding body, an equivalent linear-elastic model can be developed in which the material non-linearity and inertial effects are represented as supplementary pseudo-forces which act in addition to the physical loading. The pseudo-forces can be decomposed into constant load-sets multiplied by (deformation-dependent or displacement-dependent) scaling factors. If the scaling factors can be determined, the overall non-linear response can be found from the linear-elastic model using the principle of superposition. For the class of problem in which the material non-linearity is present in only localised regions, a reduced system of non-linear equations whose unknowns are the scaling factors may be derived using an influence matrix technique. This 'reduction procedure', which we refer to as the Pseudo-Force Influence Method (PFI-Method), is the topic of this thesis.

This dissertation is split into three parts. The contents of each are now briefly summarised.

Part I (chapter 1)
The pseudo-force concept and objectives of this thesis

In Part I, we explain why non-linear assessments of offshore structures may be required and discuss why general purpose finite element programs are not always suitable for such studies. The pseudo-force concept is introduced and proposed as an alternative approach that can provide the non-linear response using linear-elastic software.

A historical review of the development of pseudo-force and related methods reveals that these methods have been used primarily to determine the response of modified linear-elastic structures, and that the heuristic approach adopted by several researchers is not readily extended to complex non-linear problems.

Our primary objective is to develop, using pseudo-force principles, an efficient non-linear analysis tool for the assessment of offshore braced frames. A secondary objective is to develop the pseudo-force formulation within a continuum mechanics framework to demonstrate formally that the PFI-Method is simply a reformulation of the displacement-based stiffness method that is often employed in conventional finite element packages.

Part II (chapters 2 to 5)
The PFI-Method for braced frames

In Part II, we consider offshore braced frame structures, and in particular their non-linear response when exposed to severe storms. Before advancing the theory of the PFI-Method for such structures, we begin in chapter 2 by addressing the following: governing failure modes of braced frames; construction of representative non-linear structural models; procedures for static, cyclic and dynamic analyses, and criteria with which to judge the structure's adequacy.

Consideration of the failure modes of offshore braced frames leads to the conclusion that the axial capacity of a few members governs the overall strength and that the bracing configuration plays a key role in the ability of the structure to re-distribute load from buckling members. Some important aspects of non-linear structural modelling are addressed with emphasis on how to model the axial capacity of the members using non-linear bar elements. A member model based on plastic hinge theory is developed and a hysteretic algorithm for axial member capacity is described.

Using the principle of virtual work, the PFI-Method is developed in chapter 3 for statically responding structures in which the non-linear member behaviour can be described using bar elements. The method leads to a reduced system of non-linear equations whose dimension is found to match the number of non-linear bars employed. Consequently, the PFI-Method is expected to be very efficient if the failure mode is controlled by only a few members, as is usually the case for offshore braced frames. General 'arc-length' iterative procedures are discussed for the solution of the reduced system and a particularly effective method based on deformation control with initial stiffness iterations is recommended. The construction of a simulation system for non-linear analysis is described. This employs any linear-elastic program together with a stand-alone routine to solve the reduced system equations.

In chapter 4, dynamic effects are included, while still restricting material non-linearity to bar elements. If the mass of the structure can be lumped to a few points, D'Alembert's principle immediately converts the inertial resistance to equivalent dynamic pseudo-forces. Otherwise, a modal transformation is first employed. Similarities and differences between the dynamic PFI-Method and the non-linear modal superposition technique are explained. The extension of the simulation system for non-linear dynamics is elaborated upon. In both chapters 3 and 4, the physical interpretation of the influence matrices is given but their formal construction is postponed until chapter 7.

Chapter 5 puts the theory developed in chapters 3 and 4 into practice. Several examples of static, cyclic and dynamic response are presented. The problems considered, which are analysed using the described simulation system, range in complexity from a single-degree-of-freedom spring to a large structure. These validate the accuracy of the PFI-Method against analytical solutions and finite element packages, and confirm the effectiveness and efficiency of the approach.

Part III (chapters 6 and 7)
A more formal treatment of the PFI-Method

In chapter 6, continuum mechanics principles and plasticity theory are employed to provide a framework for the more general treatment of the PFI-Method which is developed in chapter 7. The resistance of a finite element is derived within a co-rotational reference system which is suited to large rotation, small strain, computations. The element resistance is developed in terms of its deformation modes. Only later are rigid body modes considered. Symbolic notation is used which enables the geometrically non-linear stiffness matrices to be expressed explicitly in terms of the geometrically linear matrices.

In chapter 7, a general theory for the PFI-Method is derived using the co-rotational approach developed in chapter 6. The symbolic notation adopted in chapter 6 allows the influence matrices to be formally defined and symmetries to be identified. Moreover, for geometrically linear problems, the equivalence of other related techniques such as the initial strain method also become apparent with this notation.

Both nodal and element PFI-Methods are developed, the distinction reflecting whether or not the pseudo-forces are summed at common nodes. The number of pseudo-forces required to represent material non-linearity is shown to equal the number of deformation modes in the element. A procedure for incorporating global geometric non-linearity without diminishing the overall effectiveness of the PFI-Method is discussed. Finally, the efficiency of the PFI-Method is compared to that of a conventional solution procedure operating on the global system matrix.

Part I

The pseudo-force concept and objectives of this thesis

Chapter 1

GENERAL INTRODUCTION

1.1 MOTIVATION FOR THIS WORK

1.1.1 Structural integrity of offshore platforms

This work has been driven primarily by the need for efficient non-linear analysis capabilities for the assessment of offshore braced-frame structures (Fig. 1.1) in water depths of up to 200m.

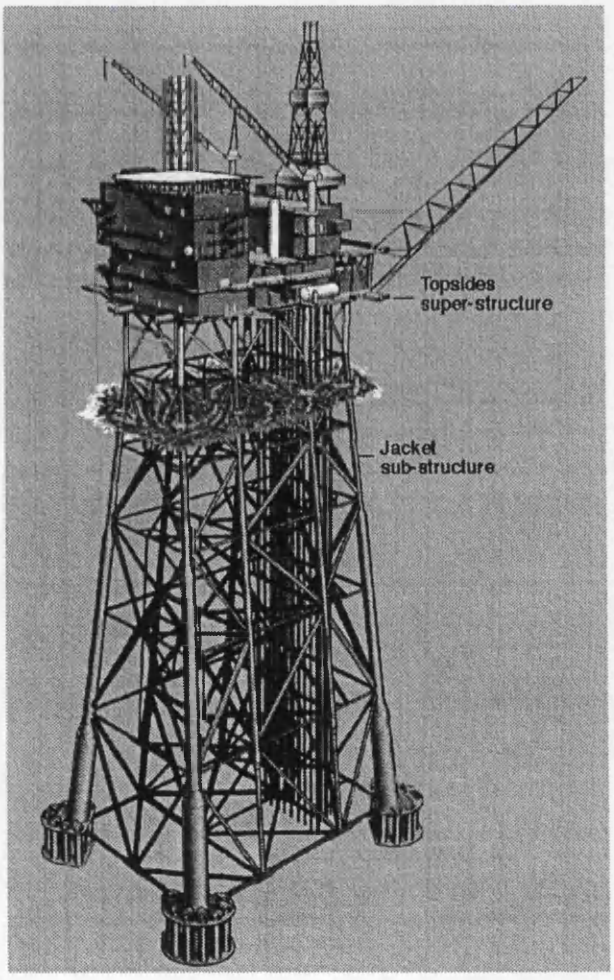

Fig. 1.1 Offshore braced-frame structure

From the offshore operator's perspective, non-linear methods are employed primarily to demonstrate the fitness for purpose of existing structures; and in particular to provide assurance of their ability to resist severe storm induced loading. Many of these have been designed to out-dated codes, or have suffered damage at some time during their operation. Moreover, with the discovery of new oil or gas reservoirs in close proximity to operating fields, an attractive economical option is to make use of existing facilities. This may result in demands being placed upon the structure outside the original design intent. Conventional 'first component failure' assessment procedures, based on linear-elastic analyses, often show these structures to be inadequate. On the other hand, a non-linear 'system strength' approach, in which the collapse resistance of the frame is determined, can usually demonstrate that these structures are perfectly satisfactory - and therefore non-essential repair/remedial work, which is extremely expensive offshore, can be avoided.

The design of new platforms can also be improved by utilising non-linear models, enabling weak links to be identified and removed, and generally leading to a much improved performance for the same initial cost.

1.1.2 Developments in numerical computations for non-linear braced frames

That the performance of offshore structures is best measured by their collapse resistance (as opposed to the onset of yielding or buckling in a single member) has long been recognised. However, although early publications on this subject discussed the governing failure modes (MARSHALL & BEA, 1976), and introduced concepts such as reserve strength (LLOYD & CLAWSON, 1984), it was not until the late 1980's that numerical methods and computing power had reached the stage that a computational collapse analysis of a space-frame with buckling members was possible. In Shell, the first study was completed in 1986 using the INTRA and MARC programs on a Cray-1 supercomputer. This study took one man year of effort. A second study was completed in 1988 (STEWART *ET. AL.*, 1988). In both studies, the solution algorithm often failed to converge when members buckled and several runs using different iteration/load-step strategies were required to determine the collapse load.

Although the robustness of commercially available general purpose non-linear f.e. programs continues to improve, these are not usually suited to routine application and require considerable learning time to use effectively and correctly. More recently, special purpose programs for the analysis of braced frames such as USFOS (SØREIDE *ET AL.*, 1992) have emerged, but nevertheless the non-linear assessment exercise remains non-trivial.

1.1.3 Primary objective in this work: non-linear response of frames using linear-elastic software

For the engineer faced with a non-linear assessment and familiar with a certain linear-elastic analysis package, it would clearly be extremely beneficial if this software and associated structural model could be used without modification to determine the static, cyclic, or dynamic capacity of a structure. Achieving this goal is a prime objective of this thesis. Of course to be of practical use,

any proposed method must be accurate and efficient.

The technique developed and presented is based on the pseudo-force concept, whereby non-linear and inertial resistance contributions are represented as pseudo-forces that act in addition to the physical loading on a linear-elastic model. The problem then is to determine these pseudo-forces: once the pseudo-forces have been found, the linear-elastic analysis program may be used to determine the non-linear response. Typically, the physical loading can be represented as a constant load-set (comprising dead loading, buoyancy loading and functional loading) and a load-set that is scaled, representing the environmental forces. For each value of the scaling factor (or for each time step in a dynamic analysis) different pseudo-forces are determined.

The attractiveness of the proposed method for frame analysis lies in the fact that for any given set of physical forces, the pseudo-forces are calculated using a stand-alone computational algorithm that is completely portable. The input data required for this stand-alone module are the non-linear behaviour of individual members and the elastic characteristics of the structure (which may be provided using any linear-elastic structural analysis program).

1.2 THE PSEUDO-FORCE CONCEPT

The classical approach to mathematical modelling of a non-linear body treats plasticity, geometric non-linearity, and dynamic resistance as intrinsic properties of the body, while the physical external loads are considered to cause the motion of the body. The pseudo-force concept offers an alternative interpretation. As already mentioned, an equivalent problem is derived in which the inelastic material properties, the geometric non-linearity and the dynamic resistance are represented as supplementary (pseudo) forces ($\underline{F}^{NL}$, $\underline{F}^{\Delta}$, $\underline{F}^{D}$, respectively) acting on a linear-elastic reference body (Fig. 1.2). Well known concepts in linear-elastic analysis are then applicable, such as the principle of linear superposition and the response influence technique.

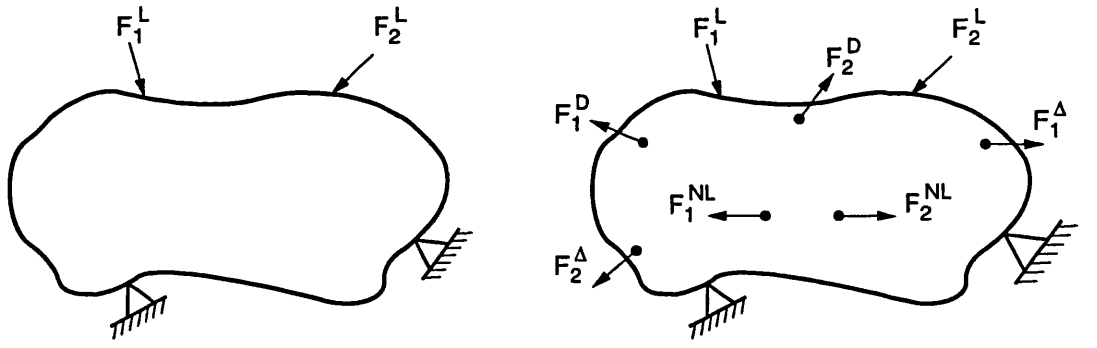

(a) Forces acting on non-linear body *(b) Forces acting on linear-elastic body*

Fig. 1.2 Equivalent representation of a non-linear problem.

For the most general problem class, the total response $\underline{r}$ of the linear-elastic reference body may be interpreted as the sum of each individual response such that we may write

$$\underline{r} = \underline{r}^L + \underline{r}^{NL} + \underline{r}^{\Delta} + \underline{r}^D \tag{1.1}$$

in which

$\underline{r}^L$ is the linear-elastic response produced by the physical loading $\underline{F}^L$;

$\underline{r}^{NL}$ is the linear-elastic response produced by pseudo-forces $\underline{F}^{NL}$ associated with plasticity;

$\underline{r}^{\Delta}$ is the linear-elastic response produced by pseudo-forces $\underline{F}^{\Delta}$ associated with geometric non-linearity; and

$\underline{r}^D$ is the linear-elastic response produced by pseudo-forces $\underline{F}^D$ associated with dynamic resistance.

Thus the original problem is transformed into one of finding the individual pseudo-forces and their corresponding response contributions derived from the linear-elastic reference model.

The pseudo-forces can be decomposed into constant load-sets multiplied by (deformation or displacement) dependent scaling factors. Using the concept of influence matrices, the original non-linear problem, which may have several thousand degrees of freedom, can be reduced to a much smaller (non-linear) system whose unknowns are the pseudo-force scaling factors. Once the scaling factors have been determined, the overall response is found from the linear-elastic model by adding the weighted responses of the constant load-sets to that produced by the physical loading (i.e. superposition principle). Provided all pseudo-forces are identified, the reduced system contains all the information necessary to describe exactly the non-linear response. The computational procedure developed is referred to as the ***Pseudo-Force Influence Method*** (PFI-Method).

For the same discretised description of a structure, the PFI-Method will produce results identical to more conventional non-linear finite element procedures. While completely general in concept, the PFI-Method is best suited to the class of problem in which

(a) plasticity is present in only a small number of elements;

(b) inertia and damping properties can be assigned to a few nodal freedoms or alternatively described using a few mode shapes; and

(c) geometric non-linear effects are either negligible or can be approximated by making use of simplified displacement fields.

Steel braced-frame structures (e.g. offshore structures) are one class of problem that generally satisfy these requirements.

1.2.1 The approach for bar elements and more general elements

To give an appreciation of the overall pseudo-force concept, we first develop the method specifically for non-linear bar elements (chapters 3 to 5). In this development, we state the physical

interpretation of the influence matrices but do not define them in formal mathematics. (The influence matrices, being intrinsic properties of the elastic body, need not be formulated explicitly to progress the pseudo-force method). In most cases, non-linear bar elements will suffice for the modelling of braced frame structures.

In chapters 6 and 7, we adopt a more formal approach, developing the pseudo-force method from continuum mechanics and plasticity theory. There are several advantages to this more rigorous treatment of the PFI-Method. Firstly, the links between the pseudo-force method and any other procedure such as the global stiffness method employed in conventional finite element packages will become clear. Secondly, the influence matrices can be explicitly defined and symmetries identified. And thirdly, for geometrically linear problems, the equivalence of other techniques related to the pseudo-force concept such as the initial strain method become immediately apparent.

1.3 PSEUDO-FORCE METHODS AND RELATED TOPICS IN PUBLISHED LITERATURE

Given a large model of a structure, it seems self-evident that if the properties of only a few elements are altered, this should not entail carrying out a complete re-analysis to obtain the new response. There is a large amount of literature on efficient methods for the ***static re-analysis*** of linear-elastic structures, and the philosophical nature of this problem is similar to that of finding the non-linear response of a structure in which the behaviour of only a few elements differs from linear-elastic. We therefore include a review of methods for static re-analysis before progressing to review the procedures used for non-linear problems.

1.3.1 Methods for static re-analysis of linear-elastic structures

Since the 1950's several static re-analysis techniques have emerged that use the original linear-elastic model as the starting point for the modified response. The extensive literature review conducted by ABU-KASSIM & TOPPING (1987) (which updates a previous literature survey performed by ARORA, 1976) provides a good impression of the variety of approaches considered previously. The following provides an non-exhaustive list of the key-words under which most of this work may be found:

- Re-analysis methods;
- Theorems of Structural Variation;
- Pseudo-force, or Pseudo-load method;
- Initial strain concepts;
- Linear Superposition methods;
- The Virtual Distortion Method;
- Modification/optimisation/re-configuration methods;
- Static condensation/substructuring methods.

These procedures can be broadly classified into two categories: pseudo-force (and related) methods, and direct modification methods which operate on the global system matrix. All methods strive to find a reduced system of equations for the response of the freedoms connected to the modified elements.

In pseudo-force and related methods, the response of the modified structure is simulated by adding constraints, in the form of either pseudo-forces or initial deformations, to the original linear-elastic model. The usefulness of this approach depends crucially on how efficiently the constraints can be obtained.

It is convenient to distinguish between nodal and element pseudo-force methods. In nodal pseudo-force methods, the pseudo-forces are applied at nodal points in the global co-ordinate system and pseudo-forces applied at common nodes are summed. In the element pseudo-force method, the pseudo-forces are associated with individual elements, and are applied in the local element co-ordinate system; they are not summed at common nodes. The initial strain (or thermal load) technique is equivalent to the element pseudo-force method for geometrically linear problems.

The use of the initial strain technique to simulate the response of modified structures was pioneered by Argyris and his co-workers (ARGYRIS & KELSEY, 1956 1960, 1961; ARGYRIS, 1964). A procedure similar to that proposed by Argyris *et al.* was later derived by MELOSH & LUIK (1968). In these early publications of the initial strain technique the ***Matrix Force Method*** was employed, but these same procedures can also be derived using the displacement based stiffness method as in the ***Virtual Distortion Method*** (VDM) of Holnicki-Szulc/Mroz/Gierlinski (HOLNICKI-SZULC & MROZ, 1985; HOLNICKI-SZULC, 1987, 1989, 1991; HOLNICKI-SZULC & GIERLINSKI, 1989).

Several *heuristic* pseudo-force and initial strain procedures have been developed. In this approach, the constraints are sought by appealing both to the classical theorems of structural mechanics (e.g. Betti's law, Castigliano's theorem, superposition, etc.) and a certain amount of intuition. Several authors, including MAJID and his co-workers (1973; 1974; 1978), ATREK (1985), and HOLNICKI-SZULC & GIERLINSKI (1989) have followed this route. The rather trivial problem of obtaining the updated structural response if a single bar element is modified has been discussed by MAJID & ELLIOT (1973). AL-BAKRI (1977) later accounted for simultaneous modifications of several bars in an optimisation study of transmission-line support towers.

Of the direct modification methods, static condensation or substructuring (see for example, ARORA & GOVIL, 1977) is perhaps the best known. A direct method proposed by ARGYRIS *ET AL.* (1971) is of particular interest as it may be shown to be equivalent to a nodal pseudo-force method derived using matrix algebra by WANG *ET AL.*, (1983), as we will demonstrate in chapter 7.

It is interesting that many of the articles on pseudo-force or related methods present essentially similar methods from a different perspective; several methods that were first developed in the 1950's were independently re-discovered in the 1970's. Perhaps the reason stems from the fact that most work in this area has been problem oriented and driven by specialists with interests in different fields. Another contributing factor may be that a heuristic approach has been adopted in many articles and as a result the authors may not recognise the similarity between their suggested approach and that put forward previously by others.

Historically, pseudo-force and related concepts have often been misunderstood. The exchange of articles between ARGYRIS & KESLEY (1960, 1961) and GRZEDZIELSKI (1961), who each took firm positions on their alternate procedures, makes interesting reading.

In chapter 7 of this work, where the PFI-Method is developed for general non-linear problems using fundamental principles of continuum mechanics, static re-analysis procedures emerge as a special case (see sections 7.4.1 and 7.5.2)

1.3.2 Methods for static and dynamic analysis of non-linear structures

The idea that the initial strain technique could be used to simulate the response of non-linear structures appears to have been first suggested by ARGYRIS (1964) who also noted that only a reduced problem need be solved to obtain the magnitude of the initial strains. His treatment of the problem using matrix algebra and the Force Method is applicable to general element types.

Heuristic arguments can be also be used to develop (element) pseudo-force and initial strain methods for structures with simple non-linear element types. HOLNICKI-SZULC & GIERLINSKI (1989) used initial strains and the concept of influence matrices to obtain a reduced system of equations that simulated non-linear behaviour (such as yielding, strain-hardening and fracture) of bars. This procedure was re-formulated by STEWART & VAN DE GRAAF (1990) into a pseudo-force method that included strain softening of the non-linear bar element, thus enabling member buckling to be simulated. They also showed that the reduced system equations could be solved outwith the linear-elastic software package and presented a portable simulation system for static analysis.

The heuristic approach provides physical insight and is rather straightforward for bar elements but it is difficult to extend to more general elements with non-linear material properties.

Nodal pseudo-force methods can also be used for non-linear analysis. The method proposed by WANG *ET AL.*, (1983) for static re-analysis has been extended for non-linear structures by ABU-KASSIM & TOPPING (1985).

The above methods all attempt to find 'exact' solutions to the discretised problem. Approximate procedures based on the Rayleigh-Ritz concept are also very popular. These ***reduced-basis techniques*** approximate the nodal displacement field using a small number of *Ritz basis vectors*. For static analysis the Ritz vectors are typically formed from either the linear buckling modes (NAGY, 1979; NAGY & KÖNIG, 1979) or the updated stiffness matrix (NOOR, ANDERSON & PETERS, 1979; NOOR & PETERS, 1980) whereas for dynamic analysis, either the initial mode shapes (NICKELL, 1976; STRICKLIN & HAISLER, 1977; MORRIS, 1977; CLOUGH & WILSON, 1979; BATHE & GRACEWSKI, 1981; KUKRETI & ISSA, 1984) or updated mode shapes (IDELSOHN & CARDONA, 1985; MOHRAZ, *ET AL.* 1991) are used. Procedures that are based on the initial configuration of the structure are written in pseudo-force form. The accuracy of reduced basis methods depends crucially on the appropriateness of the basis vectors selected. A comprehensive review of reduction methods is given by NOOR (1981, 1994).

For the response of geometrically linear structures with local material non-linearity and, in the case of dynamics, with masses assigned to only a few discrete points, we are interested in an exact formulation of the reduced problem. Therefore for this problem class the reduced basis methods

are only of passing interest. However, for geometrically non-linear problems or for dynamic problems in which the mass is distributed over the body, an approximate procedure is essential to obtain a reduced system. Estimating the influence of both global geometric non-linearity and distributed inertial resistance using a reduced basis technique, while evaluating the effect of local material non-linearity exactly with the PFI-Method, provides an attractive solution option, as we will discuss in chapter 4 and chapter 7.

1.4 SUMMARY OF OBJECTIVES

Before leaving this chapter, we summarise our objectives. These are:

(1) to develop, using a pseudo-force technique together with standard linear-elastic finite element software, a practical, efficient and accurate computational tool for non-linear (dynamic) response analysis of framed (offshore) structures; and

(2) to develop the pseudo-force method within as general a framework as possible, thereby formalising the mathematics of the procedure and consequently enabling it to be directly compared with more conventional solution procedures commonly used in finite element programs.

In chapters 2 through 5 we address the first of these objectives while the second is the scope of chapters 6 and 7.

1.5 REFERENCES

ABU-KASSIM, A.M. AND TOPPING, B.H.V. (1985), "The theorems of structural variation for linear and non-linear finite element analysis", *Civil-COMP. 85, Second int. conf. on Civil & Struct. eng. comp. (U.K.).*, pp159-171.

ABU-KASSIM, A.M. AND TOPPING, B.H.V. (1987), "Static re-analysis: a review", *Jrnl. of Struct. Eng.*, ASCE, **113**, pp1029-1045.

AL-BAKRI, M.A.E. (1977), *Optimum design of transmission towers*, PhD thesis, Univ. of Surrey.

ARGYRIS, J.H., AND KELSEY, S. (1956), "The matrix force method of structural analysis and some new applications", Ministry of Supply, *Aeronautical Research Council Reports & Memoranda*, No. 3034, UK.

ARGYRIS, J.H. AND KELSEY, S. (1960), "Initial strains in the matrix force method of structural analysis", *Jrnl. of Royal Aero. Soc.*, **64**, pp493-495.

ARGYRIS, J.H. AND KELSEY, S. (1961), "The validity of the initial strain concept", *Jrnl. of Royal Aero. Soc.*, **65**, pp129-138.

ARGYRIS, J.H. (1964), "Recent advances in matrix methods of structural analysis", *Progress in Aeronautical Sciences*, **4**, (Küchemann & Sterne Eds.), Pergamon Press.

ARGYRIS, J.H., BRONLUND, O.E. AND ROY, J.R. (1971), "A direct modification procedure for the displacement method", *AIAA Journal*, 9(9), pp1861-1864.

ARORA, J.S. (1976), "Survey of structural re-analysis techniques", *ASCE J. Struct. Division*, **112**, 783-788.

ARORA, J.S. AND GOVIL, A.K. (1977), "Design sensitivity analysis with substructuring", *J. Eng. Div., ASCE*, **EM4**, pp537-548.

BATHE, K.J., AND GRACEWSKI, S. (1981), "On nonlinear dynamic analysis using substructuring and mode superposition", *Computers & Structs.*, **13**, pp699-707.

CLOUGH, R.W. AND WILSON, E.L. (1979), "Dynamic analysis of large structural systems with local nonlinearities", *Computer Methods in Applied Mechanics & Engineering*, **17/18**, 107-129.

GRZEDZIELSKI, A.L.M. (1961), "The initial strain concept", *Jrnl. of Royal Aero. Soc.*, **65**, pp127-129.

HOLNICKI-SZULC, J., AND MROZ, Z. (1985), "Active control of stresses and deflections of elastic structures by means of imposed distortions", *Proc. 2nd Int. Syp. Struct.Control*, Univ. of Waterloo, Ontario.

References (continued)

HOLNICKI-SZULC, J. (1987), "Degradation of elastic structures simulated by initial distortions", *Mech. of Struct. & Machines*, **15**, pp1-15.

HOLNICKI-SZULC, J. (1989), "Optimal structural remodelling - simulation by virtual distortions", *Comm. App. Num. Meth.* **5**, pp289-298.

HOLNICKI-SZULC, J. AND GIERLINSKI, J.T. (1989), "Structural modifications simulated by virtual distortions", *Int. J. of Num. methods in Eng.*, **28**, pp645-666.

HOLNICKI-SZULC, J. (1991), *Virtual Distortion Method*, Lecture notes in engineering, **65**, (C.A. Brebbia & S.A. Orszag, Eds.), Springer-Verlag.

IDELSOHN, S.R., AND CARDONA, A. (1985), "A reduction method for nonlinear structural dynamic analysis", *Computer Methods in Applied Mechanics & Engineering*, **49**, pp253-279.

INTRA *Inelastic Tower Response Analysis program*, ISEC Inc., San Francisco.

KUKRETI, A.R., AND ISSA, H.I. (1984), "Dynamic analysis of nonlinear structures by pseudo-normal mode superposition method", *Computers & Structs.*, **19**(4), pp653-663.

LLOYD, J.R., AND CLAWSON, W.C. (1984), "Reserve and residual strength of pile founded offshore platforms", *Int. Symp. on The role of Design and Redundancy in Marine Structural Reliability*, (Eds. Faulkner et al.), Nat. Acad. Press.

MAJID, K.I. AND ELLIOT, D.W.C. (1973), "Forces and deflections in changing structures", *Struct. Eng.*, **51**(3), pp93-101.

MAJID, K.I. (1974), *Optimum Design of Structures*, Butterworths.

MAJID, K.I, SAKA, M.P. & CELIK, T. (1978), "The theorems of structural variation generalised for rigidly jointed frames", *Proc. Instn Civ. Engrs*, Part 2, **65**, pp839-857.

MARC *General purpose finite element program*, Marc Research Corporation, Paulo Alto.

MARSHALL, P.W, AND BEA, R.G. (1976), "Failure modes of offshore platforms", *Intl.Conf. on the Behaviour of Offshore Structures* (BOSS), Trondheim, Norway.

MELOSH, R.J. AND LUIK, R. (1968), "Multiple configuration analysis of structures", *ASCE J. Struct. Division*, **ST11**, pp2581-2596.

MOHRAZ, B., ELGHADAMSI, F.E., AND CHANG, C-J. (1991), "An incremental mode superposition for nonlinear dynamic analysis", *Earthquake Eng. & Struct. Dyn.*, **20**, pp471-481.

MORRIS, N.F. (1977), "The use of modal superposition in nonlinear dynamics", *Computers & Structs.*, **7**(1), 65-72.

NAGY, D.A. (1979), "Modal representation of geometrically nonlinear finite element behaviour by the finite element method", *Computers & Structs.*, **10**, pp638-688.

NAGY, D.A., AND KÖNIG, M. (1979), "Geometrically nonlinear finite element behaviour using buckling mode superposition", *Comp. Meth. Appl. Mech. & Eng.*, **19**, pp447-484.

NICKELL, R.E. (1976); "Nonlinear dynamics by mode superposition", *Computer Methods in Applied Mechanics & Engineering*, **7**(1), pp107-129.

NOOR, A.K., ANDERSON, C.M., AND PETERS, J.M. (1979), "Global-local approach for nonlinear shell analysis", *Proc. 7'th ASCE Conf. Electronic Comp.*, pp634-657.

NOOR, A.K., AND PETERS, J.M. (1980), "Reduced basis technique for nonlinear analysis of structures", *AIAA J.*, **18**(4), pp455-462.

NOOR, A.K. (1981), "Recent advances in reduction methods for non-linear problems", *Computers & Structs.*, **13**, pp31-44.

NOOR, A.K. (1994) "Recent advances and applications of reduction methods", *Appl. Mech. Rev.*, **47**(5), pp125-146.

SØREIDE, T.H., AMDAHL, J.A., EBERG, E., HOLMÅS, T. AND HELLAN, Ø. (1992), "USFOS - A computer program for progressive collapse analysis of steel offshore structures", Theory manual, SINTEF, Norway.

STEWART, G., EFTHYMIOU, M. AND VUGTS, J.H. (1988), "Ultimate strength and integrity assessment of fixed offshore platforms", *Intl.Conf. on the Behaviour of Offshore Structures* (BOSS), Trondheim, Norway.

STEWART, G. AND VAN DE GRAAF, J.W. (1990), "A methodology for platform collapse based on linear superposition", *Offshore Technology Conference*, OTC 6311, Houston, Texas.

STRICKLIN, J.A. AND HAISLER, W.E. (1977), "Formulations and solution procedures for nonlinear structural analysis", *Computers & Structs.*, **7**, pp125-136.

USFOS: see SØREIDE *ET AL.* (1992).

WANG, B.P., PILKEY, W.D., AND PALAZZOLO, A.B. (1983), "Re-analysis, modal synthesis and dynamic design", in *State-of-the-art finite element technology*, ch. **8**, pp225-295, A. Noor & W. Pilkey (eds.), ASME, New York.

Part II

The PFI-Method for braced frames

Chapter 2

OFFSHORE BRACED-FRAME STRUCTURES

2.1 INTRODUCTION

Jacket structures

The first offshore structure was installed in 1947 in 7m of water (VUGTS, 1989). To date there are more than 6000 offshore structures world-wide. The majority of these are in water depths of less than 200 m and are bottom founded steel space frames (sub-structures) that support modular units (topside super-structure) for drilling and oil and gas production. An example of a typical North Sea platform is shown in Fig. 2.1.

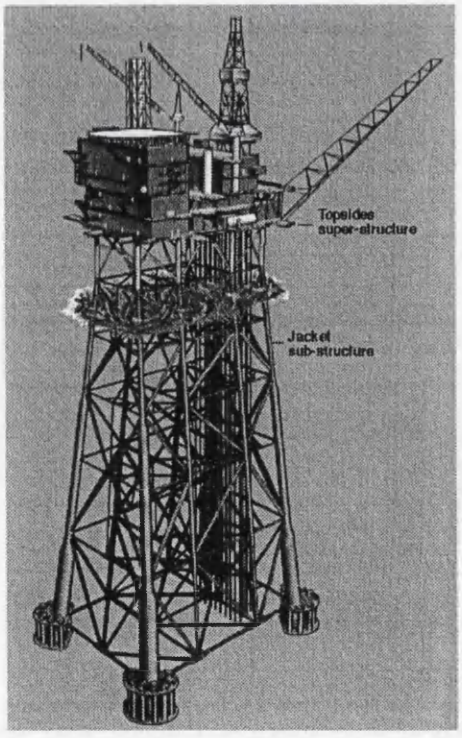

Fig. 2.1 Typical North Sea platform

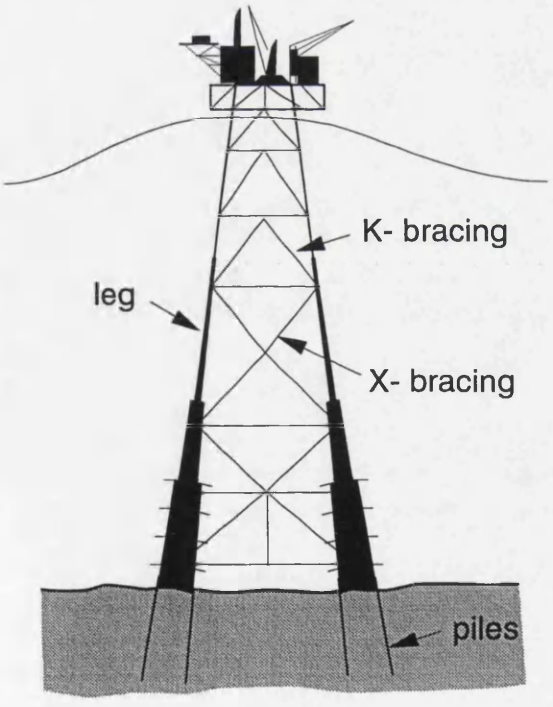

Fig. 2.2 X and K bracing arrangements

The sub-structure, of which there are two types, is commonly referred to as a jacket structure. The conventional *template jacket* has founding piles that are driven inside the legs and welded to

the top of the frame. The name arises because the sub-structure's legs fit over the piles rather like the sleeves of a "jacket", and also the legs act as a template for piling. These structure types are typical of shallow water developments such as those in the southern North Sea or close to shore in the Gulf of Mexico. For larger, heavier structures, such as those in the northern North Sea, one pile per leg is insufficient to support the overall weight and resist the environmental forces. The piles are then placed externally in groups and are grouted to the base of the legs. These *tower frame* structures (of which the structure in Fig. 2.1 is an example) are also commonly (but less correctly) referred to as jacket structures. The tower frame acts like a cantilever with the base being the most heavily loaded portion whereas in a template jacket, the critical area is at the top of the legs where the pile axial forces enter the structure.

The dominant forces acting on these structures are gravity loads (from the topside equipment and self weight of the platform), and environmental forces that arise from the combined action of waves, wind and current. The fluid loading on each member comprises a viscous drag term that is proportional to the square of the fluid velocity and (a less significant) inertial term that is proportional to the fluid acceleration (MORISON *ET AL.* 1950). In the linear response range (that is before members start to buckle or yield), dynamic effects can usually be disregarded as the natural period of the structure (around 2 secs.) is far from the excitation period (about 15 secs. in the North Sea) of large waves.

Jacket structures resist applied loading primarily by mobilising the axial strength of members. Even at large lateral deflections, the shear resistance that develops in the legs (and piles in a template jacket) is generally of secondary importance when compared to the lateral resistance offered by the vertical bracing system. The type of bracing configuration plays a key role in determining the overall non-linear behaviour of the frame. Two common configurations (X-bracing and K-bracing) are identified in Fig. 2.2.

It is required to prove the integrity of these structures when exposed to extreme storms.

Linear or non-linear analysis ?

Designs of new offshore structures and re-assessments of existing ones usually rely on linear-elastic models to determine the internal forces in each component as a result of the design loading. Compliance with codes and guidelines (such as API-RP2A) is achieved if, for all components, the strength exceeds the induced forces by an adequate margin of safety. This "first component failure" procedure clearly does not provide the true maximum load-bearing capacity of the structure.

There are two reasons why this maximum capacity or "collapse resistance" may be of interest. Firstly, a better understanding of how structures behave can lead to improvements in design, resulting in safer structures for the same cost. But the main reason is that in many cases, demands are often placed on *existing structures* that are outside their original design intent (examples include additional production equipment to process the oil and gas from a nearby newly found reservoir, and damage from dropped objects). It may not then be possible to verify the structure to existing design recommendations. As strengthening an existing structure is prohibitively expensive, it is worthwhile to identify (and make use of) any hidden reserves of strength beyond the component-level capacity.

To quantify any "reserve strength", a non-linear structural model is required together with an appropriate assessment procedure and acceptability criteria with which to judge the adequacy of the results. Setting out the methodology of how these may be realised is the primary aim of the remainder of this chapter.

Understanding the failure mode characteristics of braced frames is a pre-requisite to developing non-linear models that can adequately represent these. We therefore go into this aspect in some depth. Since the frame strength is determined by the strength of its component parts, the behaviour and modelling of the individual members are considered in detail. The axial member strength contributes most to the overall capacity of the structure and a simple model to determine this is proposed.

We begin by developing the overall framework of the assessment procedure.

2.2 ASSESSMENT PROCEDURES FOR STRUCTURES EXPOSED TO EXTREME STORM LOADING

2.2.1 Storms

Storms may be defined as events in which the maximum sea-state intensity (measured by the significant wave-height) exceeds a given threshold, for example 5m. This definition ensures independence of individual storms. For the North Sea, it results in about four winter storms per year. An extreme storm may be defined as one that will cause (near) collapse of the structure.

Characterising storms

The profile of a storm consists of a number of sequential sea-states whose intensities build up to a peak and then decay (Fig. 2.3).

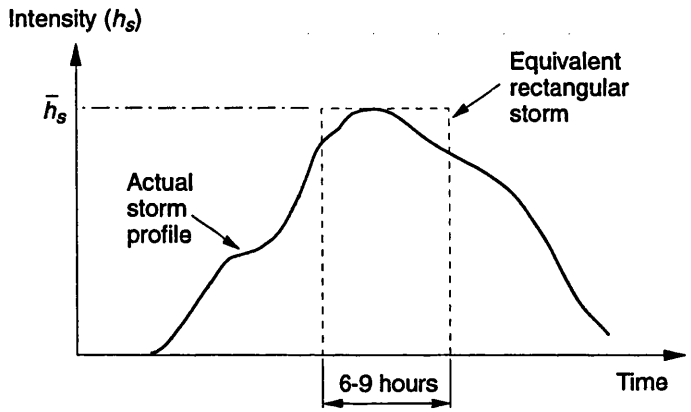

Fig. 2.3 Equivalent rectangular storm

By considering each sea-state in the storm, one can derive an equivalent rectangular storm (BORGMAN, 1970; TUCKER, 1991). This has constant intensity $\bar{h}_s$ with an associated duration of a few hours (typically 6 to 9 hours for the North Sea) comprising around 2000 waves. The

(conditional) probability of non-exceedance of wave heights h in this equivalent storm is given by the Rayleigh distribution (CARTWRIGHT & LONGUET-HIGGINS, 1956):

$$F_R(h|\bar{h}_s) = 1 - e^{-2(h/\bar{h}_s)^2} \quad . \tag{2.1a}$$

where the sub-script 'R' denotes the Rayleigh distribution. If there are N waves in the equivalent storm, the probability of non-exceedance of the largest wave h_{max} is given by

$$F_{ST}(h_{max}|\bar{h}_s) = [F_R]^N \quad . \tag{2.1b}$$

This may be referred to as the short-term variability in maximum wave-height, and is denoted by the sub-script, 'ST'.

Maximum wave-height distribution and return period

If the probability density function of storm occurrences $f(\bar{h}_s)$ can be established (for example from hindcast data, see WARD & CARDONE, 1978), then from the integral form of the total probability theorem we get the long-term (LT) maximum wave-height cumulative distribution as

$$F_{LT}(h_{max}) = \int_0^\infty F_{ST}(h_{max}|\bar{h}_s) f(\bar{h}_s) d\bar{h}_s \quad . \tag{2.2a}$$

This gives the probability that the largest wave in a storm selected at random will be less than h_{max}. If there are ν storms per year, then the cumulative distribution of the annual maximum wave-height is given by

$$F_a(h) = [F_{LT}(h)]^\nu \quad . \tag{2.2b}$$

The wave that has a return period R years (i.e. occurs on average once in R years) is known as the R-year wave and its height is calculated from the relationship

$$F_{LT}(h_R) = 1 - \frac{1}{R\,\nu} \quad . \tag{2.3}$$

Typically the 100-year wave height is used as a reference value for design.

2.2.2 Assessment procedure for static collapse (pushover) analysis

In a static pushover analysis (Fig. 2.4), we use a non-linear structural model to evaluate the collapse resistance of the structure. Inertial effects introduced by motion of the structure are ignored in this type of assessment.

Collapse resistance

The design environmental load-set $\underline{F}^W_{100}$ which results from the 100-year wave with associated current and wind (API-RP2A) is a useful reference level load for non-linear analysis. If, in our non-linear structural analysis we first apply the (factored[1]) still-water gravity and buoyancy loading, $\underline{F}^G$, and then progressively increase $\underline{F}^W_{100}$ by a scaling factor λ, the structure will eventually collapse when the scaling factor reaches λ_{ult} (Fig. 2.4). Associated with the force vector $\underline{F}^W_{100}$, we may select a suitable global force measure (such as total horizontal force or total applied overturning moment about the sea-bed). This scalar quantity is denoted by F^W_{100}. The collapse load $\lambda_{ult} F^W_{100}$ is called the ***pushover strength*** of the structure (LLOYD & CLAWSON, 1984). The factor λ_{ult} is a measure of the safety margin - Lloyd and Clawson call it the ***reserve strength factor*** (RSR) - and it can be related to the probability of failure, as will be discussed briefly later in this section.

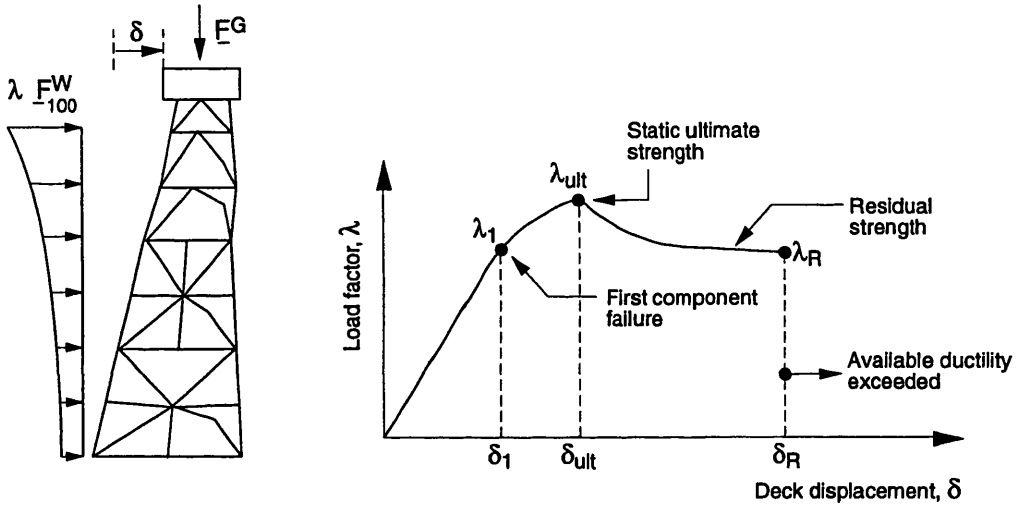

Fig. 2.4 Static pushover analysis

Several static pushover analyses are reported in the literature. In addition to the already mentioned publication by Lloyd and Clawson, the reader is referred to the work of STEWART *ET AL.*, (1988), TITUS & BANON (1988), HELLAN *ET AL.* (1994) which give insight into methodologies for such analyses and to the publications by NORDAL (1990), VAN DE GRAAF & TROMANS (1991), HELLAN *ET AL.* (1993), and SI *ET AL.* (1993) which provide details of application studies. The review paper by BOLT & BILLINGTON (1993) gives a good overview, comparing and contrasting the different methodologies used.

Failure mode classification

The pushover curve, in which the global environmental load factor is plotted against the displacement of the deck, provides a good insight into structural performance. Additionally,

1. The reasons for factoring this (by 1.15) are discussed at the foot of the next page.

referring to Fig. 2.4, certain non-dimensional measures may be used to characterise the structure:

$$RF = \frac{\lambda_{ult}}{\lambda_1}; \qquad \alpha = \frac{\lambda_R}{\lambda_{ult}}; \qquad \mu_{lim} = \frac{\delta_R}{\delta_{ult}}. \tag{2.4}$$

The ***redundancy factor*** (*RF*) was introduced by STEWART *ET AL.* (1988). It is a measure of the reserve strength beyond first component failure (λ_1). It therefore indicates how much has been gained by the non-linear assessment over the linear-elastic stress analysis.

The ratio α of the post-ultimate (or residual) strength (λ_R) to the collapse strength may be referred to as the robustness factor. The robustness factor together with the limiting ductility factor μ_{lim} (which is a measure of the maximum allowable deformation), provide a means of classifying the failure mechanism as either:

(a) *ductile,* implying $\alpha \cong 1$ *and* $\mu_{lim} >> 1$;

(b) *brittle,* implying $\alpha << 1$ *or* $\mu_{lim} \cong 1$; or

(c) *semi-brittle,* if somewhere between the two extremes.

Ductile structures are preferred over brittle structures as their dynamic load-bearing capacity is greater (see section 2.2.4). Whether a structure behaves in a ductile or brittle manner depends on its bracing configuration. This is discussed in detail in section 2.3.

Probability of failure

Early studies on the failure probability of offshore platforms (see for example: MARSHALL, 1969; MARSHALL & BEA, 1976; ANDERSON, SILBERT & LLOYD, 1982) gave valuable insight into the parameters that controlled structural safety but did not attempt to provide any guidance on acceptable margins between the design load and the pushover resistance.

The pushover factor λ_{ult} can be related to the probability of failure if two assumptions are made. The first step involves replacing the random system strength R by its characteristic value[1] R_{char}. This can be justified (STEWART ET *AL.*, 1988) by consideration of each component's strength variability and bias (the ratio between its mean and characteristic strength). Recent collapse analyses studies by SIGURDSSON *ET AL.* (1994) using USFOS together with Monte-Carlo simulation

1. The assessment check for a structural component may be expressed as $\gamma_W F_{100}^W > R_{char}^c / \gamma_c$ where: R_{char}^c is the component's characteristic strength (typically taken to be an estimate of the lower 5-percentile strength), γ_c is a resistance factor, and γ_W is a load factor. For different component types, the resistance factor may vary. For steel members a value of $\gamma_c = 1.15$ is often selected while for foundation elements 1.3 is considered appropriate (DnV, 1977). API-LRFD recommends similar factors. The component assessment criterion may also be expressed as $\lambda F_{100}^W > R_{char}^c$, where $\lambda = \gamma_W \gamma_c$. We would now like to establish a similar relationship for the complete system. In doing so we should ensure that if there is no reserve beyond first component failure, the criterion exactly matches that for a component. The problem is that γ_c is not the same for all components. Let $\gamma_s = 1.15$ be the factor for steel members with characteristic resistance R_{char}^s and (*Footnote continued at bottom of next page*)

techniques also support this approach. Secondly, it is (reasonably) assumed that the long-term probabilistic force distribution on the structure is dominated by the statistical randomness of the wave-height. Taking the total horizontal force to wave-height relationship as

$$F^W = F^W_{100}\left(\frac{h}{h_{100}}\right)^{\beta} \tag{2.5}$$

with β close to 2.0 for a drag dominated structure, the structure collapses when F^W exceeds the characteristic system strength $R_{char.}$ That is the notional[1] annual probability of failure P_a may be calculated from

$$P_a = P(F^W > R_{char}) = P(F^W > \lambda_{ult} F^W_{100}) = P(h_{max} > \lambda_{ult}{}^{1/\beta} h_{100}) = 1 - F_a(\lambda_{ult}{}^{1/\beta} h_{100}) \tag{2.6}$$

where F_a is the annual wave-height cumulative distribution given by (2.2b).

This was the approach followed by the writer and his colleagues in 1988 (STEWART ET *AL.*, 1988) and it led to the conclusion that for the North Sea, a collapse load factor of $\lambda_{ult} = 1.5$ corresponding to a (notional) failure probability of around 10^{-4} per annum was acceptable - which is more or less the accepted norm for manned installations (see NPD regulations, 1985). A more rigorous procedure for estimating the collapse probabilities of platforms, taking account of the probabilistic combinations of wave, current and wind, and using well calibrated hydrodynamic models has recently been employed by TROMANS & VAN DE GRAAF (1992) and SI *ET AL.* (1993). It is claimed by these authors that their results are indicative of 'true' failure rates as opposed to the notional failure rates quoted in earlier work.

2.2.3 Assessment procedure for cyclic shakedown analysis

The pushover strength measures the capability of the structure to resist the forces associated with the passage of a single large wave. However, the severe storm that generates this large wave

---

Footnote continued from previous page

let $\gamma_f = 1.3$ be the factor for foundation elements with characteristic resistance R^f_{char}. If, in our non-linear structural model, we use the characteristic strength of each component, modified by the relevant material factor, the system strength (for a given value of still-water load, $\underline{F}^G_o$) would be $R^*(\underline{F}^G_o; \underline{R}_s / \gamma_s; \underline{R}_f / \gamma_f)$. We could then impose the requirement $\gamma_W F^W_{100} > R^*$ which reduces to the component check for a system with no reserve strength. However, to avoid modifying the resistance of all of the steel members we extract the material factor γ_s as a common factor and write the system strength as $R^* = (1/\gamma_s) R_{char}\{\gamma_s \underline{F}^G_o; \underline{R}_s; \gamma_f / \gamma_s \underline{R}_f\}$. The system collapses when $\gamma_W F^W_{100} > R^*$, or equivalently when $\lambda F^W_{100} > R_{char}$, where $\lambda = \gamma_W \gamma_s$. From this we see that to obtain a measure of characteristic system strength R_{char}, we build a model using the characteristic strength of the steel members, and a modified strength for other components and perform a static pushover analysis with a factored still-water load $\underline{F}^G = \gamma_s \underline{F}^G_o$.

1. Notional, meaning that we do not believe this to be the actual probability of failure because our calculations include a certain degree of approximation and may not include all aspects of the problem.

will contain several large waves. It is then important to know whether the cumulative effect of these waves can lead to low cycle fatigue-induced fracture of a member or members, resulting in a system strength below that predicted by the pushover analysis. As with the pushover analysis, inertial effects are not included.

A representative storm loading history for investigating extreme storm cyclic effects has been proposed by the writer and a colleague (STEWART & TROMANS, 1993). We used the long-term wave-height distribution to get the largest individual wave and the method of ***order statistics*** (WILKS, 1948; GUMBEL, 1958; BALAKRISHNAN & COHEN, 1991) to determine the other most probable largest waves in the same storm. For any given target failure rate ($1/R$), we defined the extreme loading to be the R-year wave, h_R, plus the largest waves in the R-year storm. This sequence was then converted back to equivalent 100-year conditions leading to the concept of a ***design storm*** (Fig. 2.5), described by the following ordered wave-heights:

$$h_1 = h_{100}, \qquad h_m = h_{100}\xi_R\sqrt{1-\frac{\log m}{\log N}}\ , \ m = 2,3,\ldots; \quad \xi_R < 1 \tag{2.7}$$

where N ($\cong 2000$) is the number of waves in an equivalent rectangular storm. We defined the multiplier ξ_R as the ***short-term variability factor*** which was calculated to be

$$\xi_R = (h_{s_R}\sqrt{0.5\ln N})/h_R \tag{2.8}$$

which is simply the ratio between the most probable largest wave in the R-year storm (of intensity h_{s_R}) divided by the R-year wave height. The force history resulting from this wave sequence is then factored by λ to represent the forces imparted by the R-year storm.

In the North Sea, for a target annual failure rate of 10^{-4}, (R=10^4), ξ_R was found to lie in the range 0.77 to 0.87, with the lower and upper values corresponding to the southern and northern sectors, respectively. The largest waves may come in any order, but it is anticipated (and supported by analysis - see HELLAN *ET AL.*, 1993) that descending order (i.e. largest first) is the most onerous.

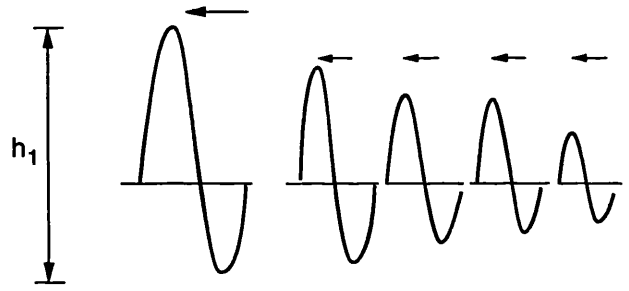

Fig. 2.5 Sequence of waves in a design storm

From eqns. (2.5) and (2.7), and the data on ξ_R, it is apparent that in the North Sea the force generated by the second largest wave (on statistical average) is at most 75% of the largest. In addition, from practical experience for areas with low current (less than 0.5 m/sec) the reverse forces generated by the trough of the wave are at most about 35% of the forward forces that are exerted as the crest passes through the structure. If the current is increased, the reverse force can

be close to zero. Therefore the cyclic action in extreme storms is relatively mild and is strongly biased in the forward direction. It is quite different from the severe load reversals experienced during earthquakes.

The work by Shell Research on cyclic storm loading was made available to an industry collaborative project organised by SINTEF. Cyclic analyses were performed on six platforms for several loading directions using a specially developed version of the USFOS program. A load-set history was derived from the waves defined by (2.7) and scaled to 98% of the pushover capacity, λ_{ult}. The structure was deemed to have passed the cyclic assessment if it eventually responded elastically to the loading history - that is if shakedown to an elastic state was possible. The conclusions were that in general the pushover resistance was an adequate ultimate strength indicator. However in two cases it was found that certain highly deformed buckled members underwent reversed plasticity for all cycles unless the load factor was reduced - that is (according to the proposed acceptance criterion) the pushover capacity overestimated the available structural strength.

The results from this project, which are believed to be the first of its kind, were presented as a series of four papers at the Offshore Mechanics and Arctic Engineering (OMAE) conference in Glasgow, 1993 (STEWART *ET AL.*, STEWART & TROMANS, EBERG *ET AL.*, HELLAN *ET AL.*). The quantification of member ductility exhaustion, which plays a crucial role in determining whether fracture of the member is likely, remains an ongoing subject of research.

2.2.4 Assessment procedure for dynamic collapse analysis

Although for a static response analysis, equilibrium cannot be achieved if the load factor is increased beyond λ_{ult}, dynamic equilibrium is always possible. Because wave forces are time-dependent, and as the platform's mass (and added mass) mobilises inertial resistance, it is quite conceivable for the peak dynamic loading to exceed the static ultimate capacity by a considerable margin before the deformations become unacceptable (μ_{lim} exceeded in Fig. 2.4). 'Failure' now becomes a question of how much deformation can be tolerated.

The possibility of resisting peak environmental forces larger than the static ultimate capacity is improved if the mass is large (increased inertial resistance) and the failure mechanism is ductile (STEWART, 1992). This gives quantifiable evidence to the intuitive view that structures with ductile failure modes are inherently safer than those with brittle modes. Recently, BEA & YOUNG (1993) have investigated the response of some Gulf of Mexico platforms using recorded loading histories from hurricanes. Their conclusions are similar to those reported by the writer in 1992.

To calculate the dynamic capacity, the time history of force associated with the passage of the 100-year wave is factored by λ and applied to the structure. The procedure is repeated for increasing values of λ until the deformation limit is reached at λ^D_{ult}. This dynamic collapse load factor is then used as the load-bearing capacity of the structure in the integrity check. Note that the largest waves in a storm do not occur contiguously and therefore only one extreme wave need be considered in the time history of force. The ratio of maximum dynamic to static resistance given by $\psi^{ult} = \lambda^D_{ult} / \lambda_{ult}$ may be called the ***ultimate dynamic overload ratio*** and provides a measure of the importance of inertial effects.

As with cyclic storm analyses, dynamic collapse in extreme storms is a new topic of research.

2.3 RESISTANCE OF BRACED-FRAME STRUCTURES

We now turn our attention to developing a detailed understanding of how braced frames resist load and how these structures fail. Before we discuss the failure modes of such frames, we first consider the response behaviour of the structural members in the space frame. As will be discussed in detail in section 2.3.2, it is primarily the axial resistance of the members that determines the overall frame capacity. We therefore focus initially on individual member axial-load/shortening characteristics.

2.3.1 Load-shortening characteristics of axially loaded members

The behaviour of (both fabricated and seamless) tubular columns under increasing axial deformation has been reported by BOUKAMP (1975), CHEN & ROSS (1977), SMITH *ET AL.* (1979), and SHERMAN (1980), while the cyclic hysteretic response has been studied by POPOV & BLACK (1981), ZAYAS *ET AL.* (1982) and GRANLI (- - -). These tests show that yielding is very localised and that the response can be described in terms of plastic hinge development.

The ideal axial hysteretic response of a simply-supported axially loaded member is depicted in Fig. 2.6 (reproduced in part from CHEN & HAN, 1985). Consistent with experimental evidence, the general inelastic behaviour can be explained by the presence of a central plastic hinge that becomes activated when the axial force and bending moment reach a bounding yield surface[1] (Fig. 2.6c). The equation of this surface is derived from the cross-section geometry.

The response curve is split into several parts (MARSHALL *ET AL.*, 1977). In the first of these (O-A), the load increases up to the buckling capacity at which point a plastic hinge forms. Beyond the peak, the hinge rotation and lateral midspan deflections increase, causing an increase in the bending moment. To satisfy the yield surface constraint, the axial force decreases. The response now progresses along the post-buckling branch (A-B). Upon reversing the increment of deformation, the column unloads elastically (B-C). The load is now zero but the column has residual deformations. The applied force now becomes tensile. Straining remains elastic until point D at which time the plastic hinge is activated again. Along path D-E, the hinge is "opened" and the column straightens. Eventually, the tensile strength of the member is reached and (in the absence of strain hardening) the response is horizontal along path E-F. Unloading from this point, along F-G, is elastic. The area under the curve O-G represents the plastic energy dissipation in one cycle.

1. This is rather simplistic. To describe the behaviour accurately, the yield surface must harden in such a way that the "Bauschinger effect" is reproduced (see EBERG *ET AL.*, 1993).

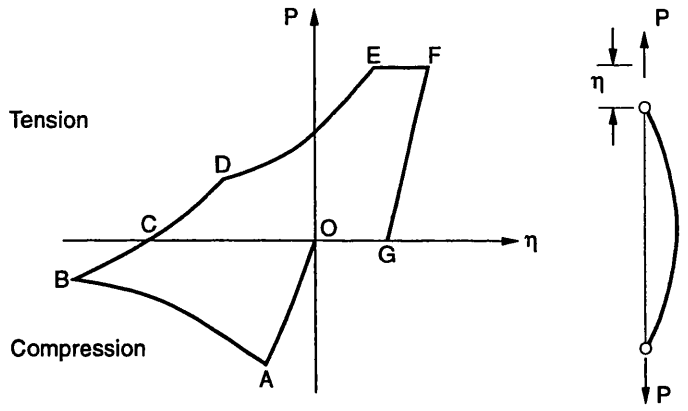

(a) Axial hysteretic response

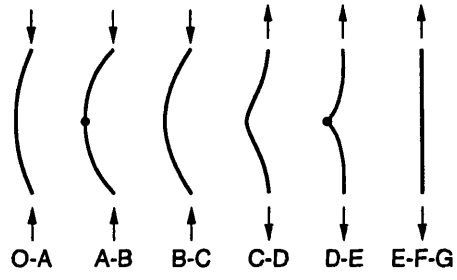

(b) Deformed shape at various stages of load history

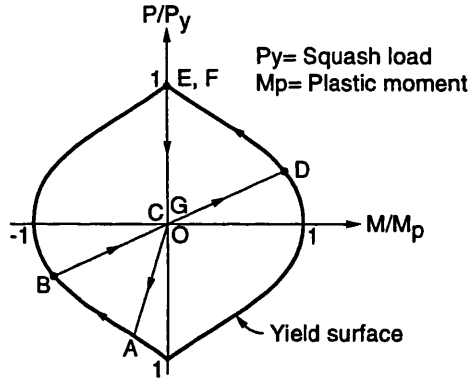

(c) Force history in central hinge

Fig. 2.6 Hysteretic brace response

The buckling load (point A) depends on the following:

(a) the geometry (length, cross sectional area)

(b) the boundary conditions (which determine the effective length factor, k)

(c) the material properties (yield stress, Young's modulus)

(d) residual stresses introduced by the production process

(e) geometrical imperfections (out of roundness, out of straightness)

A review of how each of these parameters influences the member buckling strength is given in appendix A.

There are a number of other factors (local buckling, damage, ultimate tensile strain) that need to be taken into consideration that may result in modification to the ideal hysteresis curve shown in Fig. 2.6. Local buckling is an instability of the tube wall. It becomes more likely as the diameter to thickness (D/t) ratio increases. For the D/t range (30 to 60) typically used in offshore structures, if this instability occurs it initiates after the plastic hinges have developed. The formation of the

local buckle or wrinkle can be very detrimental to the member's overall load-bearing capacity. The loss in strength after local buckling is much greater for members with high D/t ratios than for those with low D/t ratios (SMITH *ET AL.*, 1979). Experimental studies (SHERMAN, 1980; GRANLI, - - -; ZAYAS *ET AL.* 1982; POPOV & BLACK, 1981) have shown that the combination of local buckling and alternating plasticity causes the member capacity to degrade rapidly and eventually fracture. Further details on local buckling are given in appendix A.

The effect of dents on the compressive strength of tubular columns has been extensively investigated by TABY & MOAN (1985), TABY (1986) and YAO *ET AL.* (1987). For columns having D/t in the range 30 to 50 it is reported that for a dent at midspan of 10% of the diameter, the reduction in buckling load is about 30%. As with local buckling, the high strains that develop in the dented region are likely to make these columns very susceptible to fatigue-induced fracture under alternating plasticity.

In the tensile stretching regime (Fig. 2.6, path E-F), MARSHALL *ET AL.* (1977) recommend that the member is disconnected from the structural model after an axial deformation of 1% of the member length (i.e. 1% average axial strain). This is far less than the ductility expected from tensile coupon tests (20% or so) and accounts for strain concentrations at the connecting joint.

2.3.2 Failure modes of jacket structures

A comprehensive description of failure mode characteristics for frames is given by LLOYD & CLAWSON (1984), MARSHALL & BEA (1976), and GATES *ET AL.* (1977). Numerical studies by STEWART *ET AL.* (1988), and VAN DE GRAAF & TROMANS (1991) give further insight into actual platform ultimate behaviour, while the recent work by HELLAN *ET AL.* (1993) documents and discusses the pushover and cyclic resistance of six different platforms for several wave attack directions. BOLT & BILLINGTON (1993) have collated and compared the findings from a large number of numerical studies, and their paper provides a useful reference.

The cyclic response of X-braced, and diagonally braced plane frames has been studied experimentally by ZAYAS *ET AL.* (1982) and OGAWA (1987), while BOLT *ET AL.* (1994), have investigated the pushover behaviour of a plane frame with various bracing configurations.

These desk studies, numerical simulations and experiments all support the view that it is primarily the axial resistance of (a few critical) members that controls the non-linear response and collapse strength of the frame. We now describe in more detail typical failure modes under increasing lateral loading to provide a little more insight into frame characteristics.

Primary failure mechanisms

There are two primary failure mechanisms for jacket structures. The first is a sidesway mechanism which is triggered by bracing failures, an example of which was shown in Fig. 2.4. This failure mode is common for 'end-on' and 'broadside' loading directions (Fig. 2.7) and has received most attention in the literature as it is often governing. The second failure mode results from the overturning resistance being exceeded and is precipitated by leg yielding in tension or compression, or by pullout/punch-through of the piles. This is the most likely mode for 'diagonal'

wave attack directions, with the legs and piles farthest from the axis of rotation of the structure failing first (VAN DE GRAAF & TROMANS, 1991).

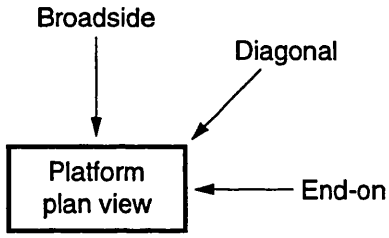

Fig. 2.7 Wave attack directions

Failure of an individual vertical bay

Although a jacket structure with its many members may appear at first sight to be very complex, the failure mode characteristics can be rather well envisaged if an individual vertical bay (Fig. 2.8a) is first studied. It is instructive to consider the sidesway mechanism in some more detail to develop some understanding of the general concepts.

For X-braced and K-braced configurations subjected to increasing horizontal load, one of the diagonal braces develops compression while the other develops tension. The brace dimensions are usually equal and, because the buckling load is always less than the tensile yield load, the compression member is the weaker of the two. Provided the horizontal bracing is strong enough to transfer any load-shedding from the compression member after it buckles, the ultimate resistance to lateral loading is achieved when the sum of the (horizontal components of the) axial force in the two diagonal bracing members, plus the portal shear resistance, reaches a maximum (Figs. 2.8b & 2.8c). If the horizontal brace is not adequate the resistance can be greatly reduced. As the axial stiffness of the bracing is far greater than the sidesway stiffness of the portal frame (about 20:1 is typical), the bracing members fail first. Only at large lateral deformations is the portal capacity fully mobilised but by then the compression member's strength has usually diminished (softened) significantly and the increased resistance from portal capacity can rarely compensate. Consequently, for X-braced sidesway mechanisms with adequate horizontal brace strength, the maximum resistance of a single bay invariably occurs at a load level at or just above that corresponding to tension member yielding. After the peak, the response is rather ductile.

For the K-braced configuration, when the compression member buckles the axial force in both members reduces (by equilibrium) and this corresponds to the ultimate capacity. When the lateral deformation is increased beyond the ultimate, the post-ultimate resistance drops dramatically (Fig. 2.8c), since both braces are now shedding load at the same rate.

The superior performance of X-bracing over K-bracing was found in the large scale tests reported by BOLT *ET AL.* (1994). These tests also confirmed the observation made by Zayas and his colleagues that for X-braced frames the tension member (acting like a taught wire) provides out of plane restraint of the compression member at its midpoint, forcing buckling to take place in one

half of the compression brace (Fig. 2.8a). The half with the largest imperfections buckles preferentially while (by equilibrium) the remaining part unloads and remains elastic.

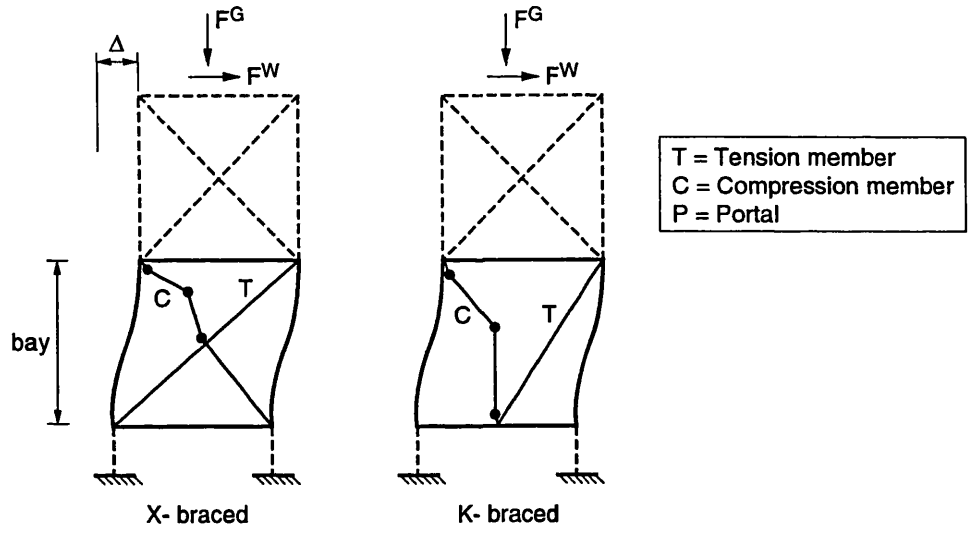

(a) Framing types

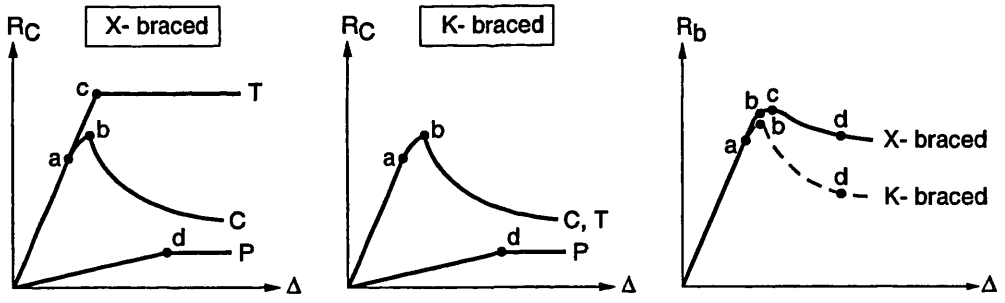

(b) Component resistance (R_c) *(c) Strength of bay (R_b)*

Fig. 2.8 Strength of X and K bracing systems

System strength

An overall sidesway mechanism develops in the structure when all of the bays at any one level fail[1]. The structure's ultimate strength therefore depends on the sum of the bay resistances at the critical level. In system reliability terminology, the bays form a parallel system. As we have just seen, if the bays are X-braced, there usually exists additional (or reserve) strength beyond first member failure. In addition, there is potential for load-shedding among adjacent bays as the drop in the resistance in any one of them is not too great after its maximum capacity has been achieved.

1. Sometimes there is an interaction between bays in the same vertical frame, resulting in a two-bay portal mechanism. The portal stiffness and portal strength contributions are then much less than those for one bay alone.

Therefore X-braced systems can exhibit reasonable reserve capacity (20% or so is not untypical - STEWART *ET AL.*, 1988; HELLAN *ET AL.*, 1993) and tend to have ductile failure modes. On the other hand, because of the rapid load-shedding associated with K-bracing, complete collapse can occur soon after buckling of the first member and the residual strength is generally rather small (HELLAN *ET AL.*, 1993; SI *ET AL.*, 1993). That is the failure mode tends to be brittle.

2.4 THE NON-LINEAR STRUCTURAL MODEL

Having reviewed the primary features of braced frames, it is now appropriate to consider how these may be modelled to enable the non-linear response to be found.

2.4.1 Review of alternative member models

Many models have been developed to describe the monotonic and cyclic behaviour of bracing members subjected to axial loading. Each have certain attractions and drawbacks in terms of functionality, complexity and numerical efficiency - factors that have to be taken into account when considering how to model the structural system as a whole. One of the most important aspects of member modelling is to ensure that the predicted buckling strength is calibrated against a recognised buckling curve which is representative of actual column strength. We use the Toma-Chen buckling curve (see appendix A) for this calibration.

Non-linear springs (phenomenological models)

In the phenomenological approach, the brace member is represented by a non-linear axial spring. The properties of the spring are developed using a path dependent algorithm whose logic is tuned to match the desired behaviour. Algorithms for these 'phenomenological models', (so-called because the behaviour is usually obtained from phenomena observed during tests) have been proposed by MARSHALL *ET AL.* (1977), and ZAYAS *ET AL.* (1980), among others which are also discussed in the report of Zayas *et al.* Alternatively, the spring's monotonic properties may be obtained from any one of the beam-column models described below with only the hysteretic response being defined using an algorithm based on test data. Computationally, this element type is extremely efficient.

Plastic hinge beam-column models

The plastic hinge concept, which is based on Koiter's concept of generalised force space yielding surfaces (KOITER, 1953), is widely used. Hinges are allowed to form at the ends and centre of the element. The hinge deformations (rotations and displacements) are found using the basic relationships of plasticity theory (flow rule, normality), and a yield surface that is described in terms of forces (axial force and bending moment). An efficient beam-column finite element may then be developed (NONAKA, 1973; TOMA & CHEN 1982; TABY & MOAN, 1985; UEDA *ET AL.*, 1985; HILMY, 1984; ABBASSIAN *ET AL.*, 1991; SØREIDE *ET AL.*, 1992). In appendix B, we derive a very simple but effective beam-column element based on the plastic hinge concept.

The plastic hinge method generally works well for monotonic compressive deformations. Even the influence of local buckling and dents can be (semi-empirically) incorporated (TABY & MOAN, 1985). However, for cyclic behaviour, which is strongly influenced by the "Bauschinger effect", it is not straightforward to obtain an accurate response. POWELL & FU-SONG CHEN, (1984) achieved a certain degree of success using multiple yield surfaces that followed closely the work of ZIEGLER (1959) and MRÓZ (1969). Recently, using similar concepts and motivated by the works of DAFALIAS & POPOV, (1975) and HILMY (1984), EBERG *ET AL.* (1993) have formulated and implemented into the USFOS finite element program, an advanced hinge model that uses two yield surfaces. A stress-strain curve whose characteristics depend on the dissipated energy in the hinge is employed. The complexity of such elements is one reason why phenomenological brace models have been favoured previously for cyclic analysis.

General non-linear beam models

More general non-linear models allow gradual yielding along the element length and over the cross-section. Because of the high curvature gradient that develops at midspan (and at the ends if fixed) when a column buckles, several of these 'distributed plasticity' elements are required to get an accurate response (STEWART *ET AL.*, 1988, found six to be the minimum). The cross-sectional stiffness is either input directly in the form of (axial-load dependent) moment-curvature relationships (SUGIMOTO & CHEN, 1985; POWELL & FU-SONG CHEN 1986), or integrated numerically from the stress distribution (see for example CHAN, 1989). This latter approach is employed in general purpose f.e. codes such as MARC. In both models, numerical integration along the length is necessary to form the element incremental stiffness. Sugimoto and Chen, have included the growth of a local buckle in their model.

The combination of numerical integration and several elements makes this beam-column model much less efficient than those derived from the plastic hinge concept.

Non-linear shell finite elements

Describing the member geometry using non-linear shell elements is the most accurate model but the processing time is non-trivial, especially if cyclic behaviour is to be described, and convergence of the solution may not always be achieved. The non-linear shell model is most useful for deriving axial response curves for severely damaged members or those with high D/t ratios outside the range of validity of the simpler beam models.

2.4.2 The proposed member model

In this work we will develop a non-linear analysis capability that employs phenomenological non-linear axial spring elements to represent the member axial strength characteristics.

The properties of this spring are derived as follows:

1. Generate the monotonic part of the load-shortening curve with any suitable member model or use experimental data; this step is done as a pre-processing activity *before* the system analysis is run.
2. In the system analysis, use a path dependent algorithm that takes into account the monotonic curve and observed characteristics from experimental data to generate the hysteretic part of the response curve.

Monotonic behaviour

In appendix B, the development of a member model based on the plastic hinge concept is described. Figure 2.9 shows the performance of this model against Taby's DENTA-II program (TABY, 1988). Also shown are test data obtained by SHERMAN (1980). For both member models, we imposed an artificial out of straightness of 0.3% of the length to ensure buckling at the Toma & Chen load (see appendix A). As expected, the predicted response lies below the test data until local buckling occurs (at a deformation of 1.5 inches).

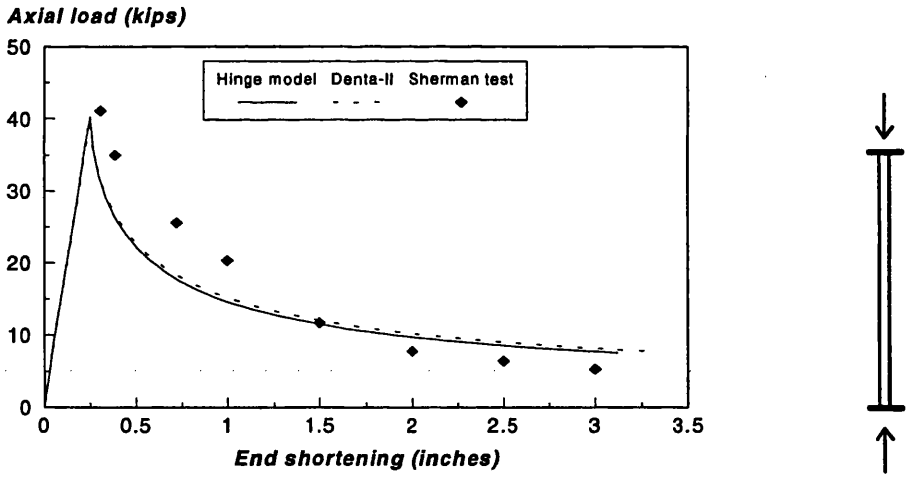

Member data: $D = 0.114$ m; $t = 2.3$ mm; $l = 5.72$ m; $k = 0.5$; $\sigma_y = 289$ MPa

Fig. 2.9 Comparison of plastic hinge member models and experimental data

It is observed that the agreement with our simple model and DENTA-II is excellent. Because DENTA-II offers the option of more general boundary conditions and includes the influence of both local buckling and dents, we use it in preference to our simpler member model to generate the monotonic properties of the phenomenological spring. Others who wish to develop a member model may find the simple procedure given in appendix B useful.

Cyclic behaviour

The essential features of the phenomenological algorithm that has been developed for cyclic response behaviour are shown in Fig. 2.10. It was realised as follows:

o-a-b-z	:	monotonic compression curve (input data)
b-c	:	linear-elastic unloading in compression based on member stiffness
c-d	:	linear-elastic loading in tension (with $P_d = 2/3\ P_b$)
d-e	:	inelastic tension, where $P_e = P_y$
e-f	:	strain hardening in tension (hardening slope specified as input)
f-g	:	linear-elastic unloading in tension (end of first cycle).

At the end of the first cycle, the monotonic curve o-a-b-z is shifted onto point g, with the force along h-i limited to P_b. This represents buckling degradation. The above process is then repeated for subsequent cycles. Two additional aspects are also implemented:

(a) If unloading in tension from path d-e, and then reloading, the path followed is d*-e, where P_{d^*} is the higher of P_d and the load when the deformation increment was reversed.

(b) In the first cycle, we load inelastically along d-e. In subsequent cycles, we follow a path l-m, where $\eta_m = \eta_f + \min\{(\eta_f - \eta_e), (\eta_h - \eta_j)\}$.

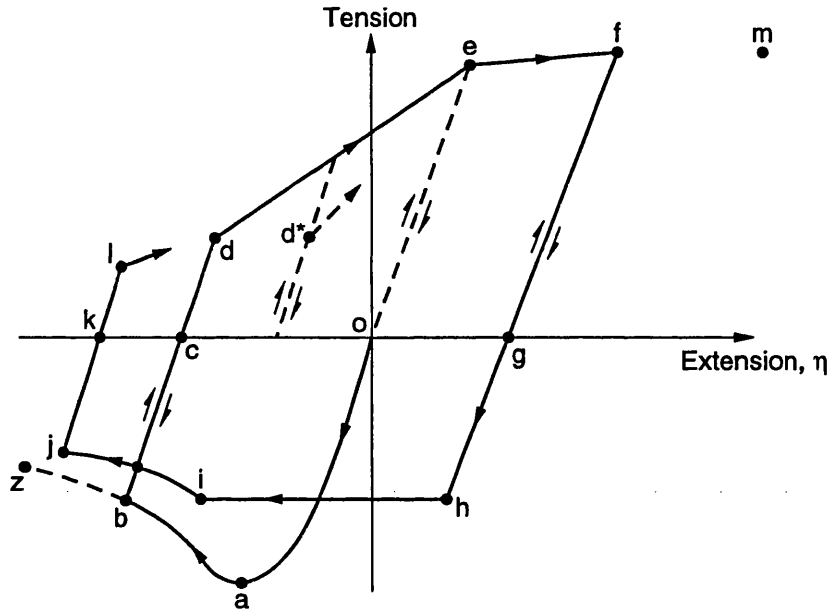

Fig. 2.10 Phenomenological spring characteristics

This hysteresis algorithm is compared in Fig. 2.11 with test data from GRANLI (- - -) and with the response curve generated by the USFOS program. The agreement is satisfactory. No general claims about the accuracy of this cyclic algorithm are made; it has not been sufficiently tested. Its main purpose is to provide a cyclic model to demonstrate that the pseudo-force method developed in chapter 3 can deal with arbitrary load histories without difficulty. An alternative considered was to use our plastic hinge member model to incrementally generate the axial resistance of the non-linear member throughout its deformation history. There are two reasons why this was not adopted. Firstly, the procedure outlined above is preferred as it not only

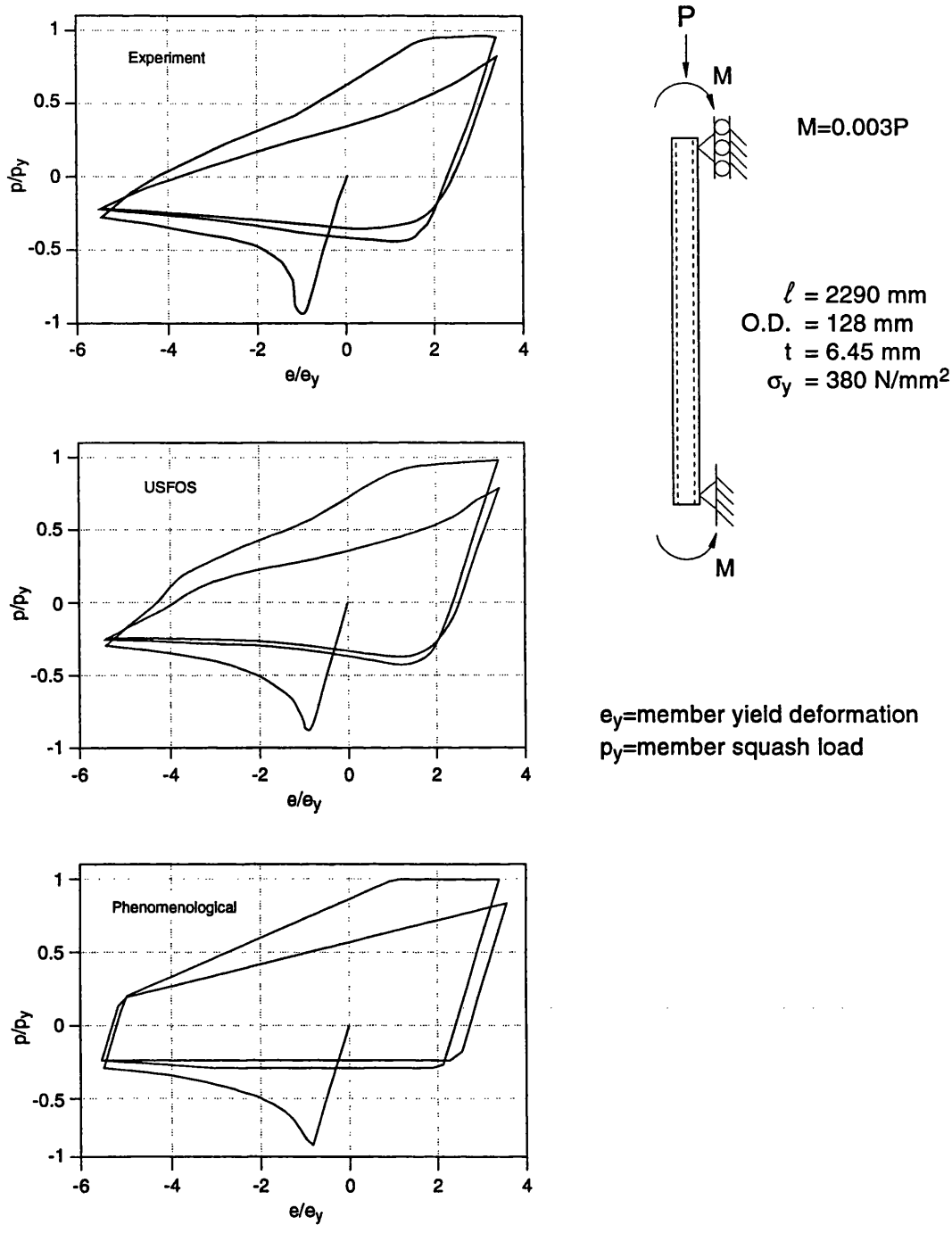

Fig. 2.11 Comparison of test data and cyclic models

provides a very efficient and simple method for generating the member's axial resistance properties, but it also has the advantage that convergence of the system analysis is not affected by the size of the loading increment (since for any given deformation history the force in the member is readily calculated). Secondly, a simple hinge model is generally not suitable for modelling cyclic plasticity (see section 2.4.1) and the effort to develop a more advanced model is non trivial.

2.4.3 The system model

From the previous discussions on frame failure modes, it was concluded that the axial strength of the members predominantly controlled the overall behaviour. We would anticipate that the phenomenological non-linear axial spring would be a satisfactory member model if put to proper use. Zayas and his co-workers (ZAYAS *ET AL.*, 1982) used phenomenological brace models in the program INTRA to numerically simulate their experimental frame tests and obtained good overall agreement. The author and his colleagues (STEWART *ET AL.*, 1988) also found good agreement between INTRA with phenomenological springs for brace members and MARC where Bernoulli-Euler beam elements were employed. Phenomenological brace models have also been used by MARSHALL *ET AL.* (1977), LLOYD & CLAWSON (1984), TITUS & BANON (1988), and several others as an effective way to model non-linear brace behaviour in large structures.

We now provide some guidance on how to employ phenomenological axial springs in a system model.

Boundary conditions for the member model

The phenomenological element allows the engineer to determine the member axial response curve using whatever information is at his disposal. Once the properties of the element have been assigned, it is extremely efficient computationally. The main disadvantage is that because the non-linear member response is developed in isolation of the frame, the effective buckling length has to be estimated somehow. For X-bracing, the experimental observations of ZAYAS *ET AL.* (1982) indicate a suitable choice for the effective length factor is k=0.7, corresponding to one end fully restrained (at the leg connection) and the other pin-ended (at the cross intersection). For K-braced frames k=0.7 is appropriate if the connection at the horizontal is not torsionally restrained out of plane, otherwise k=0.5 may be more suitable. Leg members are always very stocky (even if a k-value of 1.0 is assigned) and will generally achieve their plastic axial (squash) strength without buckling. If desired, the charts given in BS5950 (1985) provide a more refined procedure for estimating the effective member length based on the relative stiffness of the member to that of the surrounding frame.

These suggested effective length values assume rigid connections. In practice the connection (or joint as it is called) will have some flexibility and this suggests an adjustment of the member k-values to account for rotational joint stiffness. The flexibility of unstiffened joints has been studied by EFTHYMIOU (1985). If the results from these studies are taken into account, the revised effective buckling length is not usually very dramatic and in practice it generally suffices to use the node-to-node member length (which is slightly longer than the true member length) as input to the phenomenological model. Using this approach, the experimental frame tests results reported by ZAYAS *ET AL.* (1982) and BOLT *ET AL.* (1994) can be well reproduced numerically. Alternatively one can use the effective length factors suggested in API-RP2A directly as these are rather conservative.

Local fluid loading, frame effects, local buckling and yielding of connections

When determining the phenomenological brace axial response curve, local fluid loading acting on members should be taken into account (particularly for those in the wave active zone - that is from the free surface down to about three times the wave-crest height).

Side-sway-induced end moments have only a small influence on the axial strength of members and can be neglected (LLOYD & CLAWSON, 1984). From the modelling point of view this is rather convenient. It means that the member bending and axial resistances can be de-coupled, and represented as two parallel elements: a standard linear-elastic beam element with no axial strength for the bending resistance and a non-linear spring for the axial resistance (STEWART *ET AL.*, 1988).

For pushover analyses, the member response is typically monotonic and local buckling effects can be included in the member capacity formulation. On the other hand, if local buckling is anticipated in any member during a cyclic analysis, it is prudent (as recommended by MARSHALL *ET AL.*, 1977) to assume that the member's strength is lost if the hinge tries to open (i.e. if the member dissipates energy after the first half loading cycle).

In most new structures, the joints are generally stronger than the members. For older structures this is not always the case. The influence of joint yielding can be included in the phenomenological spring. However, experimental data on post-ultimate deformations of joints is scarce, and their ductility under cyclic loading must be questionable because of the high strain concentrations that are present near the welds. As a result, it may be more appropriate to strengthen any weak joints in the structure rather than attempt to include their non-linear characteristics in the numerical model.

Limitations of phenomenological member modelling

For brace elements the phenomenological approach has been shown to be very satisfactory, and for leg elements that yield in axial tension or squash/buckle in compression, it is also clearly valid. On the other hand, the portal capacity in a sidesway failure mode depends on both the axial force and bending moment in the leg members (Fig. 2.12) and this non-linear behaviour cannot be represented by an axial spring.

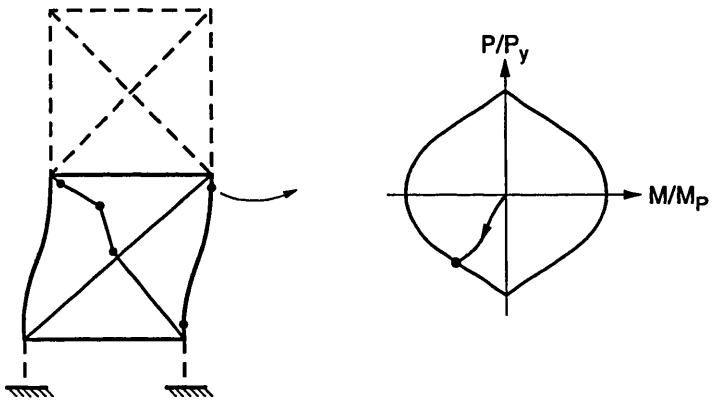

Fig. 2.12 Plastic hinge in leg member

Bearing in mind that the portal capacity provided by the legs is mostly small, and is generally reached at deformations beyond those corresponding to the ultimate frame capacity (see Fig. 2.8), it is often not necessary to account for this aspect of leg non-linearity. Ignoring the effect of yielding on portal capacity will result in an upper bound solution beyond the deformation at which the first leg becomes plastic. A lower bound solution can be obtained by restricting the axial capacity to the axial force in the leg when the yield surface is reached. Therefore (narrow) bounds on the resistance curve can be obtained.

Foundation modelling

The axial pull-out/punch-through capacity and lateral resistance of the founding piles must be adequately represented in the non-linear structural model. Pile/soil axial response curves may be established by consideration of the skin friction acting along the length of the pile, the pile flexibility, and the end bearing capacity (HOLMQUIST & MATLOCK, 1976). In many cases, it has been found that the lateral foundation resistance can be taken as linear-elastic (STEWART *ET AL.*, 1988, VAN DE GRAAF & TROMANS, 1991). If non-linear lateral behaviour of the soil is to be included, MARSHALL *ET AL.* (1977) give a good overview of how to proceed. Non-linear axial spring elements can be used to represent both the lateral and the axial foundation resistance.

Conclusions on phenomenological spring element

We conclude that it should be possible to predict adequately non-linear structural behaviour by making use of

(a) phenomenological non-linear springs for the non-linear axial resistance of critical members or foundation piles and parallel linear-elastic beam elements for their bending resistance; and

(b) general linear-elastic elements for any other part of the structure that does not exhibit non-linearity.

The validity of this approach will be demonstrated by example in chapter 5.

Comment on integrated beam models

Before leaving this section, we remark that a more sophisticated model would be to represent the entire structure with non-linear beam or plastic hinge elements whose response history is derived implicitly from the system incremental stiffness matrix. The non-linear beam element is available in general purpose f.e. codes such as MARC while the plastic hinge approach is used in USFOS. In this type of model the effective length of the member is determined by the system (which may be an advantage but also a hindrance as some modelling flexibility is lost). The computational efficiency is far less than that for the non-linear spring element and (from experience) it is more likely that convergence difficulties will be encountered.

In chapter 5, we provide further verification of the phenomenological approach by comparing results against those obtained from the USFOS program.

2.5 REFERENCES

ABBASSIAN, F., LAU, T.B., AND ZINTILIS (1991), "3-D inelastic behaviour of tubular members supported on non-linear rotational springs", *J. Offshore Mechanics and Arctic Engineering*, **113**, pp320-326.

AMERICAN INSTITUTE OF STEEL CONSTRUCTION, *AISC Specification for the design, fabrication and erection of structural steel for buildings*, Chicago.

ANDERSON, W.D., SILBERT, M.N., AND LLOYD, J.R. (1982), "Reliability procedure for fixed offshore platforms", *J. of the Structural Div.*, ASCE, **108**, No. ST11.

AMERICAN PETROLEUM INSTITUTE, *API-RP2A Recommended practice for planning, designing and constructing fixed offshore platforms.*

AMERICAN PETROLEUM INSTITUTE, *API-RP2A-LRFD Recommended practice for planning, designing and constructing fixed offshore platforms - load and resistance factor design.*

BALAKRISHNAN, N., AND COHEN, A.C. (1991), *Order statistics and inference*, Academic Press Inc.

BOUKAMP, J.G. (1975), "Buckling and post-buckling strength of circular tubular sections", *Offshore Technology Conference*, OTC 2204, Houston, Texas.

BEA, R.G. ET AL. (1982), "Application of reliability methods in design and analysis of fixed offshore platforms", *Journal of the Structural Division*, ASCE.

BEA, R.G. , AND YOUNG, C. (1993), "Loading and capacity effects on platform performance in extreme condition storm waves and earthquakes", *Offshore Technology Conference*, OTC 7140, Houston, Texas.

BEEDLE, L.S., AND TALL, L. (1960), "Basic column strength", *Journal of the Struct. Division*, ASCE, **86**, (ST7).

BOLT, H.M., AND BILLINGTON, C.J (1993), "Reserve, residual and ultimate strength analysis of offshore structures: state of the art review", *Intl. Offshore and Polar Engineering Conf.* (ISOPE), Singapore.

BOLT, H.M., BILLINGTON, C.J, AND WARD, J.K. (1994), "Results from large-scale ultimate load tests on tubular jacket frame structures", *Offshore Technology Conference*, OTC 7451, Houston, Texas.

BORGMAN, L.E. (1970), "Maximum wave height probabilities for a random number of random intensity storms", *Proc. 12"th Coastal Eng. Conf.*, **1**, 53-64, Washington.

BRITISH STANDARDS INSTITUTION BS 5959 - Part 1 (1985), *Structural use of steelwork in building, Part 1 - Code of practice for design in simple and continuous construction: hot rolled sections.*

CARTWRIGHT, D.E., AND LONGUET-HIGGINS, M.S. (1956), "The statistical distribution of the maxima of a random function", *Proc. Royal Soc.* Ser. A, 237 (1209), 212.

CHAN, S.L. (1989), "Inelastic post-buckling analysis of tubular beam-columns and frames", *J. Eng. Structs.*, **11**, pp23-30.

CHEN, W.F., AND ATSUTA, T. (1976), *Theory of beam-columns*, **Vol. 1**, McGraw-Hill, New York.

CHEN, W.F., AND HAN, D.J. (1985), *Tubular members in offshore structures*, Pitman.

CHEN, W.F., AND ROSS, D.A. (1977), "Test of fabricated tubular columns", *Journal of the Structural Division*, ASCE, **103**, (ST3), Proc. paper 12809, pp619-634.

CHEN, W.F., AND ROSS, D.A. (1978), "Test of fabricated tubular columns", Fritz Engineering Laboratory Report No. 393.8, Lehigh University, Bethlehem, USA.

DAFALIAS, Y.F., AND POPOV, E.P. (1975), "A model for nonlinear hardening materials for complex loading", *Acta Mechanica*, **21**, pp173-192.

DET NORSKE VERITAS (DnV) (1977), *Rules for the design, construction and inspection of offshore structures*, Høvik, Norway.

EFTHYMIOU, M. (1985), *Local rotational stiffness of unstiffened tubular joints*, Report No. RKER.85.199, Shell Research, Rijswijk, The Netherlands.

EBERG, E., HELLAN, Ø., AND AMDAHL, J. (1993), "Nonlinear re-assessment of jacket structures under extreme storm cyclic loading, **Part III**: The development of structural models for cyclic response", *Int. Conf. on Offshore Mechanics and Arctic Engineering* (OMAE), Glasgow, Scotland.

GATES, W.E., MARSHALL, P.W., AND MAHIN, S.A. (1977), "Analytical methods for determining the ultimate earthquake resistance of fixed offshore structures", *Offshore Technology Conference*, OTC 2751, Houston, Texas.

GRAAF, J.W. VAN DE, AND TROMANS, P.S. (1991), "Statistical verification of predicted loading and ultimate strength against observed storm damage for an offshore structure", *Offshore Technology Conference*, OTC 6573, Houston, Texas.

GRANLI, T. (- - -), *Behaviour of tubular beam columns under cyclic loading*, PhD thesis, The Norwegian Institute of Technology, (to appear).

GUMBEL, E.J. (1958), *Statistics of extremes*, Columbia University Press.

HELLAN, Ø., TANDBERG, T., AND HELLEVIG, N.C. (1993), "Nonlinear re-assessment of jacket structures under extreme storm cyclic loading, **Part IV**: Case studies on existing North Sea platforms", *Int. Conf. on Offshore Mechanics and Arctic Engineering* (OMAE), Glasgow, Scotland.

HELLAN, Ø., MOAN, T., AND DRANGE, S. O. (1994), "Use of nonlinear pushover analysis in ultimate limit state design and integrity assessment of jacket structures", *Intl.Conf. on the Behaviour of Offshore Structures* (BOSS), Massachusetts Institute of Technology, USA.

References (continued)

HILL, R. (1950), *The mathematical theory of plasticity*, Clarendon press, Oxford.

HILMY, S.I (1984), *Adaptive nonlinear dynamic analysis of three dimensional steel framed structures with interactive computer graphics*, PhD thesis, Cornell University, USA.

HOLMQUIST, D.V., AND MATLOCK, H. (1976), "Resistance/Displacement relationships for axially loaded piles in soft clay", *Offshore Technology Conference*, Houston, Texas.

INTRA: *Inelastic Tower Response Analysis program*, ISEC Inc., San Francisco. (1987 version I02)

JOHNSON, B.G. (ed.) (1966), *Guide to design criteria for metal compression members*, Wiley, New York. (2'nd ed.).

JOHNSON, B.G. (ed.) (1976), *Guide to stability design criteria for metal structures*, Wiley, New York. (3'rd ed.).

KOITER, W.T. (1953), "Stress-strain relations, uniqueness and variational theorems for elastic-plastic materials with a singular yield surface", *Quart. Appl. Math.* **11**, pp350-354.

KOROL, R.M. (1978), *Inelastic buckling of circular tubes under bending, part II - experimental program*, Dept. of Civ. Eng. Report, McMaster Univ., Hamilton, Ontario.

LLOYD, J.R., AND CLAWSON, W.C. (1984), "Reserve and residual strength of pile founded offshore platforms", *Int. Symp. on The role of Design and Redundancy in Marine Structural Reliability*, (Eds. Faulkner et al.), Nat. Acad. Press.

MARC: *General purpose finite element program*, Marc Research Corporation, Paulo Alto. (1986, version K2-1; 1993, version K5.2).

MARSHALL, P.W. (1969), "Risk factors for offshore structures", *ASCE J. Struct. Div.*, 95, ST 12, Dec. 1969.

MARSHALL, P.W, AND BEA, R.G. (1976), "Failure modes of offshore platforms", *Intl.Conf. on the Behaviour of Offshore Structures* (BOSS), Trondheim, Norway.

MARSHALL, P.W., GATES, W.E., AND ANAGNOSTOPOULOS, S. (1977), "Inelastic dynamic analysis of tubular offshore structures", *Offshore Technology Conference*, Houston, Texas.

MORISON, J.R., O'BRIEN. M.P., JOHNSON, J.W., AND SCHAFF, S.A. (1950), "The forces exerted by surface waves on piles", *Journal of Petroleum Technology*, Am. Inst. Mining Engrs., **189**, pp149-154.

MRÓZ, Z. (1969), "An attempt to describe the behaviour of metals under cyclic loads using a more general work-hardening model", *Acta Mechanica*, **7**, Nos. 2-3, pp199-212.

NONAKA, J. (1973), "An elastic-plastic analysis of a bar under repeated axial loading", *Int. J. Solids Structures*, **9**, pp569-580.

NORWEGIAN PETROLEUM DIRECTORATE (NPD) (1985), *Regulations for structural design of loadbearing structures intended for exploitation of petroleum resources.*

NORDAL, H. (1990), "Application of ultimate strength analysis in design of offshore structural systems", *Integrity of offshore structures* (IOS) Conference - 4, Elsevier Applied Science.

OGOWA, K., YAMANARI, M., MAKINO, Y., KUROBANE, Y., KUMANATO, U., AND YAMASHITA, M. (1987), "Buckling and post-buckling behaviour of complete tubular trusses under cycling", *Offshore Technology Conference*, OTC 5439, Houston, Texas.

POPOV, E.P., AND BLACK, G.R. (1981), "Steel struts under severe cyclic loadings", *Journal of the Structural Division*, ASCE, **107**, (ST9), Proc. paper 16497, pp1857-1881.

POWELL, G.H., AND FU-SONG CHEN, P. (1986), "3D beam column element with generalised plastic hinges", *ASCE J. Eng. Mech.* **112**, No. 7.

SHANLEY, F.R. (1947), "Inelastic column theory", *Journal of Aeronautical Science*, **14**, No. 5, pp261-267.

SHERMAN, D.R. (1980), *Post local buckling behaviour of tubular strut type beam-columns: an experimental study*, Report to Shell Oil Company, Houston, Texas.

SHERMAN, D.R. (1983), *Bending capacity of fabricated pipes*, Dept. of Civ. Eng. Report, Univ. of Wisconsin, Milwaukee, Wisconsin.

SIGURDSSON, G., SKJONG, R., SKALLERUD, B., AND AMDAHL, J. (1994), "Probabilistic collapse analysis of jackets", *Int. Conf. on Offshore Mechanics and Arctic Engineering* (OMAE), Houston, Texas.

SI, M.B.I., VANDERSCHUREN, L., GRAAF, J.W. VAN DE, AND TROMANS, P.S. (1993), "Probability of failure of a southern North Sea jacket structure under environmental loading", *Intl. Offshore and Polar Engineering Conf.* (ISOPE), Singapore.

SMITH, C.S., KIRKWOOD, W., AND SWAN, J.W. (1979), "Buckling strength and post-collapse behaviour of tubular bracing members including damage effects", *Int. Conf. on the Behaviour of Offshore Structures* (BOSS), Imperial College, London.

SOHOL, I.S., AND CHEN, W.F. (1987), "Local buckling and sectional behaviour of fabricated tubes", *J. of Struct. Eng.*, **113**, No.3. ASCE.

SØREIDE, T.H., AMDAHL, J.A., EBERG, E., HOLMÅS, T, AND HELLAN, Ø. (1992), "USFOS - A computer program for progressive collapse analysis of steel offshore structures", Theory manual, SINTEF, Norway.

STEWART, G., EFTHYMIOU, M., AND VUGTS, J.H. (1988), "Ultimate strength and integrity assessment of fixed offshore platforms", *Intl.Conf. on the Behaviour of Offshore Structures* (BOSS), Trondheim, Norway.

References (continued)

STEWART, G. (1992), "Nonlinear structural dynamics by the pseudo-force influence method - Part II: Application to offshore platform collapse", *Intl. Offshore and Polar Engineering Conf.* (ISOPE), Vol. I, San Francisco, USA.

STEWART, G., MOAN, T., AMDAHL, J., AND EIDE, O. (1993), "Nonlinear re-assessment of jacket structures under extreme storm cyclic loading, **Part I**: Philosophy and acceptance criteria", *Intl. Conf. on Offshore Mechanics and Arctic Engineering* (OMAE), Glasgow, Scotland.

STEWART, G., AND TROMANS, P.S. (1993), "Nonlinear re-assessment of jacket structures under extreme storm cyclic loading, **Part II**: Representative Environmental load histories", *Intl. Conf. on Offshore Mechanics and Arctic Engineering* (OMAE), Glasgow, Scotland.

STEWART, G. (1993), "Nonlinear response of offshore jacket structures using linear analysis programs", *Integrity of Offshore Structures Conference* (IOS), Glasgow, Scotland.

STEPHENS, J.J. *ET AL.* (1983), "Local buckling of thin-walled tubular steel members", *Proc. 3rd Int. Colloquium on stability of metal structures*, Toronto, Canada, SSRC, May, 1983, pp489-508.

SUGIMOTO, H., AND CHEN, W.F. (1985), "Inelastic post-buckling behaviour of tubular members", *J. of Struct. Eng.*, **111**, No.9. ASCE.

TABY, J. (1986), *Residual strength of damaged tubulars*, Report No. 6.10, SINTEF, Trondheim, Norway.

TABY, J. (1988) *DENTA-II: A computer program for the analysis of ultimate and post-ultimate behaviour of tubes*, program Users Manual.

TABY, J., AND MOAN, T. (1985), "Collapse and residual strength of damaged tubular members", *Intl.Conf. on the Behaviour of Offshore Structures* (BOSS), Delft, The Netherlands.

TOMA, S., AND CHEN., W.F. (1979), "Analysis of fabricated tubular columns", *Journal of the Structural Division*, ASCE, **105**, (ST11), Proc. paper 14994, pp2343-2366.

TOMA, S., AND CHEN., W.F. (1982), "Cyclic analysis of fixed-ended steel beam-columns", *Journal of the Structural Division*, ASCE, **108**, (ST6), Proc. paper 17180, pp1385-1399.

TITUS, P.G., AND BANON, H. (1988), "Reserve strength analyses of offshore platforms", *7'th Offshore South East Asia conference*, OSEA 88179, Singapore.

TROMANS, P.S., AND GRAAF, J.W. VAN DE (1992), "A substantiated risk assessment of a jacket structure", *Offshore Technology Conference*, OTC 7075, Houston, Texas.

TROMANS, P.S., EFTHYMIOU, M., GRAAF, J.W. VAN DE, VANDERSCHUREN, L., AND TAYLOR, P.H. (1992), "Extreme storm loading on fixed offshore platforms", *Intl. Conf. on the Behaviour of Offshore Structures* (BOSS), London, UK.

TUCKER, M.J. (1991), *Waves in ocean engineering*, Ellis Horwood.

UEDA, Y., RASHED, S.M.H., AND NAKACHO, K. (1985), "New efficient and accurate method on nonlinear analysis of offshore tubular frames", *J. of Energy Res. Tech.*, **107**, pp204-211.

USFOS: *A Computer Program for Progressive Collapse Analysis of Steel Offshore Structures*, SINTEF Report STF71 F88038 Rev. 1993, Trondheim, Norway.

VUGTS, J.H. (1989), "Bottom founded platforms: an overview", *Deep Offshore Technology Conference*, Marbela, Spain.

WARD, E.G., AND CARDONE, V.J. (1978), "Statistics of hurricane waves in the Gulf of Mexico", *Offshore Technology Conference*, OTC 3229, Houston.

WILKS, S.S. (1948), "Order statistics", *Bull. Amer. Math. Soc.*, **54**.

YAO, T., TABY, J., AND MOAN, T. (1988), "Ultimate and post-ultimate strength behaviour of damaged tubular members in offshore structures", *J. Offshore Mech. & Arctic Eng.*, **110**, pp254-262.

ZAYAS, V.A., MAHIN, S.A, AND POPOV, E.P. (1980), *Cyclic inelastic buckling of tubular steel braces*, Report No. UCB/EERC-80/16, Earthquake Eng. Research Centre, Univ. of Calif., Berkeley.

ZAYAS, V.A., MAHIN, S.A, AND POPOV, E.P. (1982),"Ultimate strength of steel offshore structures", *Intl.Conf. on the Behaviour of Offshore Structures* (BOSS), Boston.

ZIEGLER, H. (1959), "A modification of Prager's hardening rule", *Quarterly of Applied Math*, **17**, p45.

Chapter 3

THE PSEUDO-FORCE INFLUENCE METHOD FOR STRUCTURES WITH NON-LINEAR BAR ELEMENTS

- Statics -

3.1 INTRODUCTION

In this chapter, we consider structures represented mostly by linear-elastic elements (of any type), but which have a few critical members whose axial resistance is modelled using non-linear phenomenological spring or bar elements. As discussed in chapter 2, the non-linear model for an offshore brace-framed steel structure can generally be represented in this way.

A technique based on linear superposition which we call the ***Pseudo-force Influence Method*** (PFI-Method) is suited to this class of problem. The theoretical foundations behind the method for static (pushover and cyclic) analyses of framed structures are set out, and suitable (incremental) solution algorithms are discussed. The PFI-Method allows the non-linear and linear-elastic contributions of the response to be solved separately and later combined. Because of this, a simulation system to obtain the non-linear structural response can be developed around any standard linear analysis program. In the procedure developed, the linear-elastic model is used in its original form and no modification is made to the linear-elastic program's source code.

Although we consider only the geometrically linear theory at present (leaving details on large displacements until later in chapter 7), the phenomenological bar's constitutive behaviour represents both material and geometrical non-linearity of the critical member. At the global level, large displacement effects are generally small for the structure type considered. This is demonstrated by example in the chapter 5.

The principles introduced are also valid for more complex element types, as we show later in chapter 7 where a more general theory is explored. The inclusion of dynamic effects is discussed in chapter 4.

3.2 NON-LINEAR PROBLEMS FROM A DIFFERENT PERSPECTIVE

The non-linear material model

In practice, the discretised structural model for a braced-framed offshore structure may require several hundred elements of various types. However, as we have discussed previously in chapter 2, for such structures only a few members generally participate in the collapse mechanism and it is usually sufficient to model the axial behaviour of these using non-linear bar elements to capture the collapse response.

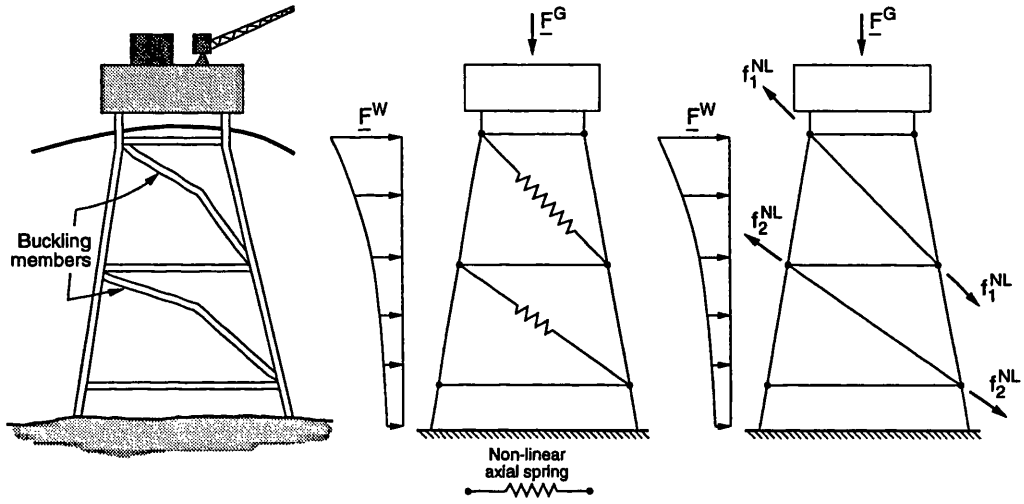

(a) Actual structure *(b) Non-linear model* *(c) Linear elastic model*

Fig. 3.1 Equivalent representation of non-linear problem

The traditional approach to the modelling problem is to represent the actual structure (Fig. 3.1a) by a ***non-linear material model*** upon which the external loading acts (Fig. 3.1b). The non-linear incremental stiffness matrix for this model would be assembled and solved iteratively for each load step. The number of degrees of freedom present in each iteration would be large (typically 2000 or so) and remain constant throughout the solution process. But there is an alternative and more elegant approach that is not only very efficient but also lends itself to the use of linear-elastic analysis techniques. The development of this alternative method is now pursued.

The linear elastic reference model

The structural model shown in Fig. 3.1c is linear-elastic. Non-linear material influences are represented by deformation-dependent pseudo-forces, of magnitude f^{NL}, acting on the member ends. If these pseudo-forces are selected such that the deformations in models Figs. 3.1b & 3.1c are identical, then clearly each model is just an alternative way of representing the same problem. We refer to the model in Fig. 3.1c as the ***equivalent linear-elastic reference model.*** For this

linear-elastic model, the principle of superposition applies and the total response can be obtained by summing the individual responses of all of the separate load-sets acting.

We can therefore describe this alternative procedure as a linear superposition technique in which a set of supplementary (pseudo) forces are applied to a linear-elastic structural model in addition to the actual loading, to reproduce exactly the effect of non-linear material behaviour. Using the principle of virtual work and a reduction technique based on influence coefficients, a (small) system of non-linear equations can be derived, the solution of which yields the pseudo-forces. In the next chapter, we show that dynamic effects can also be included as pseudo-forces acting at the nodal points of the reference structure. We now discuss this ***Pseudo-force Influence Method*** (PFI-Method) in more detail for problems in statics.

3.3 PFI-METHOD - THEORETICAL FOUNDATIONS FOR PROBLEMS IN STATICS

This section summarises the (geometrically-linear, materially non-linear) theory of the PFI-Method for problems in statics in which the response of non-linear members can be emulated using a two-noded non-linear bar or spring element. We recall that in the previous chapter, we discussed how the properties of such an element could be generated.

Referring to the equivalent linear-elastic reference model shown in Fig. 3.1c, the influence of non-linear material properties in each 'non-linear'[1] bar i is represented by a pair of equal but opposite deformation-dependent pseudo-forces, of magnitude f_i^{NL}, acting along the bar's axis. By our convention, f_i^{NL} is positive if the pseudo-forces are trying to elongate the bar. These local element forces on bar i may be expressed as

$$\underline{q}_i^{NL} = \underline{a}\, f_i^{NL} \tag{3.1}$$

in which: $\underline{q}_i^{NL}$ are the local ***pseudo-forces***; $\underline{a} = [-1 \;\; 0 \;\; 1 \;\; 0]^T$ may be interpreted as a self-equilibriating ***unit (natural) load-set***, which if applied in isolation to the structure produces tension in the bar; and f_i^{NL} is the ***natural load-set scaling factor***. The reason for adopting this particular interpretation of the pseudo-force decomposition will be more apparent when a general theory is developed in chapter 7.

3.3.1 Equivalence of models by virtual work

The conditions for equivalence of the two models shown in Figs. 3.1b & 3.1c can be established using the principle of virtual work (see, for example, MALVERN, 1969). In a typical element i, the virtual work associated with the straining of the element in the non-linear material model of Fig. 3.1b is

$$\delta W_i = \delta\eta_i p_i \tag{3.2}$$

1. We refer to elements in the linear elastic model as 'non-linear' if their counterparts in the non-linear material model undergo inelastic straining.

where δ denotes 'the variation in', η_i is the elongation and p_i is the axial force in the bar which is a non-linear function of η_i.

For the linear-elastic structural model of Fig. 3.1c, the virtual work associated with straining in the same element is

$$\delta W_i = \delta\eta_i k_i \eta_i - \delta \underline{v}_i^T \underline{q}_i^{NL} \tag{3.3}$$

where $\underline{v}_i$ is the local nodal displacement in the direction of the bar's local axis and k_i is the linear-elastic bar stiffness. The relationship between $\underline{v}_i$ and the axial deformation η_i is

$$\eta_i = \underline{a}^T \underline{v}_i ; \quad \underline{a}^T = [-1 \;\; 0 \;\; 1 \;\; 0]. \tag{3.4}$$

Substituting (3.1) into (3.3), and using (3.4), provides the virtual work of the element in the linear-elastic model as

$$\delta W_i = \delta\eta_i (k_i \eta_i - f_i^{NL}) . \tag{3.5}$$

Comparing equations (3.2) and (3.5), it is apparent that both models are equivalent if and only if

$$f_i^{NL} = k_i \eta_i - p_i \tag{3.6}$$

and so the magnitude f_i^{NL} of the pseudo-forces is simply equal to the difference between the linear-elastic and inelastic force in the bar (Fig. 3.2). For elements that remain linear elastic, there are no associated pseudo-forces.

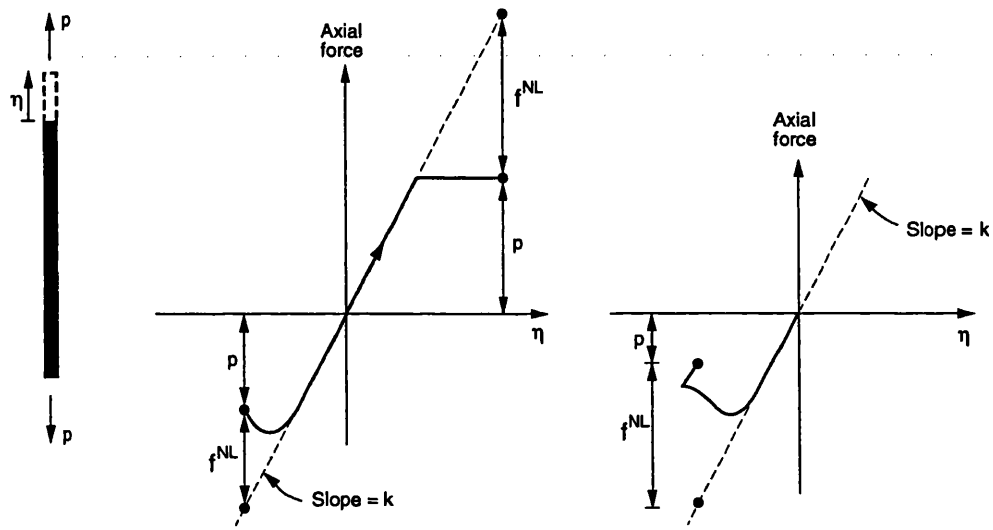

(a) Monotonic response (no incremental strain reversal)

(b) Cyclic response

Fig. 3.2 Inelastic correction forces f^{NL} for bar element

3.3.2 A direct heuristic approach

The same result can be achieved using a direct heuristic approach which gives additional insight into the method. We first consider a linear-elastic structural model with only the physical loading applied. In a typical bar i with deformation η_i, the linear-elastic resistance is $p_i^* = k_i \eta_i$. Now imagine this bar being removed from the structure and being replaced by forces acting at the nodes to which the bar was attached, such that the displacements in the structure remain unchanged. Clearly the magnitude of each nodal force would be p_i^*, equal to the resistance of the bar, and these would act in opposite directions. If p_i^* is a tensile force, these nodal forces act towards the centre of the bar and, with respect to a local co-ordinate system directed along the bar's axis, are given by $-p_i^*[-1 \;\; 0 \;\; 1 \;\; 0]^T$. To emulate non-linear behaviour, with the member resistance modified to p_i, we could apply end forces $-p_i\,[-1 \;\; 0 \;\; 1 \;\; 0]^T$ instead. However, an alternative is to keep the linear-elastic bar in place and apply pseudo-forces to the bar ends. These pseudo-forces are given by $f_i^{NL}[-1 \;\; 0 \;\; 1 \;\; 0]^T$ where the load multiplier f_i^{NL} is given by

$$\begin{aligned} f_i^{NL} &= p_i^* - p_i \\ &= k_i \eta_i - p_i \end{aligned} \tag{3.7}$$

which agrees identically with (3.6).

3.3.3 Response by superposition

For the response of the linear-elastic reference model, linear superposition applies, and the deformation in any of the M 'non-linear' elements is simply

$$\eta_i = \eta_i^L + \sum_{j=1}^{M} D_{ij}^{\eta\eta} f_j^{NL} \qquad i = 1, M \tag{3.8}$$

in which

- η_i^L is the axial deformation in the 'non-linear' element when the external loading $\underline{F}^L$ alone is applied to the linear elastic model;
- $D_{ij}^{\eta\eta}$ are the coefficients of a symmetric[1] ***deformation influence matrix*** of dimension (M, M). These give the axial deformation in 'non-linear' element i for a pair of tensile unit loads applied to the ends of 'non-linear' element j in the equivalent linear-elastic model (Fig. 3.3).

1. The matrix $\boldsymbol{D}^{\eta\eta}$ is symmetric by Betti's Law. We will prove this for the general case in chapter 7 when a more general theory of the PFI-Method is presented, for which the bar element is a special case.

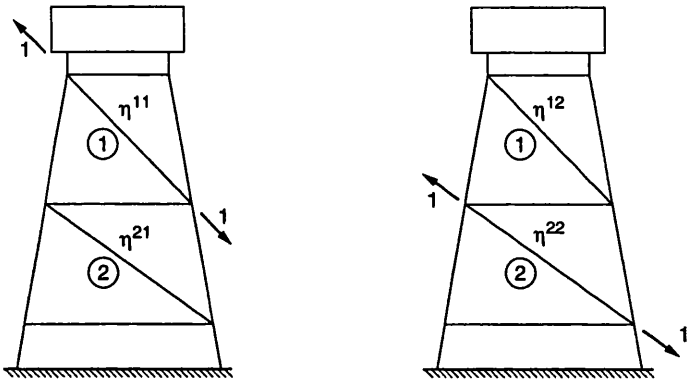

Fig. 3.3 Influence matrix $D^{\eta\eta}$ for structure with two non-linear members

Equation (3.8) can be written more compactly in the matrix form

$$\underline{\eta} = \underline{\eta}^{L} + \boldsymbol{D}^{\eta\eta}\, \underline{f}_{\eta}^{NL} \tag{3.9}$$

where it is understood that only contributions from the M non-linear bar elements are included in this set of equations. The subscript η highlights the fact that the pseudo-force multipliers are deformation dependent.

We refer to (3.8) or (3.9) as the ***reduced system equations***. The idea that non-linear problems could be solved by considering a smaller sub-system (reduced system) was apparently first noted by ARGYRIS (1964).

The two terms on the right-hand side of equation (3.9) have obvious interpretations. The first is the linear-elastic response under the action of the actual loads; the second is a correction for material non-linearity. Consequently we may write (3.9) as

$$\underline{\eta} = \underline{\eta}^{L} + \underline{\eta}^{NL} \,. \tag{3.10}$$

For the collapse analysis of space-framed offshore jacket structures, the number of non-linear members that comprise the reduced system is very small (typically 10 and often fewer). The response $\underline{\eta}^{L}$ of these elements and the associated deformation influence matrix $\boldsymbol{D}^{\eta\eta}$ can be obtained from any standard linear-elastic finite element software. Given the non-linear response behaviour of the bar elements, the reduced system of equations defined by (3.9) may then be solved numerically by a stand-alone program for the deformations/load-multipliers. The solution procedure is described in the next section and utilised later in the simulation system described in section 3.6.

Once the pseudo-forces have been established, any set of response variables $\underline{s}$ (e.g. stresses, nodal displacements, etc.), may be recovered. We can write this *recovery process* as

$$\underline{s} = \underline{s}^{L} + \boldsymbol{R}^{s\eta}\, \underline{f}_{\eta}^{NL} \tag{3.11}$$

in which $\boldsymbol{R}^{s\eta}$ is a rectangular matrix whose columns give the responses of interest for each unit load-set applied separately to the 'non-linear' members. Therefore when the unit load-sets are applied to determine the influence matrix $\boldsymbol{D}^{\eta\eta}$, the columns of $\boldsymbol{R}^{s\eta}$ can also be stored. So, the response variables of the entire structure can be recovered by summing the weighted individual responses. Equation (3.11) represents a data post-processing step.

3.3.4 Review of some similar developments reported in the literature

The virtual work approach described above has not been widely applied in the development of pseudo-force methods; and yet (as we will show in chapter 7) it offers a natural procedure for generalising the method using continuum mechanics principles and plasticity theory.

Until now, heuristic pseudo-force methods have been more prominent, particularly in the field of structural optimisation of linear-elastic skeletal frames where equations of the form (3.8) represent one of the ***Theorems of Structural Variation,*** apparently so-called because they enable the structural response to be determined if the properties of one or more members are varied. The rather trivial problem of obtaining the updated structural response if the properties of a single bar element are modified has been discussed by MAJID & ELLIOT (1973) and MAJID (1974). Later, AL-BAKRI (1977) accounted for simultaneous modifications of several bars in an optimisation study of transmission-line support towers.

These ideas were extended by HOLNICKI-SZULC & GIERLINSKI (1989) to include skeletal frames containing bars whose properties could be modified to represent simple non-linear behaviour such as yielding, strain hardening and fracture. Instead of applying pseudo-forces, their ***Virtual Distortion Method*** employed initial strains which is an entirely equivalent technique (for geometrically linear problems). STEWART & VAN DE GRAAF (1990) demonstrated that the pseudo-force (and therefore the initial strain) procedure was valid for more complex non-linear bar behaviour, including strain softening; thus the entire monotonic load-shortening curves of compression members could be represented. In that work, the pushover collapse capacity of a plane frame obtained using the pseudo-force approach showed good agreement with that determined independently using the non-linear analysis program USFOS (SØREIDE *ET AL.*, 1992).

This provides only a very brief historical review of heuristic developments in pseudo-force and related methods. After we have put in place the foundations of a more general theory for the PFI-Method (chapter 7) we return (section 7.5.2) to give a more complete picture of how the proposed method compares with other related work published in the literature.

3.4 SOLUTION PROCEDURE FOR STATICS PROBLEMS

We now look in some detail at how to solve the reduced system of equations given by (3.9). In earlier work on the non-linear response of frames using pseudo-force and related methods (HOLNICKI-SZULC & GIERLINSKI, 1989, STEWART & VAN DE GRAAF, 1990), the algorithms used were simple load-incrementation Newton iteration procedures. These are incapable of tracking the post-ultimate behaviour of the frame (ref. Fig. 2.4). Furthermore, these studies assumed non-linear elastic response - that is hysteretic member behaviour was not addressed.

Below we discuss more general procedures for solving the reduced system, including so-called 'arc-length methods' that are commonly employed in non-linear finite element programs. We will establish that even though the influence matrix of the reduced system is derived from a linear-elastic model, this does not preclude the use of advanced solution procedures including, if desired, a tangent stiffness formulation. In addition, we will discuss why the very simple deformation control algorithm that we adopt (STEWART, 1993) should work well while more complicated displacement-based control procedures (often implemented in finite element codes) are not always successful.

3.4.1 Preliminaries

Equilibrium in standard form

We consider the case where the forces on our structure can be represented by two separate load-sets: one is held constant and the other is incremented by a load factor λ. At any point in the solution history we can combine the total applied loading into one load-set which is held constant and introduce a new load-set which is then scaled, and so on. Therefore a more general load history involving several scaled load-sets can be accommodated provided only one of these is incremented at any one instant.

To be more specific, consider the case of pushover and cyclic analyses of an offshore structure. For the pushover analysis (refer to section 2.2.2), the loading is given by

$$\underline{F}^L = \lambda \underline{F}^W + \underline{F}^G \tag{3.12}$$

where, the load-set $\underline{F}^W$ is a vector of representative (i.e. characteristic) wave induced forces (including current and wind) and $\underline{F}^G$ represents the characteristic gravity loading. Incrementing λ provides the pushover response. The loading history for extreme storm cyclic analysis (ref. section 2.2.3), can be represented as

$$\underline{F}^L = \lambda_1 \underline{F}_1^W + \lambda_2 \underline{F}_2^W + \underline{F}^G \tag{3.13}$$

where the load-sets $\underline{F}_1^W$ and $\underline{F}_2^W$ are the characteristic values of the forward and reverse loading, respectively. The load history is described by varying the parameters λ_1 and λ_2. However, at any instant only one of the parameters is varying and so we can focus on the loading combination described by (3.12) without loss of generality.

With the load $\underline{F}^L$ applied to our structure, the deformation or 'load effect' in the 'non-linear' bar elements is given as

$$\underline{\eta}^L = \lambda \underline{\eta}^W + \underline{\eta}^G \,. \tag{3.14}$$

The equilibrium equation for the reduced system of equations given by (3.9) may then be written as

$$\underline{\eta} - \boldsymbol{D}^{\eta\eta}\, \underline{f}_{\eta}^{NL} = \lambda \underline{\eta}^{W} + \underline{\eta}^{G} \tag{3.15}$$

and (in a generalised sense) we can identify the left hand side with the system's internal resistance and the right hand side as the applied loading. This may be expressed in the general form

$$\underline{g}(\underline{\eta}, \lambda) = \underline{f}^{int}(\underline{\eta}) - \underline{f}^{ext}(\lambda) \tag{3.16}$$

with

$$\underline{f}^{int}(\underline{\eta}) = \underline{\eta} - \boldsymbol{D}^{\eta\eta}\, \underline{f}_{\eta}^{NL}\ ; \quad \underline{f}^{ext}(\lambda) = \lambda \underline{\eta}^{W} + \underline{\eta}^{G} \tag{3.17}$$

in which $\underline{g}$ is the ***residual,*** $\underline{f}^{int}$ is the structure's internal resistance and $\underline{f}^{ext}$ is the applied external force. The system is in equilibrium provided

$$\underline{g}(\underline{\eta}, \lambda) = \underline{0} \tag{3.18}$$

is satisfied.

Tangent stiffness matrix

The quantity

$$\overline{\boldsymbol{K}}_{\eta}^{t} = \frac{\partial \underline{g}}{\partial \underline{\eta}} = \frac{\partial \underline{f}^{int}}{\partial \underline{\eta}} \tag{3.19}$$

is the ***generalised tangent 'stiffness' matrix*** (of the reduced system). From (3.17) it follows that this may be written for the present work as

$$\overline{\boldsymbol{K}}_{\eta}^{t} = \boldsymbol{I} - \boldsymbol{D}^{\eta\eta} \boldsymbol{k}_{\eta}^{P}\ ; \qquad \boldsymbol{k}_{\eta}^{P} = \frac{\partial \underline{f}^{NL}}{\partial \underline{\eta}}\ . \tag{3.20}$$

The matrix $\boldsymbol{k}_{\eta}^{P}$ is the symmetric ***element inelastic matrix*** (or plasticity matrix) of the non-linear elements. For our bar elements, this matrix is diagonal.

We remark that $\overline{\boldsymbol{K}}_{\eta}^{t}$ is not banded since $\boldsymbol{D}^{\eta\eta}$ is a full matrix, and furthermore $\overline{\boldsymbol{K}}_{\eta}^{t}$ is non-symmetric even though both $\boldsymbol{k}_{\eta}^{P}$ and $\boldsymbol{D}^{\eta\eta}$ are symmetric.

Solution curves in space

The solution of (3.18) is a curve in the space defined by the variables $\underline{\eta}$ and λ. This curve can be parameterised by a scalar quantity s which represents a distance measure along the curve (RIKS,

1979). Referring to Fig. 3.4, the position $\underline{x}(s)$ and tangent $\dot{\underline{x}}(s)$ at any point on the solution curve are given as

$$\underline{x}(s)=\begin{bmatrix}\underline{\eta}\\ \lambda\end{bmatrix};\qquad \dot{\underline{x}}(s)=\begin{bmatrix}\dot{\underline{\eta}}\\ \dot{\lambda}\end{bmatrix} \tag{3.21}$$

in which the over-dot is the derivative with respect to s. If s is measure of true distance along the curve then $ds^2 = d\underline{\eta}^T d\underline{\eta} + d\lambda^2$ and $\dot{\underline{x}}(s)$ is a unit vector.

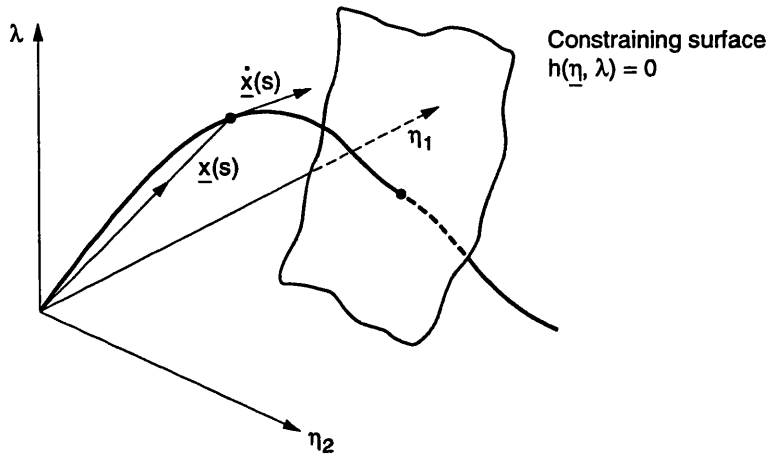

Fig. 3.4 Solution curve in space

Now on the solution curve, $d\underline{g} = \underline{0}$, and so it holds that

$$\frac{\partial \underline{g}}{\partial \underline{\eta}}\dot{\underline{\eta}}+\frac{\partial \underline{g}}{\partial \lambda}\dot{\lambda}=0 \tag{3.22a}$$

which from (3.16) and (3.19) provides

$$\overline{\boldsymbol{K}}_{\eta}^{t}\dot{\underline{\eta}}-\dot{\lambda}\underline{\eta}^{W}=\underline{0}\,. \tag{3.22b}$$

From (3.21) and (3.22b), the tangent vector to the curve in solution space is

$$\dot{\underline{x}}(s)=\dot{\lambda}\begin{bmatrix}(\overline{\boldsymbol{K}}_{\eta}^{t})^{-1}\underline{\eta}^{W}\\ 1\end{bmatrix}. \tag{3.23}$$

This clearly shows the role of the tangent stiffness as a search direction along the solution curve. Later, however, we will adopt a different search direction corresponding to the initial stiffness.

3.4.2 Arc length control

Given a known point on the solution path s_o, a neighbouring point s farther along the path may be located as the intersection of the equilibrium equation (3.18) and a constraining surface (Fig. 3.4) defined by

$$h(\underline{\eta},\lambda,s_o)=0. \tag{3.24}$$

In two dimensional space, this constraint may be viewed as an arc of radius $ds=s-s_o$. The constraint serves to limit the length of the iterative search vector. The essence of the method is depicted in Fig. 3.5.

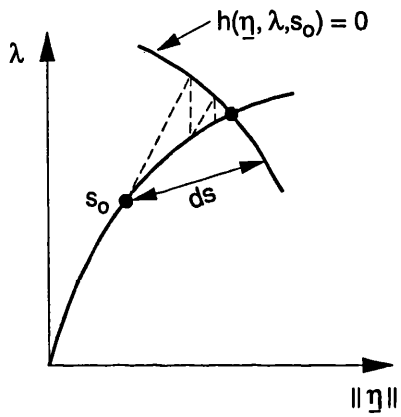

Fig. 3.5 Principles of the arc-length method

The 'arc-length method' was introduced by WEMPNER (1971), and RIKS (1972, 1979). Significant contributions were also made among others by KELLER (1977), CHRISFIELD (1980), RAMM, (1981), DUFFET & REDDY, (1986) and SCHWEIZERHOF & WRIGGERS (1986). The paper by FORDE & STEIMER (1987) provides a good overview of several of the procedures proposed to date.

In typical finite element implementations, nodal displacements/rotations are the natural variables, whereas in our PFI-Method, it is deformation freedoms that are employed. In our development of the various methods below, it is convenient to consider $\underline{\eta}$ as a generalised displacement, which may either be a displacement/rotation or a deformation.

In the arc-length method, certain control variables are selected and the constraint equation defines how these are related. Since the generalised displacement control freedoms may have different units, these must be rendered non-dimensional. We write

$$\underline{\eta}^c = V\underline{\eta} \tag{3.25}$$

where V is a rectangular matrix that selects and normalises a sub-set of control freedoms, $\underline{\eta}^c$. If deformation variables are employed, normalisation of each by its corresponding yield deformation would be an appropriate choice. For the displacement method, the displacements in the first load-step can be used to normalise subsequent control variables.

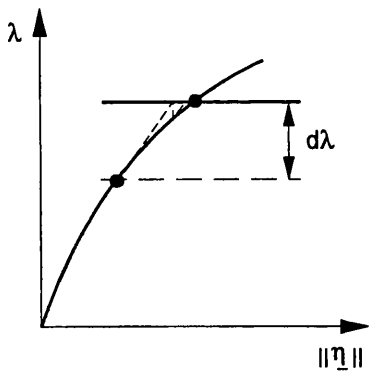

(a) *Load control*

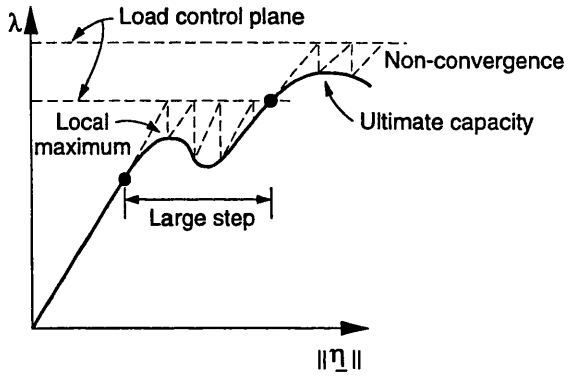

(b) *Problems with load control*

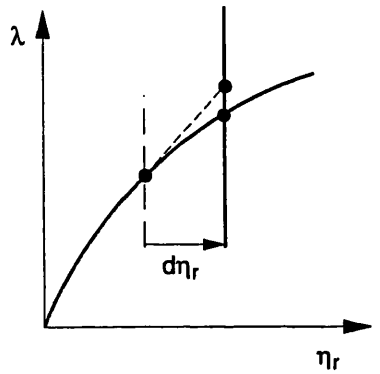

(c) *Control on single generalised displacement*

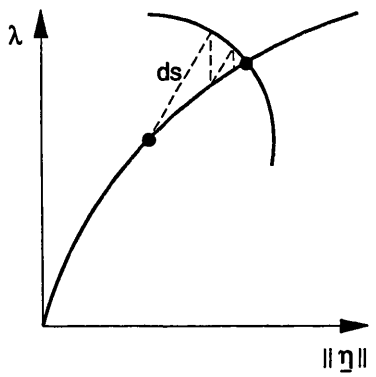

(d) *Spherical constraint*

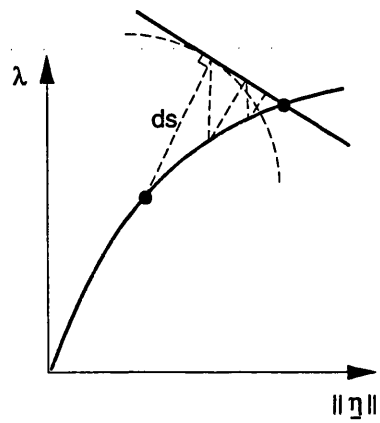

(e) *Tangent plane constraint*

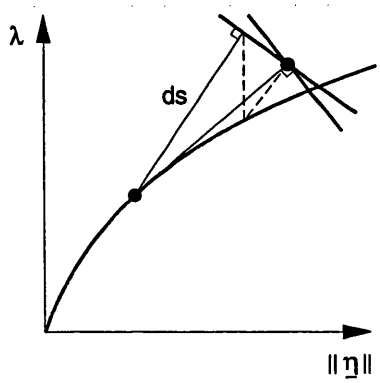

(f) *Updated tangent plane constraint*

Fig. 3.6 Possible constraints used in arc-length method

In Fig. 3.6, several possible surfaces of constraint are considered. Each of these are now discussed.

Load control

Before the work of Riks/Wempner and others in arc length techniques, the standard solution method was the simple load control procedure (Fig. 3.6a). This corresponds to a Newton iteration method (see appendix C) for the solution of (3.18). The constraint equation in this case is the plane defined by

$$h = d\lambda - ds = 0. \tag{3.26}$$

The load control method cannot trace the post-ultimate resistance of a structure and also results in large step sizes (and often non-convergence) if a local turning point exists on the solution curve (Fig. 3.6b).

Generalised displacement control on a single variable

Control on a single displacement variable has been popular for many years (see, for example, BATOZ & DHATT, 1979) and is often successful in tracking post-ultimate behaviour. The equivalent of displacement control in the PFI-Method is deformation control. As will be discussed later, deformation control is extremely effective for plasticity problems and can produce solutions to problems where conventional displacement control procedures would fail.

Control on a specific generalised displacement variable r corresponds to iterating on a vertical plane (Fig. 3.6c) and is identified with the constraint

$$h = d\eta_r^c - ds = 0. \tag{3.27}$$

Hypersphere

More general constraining surfaces have been proposed to overcome the limitations of the load control method and to improve upon the conventional displacement control procedure. WEMPNER (1971), and RIKS (1972, 1979) used a hypersphere of fixed radius (Fig. 3.6d) with all variables contained in the constraint. Subsequently, many variants of the Riks/Wempner method have been proposed.

The following equation (and its tangent plane linearisation - see below) captures the essence of the majority of these. We write the constraint as

$$h(\underline{\eta}, \lambda, s_o) = (d\underline{\eta}^c)^T d\underline{\eta}^c + \beta d\lambda^2 - ds^2 = 0 \tag{3.28}$$

where β is a scaling constant and

$$d\underline{\eta}^c = \underline{\eta}^c - \underline{\eta}_o^c \; ; \quad d\lambda = \lambda - \lambda_o \, . \tag{3.29}$$

The point $(\underline{\eta}_o, \lambda_o)$ is identified with s_o. Setting β to 0 excludes the load parameter from the constraining surface and provides a 'hypercylinder' (CHRISFIELD, 1980, and RAMM, 1981). PARK

(1982) proposes to relate β to Bergan's current stiffness parameter (BERGAN, 1980) which implies using a large value of β (tending towards load control) in the stiff regions and a low value of β (tending towards cylindrical control) in the soft regions. In the present discussion, β is assumed to take only the values 0 or 1.

Tangent hyperplane

Another option, suggested by RIKS (1979), is to linearise (3.28) about any point $(\hat{\underline{\eta}},\hat{\lambda})$ lying on the constraining surface . This yields the tangent hyperplane (Fig. 3.6e) defined by

$$h(\underline{\eta},\lambda,s_o)=(\hat{\underline{\eta}}^c-\underline{\eta}_o^c)^T d\underline{\eta}^c+\beta(\hat{\lambda}-\lambda_o)d\lambda-ds^2=0. \tag{3.30}$$

In the sub-space of the control variables, this plane lies a distance ds from the point s_o and is normal to the vector $\underline{n}=(\hat{\underline{\eta}}^c-\hat{\underline{\eta}}_o^c,\beta[\hat{\lambda}-\lambda_o])$. This plane is not generally normal to the search direction vector unless all freedoms are included in the constraint. The vector $\underline{n}$ corresponds to $\nabla_c h$ where ∇_c is the gradient operator in the control variable sub-space. To define the point $(\hat{\underline{\eta}},\hat{\lambda})$, and hence the plane, one simply scales the search direction vector until (3.30) is satisfied. Updating the tangent plane at each iteration (as proposed by SCHWEIZERHOF & WRIGGERS, 1986) provides a tighter control on step size (Fig. 3.6f) and is to be preferred if the solution path has high curvature.

Both load control ($V=0$, $\beta=1$) and generalised displacement control of a single variable ($\beta=0$ and $d\eta_r^c-ds=0$) are special cases of iterations on a plane.

3.4.3 A general solution procedure

Above we described some possible constraining surfaces. By augmenting the equilibrium equations (3.18) with one of these, the solution may be advanced from a known point s_o. That is we solve the following system of equations

$$\begin{aligned}&\underline{g}(\underline{\eta},\lambda)=\underline{0}\\&h(\underline{\eta},\lambda,s_o)=0.\end{aligned} \tag{3.31}$$

This system can be ***consistently linearised*** (DUFFET & REDDY, 1986; SCHWEIZERHOF & WRIGGERS, 1986), by employing a standard Newton iteration technique (see appendix C). At iteration k this yields

$$\overline{K}_{\eta}^{t}\Delta\underline{\eta}-\underline{\eta}^{W}\Delta\lambda=-\underline{g}_{(k)} \tag{3.32a}$$

$$\frac{\partial h}{\partial\underline{\eta}}\Delta\underline{\eta}+\frac{\partial h}{\partial\lambda}\Delta\lambda=-h_{(k)} \tag{3.32b}$$

where Δ denotes the change between two successive iterations in the current increment. These equations may be expressed as

$$\begin{bmatrix} \bar{K}_{\eta(i)} & -\underline{\eta}^W \\ \dfrac{\partial h}{\partial \underline{\eta}} & \dfrac{\partial h}{\partial \lambda} \end{bmatrix} \begin{bmatrix} \Delta \underline{\eta} \\ \Delta \lambda \end{bmatrix} = - \begin{bmatrix} \underline{g} \\ h \end{bmatrix}_{(k)} \qquad i \leq k \tag{3.33}$$

or

$$\boldsymbol{H}_{(i)} \Delta \underline{x} = - \underline{G}_{(k)} . \tag{3.34}$$

In this notation, $\underline{G}_{(k)}$ is the residual at iteration k, and $\boldsymbol{H}_{(i)}$ is the iteration matrix, the subscript $i \leq k$ indicating that any previous tangent stiffness may be used as a search direction.

A difficulty arises in the solution of (3.34) since $\boldsymbol{H}$ is non-symmetric. To circumvent this the solution is developed in two stages (DUFFET & REDDY, 1986; SCHWEIZERHOF & WRIGGERS, 1986). From (3.32a) it is apparent that

$$\begin{aligned} \Delta \underline{\eta} &= - \left[\bar{K}_{\eta(i)} \right]^{-1} \underline{g}_{(k)} + \Delta \lambda \left[\bar{K}_{\eta(i)} \right]^{-1} \underline{\eta}^W \\ &= \Delta \underline{\eta}_I + \Delta \lambda \underline{\eta}_{II} \end{aligned} \tag{3.35}$$

and from (3.32b) we get

$$\Delta \lambda = - \frac{c + \underline{a}^T \Delta \underline{\eta}_I}{b + \underline{a}^T \underline{\eta}_{II}} ; \quad \underline{a}^T = \frac{\partial h}{\partial \underline{\eta}} , \quad b = \frac{\partial h}{\partial \lambda} , \quad c = h \tag{3.36}$$

where h and its derivatives are evaluated at the current position.

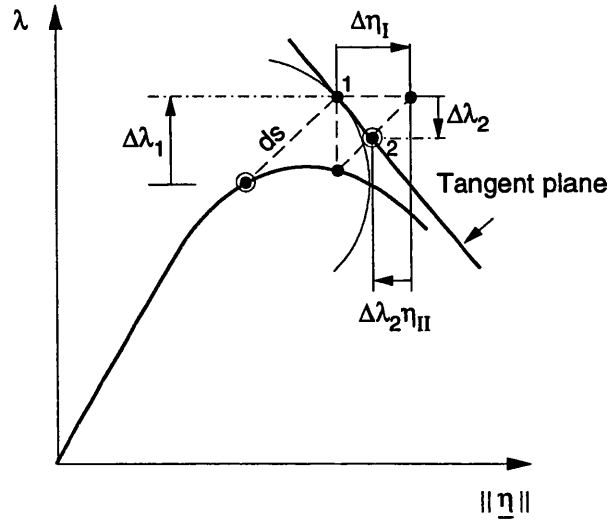

Fig. 3.7 Initial iterative procedure for all arc-length methods

Figure 3.7 shows the geometrical interpretation of $\Delta\underline{\eta}_I$, $\underline{\eta}_{II}$ and $\Delta\lambda$ for the first iteration. In subsequent iterations the procedures differ depending on how $\underline{a}, b$, and c are updated. For the hyperplane constraining surface h is identically zero after the first iteration. For general non-linear constraining functions, consistent linearisation is equivalent to the updated tangent plane method with the plane shifted closer to the constraint by an amount that depends on the residual $h_{(k)}$ as given by (3.32b). Another option is to satisfy the constraint exactly (c = 0) at each iteration by simply scaling back radially to the constraining surface. This may be called a 'radial return' method. Without further investigation, it is not immediately apparent whether the suggested radial return method is computationally more efficient than the consistent linearisation procedure as the former involves an additional scaling step in order to satisfy the constraint exactly.

All of the above procedures are encapsulated in the pseudo-code given in Box 3.1 for a predictor-corrector algorithm. The predictor step starts with an estimated load increment $d\lambda$ of unity and scales to the desired step length. The current iteration count at the start of the increment is j. The various methods are obtained by selecting appropriated values for β, $\underline{a}, b$, and c as follows:

Iteration on initial tangent plane

$$\underline{a} = 2\boldsymbol{V}^T d\underline{\eta}^c_{(j+1)}; \quad b = 2\beta d\lambda_{(j+1)}; \quad c = 0 \tag{3.37}$$

Iteration on updated tangent plane & radial return

$$\underline{a}^T = \left.\frac{\partial h}{\partial \underline{\eta}}\right|_{(k)}, \quad b = \left.\frac{\partial h}{\partial \lambda}\right|_{(k)} \quad c = 0 \tag{3.38}$$

Consistent linearisation

$$\underline{a}^T = \left.\frac{\partial h}{\partial \underline{\eta}}\right|_{(k)}, \quad b = \left.\frac{\partial h}{\partial \lambda}\right|_{(k)} \quad c = h_{(k)}. \tag{3.39}$$

Earlier we noted that $\overline{\boldsymbol{K}}_\eta$ is non-symmetric which means that some additional attention must be paid to (3.34) if it is desirable to use a symmetric solver. To get around this, we note from (3.20) that the matrix $\overline{\boldsymbol{K}}' = \overline{\boldsymbol{K}}_\eta \boldsymbol{D}^{\eta\eta}$ is symmetric and therefore we may write

$$\left[\overline{\boldsymbol{K}}_\eta\right]^{-1} = \boldsymbol{D}^{\eta\eta}\left[\overline{\boldsymbol{K}}'\right]^{-1} \tag{3.40}$$

and so loss of symmetry in $\overline{\boldsymbol{K}}_\eta$ poses no real computational difficulty.

Box 3.1 A general solution algorithm

Step 1: predictor

Initial conditions: $\lambda = \lambda_{(j)}\ ;\ \underline{\eta} = \underline{\eta}_{(j)}\ ;\ d\lambda = 1$

Estimate deformations: $\underline{\eta}_{II} = \left[\overline{K}_{\eta(i)}\right]^{-1} \underline{\eta}^{W}\ ;$

$$d\underline{\eta} = \underline{\eta}_{II} - \left[\overline{K}_{\eta(i)}\right]^{-1} \underline{g}_{(j)}\ ;\ i \le j$$

Set control deformations: $d\underline{\eta}^{c} = V\, d\underline{\eta}$

Scale to fixed arc length ds: $ds^{*} = \sqrt{(d\underline{\eta}^{c})^{T} d\underline{\eta}^{c} + \beta d\lambda^{2}}\ ;\ m = ds / ds^{*}$

$$k = j+1$$

$$d\lambda_{(k)} = m;\quad d\underline{\eta}_{(k)} = m\, d\underline{\eta}$$

Step 2: Iterative corrector

Do until converged

$$\Delta\underline{\eta}_{I} = -\left[\overline{K}_{\eta(j)}\right]^{-1} \underline{g}_{(k)}\ ;\quad j \le k$$

$$\Delta\lambda = -\frac{c + \underline{a}^{T}\Delta\underline{\eta}_{I}}{b + \underline{a}^{T}\underline{\eta}_{II}}$$

$$\Delta\underline{\eta} = \Delta\underline{\eta}_{I} + \Delta\lambda\underline{\eta}_{II}$$

If radial return then

$$d\underline{\eta}^{*} = d\underline{\eta}_{(k)} + \Delta\underline{\eta}\ ;\quad d\lambda^{*} = d\lambda_{(k)} + \Delta\lambda\ ;\quad d\underline{\eta}^{c} = V\, d\underline{\eta}^{*}$$

$$ds^{*} = \sqrt{(d\underline{\eta}^{c})^{T} d\underline{\eta}^{c} + \beta(d\lambda^{*})^{2}}\ ;\quad m = ds / ds^{*}$$

$$d\underline{\eta}_{(k+1)} = m\, d\underline{\eta}^{*}\ ;\quad d\lambda_{(k+1)} = m\, d\lambda^{*}$$

else

$$d\underline{\eta}_{(k+1)} = d\underline{\eta}_{(k)} + \Delta\underline{\eta}\ ;\quad d\lambda_{(k+1)} = d\lambda_{(k)} + \Delta\lambda$$

End if

$$k = k+1$$

End do

Internal force recovery

In any solution procedure (for problems in both statics and dynamics), the internal element forces have to be recovered and the residual vector calculated. There are two options. The first is a ***path dependent*** strategy whereby the internal force increment is calculated on the basis of the iterative deformation change $\Delta\underline{\eta}_{(k)}$. The second, which is preferred, is a ***path independent*** strategy

that calculates the internal force increment on the basis of the total incremental deformation change $d\underline{\eta}_{(k)}$. The difference between the two is shown in Fig. 3.8 for a bar element. The path dependent strategy continually updates the total deformations to the current iterative position. The initial equilibrium position is not retained and it is possible for this procedure to get lost during iterations. In the example shown, this method converges to point 2b. In the path independent strategy, we search ahead for equilibrium while remaining firmly anchored at the initial position and end up at point 2a. It is only once convergence has been achieved that we advance along the solution path.

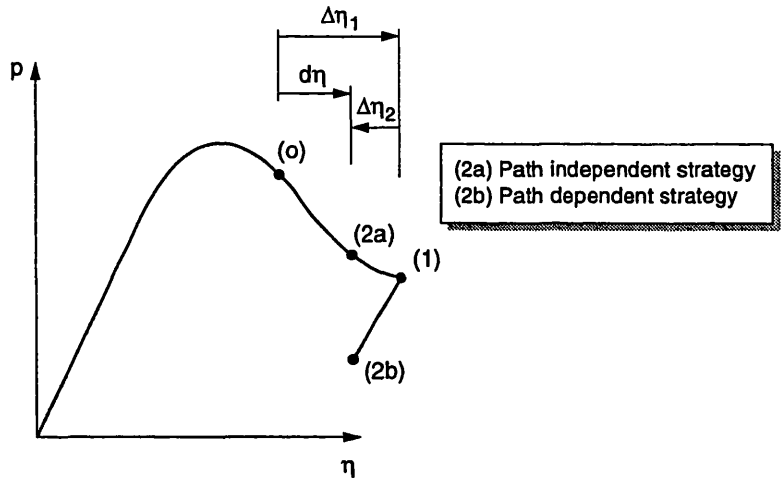

Fig. 3.8 Internal force recovery

3.4.4 Solution procedure implemented in this work

This completes our review of the theory behind the arc length method. We are now left wondering which of the alternative procedures is best. Or perhaps we should implement a variety of procedures, switching between these if one fails to converge. In many articles and texts on this subject (see for example CHRISFIELD, 1991), this latter strategy is proposed. But maybe one should first question why it is that certain procedures are not always successful.

Displacement vs deformation freedoms

The vast majority of finite element (f.e.) programs are based on displacement freedoms. A problem arises in selecting appropriate control freedoms. Since displacements are a measure of global response, there is no guarantee that the deformation in the non-linear elements will be adequately restricted if the norm of some sub-set of displacements is arbitrary constrained to lie below a certain value. This may lead to excessive iterations in one step or perhaps non-convergence. CHRISFIELD (1980) has reported improved performance by modifying the step size based on the number of iterations in the previous step. However, this improved procedure will also have some difficulties if the controlling displacements are poorly selected. The inherent problems with displacement control would suggest that displacements are not the most suitable

control variables. It seems to be rather more appropriate to steer the solution on element deformations, as it is these that really control the response. This is certainly the case for problems in which the non-linearity is caused by material properties rather than by geometrical properties.

A deformation or strain control procedure could be implemented into a general f.e. program without difficulty. In an element, a particular (Gauss point) strain increment $d\varepsilon_i$ is related to the displacement increments $d\underline{U}$ by

$$d\varepsilon_i = \underline{b}^T d\underline{U} \tag{3.41}$$

where $\underline{b}^T$ is a row of the element strain displacement matrix. The constraint is then given by

$$h = \underline{b}^T d\underline{U} - (s - s_o) = 0 \,. \tag{3.42}$$

If the largest strain in the element that is dissipating the most energy is selected as the control, it is believed that this procedure could lead to a superior performance over many of the displacement control strategies currently in use, particularly for problems that are not governed by geometrical non-linearity.

The contrast between controlling on deformations and controlling on displacement freedoms is well demonstrated by the following example. A cantilever beam of length l and bending stiffness k_b is loaded at its tip by a force F and supported by a softening non-linear rotational spring (Fig. 3.9). Given the rotation of the base θ, the moment M is known, and the applied force and the tip displacement δ can be readily calculated from

$$\delta = l\theta + F / k_b \;; \qquad F = M(\theta)/l \,. \tag{3.43}$$

From this,

$$\frac{\partial \delta}{\partial \theta} = l + \frac{1}{l k_b}\frac{\partial M}{\partial \theta} = l + \frac{k_\theta}{l k_b} \tag{3.44}$$

and so

$$\frac{\partial \delta}{\partial \theta} < 0 \quad \text{if} \quad k_\theta < -l^2 k_b . \tag{3.45}$$

The results shown in Fig. 3.9 are for the particular case of $k_b = l = 1$ for a spring with rotational resistance $M = \sin(20\theta)$. When (3.45) is satisfied, the tip displacement is reducing while the base rotation is increasing. There is then no longer a one-to-one relationship between θ and δ, and for a given value of δ, the applied force is multi-valued. Therefore, beyond a certain point, the equilibrium curve can only be traced out by controlling the deformation freedom (the base rotation) and not by controlling the tip displacement.

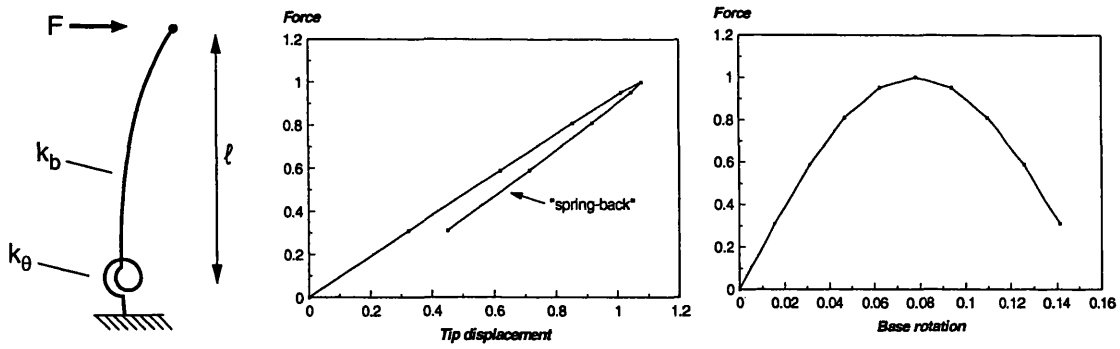

Fig. 3.9 Response of a cantilever beam supported by nonlinear rotational spring

This example captures many of the characteristics that are exhibited by the collapse mechanisms of framed structures. It illustrates that some degrees of freedom actively control the solution process while others merely follow. A ***spring-back response,*** such as that shown in Fig. 3.9, may be observed if a follower variable is selected to represent the overall behaviour of the structure. The spring back is caused by a release of elastic energy.

Control procedure implemented for the PFI-Method

As the unknowns in the PFI-Method are deformations, the method provides a natural set of freedoms for steering along the solution path. In the non-linear response range, it is suggested to steer the problem using a single deformation variable, being the one that is dissipating the most energy. In addition, because the number of unknowns in (3.9) is small, initial (elastic) stiffness iteration can be employed very effectively.

Path independent deformation control with ***initial stiffness iterations*** results in a very straightforward incremental solution procedure. The algorithm is a special case of the general procedure given in Box 3.1 above - however it is most easily derived directly from (3.35). Since, for initial stiffness iterations, $\boldsymbol{K}_{\eta_{(i)}} \equiv \boldsymbol{I}$, equation (3.35) for control freedom r, is simply

$$\Delta\eta_r = -g_{r(k)} + \Delta\lambda\eta_r^W \tag{3.46}$$

from which

$$\Delta\lambda = \frac{\Delta\eta_r + g_{r(k)}}{\eta_r^W} \,. \tag{3.47}$$

The complete algorithm is given in the Box 3.2 below in which the yield deformation of the control variable is denoted by η_r^Y.

Box 3.2 Solution procedure for deformation control

Last converged step: $\lambda = \lambda_{(j)}$; $\underline{\eta} = \underline{\eta}_{(j)}$

Deformation control: $d\eta_r = (s - s_o)\eta_r^Y$

Iteration counter: $k = j$

Do until converged:

$$\Delta\lambda = \frac{\Delta\eta_r + g_{\eta(k)}}{\eta_r^W} \; ; \qquad \Delta\underline{\eta} = \Delta\lambda\,\underline{\eta}^W - \underline{g}_{(k)}$$

$$d\lambda_{(k+1)} = d\lambda_{(k)} + \Delta\lambda \; ; \quad d\underline{\eta}_{(k+1)} = d\underline{\eta}_{(k)} + \Delta\underline{\eta}$$

$k = k+1$

End do

On the first iteration, $\Delta\eta_r = (s - s_o)\eta_r^Y$ which exactly satisfies the constraint. Therefore, for all subsequent iterations $\Delta\eta_r$ is set to zero. The selected deformation control variable η_c is that which is changing most rapidly in the previous increment. This algorithm, which is implemented in the simulation system described in section 3.6, has been tried on several examples (some of which are discussed later in chapter 5) and has not yet failed.

3.5 LIMIT POINTS AND BIFURCATION POINTS

The maximum load-bearing capacity of a structure may either be a ***limit point*** or a ***bifurcation point*** (Fig. 3.10).

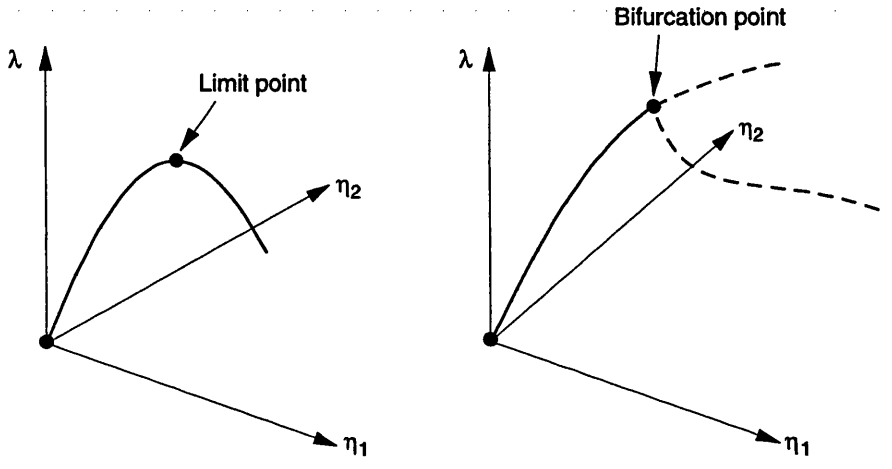

(a) Limit load *(b) Bifurcation of the solution path*

Fig. 3.10 Limit points and bifurcation points

Both limit and bifurcation points are characterised by a singular tangent stiffness matrix; however the solution passing through the limit point is unique whereas multiple solutions paths may emanate from a bifurcation point. In the case of a bifurcation point, additional information must be passed to the arc-length control procedure to select the desired path. Bifurcations are typically associated with perfect structures or those in which alternative failure modes appear at the same level of load. Adding a sufficiently large initial imperfection to the structure will transform a bifurcation point into a limit point, although there is no guarantee that the lowest equilibrium branch will be found if this is done in an arbitrary manner. However, in most practical cases, the response curve of a braced frame will be unique and the ultimate strength will occur at a well defined limit point.

3.5.1 Brief review of theory

A system with tangent stiffness matrix K is said to be in a critical equilibrium state if for at least one admissible non-zero deformation increment $\dot{\underline{a}}$, the following holds

$$\dot{\underline{a}}^T K \dot{\underline{a}} = 0. \tag{3.48a}$$

It may be shown (see for example DE BORST, 1986) that for systems having symmetric stiffness matrices, a necessary and sufficient condition for (3.48a) is that at these ***critical points***, the tangent matrix becomes singular (zero determinant), in which case (3.48a) is equivalent to

$$K \dot{\underline{a}} = 0 \,. \tag{3.48b}$$

For non-symmetric systems, a singular tangent matrix is a sufficient condition for a critical point but not a necessary condition. That is even if (3.48b) does not hold, (3.48a) can still be satisfied if $\dot{\underline{a}}$ is normal to $K\dot{\underline{a}}$. The theory of critical points takes on a simpler form for symmetric systems. We therefore re-write the equilibrium equation (3.22b) in the form

$$\overline{K}' \dot{\underline{y}} - \dot{\lambda} \underline{\eta}^W = \underline{0}; \quad \dot{\underline{\eta}} = D^{\eta\eta} \dot{\underline{y}} \tag{3.49}$$

in which the $\overline{K}' = \overline{K}_\eta^t D^{\eta\eta}$ (see eqn. (3.40)) is symmetric.

It is well known that the determinant of an $M \times M$ matrix is equal to the product of its M eigenvalues (μ), that is

$$\det \overline{K}' = \prod_{i=1}^{M} \mu_i \,. \tag{3.50}$$

Therefore $\overline{K}'$ is singular if one or more of its eigenvalues are zero showing that the occurrence of zero eigenvalues is an indicator of a critical point. Since $\det \overline{K}' = \det \overline{K}' \det D^{\eta\eta}$, and because $D^{\eta\eta}$ is positive definite (no zero eigenvalues), a singularity in $\overline{K}'$ also implies that $\overline{K}_\eta^t$ is singular.

Limit points pose no serious problem if an arc-length control solution strategy is adopted. This is because the augmented matrix $\boldsymbol{H}_{(k)}$ is not singular at a limit point provided the constraint satisfies $\nabla h^T \dot{\underline{x}} \neq 0$ (KELLER, 1977). This latter requirement ensures that the normal to the constraining surface is not perpendicular to the path tangent vector (which is why simple load control cannot track around a limit point). At a limit point only one solution (or equilibrium) path exists, the load becomes stationary ($\dot{\lambda} = 0$), and the system has only one zero eigenvalue.

In contrast to a limit point, several equilibrium paths may emanate from a bifurcation point, and on some of these paths, the load may not be stationary. Because there is no unique solution, $\boldsymbol{H}_{(k)}$ is singular at such a point and any number of zero eigenvalues can be present - although in practice it is uncommon to find more than two.

The solution paths in the vicinity of a bifurcation point may be investigated by perturbing the tangent path by the eigenvectors associated with zero eigenvalues of the tangent stiffness matrix (DUFFET & REDDY, 1986; DE BORST, 1986). Since the $M \times M$ matrix $\overline{\boldsymbol{K}}'$ is symmetric, it has a complete set of independent orthogonal eigenvectors $\underline{\phi}_i$. These are obtained from the solution of the eigenvalue problem

$$(\overline{\boldsymbol{K}}' - \mu_i \boldsymbol{I})\underline{\phi}_i = \underline{0} \qquad i = 1, M. \tag{3.51}$$

This implies that for the zero eigenvalues $\mu_1, \mu_2, \ldots \mu_r$, the following holds

$$\overline{\boldsymbol{K}}' \underline{\phi}_i = \underline{0} \qquad \underline{\phi}_i^T \overline{\boldsymbol{K}}' = \underline{0} \qquad i = 1, r \tag{3.52}$$

where the second relationship in (3.52) follows from symmetry of $\overline{\boldsymbol{K}}'$. We identify $\underline{\phi}_i$ with $\dot{\underline{a}}$ in (3.48b). The eigenvectors $\underline{\phi}_i$ $(i = 1, r)$ are said to span the null space (DUFFET & REDDY, 1986).

All possible solution paths (denoted henceforth by sub-script k) must satisfy the (modified) equilibrium equation (3.49). Furthermore, bifurcation (and limit) points satisfy the following criterion

$$\dot{\lambda}_k \underline{\phi}_i^T \underline{\eta}^W = 0 \tag{3.53}$$

which follows immediately from (3.49) and (3.52). Consequently, if there exists any path on which $\dot{\lambda}_k$ is not stationary, the null-space eigenmodes are normal to the load vector.

The continuation of the solution curve through the bifurcation point using the path tangent vector is called the fundamental solution (BUDIANSKY, 1974). Let this be denoted $\alpha \dot{\underline{y}}^*$, where $\dot{\underline{y}}^*$ has unit length and α is a scaling factor. It is easily verified using (3.49) and (3.52) that all possible solution paths in the vicinity of the critical point are described by linear combinations of the fundamental solution and null space eigenvectors. Thus,

$$\dot{\underline{y}}_k = \alpha_k \dot{\underline{y}}^* + \sum_{i=1}^{r} \beta_{ki} \underline{\phi}_i \tag{3.54}$$

and, since $\dot{\underline{\eta}} = \boldsymbol{D}^{\eta\eta} \dot{\underline{y}}$ (see equation (3.49)) we may also write

$$\dot{\underline{\eta}}_k = \alpha_k \dot{\underline{\eta}}^* + \sum_{i=1}^{r} \beta_{ki} D^{\eta\eta} \underline{\phi}_i . \tag{3.55}$$

The contribution of the eigenvectors may be regarded as introducing small imperfections into the structure to trigger deformation modes that would otherwise not be identified. Generally the imperfection amplitudes β_{ki} are chosen heuristically and α_k is then determined to comply with the arc-length constraint (see RIKS, 1972; DE BORST, 1986; WAGNER & WRIGGERS, 1988). Alternative procedures for branch switching may also be found in the paper by KOUHIA (1992). Having selected one of the bifurcated branches, the standard arc-length procedure is again adequate. Note that the number of possible solution paths (k) is not the same as the number of null space eigenvectors (r). For example, the buckling of a perfect tubular column in three dimensional space has only two null space eigenvectors, but there are an infinite number of possible solution paths since the column can buckle in any direction.

As noted by DE BORST (1986), if the load increases along the fundamental path, one zero eigenvalue is indicative of a bifurcation point. On the other hand, if the load increment on the fundamental path is stationary or decreasing, the critical point is a bifurcation point only if two or more eigenvalues are zero - otherwise it is a limit point.

In a numerical procedure, the critical point is not easily isolated and it is likely that one arrives at a position on the fundamental path just beyond the sought for point. In this case, negative eigenvalues will be found, and it is the eigenmodes associated with these which should be used as an approximation to the actual null space eigenmodes. For each negative eigenvalue, the eigenmodes satisfy

$$\underline{\phi}_i^T \overline{\boldsymbol{K}}' \underline{\phi}_i = \mu_i < 0 \tag{3.56}$$

and it is clear that the eigenmode associated with the most negative eigenvalue is the least stable. Therefore perturbing the fundamental solution by this eigenmode will usually result in the lowest branch being followed (DE BORST, 1986).

In summary

Limit Point: $\det \overline{\boldsymbol{K}}' = 0;\ \det \boldsymbol{H}_{(k)} \neq 0;\ \dot{\lambda} = 0;\ \mu_1 = 0;\ \mu_2, \ldots \mu_M > 0$

Bifurcation point: $\det \overline{\boldsymbol{K}}' = 0;\ \det \boldsymbol{H}_{(k)} = 0;\ \mu_1, \ldots \mu_r = 0$

3.5.2 Examples of bifurcation and its implication for real structures

Bifurcations in structural mechanics problems are either triggered by geometrical effects (buckling) or by the inclusion of some elements in which the strength decreases with increasing

deformation (strain softening phenomenon). These two types of phenomena are captured in the simple examples shown in Figs. 3.11 & 3.12.

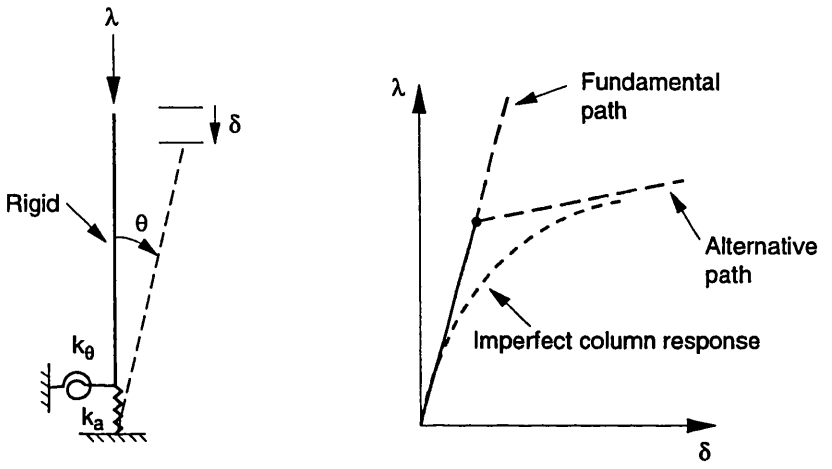

Fig. 3.11 Bifurcation caused by geometric non-linearity

In the first example shown in Fig. 3.11 (discussed in detail by BUDIANSKY, 1974), an axial force is applied to a perfectly straight rigid bar which is connected to the ground by rotational and axial linear-elastic springs of stiffnesses k_θ and k_a, respectively. Increasing the load λ produces deformations in the axial spring and the system is stable (insensitive to small random perturbations) until a certain load $\lambda_{crit} = k_\theta / l$. At this point, which corresponds to a zero eigenvalue in the stiffness matrix, adding a small lateral disturbance (a fraction of the eigen-mode) causes large rotations. If no disturbance is input, the load can be increased beyond λ_{crit} and we follow the fundamental path, which in this case is unstable. As we noted above, since the fundamental path corresponds to increasing load, one zero eigenvalue indicates a bifurcation point. Adding a small disturbance takes us on to an alternative stable equilibrium path. This same path is also reached asymptotically if a small initial rotation (imperfection) is imposed on the column. In this case the bifurcation point is no longer evident.

When we use our beam-column models to obtain the axial-load shortening curves of members in compression, we add in an initial lateral imperfection and consequently these models do not need to consider the possibility of bifurcation. Furthermore, in our present system model based upon the PFI-Method, the effect of geometrical changes at the global level are not considered and so this type of bifurcation is not an issue.

In the second example (Fig. 3.12), which is more relevant to the type of problem we are interested in, we consider a pin-jointed plane frame with two non-linear compression braces having equal buckling strengths (the problem of truss structures with many simultaneous elastic buckling members has been studied by PEEK & TRIANTAFYLLIDIS, 1992). This frame can be represented by two non-linear axial springs joined in series. The post-buckling strength of the members is represented by a softening behaviour of the springs.

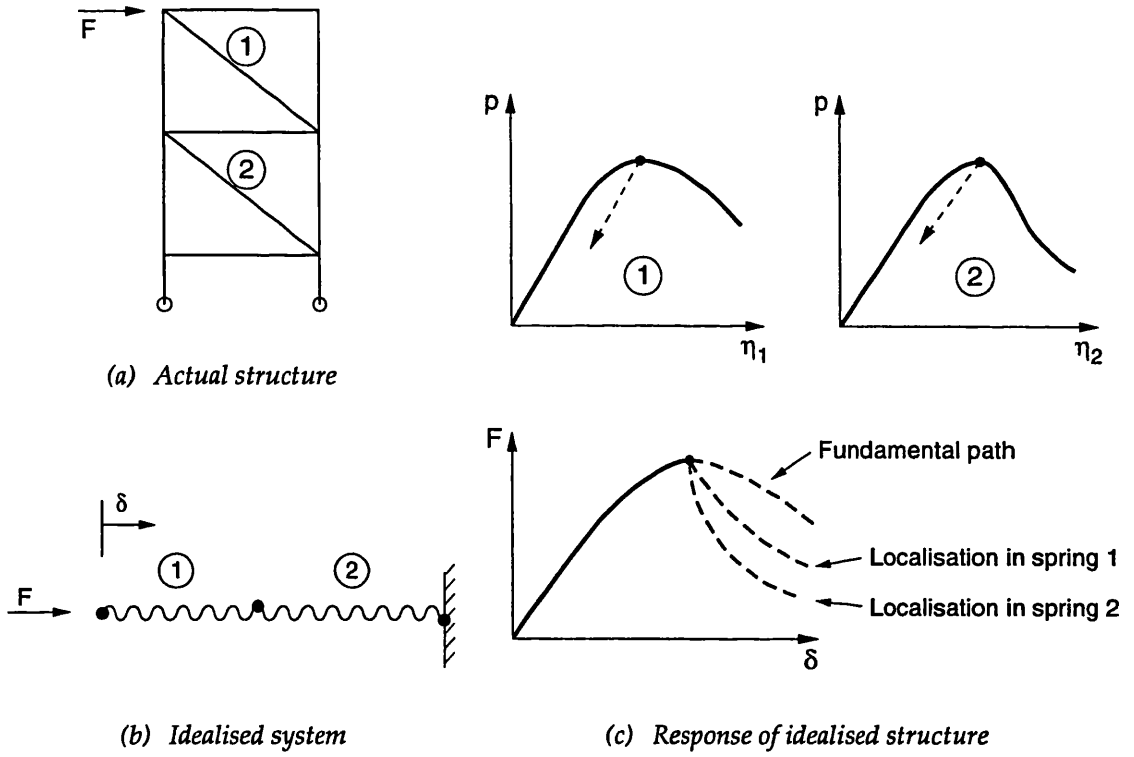

(a) Actual structure

(b) Idealised system

(c) Response of idealised structure

Fig. 3.12 Bifurcation caused by material softening

At the maximum load point of the system, both springs reach their buckling strengths and we can identify three possible solution paths (the deformation in each spring can either increase or decrease). All of these paths are stable (in the sense that adding small disturbances does not cause path switching). The most favourable post-ultimate (residual) strength is realised on the fundamental path, which corresponds to increasing deformation in both springs. Unlike the first example, the applied load now decreases beyond the bifurcation point on the fundamental path. On the other two paths, the strains localise in one of the springs and the other begins to unload elastically. At the bifurcation point, the tangent stiffness matrix has two zero eigenvalues. For the problem with n springs with equal buckling loads there are n zero eigenvalues (and n associated eigenmodes) and $2^n - 1$ possible solution paths.

If the strengths of each spring in Fig. 3.12 are given arbitrarily small (but different) perturbations, deformations will localise in the spring with the lowest strength while the other unloads elastically. Thus the bifurcation point is turned into a limit point and the equilibrium path beyond the ultimate strength of the system is determined by the softening behaviour of the localising spring. In real structures, the possibility of simultaneous buckling is remote and a limit point will usually be found. However some care should be exercised to ensure that small changes in the member strengths would not lead to a lower residual capacity. This can be verified by checking to see if any members come close to their buckling load but then unload elastically. In many respects, we can view a probabilistic Monte-Carlo analysis, in which the member properties are sampled from a certain distribution function, and the strength of the structure determined many hundreds of times, as a formalised way of investigating alternative equilibrium branches.

The two spring example has been analysed using our proposed initial stiffness deformation control algorithm. It was found that if the deformation in the spring with the greatest softening was used as the control, the method converged to the lowest descending branch; otherwise it did not converge. This suggests (but needs further effort to confirm) that if several members are buckling (softening) at the same time, then controlling the solution using the member with the steepest post-buckling slope will result in the lowest equilibrium branch being found. This straightforward approach to identifying the lowest bifurcation branch is not apparent if displacement freedoms rather than deformation freedoms are selected for arc-length control, highlighting another advantage of using deformations as the solution steering variables.

We conclude that in the unlikely event that bifurcation occurs for the type of braced frame problems we are considering, the deformation control procedure is likely to prove adequate and therefore additional numerical procedures to explicitly check for these critical points have not been implemented in our simulation system which is described below.

3.6 BUILDING A SIMULATION SYSTEM AROUND A LINEAR ANALYSIS PROGRAM

The developments discussed in this chapter have shown how to extract the non-linear aspects of a problem to obtain a reduced system that can be solved separately. This reduction process makes use of the linear-elastic response characteristics of the structure. Having found the response of the reduced system, the non-linear response of the overall structure may then be obtained as a data post-processing step. Taking advantage of this, a simulation system can be developed to obtain the response of a non-linear problem using any standard linear-elastic f.e. program. There are four main building blocks:

- a linear-elastic structural analysis or finite element program
- a linear-elastic model
- a method for generating the axial load-shortening curves of the non-linear members
- a solution procedure to solve the reduced system equations

In our implementation, these modules are entirely separate and communicate through data files. Therefore the linear-elastic f.e. program and model need not reside on the same computer as the other modules.

Figure 3.13 shows a flow diagram of how these individual modules are linked to provide a simulation system for static analysis. We now focus on how these are used to perform a non-linear pushover analysis.

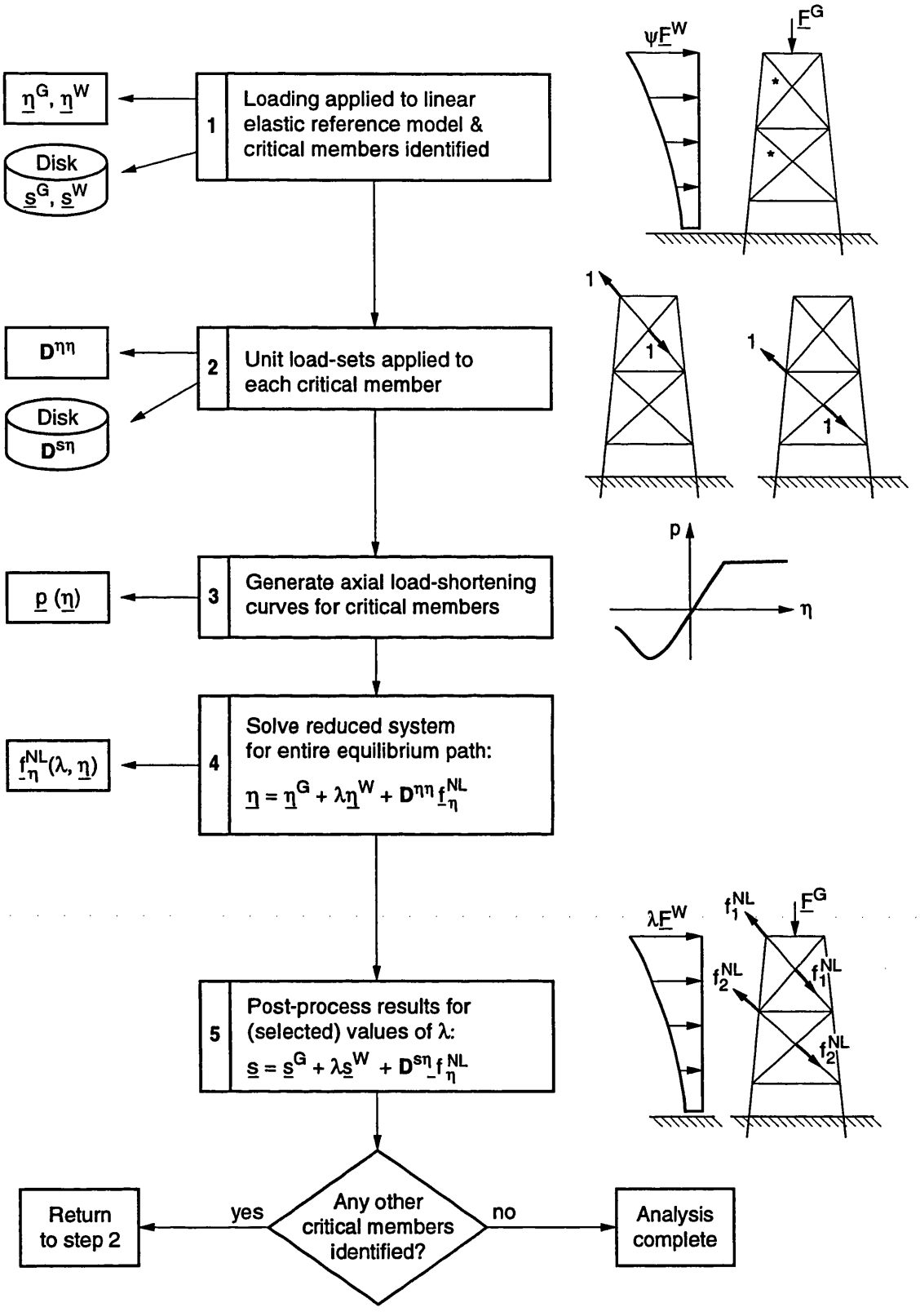

Fig. 3.13 Flow diagram of simulation system for statics problems

The steps in a non-linear pushover analysis (refer to Fig. 3.13) are:

1. Analyse the linear-elastic structure, with loading $\underline{F}^G$ and $\underline{F}^W$ applied separately, and store the response (stresses, strains, displacements, etc.) $\underline{s}^G$ and $\underline{s}^W$ on disk. Now determine (using a stress check post-processor or otherwise) a scaling factor ψ such that $\underline{F}^L = \psi \underline{F}^W + \underline{F}^G$ causes overstressing of one or more members. For these ('non-linear') members extract $\underline{\eta}^G$ and $\underline{\eta}^W$.

2. Apply unit load-sets in turn to each 'non-linear' member and store $\boldsymbol{R}^{s\eta}$, the linear-elastic response of the entire structure, on disk. Extract the axial deformations (usually best calculated from axial force divided by stiffness) of the 'non-linear' members to get the matrix $\boldsymbol{D}^{\eta\eta}$.

3. Generate (by computation or experiment - see chapter 2), the non-linear load-shortening curves for each 'non-linear' member.

4. Incrementally progress along the solution path by solving (with any suitable algorithm) the reduced system of equations (3.9). This yields (our first estimate of) the pseudo-force multipliers for the entire solution path.

5. Determine the response in the remainder of the structure for selected points on the solution path (typically at the ultimate capacity and somewhere in the residual strength range) by adding factored combinations of the individual responses, that is

$$\underline{s} = \underline{s}^G + \lambda \underline{s}^W + \boldsymbol{R}^{s\eta} \underline{f}_{\eta}^{NL}.$$

   Usually a post-processing routine is available within the linear-elastic software system to perform this operation.

6. Check for overstressing of any additional members. If so, return to step 2. Otherwise the solution history obtained in step 4 is correct.

If the above procedure is followed, the system expands in size as more members become non-linear and the problem is re-solved starting at $\lambda = 0$. With a little experience, most or all 'non-linear' members participating in the collapse mechanism can be identified at step 1. Consequently, all information required for the reduced system equations can usually be derived from one linear-elastic analysis.

The procedure for cyclic assessments is very similar to that for pushover analysis. Indeed the first stage in a cyclic assessment is a pushover analysis. This identifies the non-linear members and the linear-elastic response for the forward loading $\underline{F}_1^W$. The only additional information required for the cyclic analysis is the linear-elastic response for the reverse loading, $\underline{F}_2^W$.

The simulation system described above has been used to analyses various problems and the solutions of many of these have been verified against the USFOS program. Several examples are given in chapter 5. The inclusion of dynamic effects is discussed in the next chapter.

Major advantages

The simulation system offers many advantages to the engineer familiar with a certain linear-elastic structural analysis program. Firstly, it is not necessary to acquire a separate non-linear package (and perhaps more powerful hardware), learn how to use it and convert the existing linear-elastic model to the modified format. Secondly, the additional building blocks for the simulation system run easily on any personal computer and are quite straightforward to develop. Thirdly, upgrades of the linear-elastic f.e. program do not affect the other modules in the system. Fourthly, the simulation procedure is ideal for studying parametric variations, for example the effect on the system strength if certain members are damaged. Such an analysis takes only a few minutes as only the member load-shortening curves need be re-defined; all other input data remains unchanged.

3.7 SUMMARY OF KEY POINTS

A number of key points are worth noting about the pseudo-force technique relating to materially non-linear bar elements.

1. Only one pseudo-force multiplier (i.e. one unknown) is required for a two-noded bar element. This corresponds to modifications associated with the bar's internal resistance.
2. The pseudo-forces act along the axis of the bar - that is in the local element co-ordinate system.
3. Once the pseudo-forces are known the solution to the modified problem is obtained by linear superposition.
4. If only a small number of bar elements are to be modified, the approach is extremely efficient since it is only these bars that are included in the reduced system equations.

Although for more general elements there are more pseudo-force multipliers, these basic principles apply.

3.8 REFERENCES

AL-BAKRI, M.A.E. (1977), *Optimum design of transmission towers*, PhD thesis, Univ. of Surrey.

ARGYRIS, J.H. (1964), "Recent advances in matrix methods of structural analysis", *Progress in Aeronautical Sciences*, **4**, (Küchemann & Sterne Eds.), Pergamon Press.

BATOZ, I.L., AND DHATT, G. (1979), "Incremental displacement algorithms for non-linear problems", *Int. J. of Num. methods in Eng.*, **14**, pp1262-1267.

BERGAN, P.G. (1980), "Solution algorithms for nonlinear structural problems", *Computers & Structs.*, **12**, pp497-509.

BORST, R. DE (1986), *Nonlinear analysis of frictional materials*, PhD thesis, Delft University, The Netherlands.

BUDIANSKY, B. (1974), "Theory of buckling and post-buckling behaviour of elastic structures", *Advances in Applied Mechanics*, **14**, pp1-63.

CHRISFIELD, M.A. (1980), "A fast incremental/iterative solution procedure that handles snap-through", *Computers & Structs.*, **13**, pp55-62.

CHRISFIELD, M.A. (1991), *Nonlinear finite element analysis of solids and structures, Vol. 1*, John Wiley & Sons.

DUFFET, G.A., AND REDDY, B.D. (1986), "The solution of multi-parameter systems of equations with application to problems in nonlinear elasticity", *Computer Methods in App. Mech. & Eng.*, **59**, pp179-213.

References (continued)

FORDE, B.W.R., AND STEIMER, F.S. (1987), "Improved arc length orthogonality methods for nonlinear finite element analysis", *Computers & Structs.*, **27** (5), pp625-630.

HOLNICKI-SZULC, J., AND GIERLINSKI, J.T. (1989), "Structural modifications simulated by virtual distortions", *Int. J. of Num. methods in Eng.*, **28**, pp645-666.

KOUHIA, R. (1992), "On the solution of nonlinear finite element equations", *Computers & Structs.*, **44** (12), pp243-254.

KELLER, H.B. (1977), "Numerical solution of bifurcation and nonlinear eigenvalue problems", in *Applications of bifurcation theory* (P.H. Rabinowtz, ed.), Academic Press, New York, pp359-391.

MAJID, K.I., AND ELLIOT, D.W.C. (1973), "Forces and deflections in changing structures", *Struct. Eng.*, **51**(3), pp93-101.

MAJID, K.I. (1974), *Optimum Design of Structures*, Butterworths.

MALVERN, L.E. (1969), *Introduction to the mechanics of a continuous Medium*, Academic Press, New York.

ODEN, J.T. (1972), *Finite elements of nonlinear continua*, McGaw-Hill.

PARK, K.C. (1982), "A family of solution algorithms for nonlinear structural analysis based on the relaxation equation", *Int. J. Num.Methods in Eng.*, **18**, pp1337-1347.

PEEK, R., AND TRIANTAFYLLIDIS, N. (1992), "Worst shapes of imperfections for space trusses with many simultaneous buckling members", *Int. J. Solids & Structs.*, **29**(19), pp2385-2402.

RAMM, E. (1981), "Strategies for tracing the nonlinear response near limit points", in *Nonlinear Finite Element Analysis in Structural Mechanics* (Wunderlich, Stein & Bathe, eds.), Springer, Berlin, pp63-89.

RIKS, E. (1972), "The application of Newton's method to the problem of elastic stability", *J. App. Mech.*, **39**, pp1060-1066.

RIKS, E. (1979), "An incremental approach to the solution of snapping and buckling problems", *Int. J. of Solids & Structures*, **15**, pp529-551.

STEWART, G., AND VAN DE GRAAF, J.W. (1990), "A methodology for platform collapse based on linear superposition", *Offshore Technology Conference*, OTC 6311, Houston, Texas.

STEWART, G. (1993), "Nonlinear response of offshore jacket structures using linear analysis programs", *Conference on Integrity of Offshore Structures* (IOS), Glasgow, Scotland.

SCHWEIZERHOF, K.H., AND WRIGGERS, P.H. (1986), "Consistent linearisation for path following methods in nonlinear fe analysis", *Computer Methods in App. Mech. & Eng.*, **59**, pp261-279.

SØREIDE, T.H., AMDAHL, J.A., EBERG, E., HOLMÅS, T. AND HELLAN, Ø. (1992), *USFOS - A computer program for progressive collapse analysis of steel offshore structures*, Theory manual, SINTEF, Trondheim, Norway.

WEMPNER, G. (1971), "Discrete approximations related to nonlinear theories of solids", *Int. J. Solids & Structs.*, **17**, pp1581-1599.

WAGNER, W., AND WRIGGERS, P. (1988), "A simple method for the calculation of postcritical branches", *Eng. Comp.*, **5**, pp103-109.

Chapter 4

THE PSEUDO-FORCE INFLUENCE METHOD FOR STRUCTURES WITH NON-LINEAR BAR ELEMENTS

- Dynamics -

4.1 INTRODUCTION

In the previous chapter, we developed pseudo-force procedures to obtain the non-linear response of problems in which time dependent resistance effects were ignored. These methods are suitable for determining the static collapse resistance and cyclic resistance of offshore frames structures. To complete our structural analysis 'tool-kit' we also require a method that can solve the non-linear dynamic collapse problem. It is therefore quite natural to investigate whether the pseudo-force method may be extended to include inertial and damping resistances. As it turns out this it is quite straightforward.

We (initially) consider only those structures in which the inertial and damping properties can be adequately represented by a few discrete masses and dampers. That is the class of problems in which the structural response is dominated by low frequency vibration modes. The dynamic collapse of an offshore structure is included in this problem class since most of the effective mass is provided by the topside equipment and superstructure (typically around 20,000 tonnes for a large North Sea platform), and the structure is only lightly damped (about 3% of critical is commonly measured).

In the solution of the reduced dynamical system a two-part incremental iterative algorithm is employed. In the first step of the iterative procedure, the inertial and damping resistances are calculated by solving the equations of motion. These dynamic effects are then applied as additional forces acting on an equivalent non-linear static problem which is solved to provide the pseudo-forces associated with material non-linearity. The material pseudo-forces are then fed back into the equations of motion and the inertial and damping resistances are re-calculated. Iterations proceed until convergence is obtained. The method developed has some similarities with the mode acceleration approach (WILLIAMS, 1945) which is commonly used for the solution of linear-elastic dynamic problems.

A dynamic option is added to the simulation system discussed in the previous chapter, enabling non-linear dynamic analysis to be undertaken with any standard linear-elastic static analysis program.

4.2 PFI-METHOD: THEORY FOR PROBLEMS IN DYNAMICS

We now derive the dynamic PFI-Method, employing heuristic arguments to derive the dynamic equilibrium equations. A more formal proof of the theory is developed later in chapter 7.

Consistent with the notation employed later in chapters 6 and 7, local element variables are represented by lower case while global variables are denoted by upper case.

The dynamic non-linear material model

As with the static theory, we begin with examining the conventional discretisation of the structure. The actual structure (Fig. 4.1a) is represented in Fig. 4.1b by a number of elements, some of which may have non-linear material properties (represented by non-linear bars). Mass and damping properties are assigned to certain nodal points. In this representation, the non-linear incremental element stiffnesses are assembled into a global matrix and mass and damping 'stiffness' terms added. We may view this procedure as setting up a ***dynamic non-linear material model*** which is subjected to time-dependent forces, $\underline{F}^W(t)$.

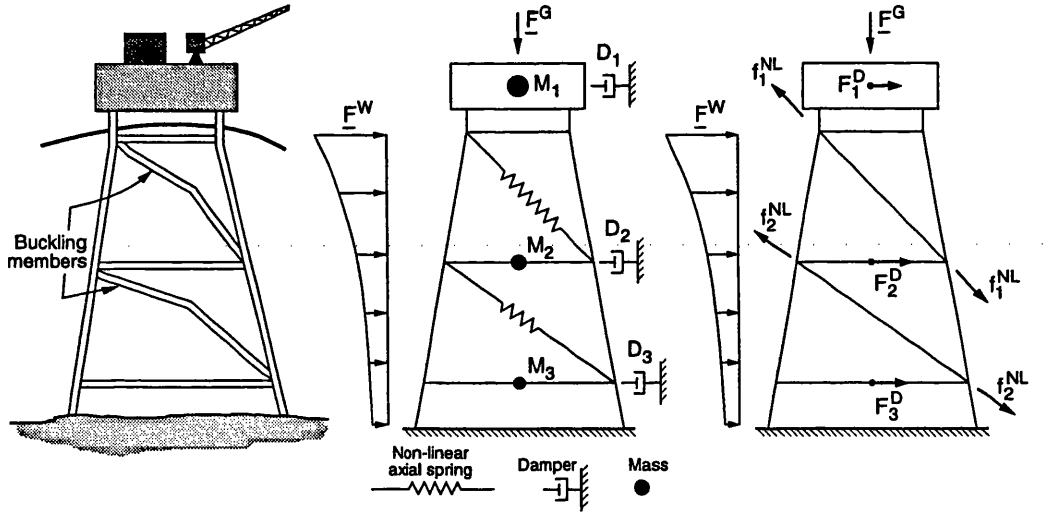

(a) Actual structure *(b) Non-linear model* *(c) Linear elastic model*

Fig. 4.1 Equivalent representation of nonlinear dynamic problem

The linear elastic reference model - dynamic pseudo-forces

For the analysis of static problems, non-linear member behaviour was emulated by applying self-equilibrating pseudo-forces of magnitude f^{NL} to a linear-elastic reference model. In addition, we now represent dynamic mass/damping effects by displacement-dependent

dynamic pseudo-forces, of magnitude F^D (Fig. 4.1c). Unlike the material pseudo-forces, the dynamic pseudo-forces are not self-equilibrating. Our task is to establish the magnitude of these pseudo-forces such that the deformations and displacements in the linear elastic reference model and the dynamic non-linear material model are equal.

The dynamic pseudo-forces are easily identified as being D'Alembert's representation of inertial/damping resistances (see, for example, CLOUGH & PENZIEN, 1974). Thus, if there are in total L mass/dampers acting on global d.o.fs. $\underline{U}$, (which represent a subset of the total nodal displacement vector), the dynamic pseudo-forces acting on these d.o.fs. are simply

$$F_i^D = -(M_i\ddot{U}_i + C_i\dot{U}_i) \qquad i = 1, L \tag{4.1}$$

or

$$\underline{F}_U^D = -(\boldsymbol{M}\ddot{\underline{U}} + \boldsymbol{C}\dot{\underline{U}}), \tag{4.2}$$

where the over-dots represent time derivatives, and $\boldsymbol{M}$ and $\boldsymbol{C}$ are diagonal mass and damping matrices, which respectively operate on the nodal acceleration and velocity vectors. The subscript U on $\underline{F}_U^D$ highlights the dependency on the global displacement. Recognising that $\underline{F}_U^D = \boldsymbol{I}\underline{F}_U^D$, where $\boldsymbol{I}$ is the identity matrix, one can see that each F_i^D may be interpreted as a load factor associated with a unit load applied to displacement freedom i (which will be a useful concept when influence matrices are considered).

Reduced-system equations for non-linear dynamics

We now imagine the linear-elastic structure acted upon by several load-sets, each of which will have an influence on all d.o.fs. U_i as well as on all non-linear element deformations. It is therefore apparent that, at any time t, the ***reduced system equations*** for the non-linear dynamic problem may be written (STEWART, 1992) as

$$\underline{U} = \underline{U}^L + \boldsymbol{H}^{U\eta}\,\underline{f}_\eta^{NL} + \boldsymbol{H}^{UU}\,\underline{F}_U^D \qquad (L \text{ equations}) \tag{4.3a}$$

$$\underline{\eta} = \underline{\eta}^L + \boldsymbol{D}^{\eta\eta}\,\underline{f}_\eta^{NL} + \boldsymbol{D}^{\eta U}\,\underline{F}_U^D \qquad (M \text{ equations}) \tag{4.3b}$$

or

$$\begin{bmatrix}\underline{U}\\ \underline{\eta}\end{bmatrix} = \begin{bmatrix}\underline{U}^L\\ \underline{\eta}^L\end{bmatrix} + \begin{bmatrix}\boldsymbol{H}^{UU} & \boldsymbol{H}^{U\eta}\\ \boldsymbol{D}^{\eta U} & \boldsymbol{D}^{\eta\eta}\end{bmatrix}\begin{bmatrix}\underline{F}_U^D\\ \underline{f}_\eta^{NL}\end{bmatrix} \tag{4.3c}$$

in which $\underline{U}^L(t)$ and $\underline{\eta}^L(t)$ are obtained from the solution of the linear static problem with applied external loading $\underline{F}^L(t)$ only, and $\boldsymbol{H}^{U\eta}$, $\boldsymbol{H}^{UU}$, $\boldsymbol{D}^{\eta U}$, $\boldsymbol{D}^{\eta\eta}$ are the (time-independent) ***reduced system elastic influence matrices.*** The $\boldsymbol{H}$ matrices are displacement influence matrices whereas the $\boldsymbol{D}$ matrices are deformation influence matrices. It will be shown later in chapter 7 (see eqn. (7.48)) that $\boldsymbol{H}^{U\eta} = (\boldsymbol{D}^{\eta U})^T$ and that both $\boldsymbol{D}^{\eta\eta}$ and $\boldsymbol{H}^{UU}$ are symmetric.

The columns of these matrices are obtained directly from the equivalent linear elastic model as follows:

H^{UU}: apply unit loads to each d.o.f. U_i (i = 1 to L) and obtain the displacements $\underline{U}$. This matrix has dimension (L, L).

$H^{U\eta}$: apply unit tensile forces to the ends of 'non-linear' element i and obtain the displacements $\underline{U}$. Repeat for i = 1 to M. This matrix has dimension (L, M).

$D^{\eta\eta}$: apply unit tensile forces to the ends of 'non-linear' element i and obtain the deformations $\underline{\eta}$. Repeat for i = 1 to M. This matrix has dimension (M, M) and is the same as that introduced previously for static non-linear analysis.

$D^{\eta U}$: apply unit loads to each d.o.f. U_i (i = 1 to L) in turn and obtain the deformations $\underline{\eta}$. This matrix has dimension (M, L).

This procedure is shown in Fig. 4.2 for a structure with two non-linear elements and two masses.

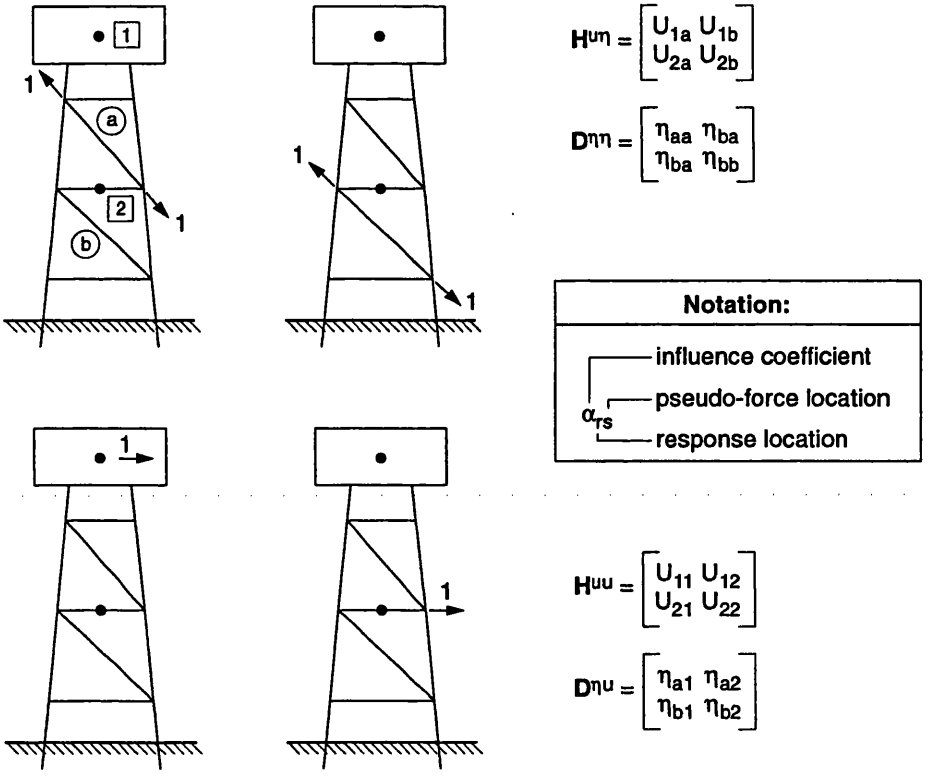

Fig. 4.2 Obtaining the influence matrices for dynamic analysis

The system (4.3a & 4.3b) may also be written as

$$\underline{U} = \underline{U}^L + \underline{U}^{NL} + \underline{U}^D \tag{4.4a}$$

$$\underline{\eta} = \underline{\eta}^L + \underline{\eta}^{NL} + \underline{\eta}^D. \tag{4.4b}$$

Thus the displacements and deformations comprise a contribution from the applied loading with corrections for material non-linearity and inertia/damping forces.

Solving the non-linear system (4.3c) (see section 4.3) for each time step yields the unknowns $\underline{f}_{\eta}^{NL}$ and $\underline{F}_{U}^{D}$, and also provides the deformations and displacements of the locations at which pseudo-forces act. As with the procedure for static problems, the deformations/stresses in the linear-elastic elements can easily be calculated as all loading on the equivalent linear-elastic model is now completely defined. Normally this is a post-processing step. Any additional elements that subsequently deform beyond their linear-elastic range can then be added to the non-linear group, and the procedure repeated. This is discussed in more detail in section 4.4, where we describe how to modify the static simulation system to include dynamic effects.

The total number of equations in the reduced non-linear dynamic system is $n = M + L$. For many problems this is only a fraction of the total number of degrees of freedom in the linear-elastic model. Typically, for dynamic collapse analyses of offshore framed structures, n is less than 20. Thus for these types of problems, the proposed method is extremely efficient.

4.3 SOLUTION PROCEDURE FOR DYNAMICS PROBLEMS

The solution procedures employed for dynamic problems are simpler than those used in static problems since equilibrium is always possible whatever the magnitude of the applied load. For static problems, we had to use special methods to trace limit points. However in dynamic problems as the structure loses strength, the excess load is absorbed by the inertial and damping resistances. The dynamic resistance limits the distance of travel along the solution curve for any increment of the external load, providing a role similar to arc length control for the static problem.

In this section, we provide an effective and efficient algorithm for the solution of the reduced system of equations (4.3c) at discrete time steps, $t = t_n$, $n = 0,1,2.....$ The method proposed is by no means the only one possible but is straightforward. We first linearise (4.3c) using the standard (modified) Newton procedure given in appendix C, leading to

$$\begin{bmatrix} \boldsymbol{I} + \boldsymbol{H}^{UU}\overline{\boldsymbol{K}}^{D} & -\boldsymbol{H}^{U\eta}\boldsymbol{k}^{P}_{\eta(i)} \\ \boldsymbol{D}^{\eta U}\overline{\boldsymbol{K}}^{D} & \boldsymbol{I} - \boldsymbol{D}^{\eta\eta}\boldsymbol{k}^{P}_{\eta(j)} \end{bmatrix} \begin{bmatrix} \Delta\underline{U} \\ \Delta\underline{\eta} \end{bmatrix} = -\begin{bmatrix} \underline{g}_{U} \\ \underline{g}_{\eta} \end{bmatrix}_{(k)} \qquad i,j \leq k \tag{4.5}$$

where the residuals at iteration k are given by

$$-\underline{g}_{U(k)} = \underline{U}^{L} + (\boldsymbol{H}^{U\eta}\underline{f}_{\eta}^{NL} + \boldsymbol{H}^{UU}\underline{F}_{U}^{D} - \underline{U})_{(k)} \tag{4.6a}$$

$$-\underline{g}_{\eta(k)} = \underline{\eta}^{L} + (\boldsymbol{D}^{\eta\eta}\underline{f}_{\eta}^{NL} + \boldsymbol{D}^{\eta U}\underline{F}_{U}^{D} - \underline{\eta})_{(k)} \,. \tag{4.6b}$$

In equation (4.5), the diagonal matrix $\overline{\boldsymbol{K}}^{D}$ is given by

$$\overline{\boldsymbol{K}}^{D} = -\frac{\partial \underline{F}_{U}^{D}}{\partial \underline{U}} \tag{4.7}$$

and this may be called the ***reduced nodal dynamic stiffness matrix*** (of dimension L x L), while k_η^P we introduced earlier (see 3.20) as the element plasticity matrix. The subscript on the element plasticity matrix in (4.5) indicates the iteration at which the matrix is updated. Note that i need not equal j and consequently, at any given iteration, different stiffness matrices may be used (if desired) in the overall system matrix given by the left hand side of (4.5).

In principle, equations (4.5) could now be solved directly for time t_n, iterating until convergence. Then the time would be incremented to t_{n+1} and so on until the solution was obtained for the overall time interval desired. However, as in the solution of the static system with a general constraint, the coefficient matrix is non-symmetric. A simpler solution procedure is therefore proposed.

The uncoupled system

The system is easily uncoupled by setting $k^P_{\eta(i)} = 0$, which corresponds to an initial stiffness procedure for estimating the displacements. At iteration k this results in

$$\Delta \underline{U} = -(\boldsymbol{I} + \boldsymbol{H}^{UU}\overline{\boldsymbol{K}}^D)^{-1}\underline{g}_{U(k)} \; ; \qquad d\underline{U}_{(k+1)} = d\underline{U}_{(k)} + \Delta \underline{U} \; . \tag{4.8}$$

which enables the accelerations and velocities to be calculated (see eqns. (4.12a) and (4.12b) below). Thus the dynamic force can be now be updated and the residual (4.6b) becomes

$$-\underline{g}_{\eta(k)} = \underline{\eta}^L + (\boldsymbol{D}^{\eta\eta}\underline{f}^{NL}_{\eta} - \underline{\eta})_{(k)} + \boldsymbol{D}^{\eta U}\underline{F}^D_{U(k+1)} \; . \tag{4.9}$$

The deformations are then obtained from

$$\Delta \underline{\eta} = -\left[\overline{\boldsymbol{K}}_{\eta(j)}\right]^{-1}\underline{g}_{\eta(k)} \; ; \qquad d\underline{\eta}_{(k+1)} = d\underline{\eta}_{(k)} + \Delta \underline{\eta} \tag{4.10}$$

where the reduced stiffness matrix $\overline{\boldsymbol{K}}_\eta = \boldsymbol{I} - \boldsymbol{D}^{\eta\eta}\boldsymbol{k}^P_\eta$ was introduced previously for static analyses (see eqn. (3.20)).

Clearly it is important that the matrix $\overline{\boldsymbol{K}}_\eta$ in (4.10) does not become singular. This is guaranteed if an initial stiffness method is used, in which case $k^P_{\eta(j)} \equiv k^P_{\eta(0)}$ is identically zero. The iteration matrix in (4.10) is then the identity operator and the calculation of the deformations is trivial, being given by

$$\Delta \underline{\eta} = -\underline{g}_{\eta(k)} \; . \tag{4.11}$$

In this entire procedure, only the matrix $(\boldsymbol{I} + \boldsymbol{H}^{UU}\overline{\boldsymbol{K}}^D)$ needs to be inverted. If a fixed time step is used the matrix $\overline{\boldsymbol{K}}^D$ is constant (see (4.14)) and only one inversion is required.

Discretisation in time

Following NEWMARK (1959) and as summarised in the text of BATHE (1982), a one step implicit scheme results if the acceleration and velocity vectors are estimated from the displacement at time t_n (the current time) and the displacement at time t_{n-1}. That is

$$\ddot{\underline{U}}_n = a_o(\underline{U}_n - \underline{U}_{n-1}) - a_2\dot{\underline{U}}_{n-1} - a_3\ddot{\underline{U}}_{n-1} \tag{4.12a}$$

$$\dot{\underline{U}}_n = a_1(\underline{U}_n - \underline{U}_{n-1}) - a_4\dot{\underline{U}}_{n-1} - a_5\ddot{\underline{U}}_{n-1} \tag{4.12b}$$

where $\underline{U}_n \equiv \underline{U}(t_n)$ and the constants $a_o - a_5$ are given by

$$\begin{aligned} a_o &= 1/(\alpha\Delta t^2); \quad a_1 = \beta/(\alpha\Delta t); \quad a_2 = 1/(\alpha\Delta t) \\ a_3 &= 1/2\alpha - 1; \quad a_4 = \beta/\alpha - 1; \quad a_5 = \Delta t(\beta/2\alpha - 1) \end{aligned} \tag{4.13}$$

The parameters α and β control the stability of the method and the time step size $\Delta t = t_n - t_{n-1}$ controls the accuracy, as we discuss in more detail below. With this discretisation in time, the dynamic matrix, as defined by (4.7), is given by

$$\overline{K}^D = (a_o M + a_1 C)\,. \tag{4.14}$$

Stability and accuracy

The Newmark method is unconditionally stable (NEWMARK, 1959; BATHE, 1982) (meaning that initial errors do not grow in time) provided $\beta \geq 1/2$ and $\alpha \geq (1/2+\beta)/4$. A common selection, that satisfies the stability requirements and is used in the studies reported later in chapter 5, is $\beta = 1/2$, $\alpha = 1/4$, corresponding to trapezoidal integration. For systems with classical proportional damping, the accuracy of the response in each mode r is governed by the ratio of the time step Δt to the (undamped) modal period, T_r. For linear problems, it is generally accepted (BATHE, 1982) that $\Delta t / T_r < 0.1$ will give reasonable integration accuracy. Overall accuracy is obtained by ensuring that the highest included mode frequency is well above that of the loading (a ratio of at most 3:1 is typically suggested). This also ensures that the loading history is adequately discretised in time. For offshore fixed frames, most of the mass is associated with the topside superstructure and the ratio of the fundamental sway frequencies to the wave excitation frequency is typically higher than 5:1. Therefore for these structures we need only be concerned with the lowest vibration modes.

For non-linear problems, the modal frequencies are time dependent since the stiffness is continuously changing. In principle, the modes should be re-calculated at each time step and the time step size adjusted accordingly to ensure accuracy. However, if the stiffness is softening, the modal frequencies will reduce and this suggests that a time step based upon the initial modal frequencies will be adequate throughout. But this overlooks the fact that abrupt changes in stiffness (which may be viewed as large changes in the pseudo-forces) will introduce high frequency vibrations. For most practical problems the higher vibration modes themselves can be ignored but the time step must be selected such that the time dependent changes in the

pseudo-forces are adequately represented, otherwise the response in the lower modes will be inaccurate. It is best to investigate this more closely on a case by case basis (for example halving the time step and noting the difference in the solution).

Various other implicit integration procedures have been proposed. Established methods are the Houbolt and Wilson-θ methods (HOUBOLT, 1950; BATHE & WILSON, 1973), and the HHT-α method (HILBER, HUGHES, & TAYLOR, 1977) which is a generalisation of Newmark's method. These alternative methods filter out high frequency modal noise whereas the Newmark method does not. They have been devised for systems with many vibration modes. However, in our PFI-Method implementation, we either pre-select a small number of mass points or, as discussed later in section 4.5.4, extract a limited number of modal frequencies. Consequently, we do not have to concern ourselves with filtering high frequency vibration modes and the standard Newmark integration procedure is perfectly satisfactory.

PFI-Method: natural frequencies

As the appropriate time step for acceptable accuracy depends on the natural frequencies of the linear-elastic reference model, we need to be able to identify and extract these frequencies. The equation of (undamped) free vibration follows from (4.3a) and (4.2) and is given by

$$\boldsymbol{H}^{UU}\boldsymbol{M}\ddot{\underline{U}}+\underline{U}=\underline{0}. \tag{4.15}$$

The steady state free vibration response therefore satisfies

$$(\boldsymbol{I}-\mu_i^2\boldsymbol{H}^{UU}\boldsymbol{M})\underline{\psi}_i=0 \qquad i=1,L \tag{4.16}$$

where μ_i are the circular eigen-frequencies (natural period $T_i=2\pi/\mu_i$) and $\underline{\psi}_i$ is the associated eigen-vector. The eigen-values are determined from

$$\det(\boldsymbol{I}-\mu^2\boldsymbol{H}^{UU}\boldsymbol{M})=0\ . \tag{4.17}$$

Any standard solution technique such as sub-space iteration (see, for example, BATHE, 1982) can be used to solve this equation.

Solution of linear dynamic problems

Although the PFI-Method has been presented as a tool for solving problems in non-linear dynamics, it may also be used for linear time dependent problems. In this case, only the displacement dependent equilibrium equation is required and from (4.3a) the linear dynamic problem is the solution to

$$\underline{U}=\underline{U}^L+\boldsymbol{H}^{UU}\underline{F}_U^D\ . \tag{4.18}$$

Since $\underline{F}_U^D$ is linear in $\underline{U}$, the Newmark method converges in one step, and the solution is

$$\underline{U}_n = (\boldsymbol{I} + \boldsymbol{H}^{UU}\overline{\boldsymbol{K}}^D)^{-1}(\underline{U}^L_n + \boldsymbol{H}^{UU}\underline{F}^D_{U_{n-1}} - \underline{U}_{n-1}) \,. \tag{4.19}$$

Summary of solution algorithm for non-linear dynamic analysis

The solution algorithm that is used in our simulation system is summarised in the Box 4.1 below.

Box 4.1 Solution procedure for non-linear dynamic analysis by PFI-Method

Time step size:

$$\det(\boldsymbol{I} - \mu^2 \boldsymbol{H}^{UU}\boldsymbol{M}) = 0; \quad T_i = 2\pi/\mu_i; \quad \Delta t = \alpha T_{\min} \quad (\alpha < 0.1)$$

Invert matrix:

$$\boldsymbol{A} = (\boldsymbol{I} + \boldsymbol{H}^{UU}\overline{\boldsymbol{K}}^D)^{-1}$$

Do for each time step

Initial conditions: $t_{n+1} = t_n + \Delta t$; $\underline{U}_{(o)} = \underline{U}_n$; $\underline{\eta}_{(o)} = \underline{\eta}_n$; etc.,

Iteration counter: $k = 0$

Do until converged

$$-\underline{g}_{U(k)} = \underline{U}^L_{n+1} + (\boldsymbol{H}^{U\eta}\underline{f}^{NL}_{\eta} + \boldsymbol{H}^{UU}\underline{F}^D_U - \underline{U})_{(k)}$$

$$d\underline{U}_{(k+1)} = d\underline{U}_{(k)} - \boldsymbol{A}\underline{g}_{U(k)}$$

$$-\underline{g}_{\eta(k)} = \underline{\eta}^L_{n+1} + (\boldsymbol{D}^{\eta\eta}\underline{f}^{NL}_{\eta} - \underline{\eta})_{(k)} + \boldsymbol{D}^{\eta U}\underline{F}^D_{U(k+1)}$$

$$d\underline{\eta}_{(k+1)} = d\underline{\eta}_{(k)} - \underline{g}_{\eta(k)}$$

$$k = k + 1$$

End do

$$\underline{U}_{n+1} = \underline{U}_n + d\underline{U}_{(k)}; \quad \underline{\eta}_{n+1} = \underline{\eta}_n + d\underline{\eta}_{(k)}; \quad \text{etc.}$$

End do

4.4 EXTENDING THE SIMULATION SYSTEM FOR NON-LINEAR DYNAMICS

The principles involved in the pseudo-force method for non-linear dynamic analysis are exactly the same as those employed in static analysis. Therefore the basic structure of the simulation system described in section 3.6 remains unchanged.

Although, in principle, it is possible to solve any non-linear dynamic problem for the class of structure under consideration, in practice the simulation system that we describe below is best suited to problems of dynamic collapse. We presume that before the non-linear dynamic analysis is performed, the results of the non-linear static analysis are available, and therefore the non-linear members in the static failure mode are known (although the number of non-linear members can expand during the dynamic analysis).

The building blocks in our simulation system are now

- a linear-elastic structural analysis (or finite element) program
- a method for generating the axial load-shortening curves of the non-linear members
- a matrix inversion routine
- an eigenvalue extraction routine to determine the appropriate time step
- a solution procedure to solve the reduced system equations

The steps involved in the entire simulation procedure are:

1. Perform static pushover analysis as described in section 3.6.
2. Apply unit loads to the mass/damper d.o.fs. in linear-elastic reference structure to determine the influence matrix $\boldsymbol{H}^{UU}$.
3. Determine an appropriate time step based on the lowest vibration mode.
4. Invert the matrix $(\boldsymbol{I}+\boldsymbol{H}^{UU}\overline{\boldsymbol{K}}^{D})$.
5. Apply unit loads to the linear-elastic reference structure to determine the influence matrix $\boldsymbol{D}^{\eta U}$ (recall that $\boldsymbol{H}^{U\eta}$ is the transpose of this). (If returning from step 8, update $\boldsymbol{D}^{\eta\eta}$ and generate load-shortening curves for additional non-linear members).
6. Apply the time history of loads to the linear-elastic reference structure and obtain the response vectors $\underline{U}^{L}(t)$ and $\underline{\eta}^{L}(t)$ for the mass d.o.fs. and non-linear members, respectively.
7. Solve the reduced system of equations for all time steps.
8. Post-process at appropriate time steps and check if any other members should be included in the non-linear set. If additional members found, return to step 5.

The implementation of this simulation system has been verified against the MARC general purpose finite element program and, for the examples considered, gave exactly the same results. Some examples are discussed in chapter 5.

The development of this simulation system opens up the possibility of performing non-linear structural dynamics on very large structures with low-cost personal computers. As with its static counterpart, the dynamic simulation system is ideally suited to parametric sensitivity analysis. For example, in dynamic collapse analyses, we are interested in the maximum deformation when the structure is exposed to waves of different magnitude. Once the base-case problem has been set up, subsequent analyses involve repeating steps 6 to 8 for the various force histories under

consideration. Also, repeating the analyses for a different structural mass involves modifying only the diagonal mass matrix and the entire analysis can be re-run without further information from the linear f.e. program.

4.5 PFI-METHOD AND MODAL SUPERPOSITION TECHNIQUES

The matrix equations of motion that result from a finite element discretisation of a structure invariably involve many degrees of freedom. To perform a dynamic analysis by direct time integration of this system requires significant computational resources. Therefore much research has been undertaken to develop more efficient schemes aimed at reducing the degrees of freedom. Such techniques are called reduction methods (NOOR, 1981, 1994), and the most popular class of these is based on modal superposition. These methods are suited to the class of problem in which the frequency content of the loading is low compared with the majority of the vibration modes of the structure (CLOUGH & WILSON, 1979). This covers many practical problems in structural dynamics. It is the intention of this section to compare and contrast the dynamic PFI-Method with procedures based on modal superposition. Although we have previously considered only those structures in which material non-linearity is represented by bar elements, the techniques developed in this section are universally applicable.

Reduction methods use the Rayleigh-Ritz technique (NOOR, 1981) to approximate a large number of unknowns N by a linear combination of a much smaller set of unknowns, r. This is achieved by a linear operator Φ_r which maps the original (physical) basis $\underline{U}$ (containing all displacement freedoms) to a reduced (generalised) basis $\underline{x}_r$. Thus,

$$\underline{U}^* = \Phi_r \underline{x}_r \tag{4.20}$$

where $\underline{U}^*$ is the approximation to $\underline{U}$.

In modal superposition methods, the columns $\underline{\phi}_i$ of the transformation matrix Φ_r are taken to be the r lowest free vibration modes. These are obtained by solving the eigenvalue problem

$$(\boldsymbol{K} - \omega_i^2 \boldsymbol{M})\underline{\phi}_i = \underline{0} \qquad i = 1, r \tag{4.21}$$

where ω_i is the circular frequency associated with eigen-mode $\underline{\phi}_i$, $\boldsymbol{M}$ is the mass matrix (which need not be diagonal) and $\boldsymbol{K}$ is a stiffness matrix which, for non-linear problems may or may not be the initial linear-elastic stiffness.

To do justice to our comparison of the dynamic PFI-Method and modal superposition methods, it is necessary to review the modal methods in some detail. We start with linear systems as the methods applied to non-linear systems use very similar ideas.

4.5.1 Linear systems analysis by modal superposition

(a) Classical modal superposition

Consider the equilibrium equations for a linear-elastic structural system

$$M\ddot{\underline{U}}+C\dot{\underline{U}}+K^E\underline{U}=\underline{F}^L \tag{4.22}$$

in which M is the mass matrix, K^E is the stiffness matrix, C is the damping matrix, and $\underline{F}^L$ is the applied load.

Applying the transformation (4.20), and assuming Rayleigh modal damping[1], the system of equilibrium equations (4.22) are transformed to a reduced set of uncoupled differential equations given by

$$I_r\ddot{\underline{x}}_r+C_r\dot{\underline{x}}_r+\Omega_r^2\underline{x}_r=\Phi_r{}^T\underline{F}^L \tag{4.23a}$$

where

$$I_r=\Phi_r{}^TM\Phi_r \qquad C_r=\Phi_r{}^TC\Phi_r \qquad \Omega_r^2=\Phi_r{}^TK^E\Phi_r\ . \tag{4.23b}$$

The matrix I_r is the identity matrix, C_r is a diagonal damping matrix, and Ω_r^2 is a diagonal matrix whose entries ω_i^2 are the circular frequencies of the linear-elastic system.

We remark that if all modes are included, the superposition method does not involve any approximation and is then simply a change of variable transformation. As such it will yield exactly the same results as a direct solver operating on (4.22) provided the same time marching scheme is used for both approaches. If, however, all modes are included, there is no computational advantage in using the modal method. That is to gain computational efficiency a truncated set of modes must be employed.

In the classical modal superposition method (see for example CLOUGH & PENZIEN, 1974), equation (4.23a) is solved for $\underline{x}_r$ and the displacements are recovered from (4.20). Because only a truncated set of modes are used to approximate the displacements, the local stresses may not be recovered sufficiently accurately using this displacement field. The accuracy of the stresses can be greatly improved by using the *Mode Acceleration Method*, which we now discuss.

(b) Mode Acceleration Method

The mode acceleration method was introduced by WILLIAMS in 1945. Several variants of the method have since been developed (MADDOX, 1975; HANSTEEN & BELL, 1979; CORNWELL *ET AL.*, 1983) but all essentially perform similar operations in a slightly different way. A review of the various methods is given in the publication of SORIANO & VENÂNCIO-FILHO (1988). The idea behind the method is very simple. The modal accelerations and velocities obtained from the

1. For Rayleigh damping, the damping matrix takes the form $C=\alpha M+\beta K^E$, where α and β are constants selected to represent the damping properties of any two modes (usually the lowest two). If we restrict the damping matrix C to be diagonal, then β must be zero and the damping in only one mode can be tuned.

classical procedure are used to calculate the inertia and damping forces and these are then applied to the structure as if they were equivalent static loads. A new estimate of the displacement field is then calculated from the equilibrium equations. That is the updated displacements $\tilde{\underline{U}}$ are calculated from

$$\tilde{\underline{U}} = \left[K^E\right]^{-1}(\underline{F}^L - M\Phi_r \ddot{\underline{x}}_r - C\Phi_r \dot{\underline{x}}_r). \tag{4.24}$$

Now, if the excluded modes are Φ_s with generalised freedoms $\underline{x}_s$, then the exact solution must be given by

$$\underline{U} = \left[K^E\right]^{-1}(\underline{F}^L - M\Phi_r \ddot{\underline{x}}_r - C\Phi_r \dot{\underline{x}}_r - M\Phi_r \ddot{\underline{x}}_s - C\Phi_r \dot{\underline{x}}_s). \tag{4.25}$$

By comparing (4.24) with (4.25), we see that the modal acceleration method neglects the influence of the inertial and damping forces associated with the higher modes. The static response of these modes is included in the term $[K^E]^{-1}\underline{F}^L$ and therefore the modal acceleration method is sometimes referred to as the static correction method. The method employs a well known principle of structural dynamics, namely that high frequency modes resist the applied loading primarily by developing internal forces rather than by mobilising inertial resistance.

4.5.2 Non-linear systems analysis by modal superposition

Superposition methods for non-linear structural dynamics can be based on either the pseudo-force method (NICKELL, 1976; STRICKLIN & HAISLER, 1977; MORRIS, 1977; BATHE & GRACEWSKI, 1981; KUKRETI & ISSA, 1984) or the tangent spectrum method (IDELSOHN & CARDONA, 1985; MOHRAZ, *ET AL.* 1991). In the pseudo-force approach, the eigenvectors of the linear system are used throughout whereas in the tangent spectrum method (or incremental modal superposition method) the eigenvectors associated with the current tangent stiffness are employed. Using updated eigenvectors has two advantages over the linear system eigenvectors. A damping matrix can be used that is proportional to the instantaneous stiffness (for some experiments this seems to give better agreement, MOHRAZ *ET AL.*, 1991) while for each time interval the change in the vibration modes can be monitored. However, there are two problems associated with the tangent method. Firstly, when compared to the pseudo-force method it is very inefficient computationally as the eigenvalue problem has to be solved repeatedly - for a test problem, MOHRAZ *ET AL.* (1991) showed that this procedure only marginally outperforms a direct integration method. Secondly, updating the basis vectors can lead to incompatibility in the displacement, velocity and acceleration fields, introducing a further source of possible error (IDELSOHN & CARDONA, 1985). For the majority of problems in structural mechanics, it would appear that it is preferable to use the initial eigenvectors with the non-linearity treated as pseudo-forces. It is procedures based on this approach that we now discuss.

Non-linear modal superposition using linear-elastic vibration modes

For non-linear dynamic problems, the equilibrium equation derived from a finite element procedure may be expressed as

$$M\ddot{\underline{U}} + C\dot{\underline{U}} + \underline{R}(\underline{U}) = \underline{F}^L \tag{4.26}$$

where $\underline{R}(\underline{U}) = \underline{F}_U^E - \underline{F}_U^{NL}$ is the internal nodal resistance which we have split into a linear-elastic contribution ($\underline{F}_U^E$) and an inelastic correction term ($\underline{F}_U^{NL}$). Since $\underline{F}_U^E = K^E \underline{U}$, the equilibrium equation may equally be written as

$$M\ddot{\underline{U}} + C\dot{\underline{U}} + K^E \underline{U} = \underline{F}^L + \underline{F}_U^{NL} \tag{4.27}$$

where $\underline{F}_U^{NL}$ is now identified as a vector of pseudo-forces in the global co-ordinate system. Applying the transformation (4.20) to (4.27), the reduced modal equations now become

$$I_r \ddot{\underline{x}}_r + C_r \dot{\underline{x}}_r + \Omega_r^2 \underline{x}_r = \Phi_r^T \{\underline{F}^L + \underline{F}_U^{NL}\}. \tag{4.28}$$

The eigenvectors Φ_r, being those of the linear-elastic (reference) system, are called pseudo-modes (KUKRETI & ISSA, 1984) - the true eigen-modes being those associated with the tangent stiffness.

The difference between the linear problem (4.23a) and the non-linear problem (4.28) is that in the latter the pseudo-force vector couples together the reduced equations of the non-linear system and these must now be solved iteratively for $\underline{x}_r$. The displacements are recovered from (4.20). This procedure dates back to the mid 1970s and early 1980s (NICKELL, 1976; STRICKLIN & HAISLER, 1977; MORRIS, 1977; CLOUGH & WILSON, 1979; BATHE & GRACEWSKI, 1981; GESCHWINDER, 1981; KUKRETI & ISSA, 1984) and is still being proposed in more recent literature (KUKRETI, 1989; CHANG & MOHRAZ, 1990).

The modal acceleration method can once again be used to improve the accuracy of the classical method (ELKATT & MILLER, 1989). In this case, for each time step we iteratively solve the two systems

$$\ddot{\underline{x}}_{r(k+1)} + C_r \dot{\underline{x}}_{r(k+1)} + \Omega_r^2 \underline{x}_{r(k+1)} = \Phi_r^T (\underline{F}^L + \underline{F}_{U(k)}^{NL}) \tag{4.29a}$$

$$d\underline{U}_{(k+1)} = d\underline{U}_{(k)} + K_{(j)}^{-1} \{\underline{F}^L - M\Phi_r \ddot{\underline{x}}_{r(k+1)} - C\Phi_r \dot{\underline{x}}_{r(k+1)} - \underline{R}(\underline{U}_{(k)})\}. \tag{4.29b}$$

Here we have made use of a modified Newton iteration scheme for the equilibrium iterations in which $K_{(j)}$ is the stiffness matrix at any point on the solution path. This is more general than the initial stiffness iterations employed by Elkatt and Miller.

In this form, the method is not very attractive, since the solution of (4.29b) requires an iterative process on a large system of non-linear equations. However, the effectiveness of the method can surely be greatly enhanced by applying the well known static condensation procedure (see for example CLOUGH & PENZIEN, 1974) to (4.29b), such that only those degrees of freedom upon which

$\underline{F}_U^{NL}$ acts are retained as master freedoms. We proceed by segregating the displacement degrees of freedom into two sets $\underline{U}_1$, and $\underline{U}_2$, where the first contains the master freedoms associated with nodes that are connected to non-linear elements, while the second contains freedoms that are connected solely to elastic elements. The incremental form of the equilibrium equations (4.29b) may then be written as

$$\begin{bmatrix} K_{11_{(j)}} & K_{12} \\ K_{21} & K_{22} \end{bmatrix} \begin{bmatrix} \Delta\underline{U}_1 \\ \Delta\underline{U}_2 \end{bmatrix} = \begin{bmatrix} \underline{F}_1^L + \underline{F}_1^D - \underline{R}_1 \\ \underline{F}_2^L + \underline{F}_2^D - \underline{F}_2^E \end{bmatrix}_{(k)} = \begin{bmatrix} \Delta\underline{F}_1 \\ \Delta\underline{F}_2 \end{bmatrix}_{(k)} \tag{4.30}$$

where $\underline{F}^D$ is the dynamic force obtained from the modal solution, and $\underline{R}_1$ and $\underline{F}_2^E$ are the respective resistance contributions from the non-linear and linear portions of the structure. The matrix $K_{11_{(j)}}$ is associated with non-linear elements while the other matrices represent stiffness contributions from linear-elastic elements. Employing the standard condensation procedure leads to the reduced system

$$d\underline{U}_{(k+1)} = d\underline{U}_{(k)} + \tilde{K}_{(j)}^{-1}\Delta\tilde{\underline{F}}_1 \tag{4.31}$$

where

$$\tilde{K}_{(j)} = K_{11_{(j)}} - K_{12}K_{22}^{-1}K_{21} \qquad \text{and} \qquad \Delta\tilde{\underline{F}}_1 = \Delta\underline{F}_1 - K_{12}K_{22}^{-1}\Delta\underline{F}_2. \tag{4.32}$$

We now only have to solve a small number of equations for the equilibrium iterations. Since the condensation procedure operates on the stiffness matrices used for the static problem and partitions the model into two sub-structures (a linear one and a non-linear one), this method may be referred to as a ***modal superposition technique with static sub-structuring***. The method appears to be new.

The combination of modal methods and condensation procedures has been suggested before but applied in a different way. ***Modal superposition with dynamic sub-structuring*** has been employed by CLOUGH & WILSON (1979), and IBRAHIMBEGOVIC & WILSON (1990). In this method, the condensation procedure is applied directly to the incremental form of the dynamic equilibrium equations (4.27) which results in the mass and damping matrices being included in the matrix partitioning. Modal superposition is used to derive the response of the linear sub-structure and the mode synthesis technique (see, for example, KERSTENS, 1984) is employed to match (or synthesise) the response of the two sub-structures across their common nodal boundaries.

Both the suggested condensation methods are most effective if the majority of non-linear elements are known in advance. This is (almost certainly) the case for a dynamic collapse analysis of a structure if a static pushover analysis has already been performed as it is unlikely that the inertial loading will modify the failure mode. Although back-substitution for the slave freedoms to check whether any more elements have strained into the non-linear response range is a computational overhead, this need not be done at each time step. If the non-linear elements are not known in advance, the methods become less efficient as the condensation/sub-structuring has to be performed each time another element becomes non-linear.

Condensation without modal superposition is also an option that has been considered (CLOUGH & WILSON, 1979; BATHE & GRACEWSKI, 1981). Although no approximation is made in the internal

linear-elastic element response, the penalty is that back-substitution is required at the end of each time step to calculate the initial conditions for the subsequent step. This diminishes the efficiency of the method.

4.5.3 PFI-Method expressed in modal form

We recall that in the PFI-Method, $\underline{U}$ includes only the L freedoms to which masses or dampers are attached. The equations (4.3a & 4.3b) obtained for the PFI-Method can be put in a form that allows comparison with the previously discussed modal methods.

Let the matrix Ψ (of dimension $L \times L$) represent all of the modes $\underline{\psi}_i$ (given by (4.16)) of the reduced system (4.3a). Denoting a generalised basis as $\underline{\xi}$, which has the same dimension as $\underline{U}$, the modal transformation becomes

$$\underline{U} = \Psi \underline{\xi} \tag{4.33}$$

and from (4.3a) and (4.3b) we obtain the governing systems of equations as

$$\tilde{I}\ddot{\underline{\xi}}_{(k+1)} + \tilde{C}\dot{\underline{\xi}}_{(k+1)} + \tilde{\Omega}^2 \underline{\xi}_{(k+1)} = \Psi^T (\underline{U}^L + H^{U\eta} \underline{f}^{NL}_{\eta(k)}) \qquad \text{(small no. of eqns.)} \tag{4.34a}$$

$$d\underline{\eta}_{(k+1)} = d\underline{\eta}_{(k)} + \left[\overline{K}_{\eta(j)}\right]^{-1} \left\{ \underline{\eta}^L + D^{\eta\eta} \underline{f}^{NL}_{\eta(k)} + D^{\eta U} \underline{F}^D_{(k+1)} - \underline{\eta}_{(k)} \right\} \text{(small no. of eqns.)} \tag{4.34b}$$

where

$$\tilde{I} = \Psi^T H^{UU} M \Psi \qquad \tilde{C} = \Psi^T H^{UU} C \Psi \qquad \tilde{\Omega}^2 = \Psi^T \Psi$$

and

$$\underline{F}^D_{(k+1)} = -\left[M\Psi \ddot{\underline{\xi}}_{(k+1)} + C\Psi \dot{\underline{\xi}}_{(k+1)} \right]. \tag{4.35}$$

The matrix $\tilde{C}$ is a diagonal damping matrix, and $\tilde{\Omega}^2$ is a diagonal matrix whose entries μ_i^2 are the squares of the circular natural frequencies. Incidentally, we note that we can write

$$\begin{aligned} D^{\eta U} \underline{F}^D &= -(D^{\eta U} M \Psi \ddot{\underline{\xi}} + D^{\eta U} C \Psi \dot{\underline{\xi}}) \\ &= -(D^{\eta M} \ddot{\underline{\xi}} + D^{\eta C} \dot{\underline{\xi}}) \end{aligned} \tag{4.36}$$

wherein $D^{\eta M} = D^{\eta U} M \Psi$ is the modal mass deformation influence matrix whose columns are the deformation in the 'nonlinear' elements when each $M\underline{\psi}_i$ is applied to the linear-elastic model, and $D^{\eta C} = D^{\eta U} C \Psi$ is the modal damping deformation influence matrix whose columns are the deformation in the 'nonlinear' elements when each $C\underline{\psi}_i$ is applied to the linear-elastic model.

Comparing the set of equations (4.29a) and (4.31) with (4.34a) and (4.34b), we see that the PFI-Method is very similar to the method we called modal superposition technique with static sub-structuring. The main differences are that whereas the modal technique with static sub-structuring is based on displacements and a global force vector, the PFI-Method employs local element deformations and material pseudo-forces that are applied in the local co-ordinate system.

The PFI-Method will be more efficient if there are few non-linear elements that do not have common nodal points. This is typically the case in offshore framed structures. For more general structures, where the non-linear regions are represented by more complex elements such as plates or shells, the modal superposition technique with static sub-structuring will result in a smaller number of degrees of freedom.

In the pseudo-force method developed so far, material non-linearity is represented by local element pseudo-forces. We refer to this as an element pseudo-force method (EPFI-Method). In chapter 7 we also explore the development of nodal pseudo-force methods (NPFI-Methods) in which the pseudo-forces are applied to the nodal points. The reduced dynamic equations of the NPFI-Method are very similar in form to those of the system of equations derived using the modal superposition technique with static sub-structuring. Both methods also have the same number of unknowns. However the stiffness matrix inversion required in (4.32) with the sub-structuring technique is avoided if the NPFI-Method is used (see chapter 7 for details).

4.5.4 Structures with many masses

The modal technique allows us to extend the PFI-Method concept to include the option of structures in which the mass is not confined to a small number of nodal points. However, the calculation of the influence matrix $\boldsymbol{H}^{UU}$ which is required to evaluate the modes shapes $\underline{\psi}_i$ (see (4.16)) now poses a problem because of the large number of unit loads that would be required to generate it. Therefore a somewhat different approach is required than that developed previously. We let $\underline{U}$ represent all of the nodal displacements and, instead of using (4.34a), adopt the direct modal form given by (4.29a). This provides

$$\boldsymbol{I}_r \ddot{\underline{x}}_{r(k+1)} + \boldsymbol{C}_r \dot{\underline{x}}_{r(k+1)} + \Omega_r^2 \underline{x}_{r(k+1)} = \Phi_r^T (\underline{F}^L + \boldsymbol{Z}_\eta^T \underline{f}^{NL}_{\eta(k)}) \tag{4.37}$$

where $\boldsymbol{I}_r$, $\boldsymbol{C}_r$, and Ω_r^2 are given by (4.23b) and $\boldsymbol{Z}_\eta^T$ is the operator that assembles the local pseudo-forces $\underline{f}^{NL}_\eta$ into the global force vector $\underline{F}^{NL}_U$ (for more details see section 7.5). We can also write (4.37) as

$$\boldsymbol{I}_r \ddot{\underline{x}}_{r(k+1)} + \boldsymbol{C}_r \dot{\underline{x}}_{r(k+1)} + \Omega_r^2 \underline{x}_{r(k+1)} = \underline{f}^L_r + \mathrm{H}^{x\eta} \underline{f}^{NL}_{\eta(k)} \tag{4.38}$$

where $\underline{f}^L_r = \Phi_r^T \underline{F}^L$ and $\mathrm{H}^{x\eta}$ is the modal displacement influence matrix given by $\mathrm{H}^{x\eta} = \Phi_r^T \boldsymbol{Z}_\eta^T$.

The problem of applying a large number of unit loads to determine the influence matrix $\boldsymbol{D}^{\eta U}$ in (4.34b) is avoided by using the relationship $\boldsymbol{D}^{\eta U} = (\boldsymbol{H}^{U\eta})^T$. Alternatively, the modal mass and modal damping influence matrices as given by (4.36) may be preferred. The deformations are then recovered from (4.34b) as before.

In principle this procedure may be implemented into a dynamic simulation system. However a drawback is that the linear-elastic structural analysis program must have an eigenmode solution option.

4.6 REFERENCES

BATHE, K.J. (1982), *Finite element procedures in engineering analysis*, Prentice-Hall, New Jersey.

BATHE, K.J., AND GRACEWSKI, S. (1981), "On nonlinear dynamic analysis using substructuring and mode superposition", *Computers & Structs.*, **13**, pp699-707.

BATHE, K.J., AND WILSON, E.L. (1977), "Stability and accuracy analysis of direct integration methods", *Earthquake Eng. & Struct. Dyn.*, **1**, pp283-291.

CHANG C.J, AND MOHRAZ, B. (1990), "Modal analysis of nonlinear systems with classical and non-classical damping", *Computers & Structs.*, **6**, pp1067-1080.

CLOUGH, R.W., AND PENZIEN, J. (1974), *Dynamics of structures*. McGraw-Hill, New York.

CLOUGH, R.W., AND WILSON, E.L. (1979), "Dynamic analysis of large structural systems with local nonlinearities", *Computer Methods in Applied Mechanics & Engineering*, **17/18**, pp107-129.

CORNWELL, R.E., CRAIG, R.R., AND JOHNSON, C.P. (1983), "On the application of the mode acceleration method to structural engineering problems", *Earthquake Eng. & Struct. Dyn.*, **11**, pp679-688.

ELKATT, M.T.H., AND MILLER, M.A. (1989), "On the accuracy of a mode superposition method in nonlinear dynamics", *Proc. 4'th Int. Conf. Civ. Struct. Eng. Comp.*, CIVILCOMP 89, Edinburgh, Scotland.

GESCHWINDER, L.F. (1981), "Nonlinear dynamic analysis by modal superposition", *J. of the Struct. Div.*, **107**, ST12, pp2325-2334.

HANSTEEN, O.E, AND BELL, K. (1979), "On the accuracy of mode superposition analysis in structural dynamics", *Earthquake Eng. & Struct. Dyn.*, **7**, pp405-411.

HILBER, H.M., HUGHES, T.J.R., AND TAYLOR, R.L. (1977), "Improved numerical dissipation for time integration algorithms in structural dynamics", *Earthquake Eng. & Struct. Dyn.*, **5**, pp283-292.

HOUBOLT, J.C. (1950), "A recurrence matrix solution for the dynamic response of elastic aircraft", *J. Aeronautical Sciences*, **17**, pp540-550.

IBRAHIMBEGOVIC, A., AND WILSON, E.L. (1990), "A methodology for dynamic analysis of linear structure-foundation systems with local non-linearities", *Earthquake Eng. & Struct. Dyn.*, **19**, pp1197-1208.

IDELSOHN, S.R., AND CARDONA, A. (1985), "A reduction method for nonlinear structural dynamic analysis", *Computer Methods in Applied Mechanics & Engineering*, **49**, pp253-279.

KERSTENS, J.G.M. (1984), *On the free vibration of modified linear mechanical systems*, PhD Thesis, Delt Univ. of Technology, The Netherlands.

KUKRETI, A.R., AND ISSA, H.I. (1984), "Dynamic analysis of nonlinear structures by pseudo-normal mode superposition method", *Computers & Structs.*, **19(4)**, pp653-663.

KUKRETI, A.R. (1989), "Dynamic response analysis of nonlinear structural systems subject to component changes", *Computers & Structs.*, **32**, pp201-212.

MADDOX, N.R. (1975), "On the number of modes necessary for accurate response and resulting forces in dynamic analyses", *J. App. Mech., ASME*, **42**, pp516-517.

MARC: General purpose finite element program, Marc Research Corporation, Paulo Alto. (1986, version K2-1; 1993, version K5.2).

MOHRAZ, B., ELGHADAMSI, F.E., AND CHANG, C-J. (1991), "An incremental mode superposition for nonlinear dynamic analysis", *Earthquake Eng. & Struct. Dyn.*, **20**, pp471-481.

MORRIS, N.F. (1977), "The use of modal superposition in nonlinear dynamics", *Computers & Structs.*, **7(1)**, pp65-72.

NEWMARK, N.M. (1959), "A method of computation for structural dynamics", *J. of the Eng. Mech. Div.*, ASCE, pp67-94.

NICKELL, R.E. (1976); "Nonlinear dynamics by mode superposition", *Computer Methods in Applied Mechanics & Engineering*, **7(1)**, pp107-129.

NOOR, A.K. (1981), "Recent advances in reduction methods for non-linear problems", *Computers & Structs.*, **13**, pp31-44.

NOOR, A.K. (1994), "Recent advances and applications of reduction methods", *Appl. Mech. Rev.*, **47(5)**, pp125-146.

SORIANO, L.H., AND VENÂNCIO-FILHO, F. (1988), "On the modal acceleration method in structural dynamics: mode truncation and static correction, *Computers & Structs.*, **29**, pp777-782.

STEWART, G. (1992), "Nonlinear structural dynamics by the pseudo-force influence method - Part I: Theoretical considerations ", *Intl. Offshore and Polar Engineering Conf.* (ISOPE), Vol. I, San Francisco.

STRICKLIN, J.A., AND HAISLER, W.E. (1977), "Formulations and solution procedures for nonlinear structural analysis", *Computers & Structs.*, **7**, pp125-136.

WILLIAMS, D. (1945), *Dynamic loads in aeroplanes under given impulsive loads with particular reference to landing and gust loads on a large flying boat*, GB RAE reports SME3309/3316.

Chapter 5

APPLICATION OF THE PFI-METHOD TO FRAMED OFFSHORE STRUCTURES

- Static, cyclic and dynamic response -

5.1 INTRODUCTION

In this chapter, the performance of the PFI-Method is assessed using various examples. The examples serve mixed functions: validation of the PFI-Method against analytical solutions or with solutions found using other f.e. programs (USFOS and MARC); demonstration of the flexibility of the method and consolidation of the concepts discussed earlier, such as spring-back; and perhaps most importantly, confirmation that the method is an efficient tool for practicing engineers to use for non-linear analysis of large offshore framed structures.

Using the principles of the PFI-Method, a stand-alone computer program called SCAPOS (Shell Collapse Analysis Program for Offshore Structures) has been developed which solves the non-linear reduced system equations (either the static equations (3.9) or the dynamic equations (4.3)). SCAPOS, together with any linear-analysis package[1] and a program for developing the member axial response curves, form the simulation system described in sections 3.6 and 4.4. We discussed the development of this simulation system in detail in these sections, but to summarise once more the function of the various building blocks may be helpful. Essentially the system comprises the four modules shown in Fig. 5.1.

5.2 STATIC AND CYCLIC ANALYSES

In this section we consider the static (pushover) response behaviour of idealised problems and structural systems. In a SCAPOS static analysis, increments of load are specified by the user. For each loading increment, a load control strategy is initially adopted with automatic switching to deformation control (see section 3.4.4) if the deformations in any member exceed a certain user specified value (typically set to 25% of the yield deformation). The analysis terminates if all load

1. For convenience, we use USFOS (with the non-linear features switched off) to analyse our linear-elastic reference models.

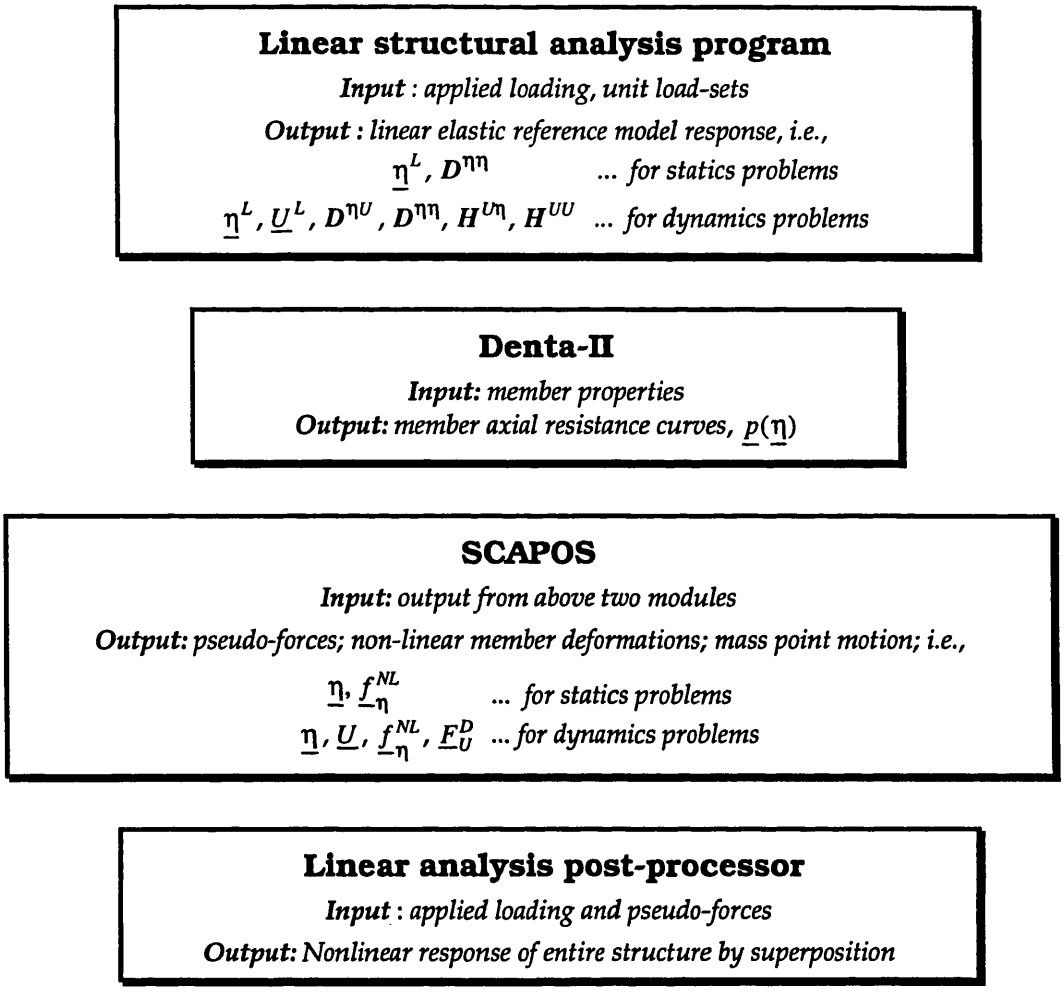

Fig. 5.1 The building blocks in the simulation system

increments have been executed or if the total deformation in any element exceeds a user specified value (typically set to 5 to 10 times the yield deformation).

Example 1: Cantilever beam on non-linear springs

For our first verification example, we consider a problem for which the analytical solution is known. Figure 5.2a shows a linear-elastic cantilevered beam (of height h and lateral stiffness k_b) connected to a rigid base which is supported by three axial foundation springs, each a distance b apart. The initial stiffness of all springs is k_o, however the outer two springs (nos. 1 & 3) exhibit non-linear behaviour when their deformations exceed η^* (with corresponding spring force p^*), as depicted in Fig. 5.2b. The cantilever tip deflects an amount δ when loaded by a force λF^W. At any point in the deformation history, the stiffness of the outermost springs can be represented as a fraction of k_o such that

$$k_1 = \alpha k_o \qquad \text{and} \qquad k_3 = \beta k_o \tag{5.1}$$

where α and β depend on the deformation in springs 1 and 3 respectively.

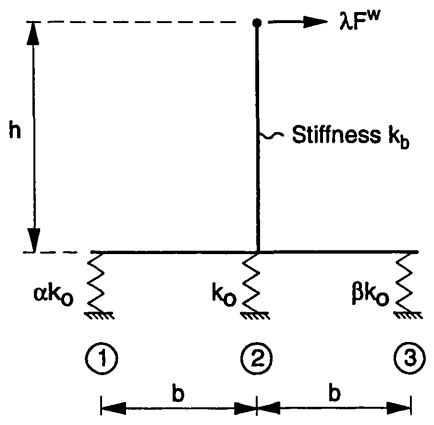

(a) Problem specification

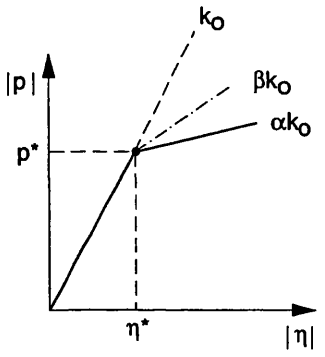

(b) Nonlinear spring characteristics

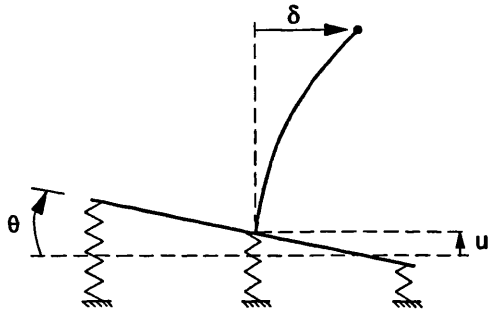

(c) Displacements

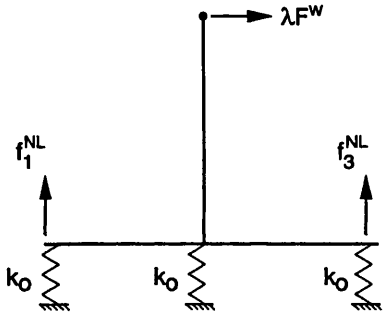

(d) Pseudo - force method

Fig. 5.2 Cantilevered beam on non-linear foundation

Analytical solution

This problem is statically determinate. Considering vertical and rotational equilibrium about the central spring yields the incremental relationships

$$du(1+\alpha+\beta)+b(\alpha-\beta)d\theta=0 \tag{5.2a}$$

$$du(\beta-\alpha)-b(\alpha+\beta)d\theta+\frac{h}{bk_o}d\lambda=0\ . \tag{5.2b}$$

Solving these equations for the displacement and rotation increments du and $d\theta$ (Fig. 5.2c) it is straightforward to relate the increment of applied load to the increment of deformation in spring no. 1 as

$$d\lambda = \frac{k_o}{F^W}\left(\frac{4\alpha\beta+\alpha+\beta}{1+2\beta}\right)\left(\frac{b}{h}\right)d\eta_1 \,. \tag{5.3}$$

Now, since $d\delta = h\,d\theta + F^W / k_b \; d\lambda$, and it may be verified that

$$d\eta_1 = \left(\frac{1+2\beta}{1+\alpha+\beta}\right)b\,d\theta \tag{5.4}$$

and it follows that the load-displacement relationship is given by

$$d\delta = \frac{F^W}{k_o}\left[\left(\frac{h}{b}\right)^2\left(\frac{1+\alpha+\beta}{4\alpha\beta+\alpha+\beta}\right)+\frac{k_o}{k_b}\right]d\lambda \,. \tag{5.5}$$

Equation (5.5) cannot be used directly if spring-back response is expected. Instead, the deformation in spring 1 is incremented and the load increment is calculated from (5.3) while the displacement increment is recovered from (5.5).

Solution by PFI-Method

The data for the problem considered are

$$F^W = 100\,MN; \quad k_o = 1600\,MN/m; \quad k_o / k_b = 8; \quad h/b = 4; \quad \eta^* = 0.125\text{m}; \quad p^* = 200\text{MN}.$$

For this data, non-linearity occurs in springs 1 and 3 at $\lambda = 1$.

From our reference linear-elastic structure (with stiffness k_o for all springs), the influence matrices and response $\underline{\eta}^L$ in the 'non-linear' springs 1 & 3 at $\lambda = 1$ can be determined as:

$$\boldsymbol{D}^{\eta\eta} = \frac{1}{3k_o}\begin{bmatrix} 5/2 & -1/2 \\ -1/2 & 5/2 \end{bmatrix}\begin{matrix}(1)\\(3)\end{matrix}; \qquad \underline{\eta}^L = \frac{F^W}{k_o}\frac{h}{2b}\begin{bmatrix}1\\-1\end{bmatrix}$$

(1) (3)

where the numbers in round brackets are the member identifiers.

Once the pseudo-forces $\underline{f}^{NL}_{\eta}$ have been established for a given load factor, the equivalent loading on the reference structure is known (Fig. 5.2d), and the response of the cantilever tip is obtained (see eqn. 3.11) from

$$\delta = \lambda\delta^W + \boldsymbol{R}^{\delta\eta}\underline{f}^{NL}_{\eta}, \quad \text{where} \quad \boldsymbol{R}^{\delta\eta} = \frac{1}{k_o}\frac{h}{2b}[1 \;\; -1] \quad \text{and} \quad \delta^W = 1.$$

The load-displacement history of the cantilever tip is now determined for three cases, namely:

Case 1: $\alpha = 0.25; \beta = 0.5$ (hardening of springs 1 & 3)

Case 2: $\alpha = -0.3; \beta = 0.5$ (softening of spring 1, hardening of spring 3)

Case 3: as for case 1 but disconnect spring 1 at $\lambda = 1.2$

The tip displacements obtained using SCAPOS for each of these cases are compared to the analytical solution in Fig. 5.3a to Fig. 5.3c, whereupon we observe that the PFI-Method gives the correct response in all three cases.

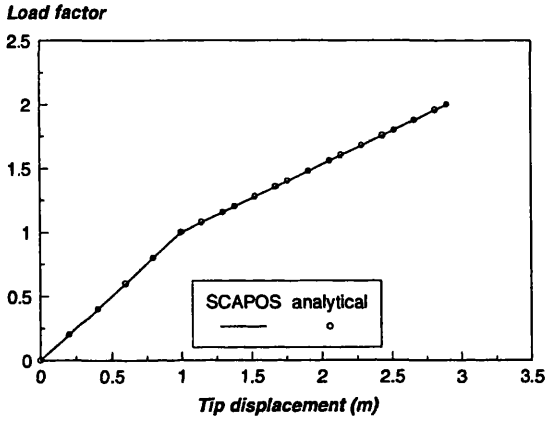

(a) *Case 1: both springs hardening*

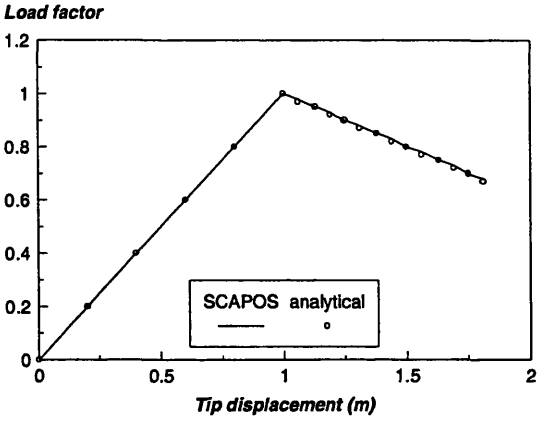

(b) *Case 2: softening of spring 1, hardening of spring 3*

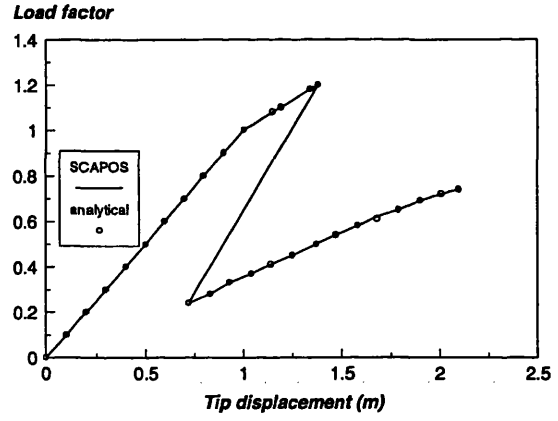

(c) *Case 3: both springs hardening, spring 1 disconnected at* $\lambda = 1.2$

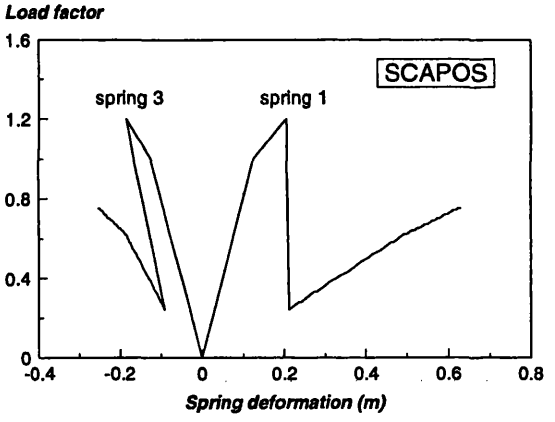

(d) *Case 3: both springs hardening, spring 1 disconnected at* $\lambda = 1.2$

Fig. 5.3 Response of cantilever beam for varying spring properties

Looking now at the particular response curves obtained, we see that for Case 1 (Fig. 5.3a), the load can always be increased whereas for Case 2 (Fig. 5.3b), a limit point is reached when $\lambda = 1$ and the stiffness thereafter becomes negative. For Case 3 (Fig. 5.3c), disconnecting spring 1 causes the load to drop and the release of elastic energy produces a spring-back response. From the SCAPOS analysis in Fig. 5.3d we see that for Case 3, immediately after disconnecting spring 1 the only (absolute) deformation increasing is that of spring 1: thus for a deformation control algorithm, this is the only possible control freedom.

These examples confirm that the incremental solution procedure for static analysis is implemented correctly in SCAPOS and that the deformation control algorithm can properly trace spring-back behaviour.

Example 2: Plane frame

The next example is a plane frame (from ZAYAS *ET AL.*, 1982). The structure is analysed in two ways. In the first approach we use the PFI-Method and represent the critical members by non-linear phenomenological bars whereas in the second analysis the USFOS program is used and the critical members are represented as non-linear elasto-plastic beam elements. The intent of this example is twofold. Firstly, to demonstrate two that the critical members in a braced frame may be represented by non-linear bar elements, and secondly to provide evidence of the satisfactory performance of the PFI-Method when used for frame analysis.

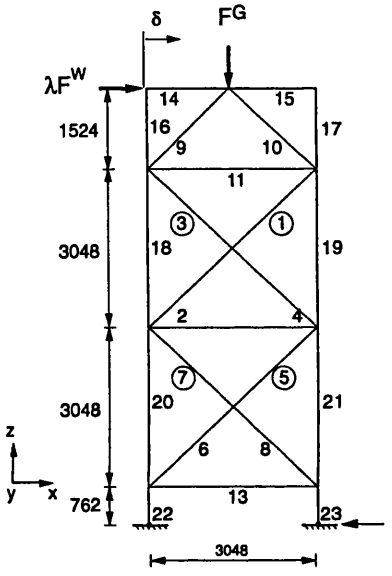

Dimensions in mm.
E = 210 MPa

Element numbers	Member size (mm)	Yield stress (MPa)
16-23	Ø 323.9x7.137	324
9, 10	Ø 152.4x3.175	248
1-4, 11-13	Ø 101.6x2.108	248
5-7	Ø 127.0x3.048	248
14, 15	1397 x 1219 x 50.3F x 26.5W	324

Pinned boundary

(a) Frame details

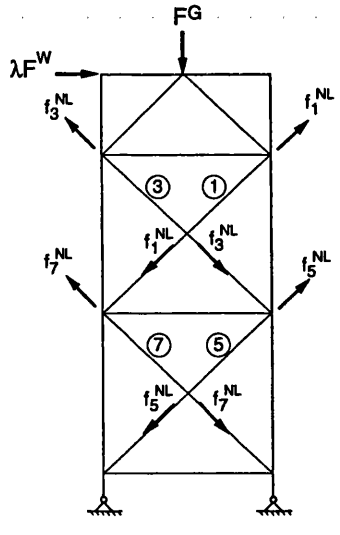

(b) Equivalent linear - elastic model

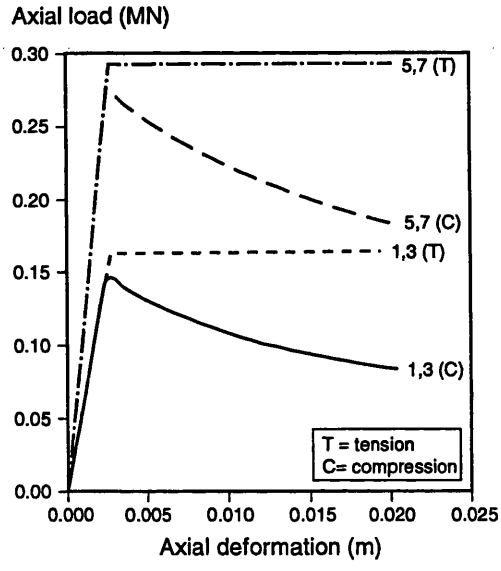

(c) Member axial response data

Fig. 5.4 Plane frame example

The frame under consideration is shown in Fig. 5.4a. It is loaded at the top by a lateral force $F^W = 0.04\text{MN}$ which is scaled by a factor λ. A constant vertical force F^G may also be applied.

The results presented below have been published previously (STEWART & VAN DE GRAAF, 1990; STEWART, 1993).

Influence matrices

From our previous discussion on failure modes of frames (chapter 2), we expect some or all of the bracing elements circled in Fig. 5.4a to play a role in the failure mechanism. The equivalent linear-elastic model therefore has pseudo-forces acting on these members (Fig. 5.4b).

The deformation influence matrix is obtained by applying unit load-sets of magnitude 1 MN to each of these members in turn (ref. Fig. 3.3). Each unit load supplies a column of this matrix (calculated from member axial force divided by axial stiffness), resulting in

$$\boldsymbol{D}^{\eta\eta} = \begin{bmatrix} \overset{(3)}{0.118E\text{-}01} & \overset{(1)}{-0.247E\text{-}02} & \overset{(7)}{0.506E\text{-}03} & \overset{(5)}{0.197E\text{-}03} \\ & 0.118E\text{-}01 & 0.197E\text{-}03 & 0.506E\text{-}03 \\ & & 0.717E\text{-}02 & -0.129E\text{-}02 \\ \text{symmetric} & & & 0.717E\text{-}02 \end{bmatrix} \begin{matrix}(3)\\(1)\\(7)\\(5)\end{matrix} \quad (\text{m/MN})$$

where the numbers in round brackets are the critical member identifiers. The deformations in the 'non-linear' members as a result of the loads $F^W = 0.04\text{MN}$ and $F^G = 0.3\text{MN}$ were found to be

$$\underline{\eta}^W = \begin{bmatrix} \underline{\eta}_3^W \\ \underline{\eta}_1^W \\ \underline{\eta}_7^W \\ \underline{\eta}_5^W \end{bmatrix} = \begin{bmatrix} -0.3791 \\ 0.3791 \\ -0.3206 \\ 0.3206 \end{bmatrix} 10^{-3}\,\text{m} \qquad \text{and} \qquad \underline{\eta}^G = \begin{bmatrix} \underline{\eta}_3^G \\ \underline{\eta}_1^G \\ \underline{\eta}_7^G \\ \underline{\eta}_5^G \end{bmatrix} = \begin{bmatrix} -0.1752 \\ -0.1752 \\ -0.2000 \\ -0.2000 \end{bmatrix} 10^{-6}\,\text{m}.$$

From this information, the linear-elastic member response $\underline{\eta}^L$ can be determined for any value of λ and any multiple of the vertical force (see eqn. (3.14)).

The lateral displacement at the point of application of the lateral load is useful for presenting the results and is given by the relationship

$$\delta = \delta^G + \lambda\delta^W + \boldsymbol{R}^{\delta\eta}\underline{f}_{\eta}^{NL}$$

where $\delta^W = 4.3815\text{x}10^{-3}\text{m}$ is the lateral displacement at $\lambda = 1$ while δ^G, the lateral displacement caused by the vertical load, is negligible. We recall (eqn. (3.11)) that the response influence matrix $\boldsymbol{R}^{\delta\eta}$ is the top displacement for each unit load-set applied to the 'non-linear' members. For this frame it is

$$\boldsymbol{R}^{\delta\eta} = [\overset{(3)}{-9.538} \quad \overset{(1)}{9.538} \quad \overset{(7)}{-8.039} \quad \overset{(5)}{8.039}]10^{-3}\,\text{m/MN}.$$

Member modelling

The member data for SCAPOS was developed following the procedure discussed in section 2.4.2 with the axial-load/shortening curves in compression for the 'non-linear' members obtained from the program DENTA-II (TABY, 1988). An initial midspan imperfection of 0.3% of the length (to ensure proper buckling behaviour - see appendix A) was used. Based on the framing pattern, a buckling effective length factor of 0.7 was considered appropriate for all of the braces, corresponding to fully clamped at one end and pinned at the other. The capacities of the tension members are calculated within SCAPOS using the yield strength and cross-sectional area. The member capacity curves are shown in Fig. 5.4c.

The beam element in USFOS is based on the same plastic hinge theory as the DENTA-II element and therefore 0.3% lateral imperfections were also introduced in the beam elements of the USFOS model.

Pushover analysis - no vertical load

The pushover response of the frame under increasing lateral load (without vertical loading) is compared to that from USFOS in Fig. 5.5a. The frame has a collapse resistance factor of $\lambda = 7.11$. It is observed that the agreement is excellent over the entire response range, including the residual (post-collapse) regime. The failure mode may be classified as ductile. It is controlled by all four bracing elements (failure sequence: 3, 1, 7, 5) with the ultimate strength being achieved when tension member 5 yields, as indicated in Fig. 5.5a. The legs behave elastically throughout as the deformations are not large enough to mobilise their plastic bending capacities. The visualisation of the failure mode shown in Fig. 5.5b was obtained using the graphical display features of the USFOS program.

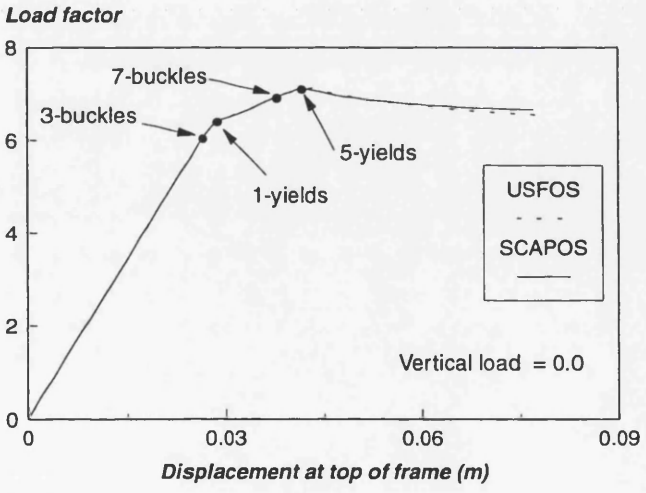

(a) *Pushover response*

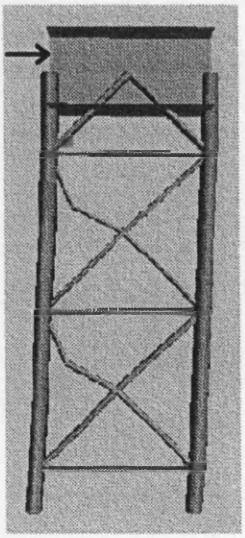

(b) *Failure mode*

Fig. 5.5 Pushover analysis of plane frame

Pushover analysis - significant vertical load

The SCAPOS program does not include the secondary effects of geometric non-linearity on global stiffness, or P-δ influences as they are commonly called. For large offshore platforms, the effective gravity load may be up to twice the environmental force causing collapse. As the platform displaces horizontally, the gravity load produces a de-stabilising moment, but this is typically only a few (1 or 2) percent of the total overturning moment and can either be ignored or included as a knockdown factor on the collapse load. To demonstrate that global P-δ influences are of minor significance for braced frames, the plane frame pushover resistance was assessed at a vertical load $F^G = 0.6\text{MN}$ which provides a vertical to horizontal loading ratio at collapse of approximately 2:1. The results of these analyses are shown in Fig. 5.6. The SCAPOS results are almost identical to those for the frame without vertical load (Fig. 5.5a) which is not surprising given the very low values of gravity loading ($\underline{\eta}^G$) found in the bracing members. For the USFOS analysis, the presence of the vertical load causes some additional deflection because of second order overturning moments, but the peak capacity remains more or less the same, confirming that P-δ influences may be neglected for this structural configuration.

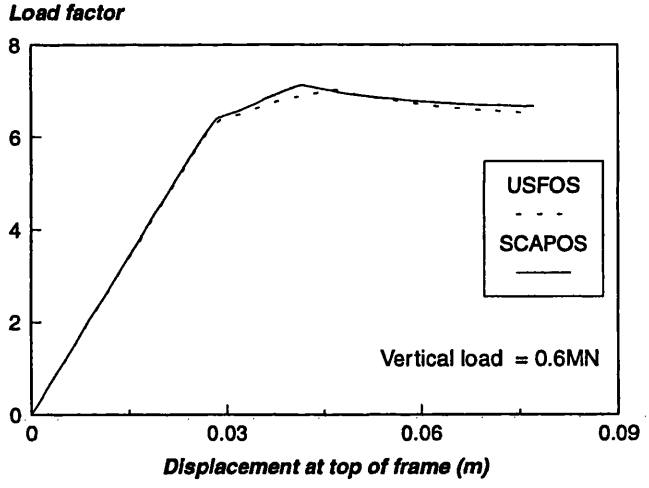

Fig. 5.6 Pushover response curve of plane frame with vertical loading applied

Fracture of tension member

The above analyses assume that all members can plastically deform without ill effect. This corresponds to ductile material behaviour. The presence of a flaw or poor quality material may reduce this ductility and lead to fracture of the member. To allow the consequences of lack of ductility to be investigated, it is possible in our simulation system to disconnect a member at any point in the analysis. This is achieved by setting the member resistance to zero after the critical deformation has been reached.

The SCAPOS results are compared with those from USFOS in Fig. 5.7a for the case in which tensile member no. 1 (see Fig. 5.4a) was disconnected when the global load reached $\lambda = 3.05$. No vertical loading was applied. The agreement between the two methods is once again very good.

With this member disconnected, the peak strength of the frame is reduced from $\lambda = 7.11$ to $\lambda = 6.25$. We observe that the deformation control algorithm employed in SCAPOS follows the spring-back response, whereas USFOS (because it switches to a load-control algorithm when the fracture option is invoked), jumps across the 'valley'.

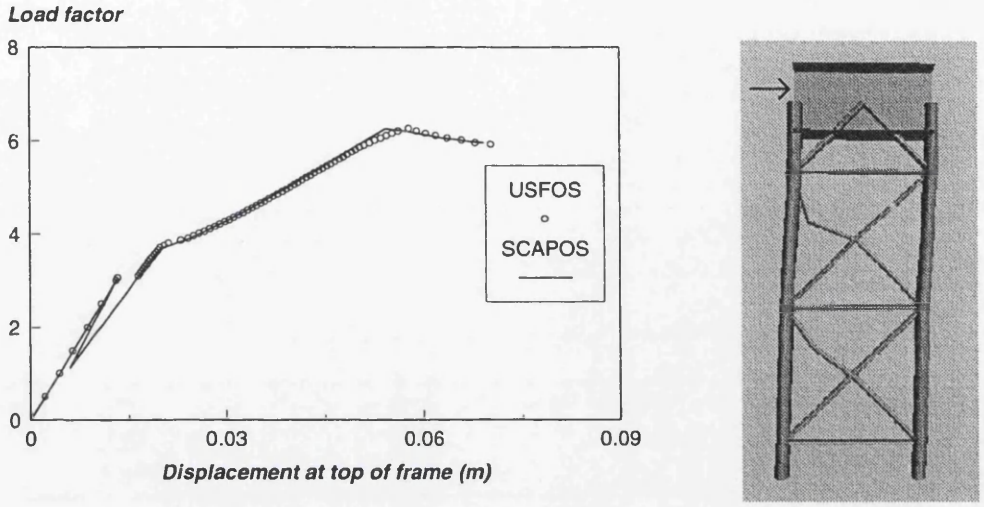

(a) Pushover of plane frame with member 1 disconnected at $\lambda = 3.05$

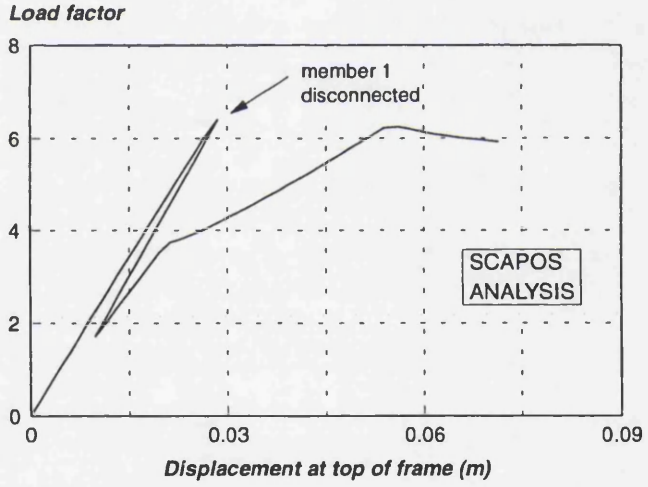

(b) Pushover of plane frame with member 1 disconnected at $\lambda = 6.4$

Fig. 5.7 Pushover of plane frame with member fracture

To further illustrate the robustness of the deformation control algorithm, we disconnected member no.1 when its yield capacity was reached, which corresponds to a global load of $\lambda = 6.4$ (Fig. 5.7b). The spring-back is now very pronounced and a brittle post-ultimate response is observed. The USFOS program is unable to track the frame behaviour for this problem. This is because the load at which fracture is initiated ($\lambda = 6.4$) is above the strength of the frame with the member removed ($\lambda = 6.25$) and consequently the load control algorithm, which is used in USFOS for member fracture problems, will not converge.

Cyclic response

The plane frame (without vertical loading) was subjected to severe cyclic loading with equal intensity in the forward and reverse directions. This loading history is representative more of earthquake motions than of extreme storm loads which are biased positively in the forward direction (forward to reverse loads ratio for storm loading ranges from about 10:1 to 2:1 depending on water depth and current).

As mentioned in section 2.4.2, a phenomenological algorithm has been implemented into our simulation procedure to model the hysteretic behaviour of members under cyclic axial loading. Furthermore, because the forward and reverse loading in this example is described by scaling the same load-set, having performed a pushover analysis a cyclic analyses using the PFI-Method requires no additional input data.

As our implemented incrementation control procedure in SCAPOS is based on member deformations, while USFOS controls on global displacements, it was not straightforward to provide equivalent cyclic loading histories for both methods. The approach taken for the USFOS analysis was to push in the forward direction until just below the collapse strength of $\lambda = 7.11$ and then to cycle the top displacement at a fixed amplitude of 50 mm. For the SCAPOS runs, the load cycles were adjusted such that the frame top displacement was approximately that obtained by USFOS. The tension members in the SCAPOS analysis were given 5% strain hardening after yielding to ensure that the desired global displacements could be reached before overall collapse occurred.

The global response of the frame and the local behaviour of member no. 3 obtained using both SCAPOS and USFOS are shown in Fig. 5.8. Given the approximate nature of the phenomenological algorithm employed in SCAPOS, the agreement between the two different approaches is remarkably good: the peak capacities of the frame on each cycle are very similar, each indicating a slight degradation in strength after the first cycle; and the overall and local hysteretic energy dissipation compares very well.

Although further enhancement of the phenomenological algorithm is possible, this example lends support to the opinion that the present algorithm is adequate to identify structures that are susceptible to cumulative cyclic damage. In such cases, as the analysis progresses one can decide (on the basis of experimental data or experience) whether the hysteretic damage in any member is too severe, and if so, this member may be disconnected from the frame using the "fracture" option. For example, let us assume that having reviewed the results from the analysis shown in Fig. 5.8 we consider that after two high intensity cycles the ductility of member 1 would be exhausted. Disconnecting this element after two cycles provides the response shown in Fig. 5.9. Whether the structural performance is adequate or not would depend on the magnitude and number of high intensity load cycles expected. This is akin to a low cycle fatigue problem.

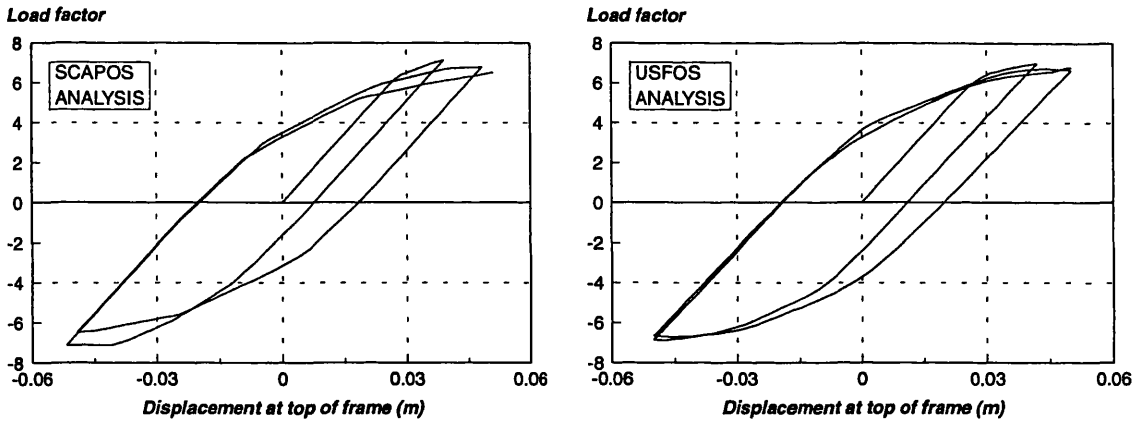

(a) Global response history

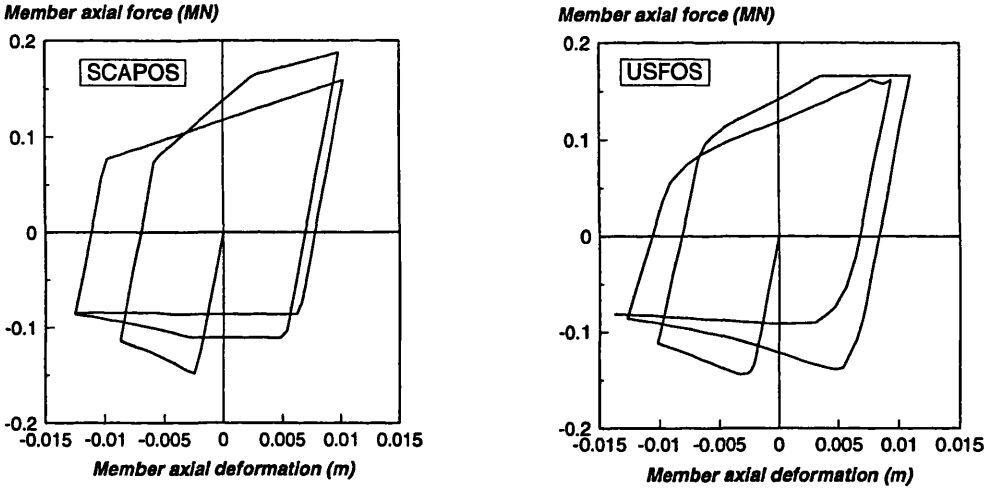

(b) Local response history of member 3

Fig. 5.8 Cyclic response of plane frame

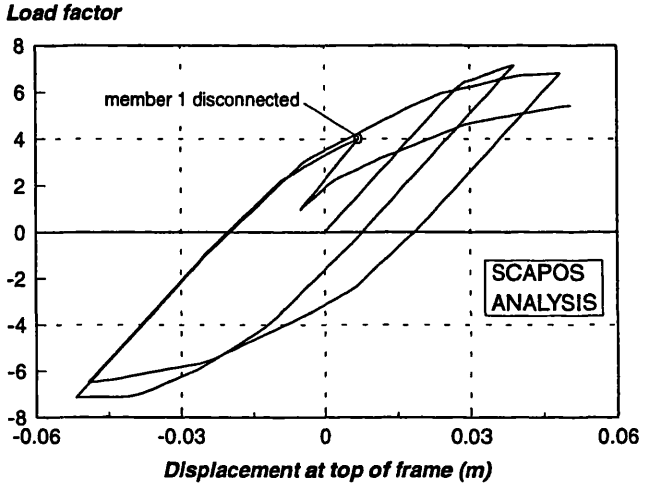

Fig. 5.9 Plane frame with member 1 disconnected after two cycles

This type of analysis could be taken one step further to derive damage response statistics for quasi-statically responding structures exposed to extreme storm loading. Although not included in the present work, it would be a simple task to automatically generate several realisations of a storm's loading and perform cyclic analyses (on the initially intact structure) for each realisation. Elements whose hysteretic energy dissipation exceeded a given value could be automatically disconnected. From such a study, the probability of collapse taking account of degradation in strength during severe storms could be determined.

Example 3: Rigid slab supported by non-linear foundation springs

In example 1, we saw that the influence matrix and other data could be generated automatically for a rigid beam resting on non-linear foundation springs. This principle can be extended to the two-dimensional problem of a rigid slab which finds practical applications in the assessment of the ultimate strength of the foundation systems of jacket structures. The results presented below have been published previously (STEWART & VAN DE GRAAF, 1990).

The model

A steel jacket platform in 140 m water depth is supported by eight pile groups as shown in Fig. 5.10. Assuming that lateral soil/pile failure does not occur, that the jacket strength is adequate, and that the capability of the foundation system to resist overturning moment and vertical loading is determined primarily by the axial resistance of the piles, the problem may be treated as a rigid slab supported by non-linear axial foundation springs.

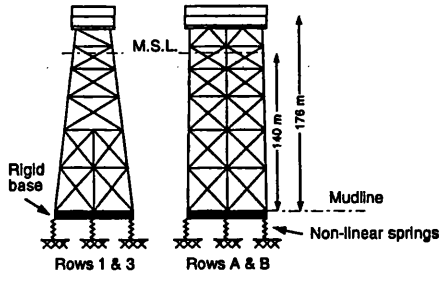

(a) Jacket details

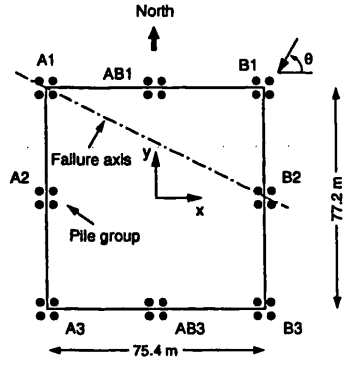

(b) Foundation arrangement

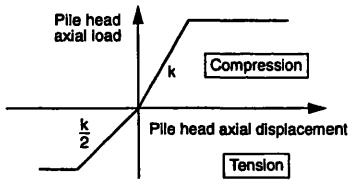

RELATIVE PILE GROUP CAPACITIES		
Pile group	Compression	Tension
A1	1.0	0.44
A2	0.86	0.46
A3	0.80	0.44
AB1	0.83	0.44
AB3	0.49	0.22
B1	1.08	0.45
B2	1.09	0.47
B3	0.94	0.44

(c) Pile data

Fig. 5.10 Platform and foundation details

The pile group axial-load/deflection curves (Fig. 5.10) are modelled as ideal elastic-plastic in compression and tension, with the stiffness in tension being half the compressive stiffness of 2800 MN/m. The pile group capacities given are normalised to the compressive strength of group A1 which has a characteristic strength of 160 MN. The characteristic pile capacities are then multiplied by a factor of 0.88 while the vertical loading is factored by 1.15. Together these factors correspond to a partial factor on foundation resistance of $\gamma_f = 1.15/0.88 = 1.3$, as discussed in section 2.2.2. The on-bottom weight of the platform is 288.9 MN, with centroid at co-ordinates (-4.2m, -3.1m), and the applied environmental overturning moment at a load factor of $\lambda = 1$ is $M^W = 10490$ MNm for all wave attack directions.

Generating the input data for the simulation system

Taking the reference linear-elastic model to comprise eight linear-elastic springs of equal stiffness (k_o = 2800 MN/m), and with the assumption of rigid body deformations at the mudline, all of the influence matrices and load-effects for this model can be determined analytically. That is no structural model is required for the linear-elastic analysis.

Referring to Fig. 5.10b, the co-ordinates of the n piles (with respect to the centroid of the pile system in the reference model) are (x_i, y_i), the eccentricity of the on-bottom weight F^G is (x_G, y_G), and the environmental overturning moment is M^W with attack direction θ. The axial deformation η_i^L in each pile in the reference model is given by

$$\eta_i^L = \eta_i^G + \lambda \eta_i^W$$

where η_i^G is the deformation caused by the gravity loading F^G and η_i^W is that caused by the environmental loading. It easily follows that

$$\eta_i^G = -\frac{F^G}{k_o}\left[1/n + x_G x_i / I_{yy} + y_G y_i / I_{xx}\right]; \quad \eta_i^W = \frac{M^W}{k_o}\left[x_i \cos\theta / I_{yy} + y_i \sin\theta / I_{xx}\right]; \quad i = 1, n$$

where

$$I_{yy} = \sum_1^n x_i^2 \quad \text{and} \quad I_{xx} = \sum_1^n y_i^2$$

are the moments of inertia of the foundation system about the x-x and y-y axes, respectively.

The deformation influence matrix is derived by applying unit tensile forces to the end of each spring in turn, giving

$$D_{ij}^{\eta\eta} = \frac{1}{k_o}\left[1/n + x_i x_j / I_{yy} + y_i y_j / I_{xx}\right], \quad i = 1, n \ .$$

Results - overturning capacity envelope for foundation

The foundation ultimate failure envelope (Fig. 5.11) was obtained by evaluating the ultimate overturning resistance for wave attack directions $0 - 2\pi$. This failure surface is asymmetric

because of the differing pile group capacities. The foundation ultimate failure surface is convex (in agreement with plasticity theory for material models that do not strain-soften) and consists entirely of straight line facets, each of which represents a different failure mode (rotation axis). From the 'flow rule' of plasticity theory, the rotation axes of the failure mechanisms are normal to these facets. A wave attack direction of 60 degrees is the most critical for this structure, corresponding to $\lambda_{ult}^{60} = 1.53$.

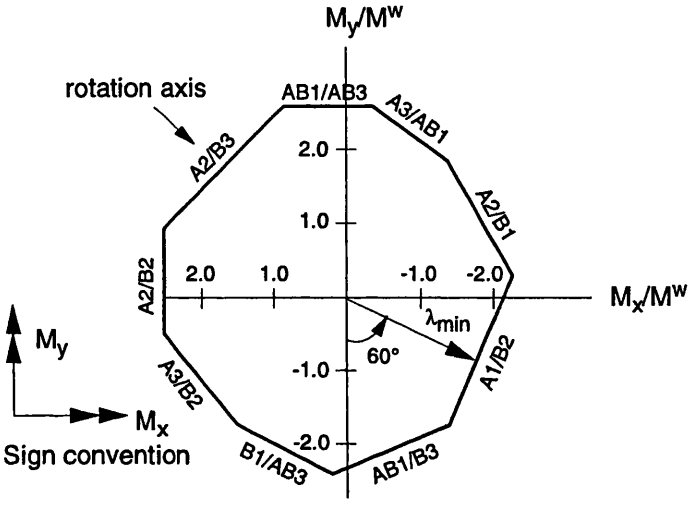

Fig. 5.11 Foundation ultimate failure surface

To verify the rigid body approach, the linear-elastic response data for the complete jacket/foundation system were obtained for the 60 degree wave attack direction using a conventional linear structural analysis package. The SCAPOS simulation was then re-run with this revised data whereupon the same failure mechanism as in the rigid body approach was identified - however the ultimate resistance was some 7% higher which is attributed to the rotational resistance of the piles at the mudline. This verification analysis confirms the usefulness of the rigid body approach as a screening tool for foundation assessments.

Example 4: Analysis of a large 3-D structure

The complexity or size of the structure is of no consequence for the non-linear analysis using SCAPOS - the controlling factor is the number of members in the failure mode. This important principle is demonstrated by the present example, as well as providing verification that for large 3-D structures, non-linear phenomenological bar elements as used in SCAPOS perform equally as well as the beam elements in USFOS.

The structure, which is shown in Fig. 5.12 is a template jacket installed in 65m of water. It is supported by 8 piles that are driven through the legs and connected at the top of the jacket. A diagonal wave-approach direction is considered.

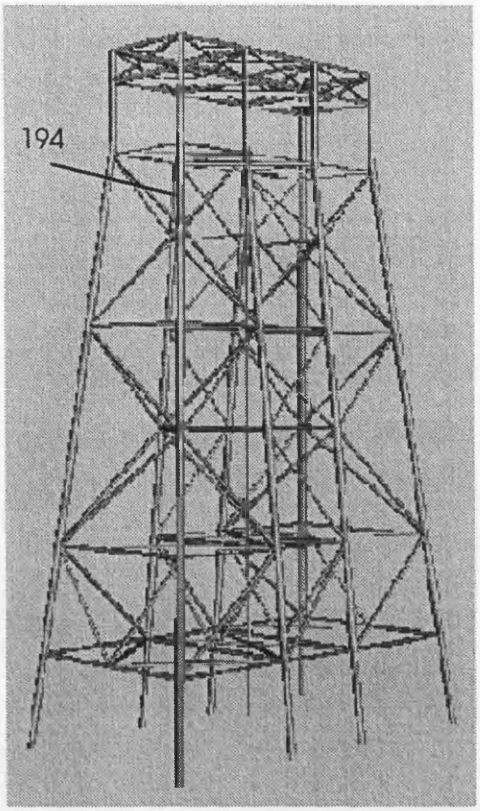

Fig. 5.12 Large 3-D Structure

Pushover analysis

The pushover failure mode is governed by 10 members that fail by buckling, squashing, or tensile yielding. Of these, 5 are leg members while the remainder are diagonal bracing members. These members are all near the water line, where the pile forces are transmitted into the jacket.

Although the linear-elastic model for this structure contains some 334 linear elements, the SCAPOS model for this problem has only 10 deformation variables, one for each of the non-linear members. The axial compression behaviour of the (diagonal) bracing members was generated using the program DENTA-II. Because both ends of these members frame into heavy legs, their effective buckling length factor was selected as 0.5.

The results are compared with those of USFOS in Fig. 5.13. The agreement is extremely good, with the collapse load differing by only 0.5%. Close to the peak load, the USFOS solution ratchets a little. This seems to be caused by recovery of equilibrium after drifting from the plastic yield surface and in certain circumstances progressing the solution further can prove troublesome. This is a common difficulty with many non-linear f.e. packages in frame analysis. The problem seems to be caused by poor arc-length control and iteration procedures that cannot cope with rapid loss of stiffness when members buckle. Perhaps deformation control with path independent iterations (as implemented in SCAPOS and discussed earlier in section 3.4.4) would improve the performance of many f.e. packages.

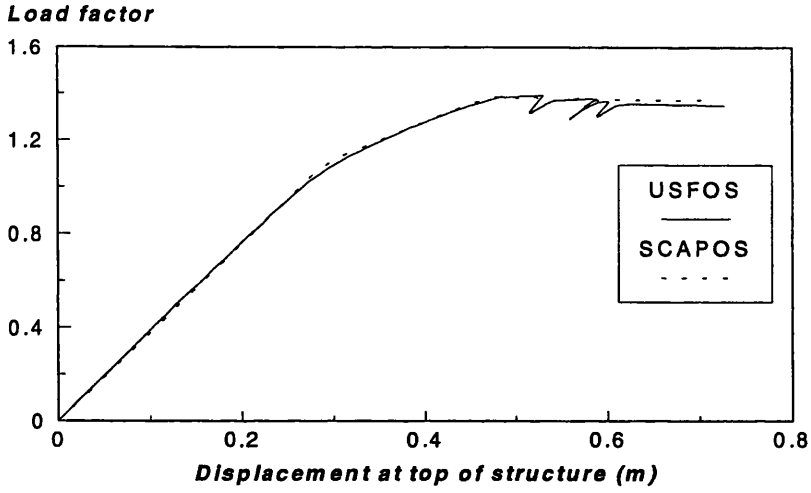

Fig. 5.13 Pushover of 3-D structure

Cyclic analysis

A cyclic analysis of this structure has also been carried out for storm loading. The normalised loading history is shown in Fig. 5.14 and corresponds to that produced by the wave-height sequence defined by (2.7), with the short-term variability factor set to unity. This load history was scaled until the largest force was 98% of the pushover capacity. Member 194 (see Fig. 5.12) is the most heavily loaded in the structure. The results at global level and for leg member 194 are given in Fig. 5.15. The agreement between SCAPOS and USFOS is again satisfactory. Both modelling approaches providing very similar response histories at the global level with the same trend in the local member behaviour.

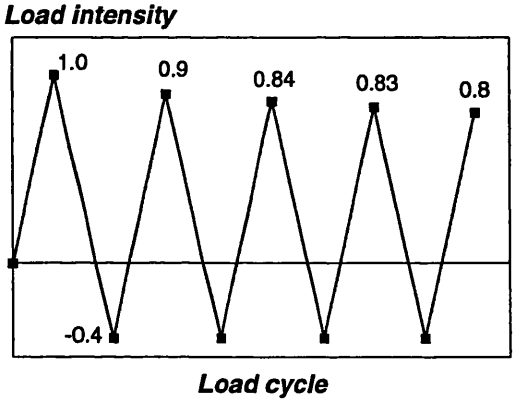

Fig. 5.14 Normalised environmental load history for cyclic analysis

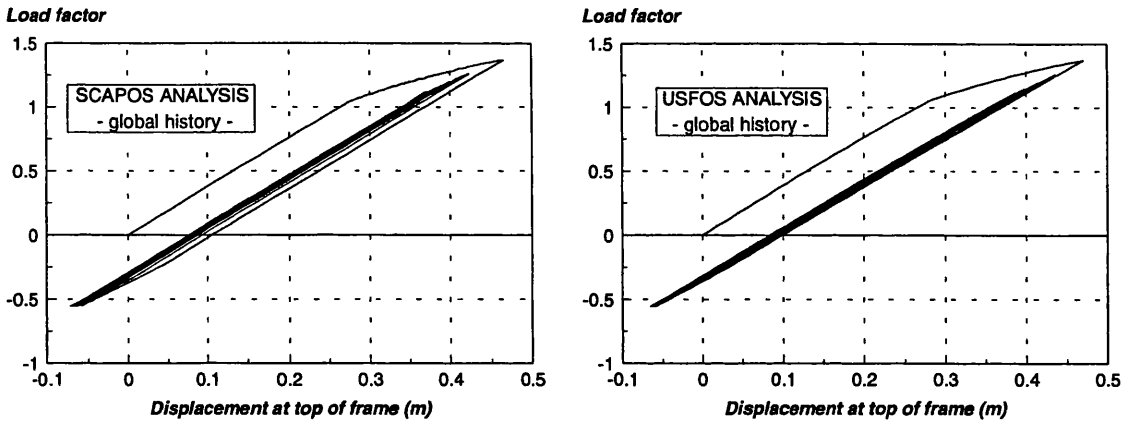

(a) Global response history

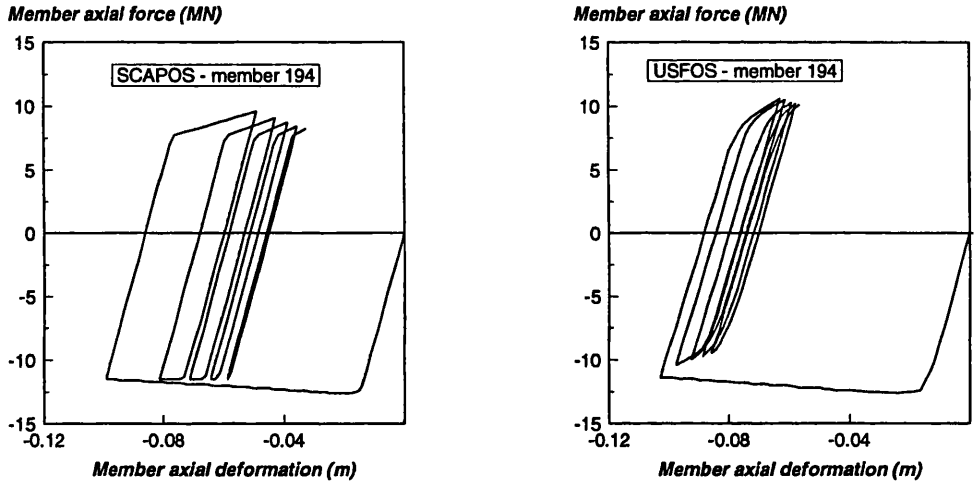

(b) Local response history of member 194

Fig. 5.15 Cyclic response of 3-D structure

The energy dissipation in member 194 (Fig. 5.15) is rather severe. To investigate the robustness of the structure to local cyclic damage, member 194 was disconnected at load-peak no. 4. The results are shown in Fig. 5.16. We observe that the residual strength upon disconnecting this member is $\lambda_R = 1.10$, which, although considerable, is not adequate to sustain the applied load ($\lambda = 1.15$) at load-peak no. 4. Consequently, the cyclic capacity of this structure is less than its pushover capacity. A pessimistic estimate of the cyclic capacity is obtained if no cyclic member strength is taken into account and the overall load profile scaled such that the load intensity of the second cycle does not exceed the residual capacity. In this example, this gives the allowable magnitude of the largest wave-force in the sequence as $\lambda_1 = 0.86\lambda_{ult}$ implying that the cyclic capacity is some 14% below the pushover capacity.

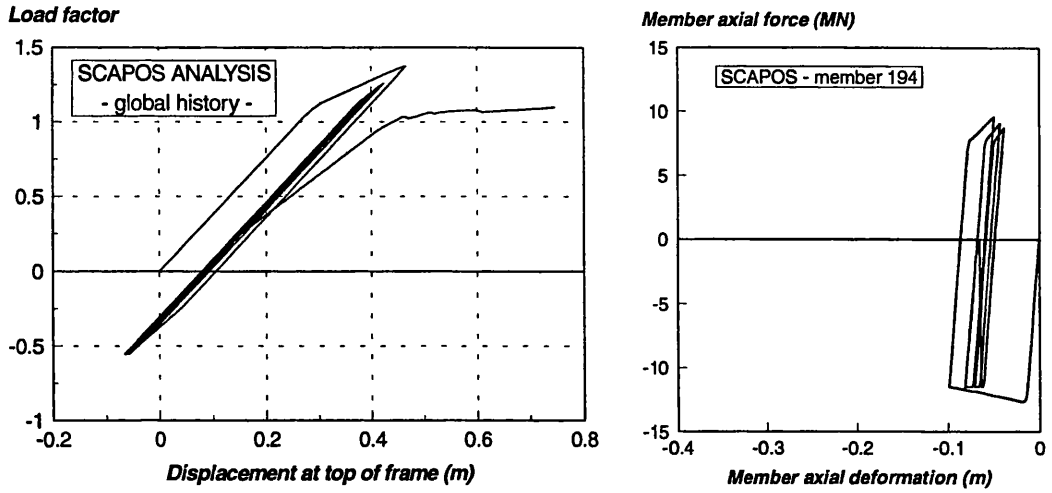

Fig. 5.16 Cyclic response of 3-D structure with member 194 disconnected at load-peak no. 4

5.3 DYNAMIC ANALYSES

We present three detailed verification examples for the PFI-Method applied to dynamic problems. In the first example, we obtain the results of a simple modified linear-elastic problem using an associated reference model and compare the SCAPOS results with the exact solution. In the second example, the response of a non-linear elastic spring is obtained and compared with the solution found using the MARC f.e. package. Finally, the SCAPOS and MARC results from a dynamic analysis of the plane frame considered previously in example 2 are presented.

Example 5: Modified linear-elastic system

We begin with a simple but effective test for the implementation of the dynamic simulation procedure using the PFI-Method.

The example, shown in Fig. 5.17a, comprises a rigid cantilever beam of length l supported by three linear elastic springs, each a distance of b apart. The spring stiffnesses are $k_1 = \alpha k_o$, $k_2 = \beta k_o$ and $k_3 = k_o$, where α and β are constants. The tip of the cantilever supports a mass m and is restrained by a viscous damper c. It is excited by a time dependent force, $F(t) = F_o \cos \omega t$ at time $t > 0$.

For our reference structure, we select equal stiffnesses k_o for all of the springs (Fig. 5.17b). For any particular input data to this problem, the SCAPOS program solves the system of equations given by (4.3c). If the reference model is different from the actual problem ($\alpha \neq 1$ or $\beta \neq 1$), time dependent pseudo-forces act on springs 1 and 2 as shown in Fig. 5.17b even though the actual problem is linear. That is, to the PFI-Method, a modified linear problem is essentially the same as a non-linear problem. This means that it is very simple to check that the dynamic solution algorithms are programmed correctly as we know the exact solution to the linear problem.

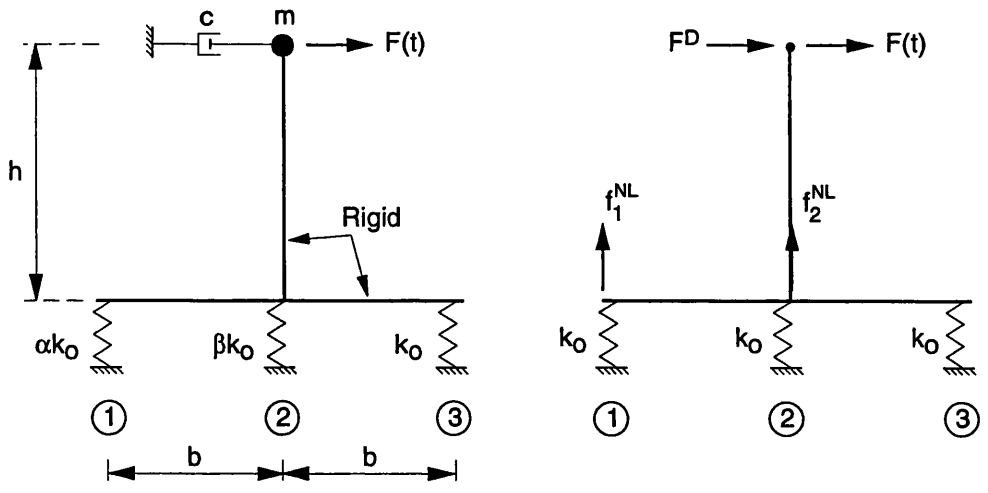

(a) Problem specification *(b) Pseudo-force approach*

Fig. 5.17 Model of cantilevered beam for dynamic analysis

Exact solution

The equation of motion for the mass point displacement U can be derived as

$$m\ddot{U}+2\zeta m\omega_o\dot{U}+k^*U=F_o\cos\omega t;\quad t>0$$

where

$k^*=k_o(b/l)^2\dfrac{4\alpha+\alpha\beta+\beta}{1+\alpha+\beta}$ is the effective stiffness,

$\zeta=2m\omega_o/c$ is the damping ratio, and

$\omega_o=\sqrt{k^*/m}$ is the natural frequency of the undamped system.

The analytical solution of this problem for zero initial conditions can be derived by following the procedure outlined by CLOUGH & PENZIEN (1974), resulting in

$$U(t)=A\cos\omega t+B\sin\omega t-e^{-\zeta\omega_o t}\left\{A\cos\omega_d t+(\zeta\frac{\omega_o}{\omega_d}A+\frac{\omega}{\omega_d}B)\sin\omega_d t\right\}$$

where

$$\omega_d=\omega_o\sqrt{1-\zeta^2};\quad A=(1-\beta^2)\rho;\quad B=2\zeta\beta\rho;\quad \beta=\frac{\omega}{\omega_o};\quad \rho=\frac{1}{(1-\beta^2)^2+(2\zeta\beta)^2}\frac{F_o}{k^*}.$$

Solution by PFI-Method

From our reference model (Fig. 5.17b), the input for the PFI-Method is easily derived. The influence matrices are obtained by applying unit loads in turn to springs 1 & 2 and to the mass point (refer to Fig. 4.2) and are given by

$$\boldsymbol{D}^{\eta\eta} = \frac{1}{k_o}\begin{bmatrix} 5/6 & 1/3 \\ 1/3 & 1/3 \end{bmatrix} \qquad \boldsymbol{D}^{\eta U} = \frac{l}{2bk_o}\begin{bmatrix} 1 \\ 0 \end{bmatrix}$$

$$\boldsymbol{H}^{UU} = \frac{1}{2k_o}\left(\frac{l}{b}\right)^2 [1] \qquad \boldsymbol{H}^{U\eta} = \frac{l}{2bk_o}[1 \quad 0]$$

and, since the force is applied at a mass point, the static response of the linear-elastic system to a force $F(t)$ is given by

$$U^L = \boldsymbol{H}^{UU} F(t) \qquad \underline{\eta}^L = \boldsymbol{D}^{\eta U} F(t)$$

where U^L is the displacement of the mass point and the entries of $\underline{\eta}^L$ are the deformations of springs 1 and 2.

We select the following base case data

$F_o = 0.873$ MN $\quad k_o = 100$ MN/m $\quad m = 2{,}850$ tonnes $\quad \zeta = 0.03 \quad l/b = 4$

$\alpha = 1/3, \ \beta = 1/2 \Rightarrow k^* = 6.82$MN/m, $\omega_o = 1.55$rad/sec (4.05 sec period).

Two forcing frequency ratios ($\omega_o/\omega = 4$ and $\omega_o/\omega = 0.99$) are considered. The first gives conditions far from resonance (similar to wave-loading on jacket structures) while the second is a test of how the system performs near resonance.

Various time steps were employed and the SCAPOS results compared with the analytical solution for each. As the time step was reduced, the SCAPOS results approached the analytical solution from which it may be concluded that the dynamic simulation procedure is implemented correctly. A time step $\Delta t = 0.2 = (1/20)(2\pi/\omega_o)$ gave answers of acceptable accuracy in both cases, as shown in Figs 5.18a and 5.18b. A time step of $\Delta t = 0.4 = (1/10)(2\pi/\omega_o)$ performed rather poorly after a few cycles, particularly in the near-resonance range.

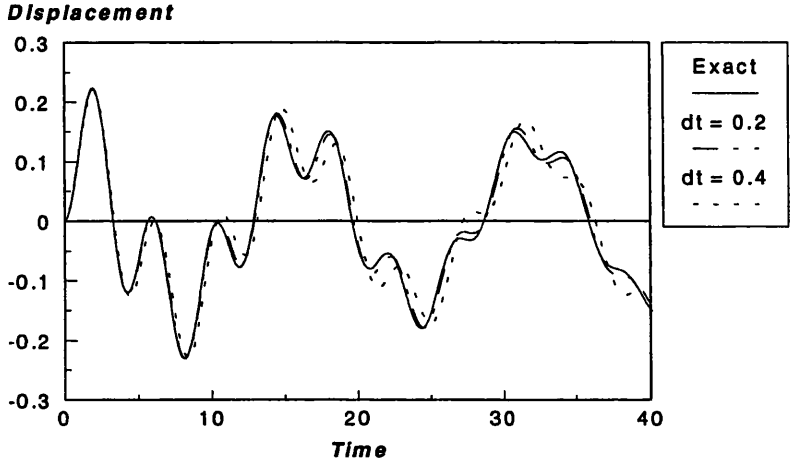

(a) Response far from resonance ($\omega_o/\omega = 4$)

Fig. 5.18 Response of cantilevered beam on modified linear-elastic springs

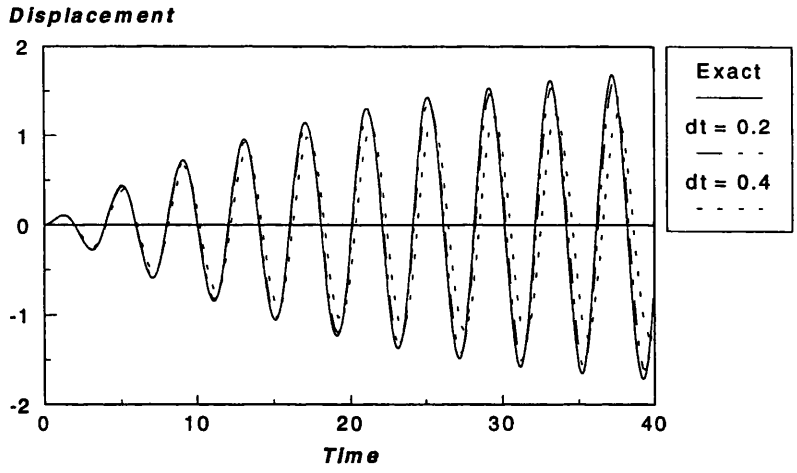

(b) Response near resonance ($\omega_o / \omega = 0.99$)

Fig. 5.18 (Contd.) Response of cantilevered beam on modified linear-elastic springs

Example 6: Single degree of freedom non-linear spring

We consider now an undamped single degree of freedom model in which the spring stiffness is non-linear elastic (Fig. 5.19). The initial stiffness is $k_o = 75$ MN/m and the mass is m = 17,100 tonnes giving an initial natural frequency of $\omega_o = 2.09$ rad / sec (3 sec. natural period). The purpose of this model is three-fold:

(1) to see if the time step size required for an accurate numerical solution should be modified as a consequence of the non-linearity;

(2) to investigate the effect on accuracy if loading with multiple frequencies is input; and

(3) to compare the PFI-Method solution with that of the MARC general purpose f.e. code for a simple example before progressing to a more complex structure.

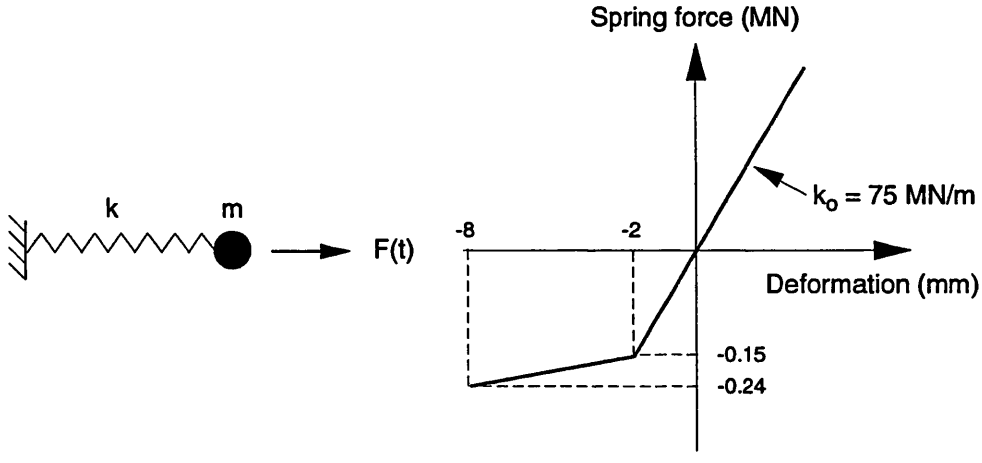

Fig. 5.19 Single degree of freedom non-linear spring

Influence matrices

The influence matrices for this problem are trivial, being given by

$$D^{\eta\eta} = D^{\eta U} = H^{UU} = H^{U\eta} = \frac{1}{k_o}[1]$$

while the static response of the linear-elastic reference system to an applied force $F(t)$ is

$$U^L = H^{UU} F(t) \qquad \eta^L = D^{\eta U} F(t).$$

Note that although there is only one degree of freedom ($U \equiv \eta$), in the PFI-Method U and η are treated separately; therefore an additional check on the solution process can be made by verifying that the two variables converge to the same value at each time step.

Loading

We consider two forcing functions given by

(a) $F(t) = F_o \sin \omega t \qquad t > 0$

(b) $F(t) = F_o \sin \omega t |\sin \omega t| \qquad t > 0$

with amplitude $F_o = 0.18$ MN and frequency $\omega = 0.39$ rad/sec (16 sec. period). After the initial transients have damped out, the first loading history supplies energy at a single frequency, whereas the second (which is representative of viscous drag loading on offshore structures) can be expanded in a Fourier Series to give

$$F(t) = \frac{8}{3\pi} F_o (\sin \omega t - \frac{1}{5} \sin 3\omega t - \frac{1}{35} \sin 5\omega t) + \text{higher order terms},$$

which is equivalent to a multi-frequency input source.

Results

The two load-cases were analysed using both SCAPOS and MARC with various time steps. The time histories of displacement for loading case (a) are compared in Fig. 5.20a while those for loading case (b) are given in Fig. 5.20b. The first observation from this set of plots is that both methods agree very well for all time steps selected. The second observation is that a time step of 1/20 of the natural period ($\Delta t = 0.15$ secs.) or less gives good accuracy for both forcing functions while a time step of 1/10 of the natural period provides reasonable accuracy for the single frequency loading but is not very accurate for the multi-frequency loading after about 4 cycles. This may be because the $\sin 5\omega t$ term in the forcing function is very close to the resonant frequency of the linear system.

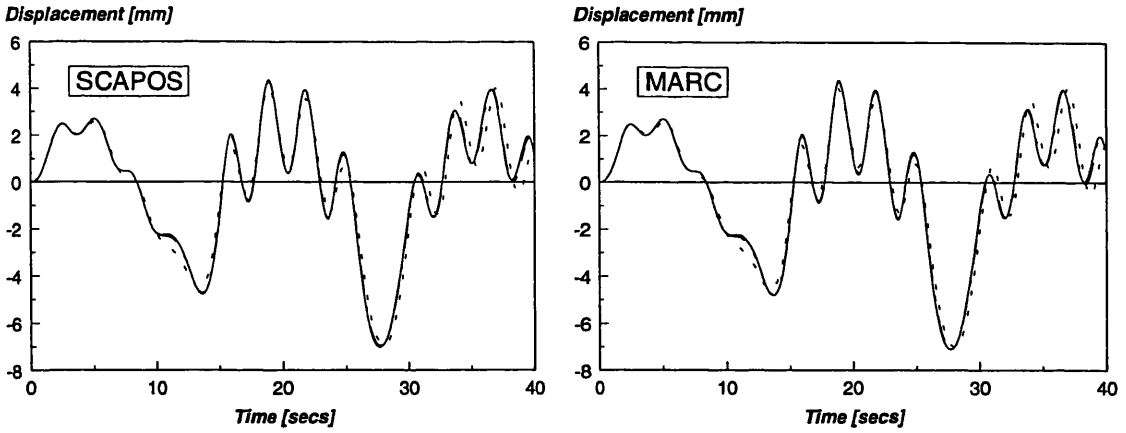

(a) Response of s.d.o.f. non-linear spring for $F(t) = F_o \sin \omega t$

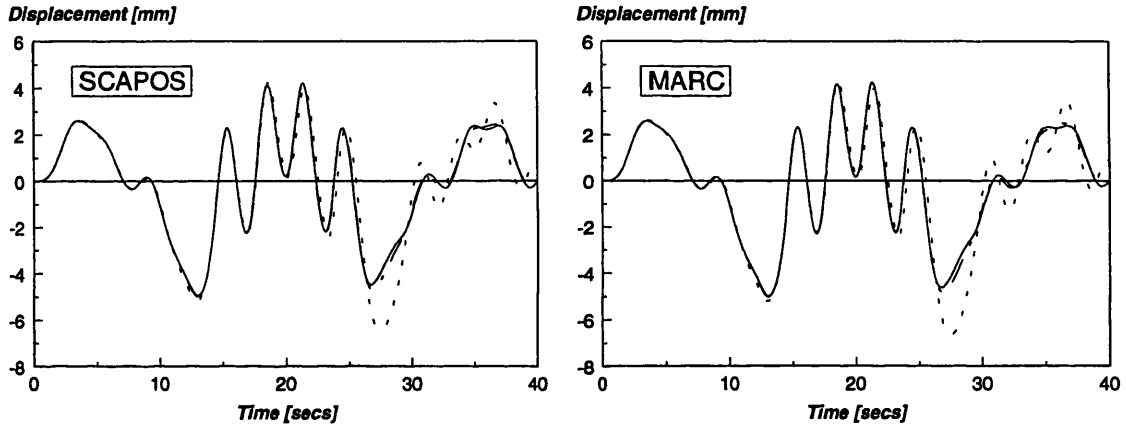

(b) Response of s.d.o.f. non-linear spring for $F(t) = F_o \sin \omega t |\sin \omega t|$

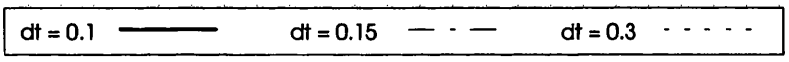

Fig. 5.20 Response of single degree of freedom non-linear spring

This example (and many others that are not reported here) leads us to the conclusion that 1/20 of the natural period of the linear-elastic system is a good initial estimate of the time step size for performing non-linear dynamic analysis. A second analysis with a reduced time step (e.g. 1/30 of the natural period) should then be carried out to confirm that the results reported are not unduly sensitive to time step size.

Example 7: Plane frame

Having verified the implementation of the PFI-Method in SCAPOS, and also the equivalence with MARC for a simple example, we now apply both methods to the dynamic collapse analysis of the plane frame considered previously in example 2. The structural model (Fig. 5.21a) is identical to that analysed before (Fig. 5.4) except that now at the top of the frame a time dependent lateral force is applied, and there is a mass of 2080 tonnes. The equivalent linear-elastic model (Fig. 5.21b) now has a dynamic pseudo-force F^D acting in addition to the material pseudo-forces f^{NL}. The initial natural frequency of this frame is $\omega_o = 2.09\,\text{rad/sec}$ (3 sec. natural period), (which is the same as that of the s.d.o.f. non-linear spring in example 6), and is representative of offshore jacket structures. Non-linear elastic behaviour of the members is assumed in this example (the hysteretic member algorithm not yet being implemented into the dynamic modules of the SCAPOS code), which means that the results are only of practical significance up to the point of maximum displacement in the non-linear response range (as thereafter the strain increments in the members reverse). This is not really a severe limitation as only the maximum response is of interest in this study. The MARC model for this frame is identical to the SCAPOS model - that is non-linear elastic springs were used to model the four diagonal braces.

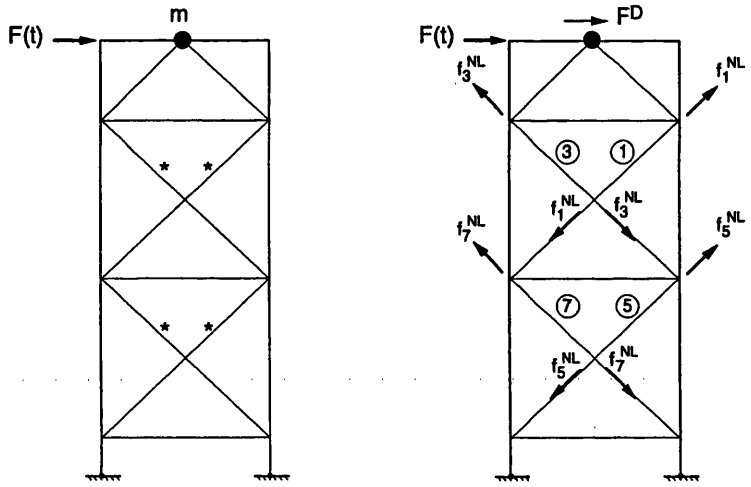

(a) Plane frame model with critical members (*)

(b) Equivalent linear-elastic model

Fig. 5.21 Models for dynamic analysis of plane frame

Loading

The forcing function is taken as $F(t) = \alpha(t) F_o \sin\omega t|\sin\omega t|$ with amplitude $F_o = 0.284$ kN (corresponding to the static pushover capacity) and frequency $\omega = 0.39$ rad./sec. (16 sec. period). The factor $\alpha(t)$ is a ramping function (commonly used in practice to prevent start-up transient dynamics in the initial load cycles) and is taken to be:

$$\alpha(t) = t/32 \quad 0 < t < 32$$
$$= 1 \quad 32 < t < 40$$

This loading history (Fig. 5.22) is quite representative of the development of an extreme event in a severe storm - although the reverse load is rather high, it has little effect on overall response as the members are non-linear elastic and dissipate no energy.

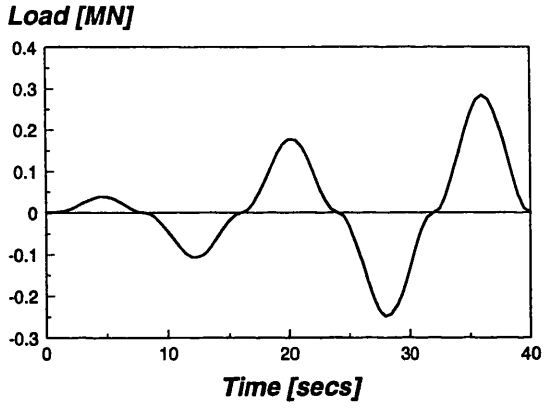

Fig. 5.22 Loading history applied to plane frame

Influence matrices

The influence matrix $D^{\eta\eta}$ was given above in example 2 (static analysis of plane frame). The other influence matrices (derived in accordance with Fig. 4.2) were found by applying a lateral load of 1 MN to the top of the frame, giving:

$$D^{\eta U} = (H^{U\eta})^T = \begin{bmatrix} -0.9496 \\ 0.9496 \\ -0.8015 \\ 0.8015 \end{bmatrix} \begin{matrix} (3) \\ (1) \\ (7) \\ (5) \end{matrix} \text{ m/MN} \qquad H^{UU} = [0.1074] \text{ m/MN}.$$

The static response of the linear-elastic reference model to an applied force $F(t)$ is

$$U^L = H^{UU} F(t) \qquad \underline{\eta}^L = D^{\eta U} F(t).$$

Results

Time histories of the results for this problem are given in Fig. 5.23. The agreement between SCAPOS and MARC is again extremely satisfactory. Indeed the largest difference in response found for all time step sizes was less than 1%. This small discrepancy is attributed to the different ways in which convergence criteria are specified in each program. The conclusions on time step size are in agreement with the recommendations suggested in the previous example: that is a time step of 1/20 of the initial natural period ($\Delta t = 0.15$ secs) provides reasonable accuracy.

For both the SCAPOS and MARC analyses, we notice a large change in the results when the time step is changed from $\Delta t = 0.15$ secs (1/20 natural period) to $\Delta t = 0.3$ secs (1/10 natural period). The divergence in the results for the two time step sizes first occurs when the first

member buckles. However the discrepancy is exacerbated by the fact that for $\Delta t = 0.15$ secs, the maximum displacement reached is 0.404m which is just below the static collapse displacement of 0.417m (Fig. 5.5), and therefore small errors in the displacement integration may take the response into the post-ultimate regime, leading to large errors in the final results. If the applied load were to be increased somewhat, taking the response for $\Delta t = 0.15$ secs also into the post-ultimate regime, the discrepancy in results using these two time step sizes would be much less.

For the larger time step of $\Delta t = 0.3$secs., the MARC program did not converge once the velocity of the top of the frame reversed (at t = 38 secs.). This is attributed to the fact that the member behaviour is taken to be non-linear elastic. As a result, when the strain increment reverses in members deformed beyond their buckling load, an incremental increase in member resistance occurs. The Newton iteration procedure in MARC then breaks down; however the constant stiffness iteration procedure in SCAPOS does not encounter any difficulty.

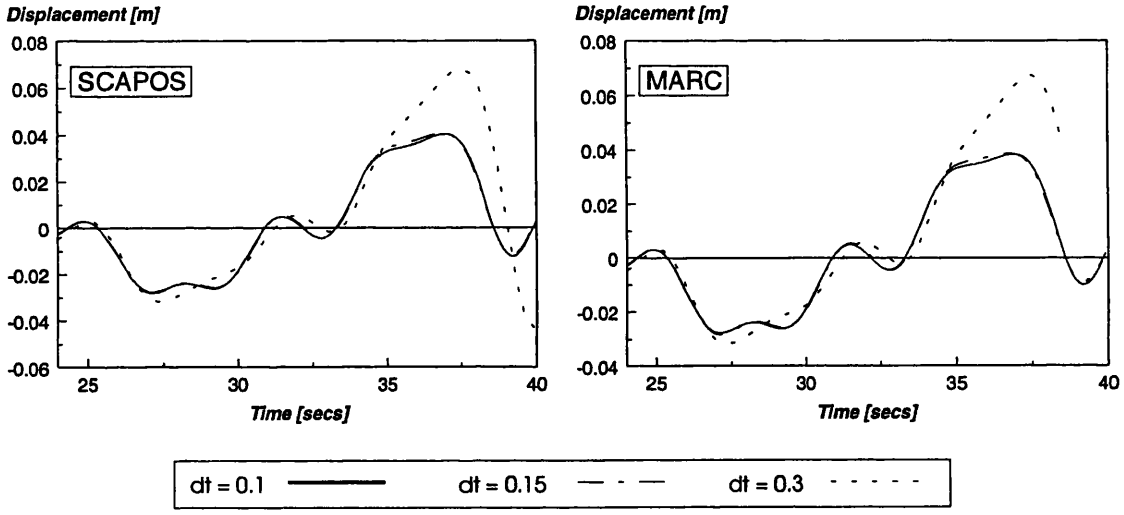

Fig. 5.23 Dynamic response of plane frame

Dynamic overload analysis

Because of the time dependent nature of the loading and the inertial resistance of the frame, the dynamic collapse resistance can exceed the static ultimate resistance by a significant margin. To investigate this, the loading history was scaled by a factor ψ (the dynamic overload ratio) and the maximum displacement of the frame recorded. The analysis was then repeated with member 1 fractured (disconnected) when it reached its tensile yield capacity. The results of these analyses are shown in Fig. 5.24 (in which the ductility is defined as the ratio of the top displacement to the static ultimate displacement).

Failure is now defined in terms of exceeding a *ductility limit*. This ductility limit, which reflects the deformations at which the frame (platform) is commercially written-off, may typically be around 5. For the intact frame, which has a ductile failure mode (see Fig. 5.5), the ductility limit is exceeded when ψ is about 1.16, indicating a 16% additional capacity over the static ultimate capacity. For the analysis in which member 1 is fractured (simulating loss of member ductility),

the failure mode is brittle (Fig. 5.7b) and the ultimate dynamic overload ratio is reduced to about 3%.

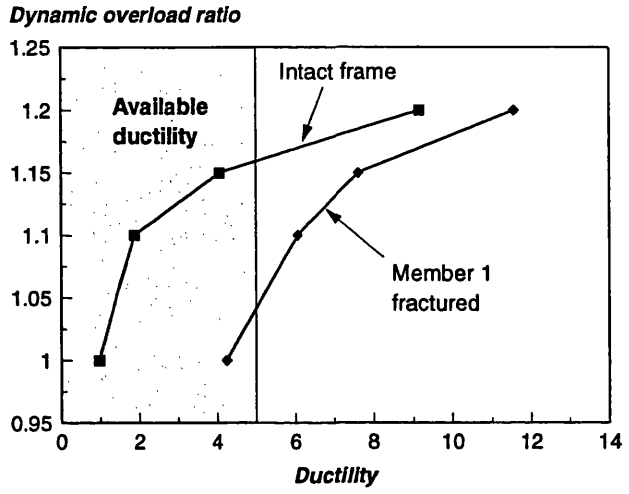

Fig. 5.24 Dynamic response of plane frame

Discussion

For the intact structure and the structure with the member fractured, the ratio of maximum dynamic load (at a ductility level of 5) to the residual strength (post-ultimate strength at large deformations) is fairly constant, being 1.24 and 1.22, respectively. This same ratio was also found in another study reported by the author[1]). It would appear that this offers a reasonable way to quickly assess the dynamic resistance from the static pushover curve. That is the maximum dynamic capacity is about 20% above the residual strength. Consequently, if the residual strength is more than 20% below the static ultimate strength, no additional benefits will be gained from the inertia of the structure. This supports the intuitive wisdom that ductile structures are safer than brittle structures.

Ductility requirements are not normally considered in the design of offshore structures in non-seismic zones. Thus, structural configurations that are not permitted in seismic zones (e.g. K-bracing in primary vertical frames) are commonly found in areas such as the North Sea, where earthquake loading is not a design event. The apparent lack of industry interest in designing ductile performance into offshore structures exposed to extreme storms can perhaps be attributed to the fact that the benefits of doing so were not visible. From the above study, however, it is clear that ductile performance is a highly desirable feature for these structures and methods for achieving this (e.g. X-bracing) should be considered in their design.

1. A full dynamic collapse study on a North Sea platform has been assessed using SCAPOS (Stewart, 1992). The model comprised a linear-elastic jacket supported by the foundation system described in example 3. Realistic time dependent wave and current loading was applied to this model.

5.4 EFFICIENCY OF THE PFI-METHOD

For all of the examples presented, the SCAPOS analyses were run on a 386/40 Mhz personal computer (PC) with mathematical co-processor (a $1,500 machine), while both USFOS and MARC were run on an IBM RS6000/350 workstation (a $50,000 machine). For a direct comparison of the efficiency of the various programs it would have been preferable to run all software on the same hardware. However several peripheral packages on the PC are used to view the data from the simulation system and it was not practical to implement these on the workstation. Furthermore, it is useful to demonstrate that a procedure utilising the principles of the PFI-Method can run on a low cost PC.

To give an impression of the efficiency of the PFI-Method, the elapsed time for the plane frame and 3-D structures was compared with that of USFOS. Using SCAPOS on the PC, the elapsed times varied between 2 secs (pushover of plane frame) and 20 secs (cyclic analysis of 3-D structure) while the equivalent runs on the workstation using USFOS (version 5.9) took between 40 secs and 55 minutes[1]. On a sample benchmark problem, the workstation to PC efficiency ratio was gauged to be around 20:1. Therefore SCAPOS is between 400 and 3300 times faster than USFOS-5.9 for the examples considered. Since non-linear frame behaviour depends on only a few elements, the elapsed time for a SCAPOS analysis is independent of the complexity of the structure whereas in USFOS the solution time increases as the model size becomes larger.

There are two additional considerations to mention. Firstly, several of the USFOS analyses had to be re-started to overcome convergence difficulties whereas in the SCAPOS analyses no convergence problems were encountered. The elapsed times quoted above show only the computational effort involved in successful runs - the actual elapsed time for USFOS was several hours in some cases. Secondly, it should be borne in mind that building the non-linear USFOS structural model can take several weeks of effort, whereas if a linear-elastic model already exists this task is not necessary when the SCAPOS simulation system is used.

5.5 CLOSING REMARKS

Hopefully, these examples will have demonstrated the practicality, flexibility, accuracy and usefulness of the PFI-Method. The only modelling decision that the engineer must take is to decide on the effective buckling length of compression members. This is fairly straightforward, and if in doubt, one can always err on the conservative side.

The examples also provide a useful insight into frame behaviour: the plane frame examples confirm the importance of the bracing members in the overall strength of the frame while the 3-D example supports the view that the non-linear collapse behaviour of large 3-D framed structures is often controlled by the axial capacity of only a few members.

1. Version 6.8 of USFOS (released 1994), which uses sparse matrix technology is considerably faster (10 minutes elapsed time for 3-D cyclic analysis).

Acknowledgements

It is appropriate to acknowledge the contributions to this chapter by several undergraduate and diploma students who have worked at Shell Research under the author's supervision. Harold Maasen helped with a variety of USFOS member calibration tests; Bart Reimsdijk developed a graphical display program for SCAPOS dynamic analysis; Roberto Danker performed the cyclic USFOS analyses; and Hjalmar Groen carried out some comparisons between SCAPOS and MARC for dynamic analyses. The efforts of Anne Arents of the Research Applications department in Shell Research were also invaluable in transforming the prototype SCAPOS software into a finished product.

5.6 REFERENCES

CLOUGH, R.W., AND PENZIEN, J. (1974), *Dynamics of structures*. McGraw-Hill, New York.

MARC: *General purpose finite element program*, Marc Research Corporation, Paulo Alto. (1986, version K2.1; 1993, version K5.2).

STEWART, G., AND VAN DE GRAAF, J.W. (1990), "A methodology for platform collapse based on linear superposition", *Offshore Technology Conference*, OTC 6311, Houston, Texas.

STEWART, G. (1992), "Nonlinear structural dynamics by the pseudo-force influence method - Part II: Application to offshore platform collapse", *Intl. Offshore and Polar Engineering Conf.* (ISOPE), Vol. I, San Francisco, USA.

STEWART, G. (1993), "Nonlinear response of offshore jacket structures using linear analysis programs", *Integrity of Offshore Structures Conference* (IOS), Glasgow, Scotland.

TABY, J. (1988), *DENTA-II: A computer program for the analysis of ultimate and post-ultimate behaviour of tubes*, program Users Manual.

USFOS: *A Computer Program for Progressive Collapse Analysis of Steel Offshore Structures*, SINTEF Report STF71 F88038 Rev. 1993, Trondheim, Norway.

ZAYAS, V.A., MAHIN, S.A, AND POPOV, E.P. (1982),"Ultimate strength of steel offshore structures", *Intl.Conf. on the Behaviour of Offshore Structures* (BOSS), Boston.

Part III

A more formal treatment of the PFI-Method

Chapter 6

BASIC PRINCIPLES OF EQUILIBRIUM
&
THE CO-ROTATIONAL APPROACH

6.1 INTRODUCTION

As we saw in Part II of this work, the pseudo-force method for bar elements is based on separating the resistance of the bar into two components: a linear-elastic resistance and an inelastic correction term. This enabled us to obtain the non-linear response by solving an equivalent linear elastic problem. Clearly, to investigate whether this technique can be applied to more general non-linear finite element problems, the basic principles of equilibrium for the discretised continuum must be fully understood. In this chapter, which is a pre-cursor to the development of the more general pseudo-force method developed in chapter 7, we first explore the fundamentals of element equilibrium, kinematics and stiffness matrices. We then form the global equilibrium equations in such a way that the contribution of individual elements can be identified. Direct linearisation of these equations provides the global stiffness matrix normally used in finite element computations.

We therefore have two principle objectives in mind in this chapter. Firstly to provide the framework for further development of the pseudo-force method, and secondly, to allow us to compare the pseudo-force method with more traditional finite element solution procedures.

Scope

Only two dimensional (planar) continuum elements are considered in this work, however generalisation to three dimensional elements is possible. Additionally, we restrict our attention to (infinitesimally) small strains but allow large rotations. This is depicted in Fig. 6.1 where the element undergoes a large rotation ϕ, but the deformation of any line segment is small. This formulation allows the description of buckling phenomena, rigid body motion and the formation of plastic yield zones in the material, but does not take account of volume changes as a result of straining. For most problems in structural mechanics this is perfectly adequate.

The equilibrium of an individual finite element is considered within a co-rotating reference frame that translates and rotates with the element (Fig. 6.1). For small strain problems, this approach provides a very natural framework for evaluating the element's resistance to deformation, since infinitesimal theory may be used to describe both the strain-displacement

relationship and the stress-strain law. Having derived the resistance contribution of an individual element, suitable geometric transformations that reflect the link between the co-rotational and the fixed reference frame are then employed to rotate and sum each element's resistance forces into the global equilibrium equations.

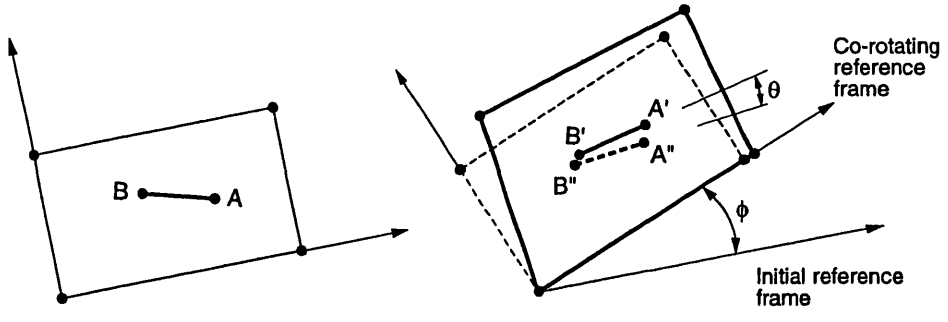

$\overrightarrow{B"A"}$: Rigid body motion of $\overrightarrow{BA}$
$\overrightarrow{B'A'}$: Deformed position of $\overrightarrow{BA}$

Small strain: $\dfrac{|\overrightarrow{A'B'}|}{|\overrightarrow{A"B"}|} \sim 1 \; ; \; \theta << 1$

Large rotations: no restriction on ϕ

(a) Undeformed position *(b) Deformed position*

Fig. 6.1 Large displacements and small strains in a co-rotating reference frame

Not surprisingly, many researchers have found the co-rotational framework to be convenient for small-strain-large-rotation finite element developments (BELYTSCHKO & HSIEH, 1973; BESSELING, 1974; MATTIASON, 1983; CHRISFIELD & COLE, 1989; CHRISFIELD, 1990; to name but a few) and the technique also has strong similarities with the ***natural method*** pursued by ARGYRIS *ET AL.* (1979). It may also be viewed as the small strain equivalent of the embedded convected co-ordinate system proposed by GREEN & ZERNA (1968) for finite strain analysis which has been employed in numerical computations by, for example, NEEDLEMAN (1981), and NEEDLEMAN & TVERGAARD (1984).

Most importantly as far as the objectives of this work are concerned, the co-rotating framework provides a unique insight into the development of the equilibrium equations at the element level which is lost if one adopts a fixed reference system. Furthermore, it enables the equilibrium to be developed at the most basic or natural level; only later are degrees of freedom related to rigid body modes included. As a consequence, the geometrically non-linear theory is obtained directly as an extension of the geometrically linear theory. These fundamental aspects play a key role in the development of both the pseudo-force method and more conventional co-rotational non-linear finite element procedures.

Organisation of this chapter

The organisation of this chapter is as follows. The notation used is first summarised and a description of the various reference systems adopted then follows. For each reference system, force and kinematic (displacement) freedoms are introduced and the correspondence between the

variables in different reference systems derived. Next, constitutive models appropriate for the co-rotating system are defined and the element stiffness matrices developed. Finally, the global equilibrium equations are assembled and the global stiffness matrices for statics and dynamics derived.

6.2 NOTATION

It is appropriate to introduce the notation used in this and the following chapter. Variables such as $\underline{v}$ represent all of the components of the vector $\vec{v}$. The individual entries of $\underline{v}$ are v_i. Matrices such as $\boldsymbol{T}$ represent all of the components of the tensor $\underline{\underline{\boldsymbol{T}}}$. The individual entries of $\boldsymbol{T}$ are T_{ij}. The transpose of $\underline{v}$ is denoted by $\underline{v}^T$ while that of $\boldsymbol{T}$ is denoted by $\boldsymbol{T}^T$.

Lower case variables are used to represent quantities that relate to either individual elements or to groups of elements. The quantities are stored *element by element*. For example the nodal displacements for a group of elements would take the form

$$\underline{u} = \left[\underline{u}_1^T \quad \underline{u}_2^T \quad \cdots \quad \underline{u}_k^T\right]^T; \quad k \le n \tag{6.1}$$

where $\underline{u}_i$ contains the complete set of nodal displacements of element i for a model having a total of n elements. These components may relate to any convenient co-ordinate system.

Similarly, upper case variables refer to nodal point values, with respect to the global co-ordinate system, stored node by node. The displacements for a group of nodes would be represented as

$$\underline{U} = \left[\underline{U}_1^T \quad \underline{U}_2^T \quad \cdots \quad \underline{U}_k^T\right]^T; \quad k \le N \tag{6.2}$$

where $\underline{U}_i$ contains the displacements of node i for a model having a total of N nodes.

Matrices relating groups of element quantities to other groups of element quantities are block diagonal. Those relating element variables to nodal variables are block rectangular. For example, if

$$\underline{a} = \boldsymbol{B}\underline{c}; \quad \underline{x} = \boldsymbol{Y}\underline{Z} \tag{6.3}$$

such that $\underline{a}_i = \boldsymbol{B}_i \underline{c}_i$; $\underline{x}_i = \boldsymbol{Y}_i \underline{Z}$, then $\boldsymbol{B}$ and $\boldsymbol{Y}$ are of the form

$$\boldsymbol{B} = \begin{bmatrix} \boldsymbol{B}_1 & & & \\ & \boldsymbol{B}_2 & & \boldsymbol{O} \\ & & \ddots & \\ \boldsymbol{O} & & & \boldsymbol{B}_k \end{bmatrix}; \quad \boldsymbol{Y} = \begin{bmatrix} \boldsymbol{Y}_1 \\ \boldsymbol{Y}_2 \\ \vdots \\ \boldsymbol{Y}_k \end{bmatrix} \tag{6.4}$$

If the matrices consist only of ones and zeros they are called boolean. Boolean matrices are normally used to select certain rows or to add rows of a matrix. Matrices with a subscript 'o' are constant, although the converse does not hold.

Stress and strain tensor components are usually represented in so-called "vector" form, that is as single-column matrices. For example, the stress tensor components are represented as

$$\underline{\sigma} = [\sigma_{11} \quad \sigma_{22} \quad \sigma_{12}]^T .$$

Nodal transformations

We make frequent use of the nodal orthogonal transformation matrix

$$R_\theta = \begin{bmatrix} R_{\theta_1} & & & \\ & R_{\theta_2} & & \boldsymbol{O} \\ & & \ddots & \\ \boldsymbol{O} & & & R_{\theta_k} \end{bmatrix}; \qquad R_{\theta_i} = \begin{bmatrix} \cos\theta_i & \sin\theta_i \\ -\sin\theta_i & \cos\theta_i \end{bmatrix} \tag{6.5}$$

where the sub-matrix R_{θ_i} operates on the freedoms of a single node.

The matrix R_θ and its derivative can also be expressed in the form

$$R_\theta = \Phi_c + \Phi_s \Omega_o \qquad \frac{\partial R_\theta}{\partial \theta} = R_\theta \Omega_o = \Omega_o R_\theta \tag{6.6}$$

in which Φ_c is a diagonal matrix of cosines, Φ_s is a diagonal matrix of sines, and Ω_o is a skew-symmetric matrix given by

$$\Omega_o = \begin{bmatrix} 0 & 1 & & & \\ -1 & 0 & & \boldsymbol{O} & \\ & & \ddots & & \\ & \boldsymbol{O} & & 0 & 1 \\ & & & -1 & 0 \end{bmatrix}; \qquad \Omega_o \Omega_o^T = I \ . \tag{6.7}$$

Identity matrices

We denote identity matrices by the symbol I. The dimension of I is usually apparent from the context. In some cases a subscript is used if the dimension needs emphasis. Thus I_n is the identity matrix of order n x n.

6.3 REFERENCE SYSTEMS

Above it was stated that a co-rotational reference system offers certain advantages over a fixed reference system. It is now appropriate to introduce the different reference systems adopted in this work. It is to be stressed that any convenient reference system may be chosen in which to represent the physical quantities of interest. The quantities themselves (e.g. vectors, tensors, etc.) are frame-invariant. So, for example, as shown in Fig. 6.2, the displacement vector $\vec{u}$ has components (u^o, v^o) with respect to reference system C_o, while in reference system C_1 this same vector has components (u^1, v^1).

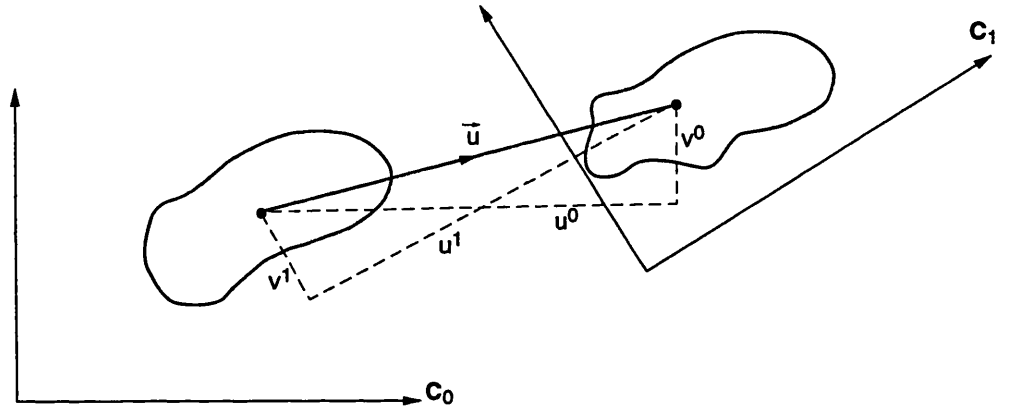

Fig. 6.2 Components of a vector in different reference systems

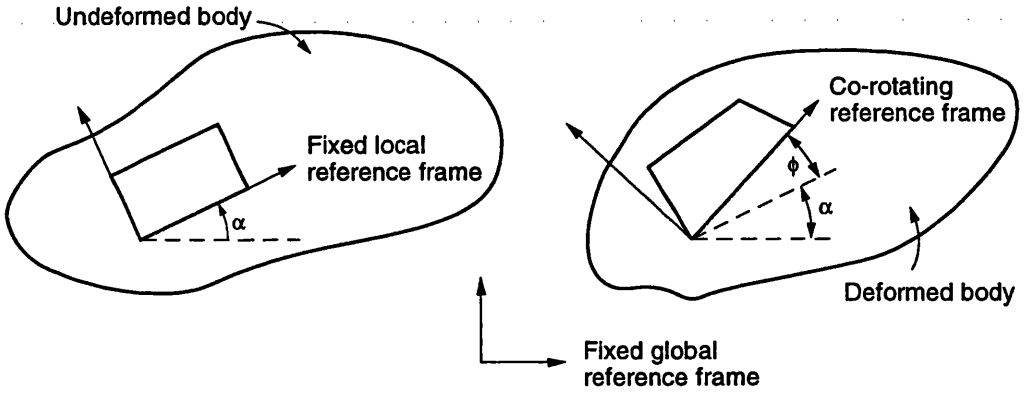

Fig. 6.3 Motion of an element within a deformable body

In Figure 6.3, an element within a body translates, rotates and deforms under the effect of loading applied to the system. The element motion may be defined by (generalised) displacement components that depend on the selected Cartesian frame of reference.

The reference systems employed (Figs. 6.4a-6.4e) are:

1. **The fixed global reference system** (Fig. 6.4a)
   The same reference system is employed for all elements. The nodal element displacements are denoted by $\underline{u}$.

2. **The local reference systems** (Figs. 6.4b, 6.4c)
   Each element has its own local (fixed and translating) reference systems. The orientation of these reference systems is determined by the initial position of the element in the undeformed state and differs from the global reference system by an angle α. In the fixed reference system absolute nodal element displacements $\underline{v}$ are employed. On the other hand, if the reference system translates by $\underline{v}_o$, being the displacements of node 1, relative displacements $\underline{w}$ are used.

3. **The co-rotating reference system** (Fig. 6.4d)
   Each element has its own local reference system that co-rotates and translates with the element. One axis of the reference system is selected as the direction of the line segment joining any two nodes (we use nodes 1 and 2), the other is orthogonal to this direction. The orientation of this reference system differs from the fixed and translational local reference system by an angle ϕ. The non-zero nodal element deformations (relative displacements in co-rotated frame) are denoted by $\underline{\eta}$. The origin of the element (at node 1) translates by $\underline{v}_o$. Thus the final position of the element can be described as a translation followed by a rotation followed by a set of deformations.

4. **The instantaneous reference systems** (Fig. 6.4e)
   To describe the incremental motion of the element, we use a local element reference system whose orientation at 'time' t coincides with that of the co-rotating system. At a short time dt later, the angle of rotation between the co-rotating system and the instantaneous local system differs by $d\phi$. If node 1 of the instantaneous frame translates with the element, then the nodal freedoms are the relative displacements $\underline{w}^*$ (Fig. 6.3e); otherwise, they are the absolute displacements $\underline{v}^*$ (not shown in Fig. 6.3).

Other co-rotational definitions can also be found in the literature. BELYTSCHKO & HSIEH (1973) for example, use the average rigid body rotation of the element, calculated from the polar decomposition of the displacement gradient tensor. In the natural method, Argyris and his colleagues (see ARGYRIS & TENEK, 1994) also use the average rigid body rotation, calculated from the infinitesimal rotation tensor. It is apparent that any convenient choice may be made, provided that the unknown deformations are independent of the rotation. The selection made in this work leads to a very simple formulation and has the advantage that the kinematic description of the rotation is described in the same manner for all element types. The other methods mentioned require element-specific calculations to determine the incremental rotation angle.

For pure rigid body rotation and deformation without shear, the co-rotational angle for all methods is identical. Otherwise, the angle ϕ adopted in the present method is infinitesimally close to, but is not identical to, the average rigid body rotation.

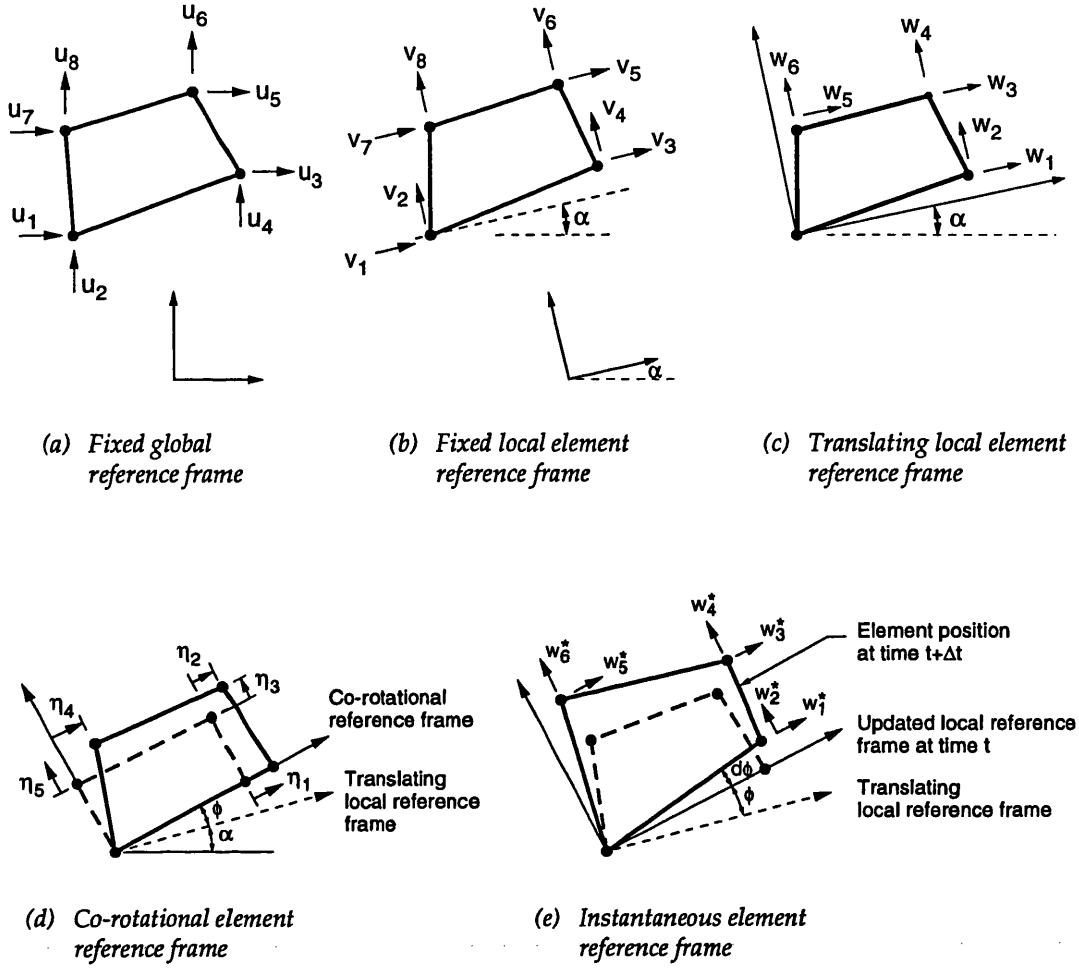

(a) Fixed global reference frame

(b) Fixed local element reference frame

(c) Translating local element reference frame

(d) Co-rotational element reference frame

(e) Instantaneous element reference frame

Fig. 6.4 Kinematics of an element in alternative reference systems

6.4 NODAL KINEMATIC RELATIONSHIPS

The kinematic relationships linking the nodal point displacements $\underline{u}$, $\underline{v}$, $\underline{w}$ (Fig. 6.4) are straightforward, and may be stated as

$$\underline{v} = R_\alpha \underline{u} \qquad \underline{u} = R_\alpha^T \underline{v} \tag{6.8}$$

$$\underline{w} = M_o \underline{v} \qquad \underline{v} = \begin{bmatrix} I_2 & O \\ \bar{I} & I \end{bmatrix} \begin{bmatrix} \underline{v}_o \\ \underline{w} \end{bmatrix} \quad \text{and} \quad M_o = \begin{bmatrix} -\bar{I} & I \end{bmatrix}. \tag{6.9}$$

where

$$\bar{I} = [I_2 \;\; I_2 \;\; \cdots \;\; I_2]^T \quad \text{and} \quad I_2 = \begin{bmatrix} 1 & 0 \\ 0 & 1 \end{bmatrix}.$$

At any instant in time, the incremental relationships between $\underline{v}$, $\underline{w}$, $\underline{v}^*$, and $\underline{w}^*$ also poses no difficulty:

$$\dot{\underline{v}}^* = \boldsymbol{R}_\phi \dot{\underline{v}} \qquad \dot{\underline{v}} = \boldsymbol{R}_\phi^T \dot{\underline{v}}^* \tag{6.10}$$

$$\dot{\underline{w}}^* = \tilde{\boldsymbol{R}}_\phi \dot{\underline{w}} \qquad \dot{\underline{w}} = \tilde{\boldsymbol{R}}_\phi^T \dot{\underline{w}}^* \tag{6.11}$$

$$\dot{\underline{w}}^* = \boldsymbol{M}_o \dot{\underline{v}}^* \qquad \dot{\underline{v}}^* = \begin{bmatrix} \boldsymbol{I}_2 & \boldsymbol{O} \\ \bar{\boldsymbol{I}} & \boldsymbol{I} \end{bmatrix} \begin{bmatrix} \dot{\underline{v}}_o^* \\ \dot{\underline{w}}^* \end{bmatrix}. \tag{6.12}$$

where the matrix $\tilde{\boldsymbol{R}}_\phi$ is simply a condensed form of $\boldsymbol{R}_\phi$ with the entries related to the node 1 freedoms removed. The tilde (~) will subsequently denote the condensed form of a matrix.

Now, in the co-rotating system let $\hat{\underline{X}} = [(X_2 \;\; Y_2) \;\; (X_3 \;\; Y_3) \;\; \ldots]^T$ denote the co-ordinates of all nodes in an element excluding node 1 (the origin) and let $\underline{\zeta}$ be the relative displacements of these same nodes, including the zero entry for the vertical relative displacement of node 2. That is the deformations $\underline{\eta}$ correspond to the non-zero entries of $\underline{\zeta}$ (Fig. 6.5).

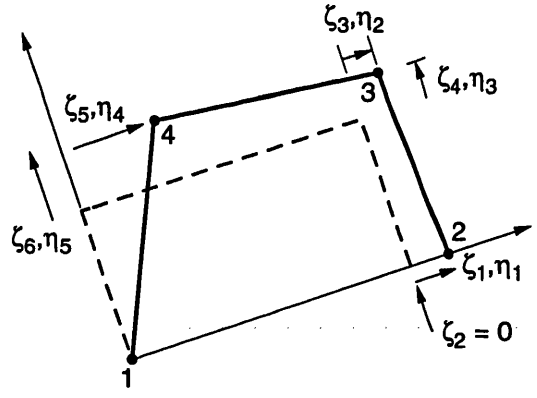

Fig. 6.5 Relative displacements, $\underline{\zeta}$ and deformations, $\underline{\eta}$ in co-rotating frame

The deformations $\underline{\eta}$ can be extracted from $\underline{\zeta}$ using a simple boolean matrix $\boldsymbol{G}_o$, such that

$$\underline{\eta} = \boldsymbol{G}_o \underline{\zeta} \; ; \qquad \underline{\zeta} = \boldsymbol{G}_o^T \underline{\eta} \; ; \qquad \boldsymbol{G}_o = \left[\begin{array}{cc|c} 1 & 0 & \underline{0}^T \\ \hline \multicolumn{2}{c|}{\boldsymbol{O}} & \boldsymbol{I} \end{array}\right] ; \qquad \boldsymbol{G}_o \boldsymbol{G}_o^T = \boldsymbol{I} \, . \tag{6.13}$$

The kinematic link between $\underline{\zeta}$ and $\underline{w}$ is provided by the following expressions

$$\underline{w} = \tilde{\boldsymbol{R}}_\phi^T \underline{\zeta} + (\tilde{\boldsymbol{R}}_\phi^T - \boldsymbol{I}) \hat{\underline{X}} \qquad \text{and} \qquad \underline{\zeta} = \tilde{\boldsymbol{R}}_\phi \underline{w} + (\tilde{\boldsymbol{R}}_\phi - \boldsymbol{I}) \hat{\underline{X}}, \tag{6.14}$$

and since $\tilde{R}_\phi$ is a function of $\underline{w}$, these relationships are non-linear. Differentiating these provides the kinematic link between the increments of instantaneous relative displacements $\dot{\underline{w}}^*$ and the co-rotating generalised co-ordinates $[\dot{\phi}\ \ \dot{\underline{\eta}}^T]^T$, which may be represented as

$$\begin{bmatrix}\dot{\phi}\\ \dot{\underline{\eta}}\end{bmatrix}=\begin{bmatrix}\tilde{\underline{h}}^T\\ \tilde{A}\end{bmatrix}\dot{\underline{w}}^* \qquad \dot{\underline{w}}^*=\begin{bmatrix}\tilde{\Omega}_o^T(G_o^T\underline{\eta}+\hat{\underline{X}}) & G_o^T\end{bmatrix}\begin{bmatrix}\dot{\phi}\\ \dot{\underline{\eta}}\end{bmatrix} \tag{6.15}$$

with

$$\tilde{\underline{h}}^T=\frac{\partial\phi}{\partial\underline{w}^*} \qquad \text{and} \qquad \tilde{A}=\frac{\partial\underline{\eta}}{\partial\underline{w}^*}=G_o\frac{\partial\underline{\zeta}}{\partial\underline{w}^*}\,. \tag{6.16}$$

Whatever its form, $\tilde{\underline{h}}$ can be split into a constant part and a deformation dependent part, such that

$$\tilde{\underline{h}}^T=\tilde{\underline{h}}_o^T+\tilde{\underline{h}}_\eta^T \tag{6.17}$$

and from (6.14) with the aid of (6.6) and (6.11) we can establish after some manipulation that

$$\frac{\partial\underline{\zeta}}{\partial\underline{w}^*}=I+\tilde{\Omega}_o(\underline{\zeta}+\hat{\underline{X}})\tilde{\underline{h}}^T\,,$$

from which (6.16) provides

$$\tilde{A}=\tilde{A}_o+\tilde{A}_\eta\,; \qquad \tilde{A}_o=G_o(I+\tilde{\Omega}_o\hat{\underline{X}}\tilde{\underline{h}}_o^T) \qquad \tilde{A}_\eta=G_o\tilde{\Omega}_o(G_o^T\underline{\eta}\tilde{\underline{h}}^T+\hat{\underline{X}}\tilde{\underline{h}}_\eta^T)\,. \tag{6.18}$$

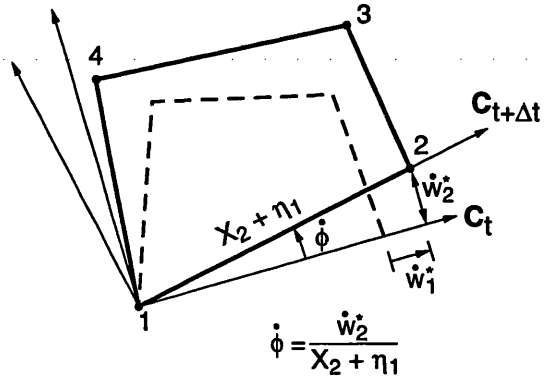

Fig. 6.6 Kinematics of incremental rotation

For our particular choice of co-rotating reference frame (see Fig. 6.6), we have

$$\dot{\phi} = \frac{\dot{w}_2^*}{X_2 + \eta_1} \equiv \frac{1}{X_2}\left(1 - \frac{\eta_1}{X_2}\right)\dot{w}_2^* \tag{6.19}$$

where X_2 is the X-coordinate of node 2, and η_1 is the extension of edge 1 - 2. From this it is apparent that

$$\underline{\tilde{h}}_o^T = \frac{1}{X_2}\begin{bmatrix} 0 & 1 & \underline{0}^T \end{bmatrix} \qquad \underline{\tilde{h}}_\eta^T = -\frac{\eta_1}{(X_2)^2}\underline{\tilde{h}}_o^T . \tag{6.20}$$

Thus by selecting the base of the element as our co-rotational reference, the element kinematic relationships take on a rather simple form and $\underline{\tilde{h}}$ is the same for all element types. Finally, from (6.10) and (6.15) it follows that

$$\dot{\phi} = \underline{h}^T \underline{\dot{v}}^* = \underline{h}^T \boldsymbol{R}_\phi \underline{\dot{v}} \qquad \underline{\dot{\eta}} = \boldsymbol{A}\underline{\dot{v}}^* = \boldsymbol{A}\boldsymbol{R}_\phi \underline{\dot{v}} \tag{6.21}$$

where

$$\underline{h}^T = \underline{\tilde{h}}^T \boldsymbol{M}_o \qquad \boldsymbol{A} = \tilde{\boldsymbol{A}}\boldsymbol{M}_o . \tag{6.22}$$

These kinematic relationships are universally applicable. For the case of small strains we simply replace $\boldsymbol{A}$ with $\boldsymbol{A}_o$ and $\underline{h}^T$ with $\underline{h}_o^T$.

6.4.1 Relationship between geometrically linear and non-linear operators

From the above we can write

$$\underline{\beta} = \begin{bmatrix} \dot{\phi} \\ \underline{\dot{\eta}} \end{bmatrix} = \begin{bmatrix} \underline{\tilde{h}}^T \\ \tilde{\boldsymbol{A}} \end{bmatrix} \underline{\dot{w}}^* = \tilde{\boldsymbol{L}}\tilde{\boldsymbol{R}}_\phi \underline{\dot{w}} ; \quad \tilde{\boldsymbol{L}} = \begin{bmatrix} \underline{\tilde{h}}^T \\ \tilde{\boldsymbol{A}} \end{bmatrix} . \tag{6.23}$$

The geometrically linear transformation is identified with $\tilde{\boldsymbol{R}}_\phi \rightarrow \boldsymbol{I}$, $\tilde{\boldsymbol{L}} \rightarrow \tilde{\boldsymbol{L}}_o$, $\underline{\dot{w}}^* \rightarrow \underline{\dot{w}}$, such that

$$\underline{\beta}_o = \begin{bmatrix} \dot{\phi}_o \\ \underline{\dot{\eta}}_o \end{bmatrix} = \begin{bmatrix} \underline{\tilde{h}}_o^T \\ \tilde{\boldsymbol{A}}_o \end{bmatrix} \underline{\dot{w}} = \tilde{\boldsymbol{L}}_o \underline{\dot{w}} ; \quad \tilde{\boldsymbol{L}}_o = \begin{bmatrix} \underline{\tilde{h}}_o^T \\ \tilde{\boldsymbol{A}}_o \end{bmatrix} . \tag{6.24}$$

It follows immediately that

$$\underline{\dot{\beta}} = (\tilde{\boldsymbol{L}}\tilde{\boldsymbol{R}}_\phi \tilde{\boldsymbol{L}}_o^{-1})\underline{\dot{\beta}}_o , \tag{6.25}$$

where, from (6.15) with $\underline{\dot{w}}^* \rightarrow \underline{\dot{w}}$,

$$\tilde{\boldsymbol{L}}_o^{-1} = \begin{bmatrix} \tilde{\Omega}_o^T \underline{\hat{X}} & \boldsymbol{G}_o^T \end{bmatrix} . \tag{6.26}$$

Therefore if the increments of deformation and rotation are first calculated according to the geometrically linear theory, we can subsequently obtain the geometrically non-linear increments via these transformations. The generalised displacements of the element at any 'time' t are given by

$$\underline{\beta}(t) = \int_o^t \tilde{L}\tilde{R}_\phi \underline{\dot{w}}\, dt = \int_o^t \tilde{L}\tilde{R}_\phi \tilde{L}_o^{-1} \underline{\dot{\beta}}_o\, dt \ . \tag{6.27}$$

6.5 ELEMENT EQUILIBRIUM - MEASURES OF GENERALISED FORCE

Having established the kinematic relationships we now turn to formulating expressions for the element resistance.

6.5.1 The generalised element resistance

Consider a body discretised into finite elements, and acted upon by external forces and boundary reactions which form an equilibrium set (Fig. 6.7a). An individual element experiences a set of forces applied at its nodal points (Fig. 6.7b), which cause it to deform thus mobilising internal resistance. The element is in equilibrium under the action of these nodal forces.

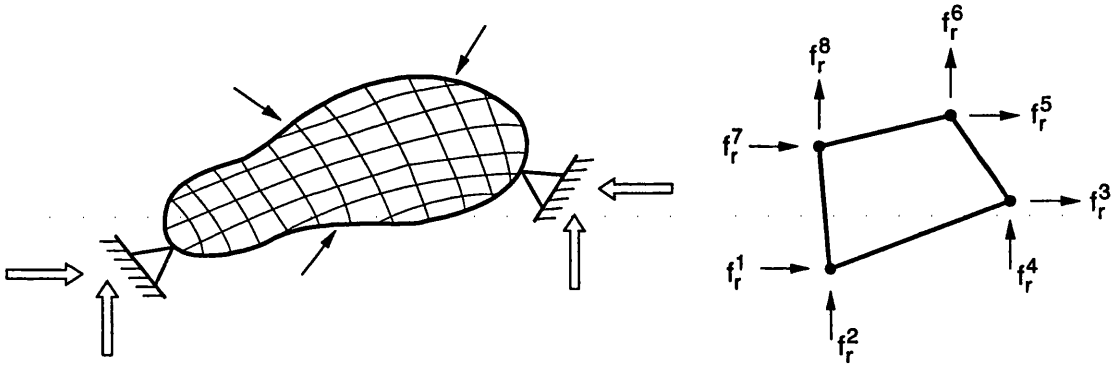

(a) Body in equilibrium under the action of external loading and boundary reactions

(b) Equilibrating set of nodal forces acting on deformed element

Fig. 6.7 Equilibrium of body and individual element

Representing the (generalised) displacement freedoms of the element in any convenient reference system by $\underline{r}$, and the corresponding work-conjugate nodal forces by $\underline{f}_r$, the principle of virtual work (see for example, MALVERN, 1969) gives

$$\delta W = \delta \underline{r}^T \underline{f}_r = \int_{V_e} \delta \underline{\varepsilon}_r^T \underline{\sigma}_r \, dV \tag{6.28}$$

in which $\underline{\sigma}_r$ and $\underline{\varepsilon}_r$ are work-conjugate measures of stress and strain, δ denotes the variation of a quantity, and the integration (assuming infinitesimal strains) is taken over the original element volume, V_e.

The variation in strain can be determined through a relationship of the form $\delta\underline{\varepsilon}_r = \boldsymbol{B}_r\delta\underline{r}$ (see section 6.6.1) where $\boldsymbol{B}_r$ is the strain displacement matrix. Thus it follows that

$$\underline{f}_r = \int_{V_e} \boldsymbol{B}_r^T \underline{\sigma}_r \, dV \tag{6.29}$$

where $\underline{f}_r$ may be called the ***generalised resistance*** of the element. In particular, in the co-rotational reference system (where we denote the infinitesimal strains as $\underline{e}^*$ and the stresses as $\underline{\sigma}^*$),

$$\delta\underline{e}^* = \boldsymbol{B}\,\delta\underline{\eta} \tag{6.30}$$

$$\underline{f}_\eta = \int_{V_e} \boldsymbol{B}^T \underline{\sigma}^* \, dV \tag{6.31}$$

and $\boldsymbol{B}$ is independent of the deformations.

6.5.2 Work-conjugate forces in various reference systems

Now let us consider the element virtual work in each of the reference systems introduced above. The virtual work is a scalar quantity and this must be invariant in all reference systems. In particular for any two reference systems denoted *r* and *s*, the following must hold

$$\delta W = \delta\underline{r}^T \underline{f}_r = \delta\underline{s}^T \underline{f}_s \,. \tag{6.32}$$

Applying this equation and using the kinematic relationships developed in section 6.4, provides the most elegant method for establishing the (work-conjugate) forces in each reference system. Thus

$$\underline{f}_u = \boldsymbol{R}_\alpha^T \underline{f}_v \qquad \underline{f}_v = \boldsymbol{M}_o^T \underline{f}_w \tag{6.33a}$$

$$\underline{f}_w = \tilde{\boldsymbol{R}}_\phi^T \underline{f}_{w^*} \qquad \underline{f}_v = \boldsymbol{R}_\phi^T \underline{f}_{v^*} \tag{6.33b}$$

$$\underline{f}_{w^*} = \tilde{\boldsymbol{A}}^T \underline{f}_\eta \qquad \underline{f}_{v^*} = \boldsymbol{A}^T \underline{f}_\eta \tag{6.33c}$$

from which

$$\underline{f}_w = \tilde{\boldsymbol{R}}_\phi^T \tilde{\boldsymbol{A}}^T \underline{f}_\eta \qquad \underline{f}_v = \boldsymbol{R}_\phi^T \boldsymbol{A}^T \underline{f}_\eta \,. \tag{6.34}$$

Although we derived the matrix $\boldsymbol{A}$ using kinematics, it is more instructive (for further development of the pseudo-force method) to consider an alternative procedure for its construction based on equilibrium considerations. This route is typically followed in the 'force method' of

structures (see PRZEMIENIECKI, 1968), but has also been employed by Argyris and his colleagues (ARGYRIS *ET AL.*, 1979) for displacement based finite elements.

In the co-rotational reference system, the deformations $\underline{\eta}$ produce straining and associated with these freedoms are generalised forces $\underline{f}_\eta$. With respect to the co-rotating reference system, three nodal point displacement freedoms are zero (corresponding to the removal of three rigid body modes - two translational and one rotational) and we may regard the element as having three boundary restraints. The reaction forces $\underline{f}_b$ on these boundary restraints together with the generalised forces $\underline{f}_\eta$ form an equilibrium set, as shown in Fig. 6.8a. The boundary reaction forces can be determined from statics as

$$\underline{f}_b = \Gamma\, \underline{f}_\eta \tag{6.35}$$

where we may call Γ the ***equilibrium matrix***. We see that the columns $\underline{\gamma}_i$ of Γ are the reaction forces when unit loads are applied in turn to each of the nodes associated with deformation freedoms (Fig. 6.8b). For an element having r rigid body modes and m deformation freedoms, Γ has dimension (r, m).

We can now denote the combined set of element forces as

$$\begin{bmatrix} \underline{f}_b \\ \underline{f}_\eta \end{bmatrix} = \begin{bmatrix} \Gamma \\ I \end{bmatrix} \underline{f}_\eta \,. \tag{6.36}$$

All that remains to be done is to order the forces to correspond to the freedom numbering in the $\underline{v}^*$ reference system. This achieved using a boolean sorting matrix S_o, and we may write

$$\underline{f}_{v^*} = S_o \begin{bmatrix} \Gamma \\ I \end{bmatrix} \underline{f}_\eta \tag{6.37}$$

and from (6.33c) follows the important result

$$A^T = S_o \begin{bmatrix} \Gamma \\ I \end{bmatrix} . \tag{6.38}$$

The matrix $\tilde{A}^T$ can be developed in a similar manner by considering equilibrium of the element with only one fixed boundary being replaced by a statically determined reaction force. This also corresponds to the removal of two rows from A^T.

For the triangular element shown in Fig. 6.8, the matrix A^T is given by

$$A^T = \begin{bmatrix} 1 & 0 & 0 & 0 & 0 & 0 \\ 0 & 1 & 0 & 0 & 0 & 0 \\ 0 & 0 & 0 & 1 & 0 & 0 \\ 0 & 0 & 1 & 0 & 0 & 0 \\ 0 & 0 & 0 & 0 & 1 & 0 \\ 0 & 0 & 0 & 0 & 0 & 1 \end{bmatrix} \begin{bmatrix} -1 & -1 & 0 \\ 0 & -a & b-1 \\ 0 & a & -b \\ 1 & 0 & 0 \\ 0 & 1 & 0 \\ 0 & 0 & 1 \end{bmatrix} = \begin{bmatrix} -1 & -1 & -1 \\ 0 & -a & b-1 \\ 1 & 0 & 0 \\ 0 & a & -b \\ 0 & 1 & 0 \\ 0 & 0 & 1 \end{bmatrix} \tag{6.39}$$

where a and b depend on the deformed geometry and are defined in Fig. 6.8. For the bar element the matrix A^T is simply the first four entries in the first column of the matrix given by (6.39).

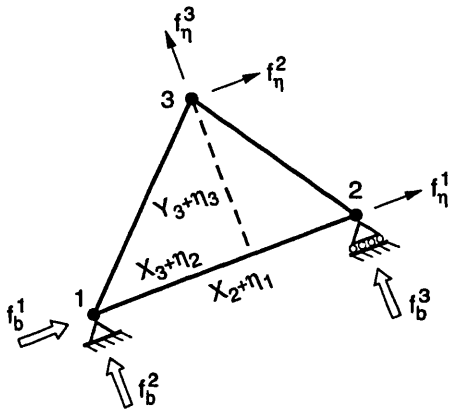

(a) Equilibrating forces acting on element

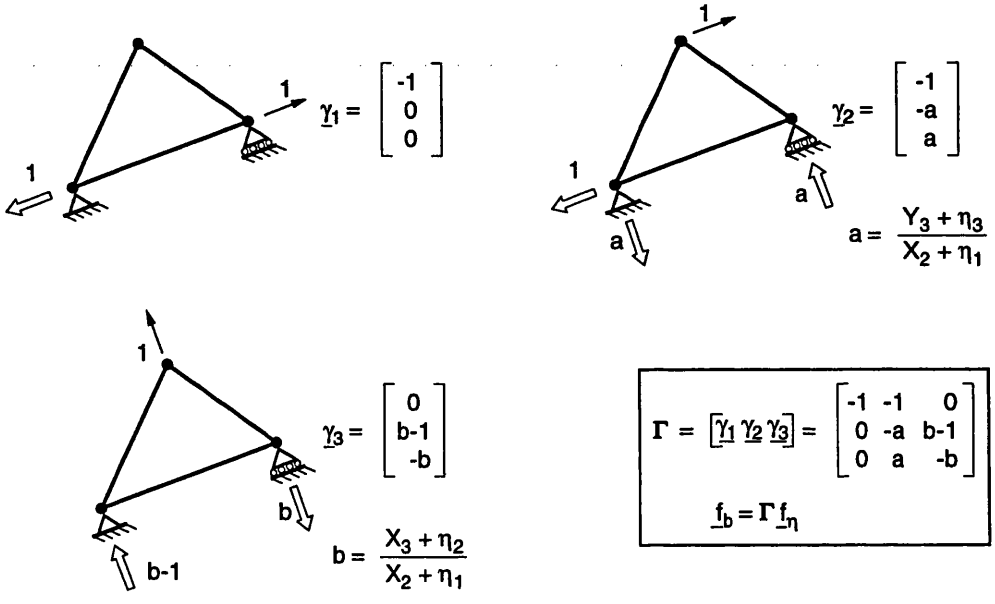

(b) Unit loads applied to deformation freedoms

Fig. 6.8 The equilibrium matrix Γ for the triangular element

Small deformations

The matrix Γ in (6.38) is based on the deformed dimensions of the element. This matrix may be split into two parts such that

$$\Gamma = \Gamma_o + \Delta\Gamma \tag{6.40}$$

where Γ_o represents the equilibrium matrix for the co-rotating element based on the element's undeformed dimensions, and $\Delta\Gamma(\underline{\eta})$ is a correction that accounts for the change in element dimensions upon straining. Inserting (6.40) into (6.38) we find that

$$A_o^T = S_o \begin{bmatrix} \Gamma_o \\ I \end{bmatrix} \qquad A_\eta^T = S_o \begin{bmatrix} \Delta\Gamma \\ O \end{bmatrix}. \tag{6.41}$$

For the bar element, A_η^T is identically zero since axial straining does not produce any boundary reaction forces normal to the bar.

Whatever the element type, if the strains are small we may ignore the contribution of $\Delta\Gamma$ and consequently (6.34) can be expressed as

$$\underline{f}_w = \tilde{R}_\phi^T \tilde{A}_o^T \underline{f}_\eta \qquad \underline{f}_v = R_\phi^T A_o^T \underline{f}_\eta \ . \tag{6.42}$$

It should be pointed out however that some care needs to be exercised in the linearisation of (6.42) otherwise the stiffness matrix will not be symmetric; retaining the full non-linear relationships (6.34) will provide symmetry without difficulty. This is discussed in more detail in section 6.7.3 below.

6.5.3 Interpreting the element forces in the fixed local reference system

We have shown how the element forces in the local reference system may be developed from the forces that act in the co-rotational reference frame. In the case of the $\underline{v}$ reference system it is apparent that this involves the formulation of an equilibrium set of forces $\underline{f}_{v^*} = A_o^T \underline{f}_\eta$ in the co-rotational system which are then rotated by R_ϕ^T to coincide with the initial element reference system.

Recalling that $R = \Phi_c + \Phi_s \Omega_o$, we may write

$$\underline{f}_v = R_\phi^T A_o^T \underline{f}_\eta = \Phi_c A_o^T \underline{f}_\eta + \Phi_s \Omega_o^T A_o^T \underline{f}_\eta \ , \tag{6.43a}$$

which is valid for a group of elements, while for an individual element we write

$$\underline{f}_v = \cos\phi (A_o^T \underline{f}_\eta) + \sin\phi (\Omega_o^T A_o^T \underline{f}_\eta). \tag{6.43b}$$

This representation is very revealing from the viewpoint of the pseudo-force method that we will discuss subsequently. In the $\underline{v}$ reference system, the forces $A_o^T \underline{f}_\eta$ are those that would be obtained from a geometrically linear theory. Now, since the operator Ω_o^T rotates the vector components in the fixed local reference anti-clockwise through 90 degrees, we see that for the geometrically non-linear bar, $\underline{f}_v$ comprises two sets of orthogonal forces whose values are simply the forces derived from the geometrically linear theory scaled by the factors $\cos\phi$ and $\sin\phi$. This is illustrated in Fig. 6.9 for a bar element. It is the second term in (6.43) that leads to the "geometric" or "initial stress" element stiffness in a finite element procedure, while the deviation from unity of the $\cos\phi$ term leads to the "initial strain" stiffness.

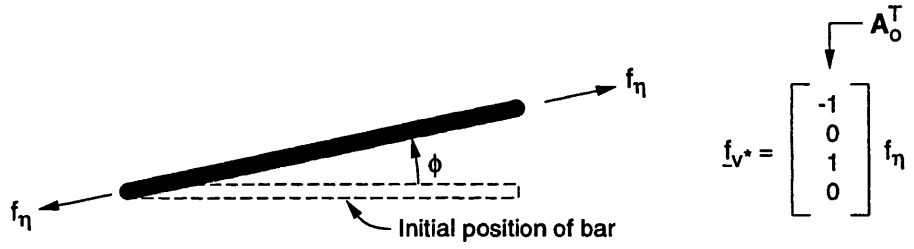

(a) Force components w.r.t. instantaneous reference frame ($\underline{v}^*$)

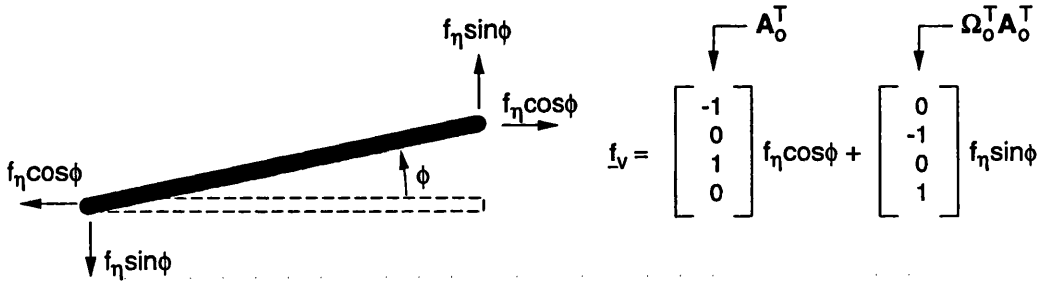

(b) Force components w.r.t. initial local reference frame ($\underline{v}$)

Fig. 6.9 Different interpretations of forces acting on a bar element

6.6 STRESS AND STRAIN RELATIONSHIPS IN A CO-ROTATING FRAME

The key to the success of the co-rotational formulation is in the simplicity of the constitutive relationships. These therefore warrant some comment before progressing.

For large displacement problems it is important that pure rigid body rotations do not cause straining. If suitable stress and strain measures can be found to satisfy this requirement, they are said to be *objective* (MALVERN, 1969; HUGHES, 1984). If we operate within a co-rotational framework, and if the strains are small, then objectivity is satisfied and the usual stress/strain measures and relationships as used in infinitesimal theory apply. The co-rotational constitutive model is therefore very simple and has a clear physical interpretation. Some of the other models

proposed for large displacement problems are much more obscure. These are discussed in some detail in appendix D, where we also look at the co-rotational formulation from a more mathematical standpoint.

6.6.1 Strain-deformation relationship

Let us first establish the relationship between the strains and the deformations in the co-rotational frame. In Fig. 6.10a, we identify a material point A with initial co-ordinates $\underline{X}$ in the fixed local reference system. This material point then translates, rotates and deforms to position A' with co-ordinates $\underline{x}^*$ measured in a moving co-rotational system (Fig. 6.10b). This co-rotational system has rotated by ϕ relative to the element's fixed (and translational) local reference system. Under pure rigid body motion, the position of A is given by A'' with co-ordinates $\underline{X}^*$. Because the strains are small (infinitesimal), $\underline{x}^*$ and $\underline{X}^*$ are indistinguishable to first order. Gradients with respect to $\underline{x}^*$ may therefore be replaced by gradients with respect to $\underline{X}^*$. Furthermore, the co-ordinate entries in $\underline{X}$ and $\underline{X}^*$ are identical and either may be referred to as material co-ordinates.

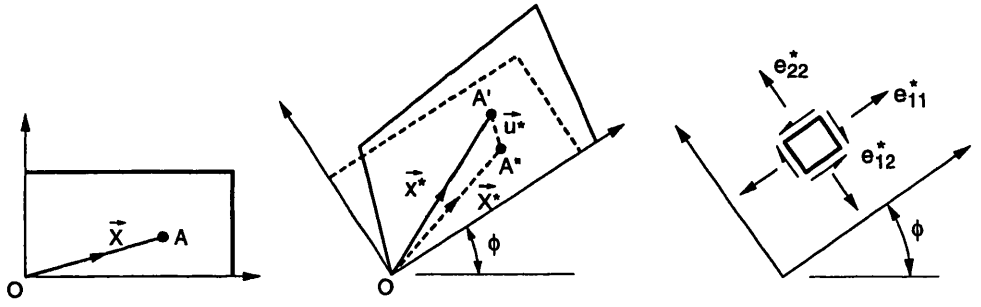

(a) Initial configuration *(b) Element deformations in co-rotational system* *(c) Strain components in co-rotating reference frame*

Fig. 6.10 Kinematics and strains in the co-rotating reference system

The deformation $\underline{u}^*$ at material point $\underline{X}^*$ within an element can be interpolated from the element deformation freedoms $\underline{\eta}$ using a matrix of shape functions N, such that

$$\underline{u}^*(\underline{X}^*) = N(\underline{X}^*)\underline{\eta} \,. \tag{6.44}$$

Now, the increments of the infinitesimal strains as measured by an observer co-rotating with the body (Fig. 6.10c) are

$$\dot{e}^*_{ij} = \frac{1}{2}\left(\frac{\partial \dot{u}^*_i}{\partial X^*_j} + \frac{\partial \dot{u}^*_j}{\partial X^*_i}\right), \qquad i,j = 1,2 \tag{6.45}$$

whereupon substituting (6.44) and using the fact that $\underline{X}^* \equiv \underline{X}$, we can write

$$\begin{bmatrix} \dot{e}^*_{11} \\ \dot{e}^*_{22} \\ \dot{e}^*_{12} \end{bmatrix} = \begin{bmatrix} \dfrac{\partial \underline{N}_1^T}{\partial X_1} \\ \dfrac{\partial \underline{N}_2^T}{\partial X_2} \\ \dfrac{1}{2}\left(\dfrac{\partial \underline{N}_1^T}{\partial X_2} + \dfrac{\partial \underline{N}_2^T}{\partial X_1}\right) \end{bmatrix} \dot{\underline{\eta}} \qquad \text{or} \qquad \dot{\underline{e}}^* = \boldsymbol{B}\dot{\underline{\eta}}\,, \tag{6.46}$$

where the strain deformation matrix $\boldsymbol{B}$ is independent of the deformation history.

6.6.2 Constitutive relationship

The constitutive relationship may be expressed in rate form as

$$\dot{\underline{\sigma}}^* = (\boldsymbol{C}^E - \boldsymbol{C}^P)\dot{\underline{e}}^* = \boldsymbol{C}^{EP}\dot{\underline{e}}^* \tag{6.47}$$

in which $\boldsymbol{C}^E$ contains the usual elastic moduli and $\boldsymbol{C}^P$ the plastic moduli. For isotropic-work-hardening associated plasticity, with a yield function (surface) $\psi(\underline{\sigma}^*)=0$, the matrix of plastic moduli are derived from the flow rule (HILL, 1950), giving

$$\boldsymbol{C}^{EP} = \boldsymbol{C}^E\left(\boldsymbol{I} - \frac{\underline{n}\,\underline{n}^T\boldsymbol{C}^E}{\underline{n}^T\boldsymbol{C}^E\underline{n} + h'(W^P)}\right); \qquad \underline{n} = \frac{\partial \psi}{\partial \underline{\sigma}^*}; \qquad W^P = \int \underline{\sigma}^{*T}\, d\underline{e}^*_p \tag{6.48}$$

where $h'(W^P)$ is the hardening index being the slope of the uni-axial true-stress/plastic-strain curve at the point where the dissipated plastic work equals W^P, and $\underline{e}^*_p$ is the plastic strain, being the total strain minus the elastic strain.

Numerically, the constitutive model would be implemented as follows. Suppose the deformations, strains and stresses at step m-1 are known. The solution of the equilibrium equations would then yield successive estimates to the updated deformations at step m. Since the $\boldsymbol{B}$ matrix is not changing within the co-rotating system, the total strain increment $D\underline{e}^*$ associated with the total deformation change is given by

$$D\underline{e}^* = \boldsymbol{B}(\underline{\eta}_m - \underline{\eta}_{m-1}) \tag{6.49}$$

and the updated stresses can then be recovered from

$$\underline{\sigma}^*_m = \underline{\sigma}^*_{m-1} + \int_{\underline{e}^*_m}^{\underline{e}^*_m + D\underline{e}^*} \boldsymbol{C}^{EP}\, d\underline{e}^*\,. \tag{6.50}$$

For plasticity problems, special procedures have been developed to perform this integration both efficiently and correctly. These ensure that drifting from the yield surface does not occur. In certain cases geometrical "return" algorithms may be employed that provide the stress increment

directly without the need for numerical integration. Details of various methods for performing the stress recovery are given by BATHE (1982), HUGHES (1984), and CHRISFIELD (1991).

6.7 STIFFNESS MATRICES

6.7.1 Generalised element tangent stiffness matrix

The solution of non-linear problems involves linearisation. The linearisation of the generalised element resistance $\underline{f}_r$ can be written as

$$\dot{\underline{f}}_r = \frac{\partial \underline{f}_r}{\partial \underline{r}} \dot{\underline{r}} = \boldsymbol{k}_r^t \dot{\underline{r}} \,. \tag{6.51}$$

where $\boldsymbol{k}_r^t$ may be called the generalised element tangent stiffness matrix.

6.7.2 Co-rotational element tangent stiffness matrix

In the co-rotating frame the element resistance was derived previously as

$$\underline{f}_\eta = \int_{V_e} \boldsymbol{B}^T \underline{\sigma}^* \, dV \tag{6.52}$$

and it is apparent by (6.51) and (6.47) that the co-rotational tangent stiffness matrix is given by

$$\boldsymbol{k}_\eta^t = \frac{\partial \underline{f}_\eta}{\partial \underline{\eta}} = \int_{V_e} \boldsymbol{B}^T \boldsymbol{C}^{EP} \boldsymbol{B} \, dV = \int_{V_e} \boldsymbol{B}^T (\boldsymbol{C}^E - \boldsymbol{C}^P) \boldsymbol{B} \, dV \,. \tag{6.53}$$

Equations (6.52) and (6.53) respectively represent the most elementary form of element resistance and stiffness matrix. The inverse of the co-rotational matrix (when it exists) is the element flexibility matrix.

If the deformation freedoms $\underline{\eta}$ are selected to correspond to pure straining modes of the element (in which case the true rigid body rotation of the element must be used to represent the co-rotating reference frame instead of the rotation of one edge) then we get Argyris' natural stiffness matrix. Although this choice may appear attractive, it does increase the complexity of the algebra. Also, the fact that the rigid body rotation for higher order elements varies spatially within the element (since the strains are not constant) complicates matters somewhat. The interested reader is referred to two papers by Argyris (ARGYRIS *ET AL.*, 1979; and ARGYRIS & TENEK, 1994) that go into the procedure in some depth.

The co-rotational tangent matrix may be split into two parts, representing the linear elastic material contribution and the inelastic or plastic contribution, giving

$$\boldsymbol{k}_\eta^E = \int_{V_e} \boldsymbol{B}^T \boldsymbol{C}^E \boldsymbol{B} \, dV \qquad \boldsymbol{k}_\eta^P = \int_{V_e} \boldsymbol{B}^T \boldsymbol{C}^P \boldsymbol{B} \, dV \,, \tag{6.54}$$

such that

$$k_\eta^t = k_\eta^E - k_\eta^P \,. \tag{6.55}$$

6.7.3 Local element tangent stiffness matrix

To derive the element tangent stiffness matrix in the fixed local co-ordinate system, we could use the chain rule of differentiation directly on (6.34), giving

$$\begin{aligned} k_v^t &= \frac{\partial \underline{f}_v}{\partial \underline{v}} = \frac{\partial (\boldsymbol{R}_\phi^T \boldsymbol{A}^T \underline{f}_\eta)}{\partial \underline{v}} \\ &= \boldsymbol{R}_\phi^T \boldsymbol{A}^T \frac{\partial \underline{f}_\eta}{\partial \underline{\eta}} \frac{\partial \underline{\eta}}{\partial \underline{v}} + \frac{\partial \boldsymbol{R}_\phi^T}{\partial \phi} \boldsymbol{A}^T \underline{f}_\eta \frac{\partial \phi}{\partial \underline{v}} + \boldsymbol{R}_\phi^T \left(\frac{\partial (\boldsymbol{A}_\eta^T \underline{f}_\eta)}{\partial \underline{\eta}} \bigg|_{\underline{f}_\eta = const} \right) \frac{\partial \underline{\eta}}{\partial \underline{v}} \end{aligned} \tag{6.56}$$

and it may be verified (by example) that this indeed provides a symmetric matrix. The last two terms, which account for changes in geometry and spatial orientation under constant force $\underline{f}_\eta$ provide the geometric stiffness matrix. If, however, we were to have differentiated the small strain form of $\underline{f}_v$ given by (6.42) instead, the last term in the geometric stiffness matrix would not be present and the overall matrix is then non-symmetric for all element types other than bars.

For a small strain formulation, it seems rather odd that we should need to carry all of the straining terms to develop a symmetric geometric stiffness matrix. Indeed for such problems we might expect that it should be sufficient to account only for the rigid body rotation in the geometric stiffness matrix. This can be achieved by following a slightly different procedure for the stiffness formulation which is now described.

We begin with the incremental form of the virtual work equation in the $\underline{w}$ reference system:

$$\delta \dot{W} = \delta \underline{w}^T \dot{\underline{f}}_w = \delta \underline{w}^T \frac{\partial \underline{f}_w}{\partial \underline{w}} \dot{\underline{w}} = \delta \underline{w}^T \boldsymbol{k}_w^t \dot{\underline{w}} \,. \tag{6.57}$$

Now, since

$$\dot{\underline{f}}_w = \frac{\partial \underline{f}_w}{\partial \phi} \dot{\phi} + \frac{\partial \underline{f}_w}{\partial \underline{\eta}} \dot{\underline{\eta}} \qquad \text{and} \qquad \delta \underline{w} = \frac{\partial \underline{w}}{\partial \phi} \delta \phi + \frac{\partial \underline{w}}{\partial \underline{\eta}} \delta \underline{\eta}, \tag{6.58}$$

we can write (6.57) in the form

$$\delta \dot{W} = \begin{bmatrix} \delta \phi & \delta \underline{\eta}^T \end{bmatrix} \begin{bmatrix} \left(\frac{\partial \underline{w}}{\partial \phi} \right)^T \\ \left(\frac{\partial \underline{w}}{\partial \underline{\eta}} \right)^T \end{bmatrix} \begin{bmatrix} \frac{\partial \underline{f}_w}{\partial \phi} & \frac{\partial \underline{f}_w}{\partial \underline{\eta}} \end{bmatrix} \begin{bmatrix} \dot{\phi} \\ \dot{\underline{\eta}} \end{bmatrix} = \begin{bmatrix} \delta \phi & \delta \underline{\eta}^T \end{bmatrix} \left[\begin{array}{c|c} \tilde{k}_{\phi\phi}^\sigma & \tilde{k}_{\phi\eta}^\sigma \\ \hline \tilde{k}_{\eta\phi}^\sigma & \tilde{k}_{\eta\eta}^\sigma + \tilde{k}_{\eta\eta} \end{array} \right] \begin{bmatrix} \dot{\phi} \\ \dot{\underline{\eta}} \end{bmatrix} \tag{6.59}$$

in which the sub-matrices with superscript 'σ' contribute to the geometric stiffness.

The increments and variations in ϕ and $\underline{\eta}$ can be expressed in terms of $\underline{v}$, as derived previously (see equation (6.21)), while the derivatives are obtained with the aid of equations (6.14), (6.33b) and (6.33c). The full stiffness matrix for k_v^t is then obtained by expanding out the matrix products. If we include all terms, we arrive at the same matrix as presented in (6.56), albeit in a different algebraic form. However, we now have the opportunity to identify that part of the geometric stiffness that comes from rigid body motion, $\tilde{k}_{\phi\phi}^{\sigma}$. We therefore write the small strain incremental virtual work as

$$\delta\dot{W} = \delta\underline{\eta}^T \tilde{k}_{\eta\eta}\,\dot{\underline{\eta}} + \delta\phi\,\tilde{k}_{\phi\phi}^{\sigma}\,\dot{\phi} \tag{6.60}$$

with the incremental work done by the remaining terms being negligible (and identically zero under rigid body motion). For a single element, the rigid body stiffness matrix $\tilde{k}_{\phi\phi}^{\sigma}$ is a scalar which we subsequently write as k_ϕ. It is given by

$$k_\phi = \hat{\underline{X}}^T \tilde{A}_o^T \underline{f}_\eta \,. \tag{6.61a}$$

Using (6.59) together with (6.14), (6.33) and (6.53), it can be shown that $\tilde{k}_{\eta\eta} = G_o \tilde{A}_o^T k_\eta^t$, and furthermore, it follows from (6.13) and (6.18) that $G_o \tilde{A}_o^T = I$. Consequently,

$$\tilde{k}_{\eta\eta} = k_\eta^t \,. \tag{6.61b}$$

Now, using the kinematic relationship (6.21), equation (6.60) can be written as

$$\delta\dot{W} = \delta\underline{v}^T R_\phi^T \left[A_o^T k_\eta^t A_o + k_\phi \underline{h}_o \underline{h}_o^T \right] R_\phi\, \dot{\underline{v}} \tag{6.62}$$

whereupon the local element tangent stiffness matrix is given by

$$k_v^t = R_\phi^T \left[A_o^T k_\eta^t A_o + k_\phi \underline{h}_o \underline{h}_o^T \right] R_\phi \,. \tag{6.63}$$

Thus using the co-rotational approach, a very elegant representation of the element tangent stiffness matrix is obtained. The geometric stiffness contribution, being the second term inside the square brackets in (6.63) is particularly simple in form while the contribution from large rotations is clearly apparent.

Comparison with other common formulations

To allow comparison with other commonly found formulations we now write

$$A_o R_\phi = A_o + A_\phi \qquad \text{with} \qquad A_\phi = A_o(R_\phi - I) \tag{6.64}$$

and the stiffness matrix k_v^t can then be expressed in the form

$$k_v^t = k_v^{EP} + k_v^\varepsilon + k_v^\sigma \tag{6.65}$$

with

$k_v^{EP} = k_v^E - k_v^P = A_o^T\, k_\eta^t\, A_o$ — the ***infinitesimal elasto-plastic*** matrix;

$k_v^\varepsilon = A_o^T\, k_\eta^t\, A_\phi + A_\phi^T\, k_\eta^t\, A_o + A_\phi^T\, k_\eta^t\, A_\phi$ — the ***initial strain***[1] matrix; and

$k_v^\sigma = k_\phi R_\phi^T \underline{h}_o \underline{h}_o^T R_\phi$ — the ***initial stress***[2] matrix.

This represents a so-called ***Total Lagrange*** formulation (see HIBBIT *ET AL.*, 1970) since the element stiffness matrices are related back to the original position of the element (i.e. the fixed local co-ordinate system). If the local co-ordinate system is updated at the end of each load increment, an ***Updated Lagrange*** procedure is obtained (see MCMEEKING & RICE, 1975; NAGTEGALL & DE JONG, 1980). In this case A_ϕ is zero and therefore k_v^ε is also zero. Both methods are however identical.

The matrix k_v^σ is important if stability problems are being considered. In the Total Lagrange procedure, k_v^ε reflects the influence of finite rotations on the element strains whereas in the Updated Lagrange method this is included in the updating procedure.

The matrix k_v^t is rank-3 deficient since it includes three rigid body modes (two displacement modes and one rotational mode). It is therefore singular. This matrix may also be derived directly from the fixed reference system (see for example, WASHIZU, 1975; ZIENKIEWIZC, 1971) using increments of the Green-Lagrange strain, but the explicit dependence on the kinematic transformation matrices A, $\underline{h}_o^T$ and R_ϕ is then obscured.

6.7.4 Element tangent stiffness matrix in global reference system

Finally, the element matrix may be rotated into a common fixed global reference system with displacements $\underline{u}$, ready for assembly into the global stiffness matrix. That is

$$k_u^t = \frac{\partial \underline{f}_u}{\partial \underline{u}} = \frac{\partial (R_\alpha^T \underline{f}_v)}{\partial \underline{u}} = R_\alpha^T \frac{\partial \underline{f}_v}{\partial \underline{v}} \frac{\partial \underline{v}}{\partial \underline{u}} = R_\alpha^T k_v^t R_\alpha \,. \tag{6.66}$$

1. Alternatively referred to as the large displacement stiffness matrix.
2. Alternatively referred to as the geometric stiffness matrix

6.8 GLOBAL EQUILIBRIUM AND LINEARISATION

6.8.1 Global equilibrium

Until now we have focused on the equilibrium at the element level. We now turn to the assembly of the element resistances into a global system of equations. Applying the principle of virtual work to the entire domain, Ω, gives

$$\delta W^{int} = \int_{\Omega} \delta \underline{e}^{*T} \underline{\sigma}^{*} \, dV = \delta \underline{u}^{T} \underline{f}_{u} \tag{6.67a}$$

$$\delta W^{ext} = \delta \underline{U}^{T} \underline{F}^{ext} \tag{6.67b}$$

where δW^{int} and δW^{ext} are the internal and external virtual work, and $\underline{U}$ and $\underline{F}^{ext}$ respectively represent the nodal displacements and applied forces, the virtual work associated with the boundary reactions being zero. Equating the internal and external virtual work provides a statement about equilibrium of the entire domain, which may be expressed as

$$\int_{\Omega} \delta \underline{e}^{*T} \underline{\sigma}^{*} \, dV = \delta \underline{u}^{T} \underline{f}_{u} = \delta \underline{U}^{T} \underline{F}^{ext}. \tag{6.68}$$

To progress further, we need to be able to relate the quantities $\underline{u}$ and $\underline{f}_{u}$ stored element-by-element, to the global nodal quantities $\underline{U}$ and $\underline{F}^{ext}$ stored node-by-node. These links are provided by

$$\underline{u} = \boldsymbol{S}_{G} \underline{U} \qquad \text{and} \qquad \boldsymbol{S}_{G}^{T} \underline{f}_{u} = \underline{F}_{ext}. \tag{6.69}$$

The operator $\boldsymbol{S}_{G}$ is a block rectangular boolean matrix that disperses the appropriate d.o.fs. in $\underline{U}$ to each element, while $\boldsymbol{S}_{G}^{T}$, which is a consequence of the equivalence of virtual work, is an operator that assembles the element forces into a global format. Making use of these operators, and the transformations already established in sections 6.4 and 6.5, the global equilibrium equation (6.68) for the entire discretised continuum may be stated as

$$\boldsymbol{S}_{G}^{T}\left(\boldsymbol{R}_{\alpha}^{T} \boldsymbol{R}_{\phi}^{T} \boldsymbol{A}_{o}^{T} \underline{f}_{\eta} \right) = \boldsymbol{S}_{G}^{T}\left(\boldsymbol{R}_{\alpha}^{T} \boldsymbol{R}_{\phi}^{T} \underline{f}_{v^{*}} \right) = \boldsymbol{S}_{G}^{T}\left(\boldsymbol{R}_{\alpha}^{T} \underline{f}_{v} \right) = \boldsymbol{S}_{G}^{T} \underline{f}_{u} = \underline{F}^{ext} \, . \tag{6.70}$$

Examining this equation from left to right, we see that the operator $\boldsymbol{A}_{o}^{T}$ converts the element forces $\underline{f}_{\eta}$ into the forces $\underline{f}_{v^{*}}$ which are then rotated into the fixed local fixed reference system by $\boldsymbol{R}_{\phi}^{T}$. A further rotation $\boldsymbol{R}_{\alpha}^{T}$ aligns these forces with the global reference system to provide $\underline{f}_{u}$, and finally $\boldsymbol{S}_{G}^{T}$ assembles the element nodal forces into the nodal resistance vector which is equated to the external loading. Herein lies the attractiveness of the notation adopted. It preserves the entire assembly process, and individual element contributions can be identified.

It is the efficient solution of this set of equations that is of interest. One solution procedure is to apply a Newton linearisation scheme directly (appendix C). This leads to the conventional f.e. approach. An alternative for structures with localised non-linearity, is to reduce the size of the system using the pseudo-force concept, as we demonstrated previously for structures with

non-linear bar elements. We will pursue the pseudo-force method in the next chapter. Let us continue here with the traditional f.e. method to complete the picture.

6.8.2 Linearisation and direct solution methods

Global tangent stiffness

We begin by writing the global equilibrium equation (6.70) in the form

$$\underline{G}(\underline{U}) = \underline{F}_U^{int} - \underline{F}^{ext} = \underline{0} \tag{6.71}$$

in which we identify the internal resistance $\underline{F}_U^{int} = S_G^T \underline{f}_u$ as the total sum of the element resistances. The sub-script 'U' indicates that the force is displacement dependent. Linearisation of this system of equations with respect to the current equilibrium point using the Newton technique described in appendix C, provides the incremental equations for the discretised continuum as

$$K^t \Delta \underline{U} = (\underline{F}^{ext} - \underline{F}_U^{int})_{(k)} \tag{6.72a}$$

$$\underline{U}_{(k+1)} = \underline{U}_{(k)} + \Delta \underline{U} \tag{6.72b}$$

where k is an iteration counter and K^t is the global tangent stiffness matrix given by

$$K^t = \frac{\partial \underline{F}_U^{int}}{\partial \underline{U}} = S_G^T k_u^t S_G = S_G^T R_\alpha^T k_v^t R_\alpha S_G \tag{6.73}$$

where the matrices k_u^t and k_v^t (see (6.66) and (6.63), respectively) are block diagonal and include all individual element stiffness matrices.

Infinitesimal theory

For future reference in chapter 7, we note that for infinitesimal displacements, the global tangent stiffness may be expressed as

$$K^t = K^E - K^P. \tag{6.74}$$

The global elastic and plastic matrices are given respectively by

$$K^E = S_G^T R_\alpha^T A_o^T k_\eta^E A_o R_\alpha S_G \qquad K^P = S_G^T R_\alpha^T A_o^T k_\eta^P A_o R_\alpha S_G \tag{6.75}$$

which correspond to the transformation and summation of the block-diagonal matrices of element stiffnesses whose entries k_η^E and k_η^P are given by (6.54).

Dynamic stiffness

The mass-inertia and viscous damping effects may be treated as equivalent external forces (D'Alembert form) such that the external loading has two contributions

$$\underline{F}^{ext} = \underline{F}^{L} + \underline{F}^{D}_{U} \tag{6.76}$$

where the applied loading $\underline{F}^{L}$ is assumed to be independent of the displacements, and the *dynamic loading* $\underline{F}^{D}_{U}$ is given by

$$\underline{F}^{D}_{U} = -(\boldsymbol{M}\ddot{\underline{U}} + \boldsymbol{C}\dot{\underline{U}}) \tag{6.77}$$

where $\boldsymbol{M}$ and $\boldsymbol{C}$ are respectively the mass and damping matrices. The incremental form of the equilibrium equation (6.71) is now

$$(\boldsymbol{K}^{t} + \boldsymbol{K}^{D})\Delta\underline{U} = (\underline{F}^{ext} - \underline{F}^{int}_{U})_{(k)} \tag{6.78}$$

where

$$\boldsymbol{K}^{D} = -\frac{\partial \underline{F}^{D}_{U}}{\partial \underline{U}} = \boldsymbol{M}\frac{\partial \ddot{\underline{U}}}{\partial \underline{U}} + \boldsymbol{C}\frac{\partial \dot{\underline{U}}}{\partial \underline{U}} \tag{6.79}$$

is the ***dynamic stiffness.***

Equation (6.78) may be written as

$$\boldsymbol{K}^{s}\,\Delta\underline{U} = -\underline{G}(\underline{U})_{(k)} \tag{6.80}$$

where $\boldsymbol{K}^{s}$ is the generalised 'stiffness' matrix and $\underline{G}(\underline{U})_{(k)}$ is the unbalanced (residual) force at iteration k.

This completes the development of the finite element procedures. It is now timely to apply the ideas expounded in this chapter to develop a more general pseudo-force method.

6.9 REFERENCES

ARGYRIS, J., BALMER, H., ST. DOLTSINIS, J., DUNNE, P.C., HASSE, H., KLEIBER, M., MALEJANNAKIS, G.A., MLEJNEK, H.P., MÜLLER, M., AND SCHARPF, D.W. (1979), "Finite element method - the natural approach", *Comp. Meth. App. Mech. & Eng.*, **17/18**, pp1-106.

ARGYRIS, J., AND TENEK, L. (1994), "Linear and geometrically nonlinear bending of isotropic and multilayered composite plates by the natural mode method", *Comp. Meth, Appl. Mech. & Eng.*, **113**, pp207-251.

BATHE, K.J. (1982), *Finite element procedures in engineering analysis*, Prentice-Hall, New Jersey.

BELYTSCHKO, T., AND HSIEH, B.J. (1973), "Non-linear transient finite element analysis with convected co-ordinates", *Int. J. Num. Meth. Eng.*, **7**, pp255-271.

BESSELING, J.F. (1974), "Non-linear analysis of structures by the finite element method as a supplement to linear analysis", *Comp. Methods in App. Mech. & Eng.*, **3**, pp173-194.

CHRISFIELD, M.A., AND COLE, G. (1989), "Co-rotational beam elements for two- and three-dimensional non-linear analysis", In: *Discretisation Methods in Structural Mechanics*, pp115-124 (Eds. Kuhn *et al.*), Springer-Verlag.

CHRISFIELD, M.A. (1990), "A consistent co-rotational formulation for non-linear three-dimensional beam elements", *Comp. Methods in App. Mech. & Eng.*, **81**, pp131-150.

References (continued)

CHRISFIELD, M.A. (1991) *Nonlinear finite element analysis of solids and structures*, Vol. I, John Wiley & Sons.

GREEN, A.E, AND ZERNA, W. (1968), *Theoretical elasticity*, Oxford University Press.

HILL, R. (1950), *The mathematical theory of plasticity*, Clarendon Press, Oxford.

HIBBITT, H.D., MARCAL, P.V., AND RICE, J.R. (1970), "A finite element formulation of problems of large strain and large displacement", *Int. J. Solids & Structs.*, **6**, pp1069-1086.

HUGHES, T.J.R. (1984), "Numerical implementation of constitutive models: rate independent deviatoric plasticity", In: *Theoretical Foundations for Large-scale Computations for Nonlinear Materials Behaviour* (Eds. S. Nemat-Nasser, R.J. Asaro, & G.A. Hegemier), Martinus Nijhoff Publishers, The Netherlands.

MCMEEKING, R.M., AND RICE, J.R. (1975), "Finite element formulations for problems of large elastic-plastic deformation", *Int. J. Solids & Structs.*, **11**, pp601-616.

MALVERN, L.E. (1969), *Introduction to the mechanics of a continuous medium*, Prentice-Hall.

MATTIASON, K. (1983), *On the co-rotational finite element formulation for large deformation problems*, Pub. 83:1, Dept. of Structural Mechanics, Chalmers University of Technology.

NAGTEGALL, J.C., AND DE JONG, J.E., (1980), "Some computational aspects of elastic-plastic large strain analysis", In: *Computational Methods in Nonlinear Mechanics*, (J.T. Oden, Ed.).

NEEDLEMAN, A. (1981), "Plasticity of metals at finite strain: theory, computation and experiment", In: *Proc. Res. Workshop* (Eds. E.H. Lee, and R.L. Mallet), Stanford University.

NEEDLEMAN, A., AND TVERGAARD, V. (1984), "Finite element analysis of localised plasticity", In: *Finite elements: special problems in solid mechanics*, Vol. 5, (J.T. Oden and G.F. Carey, Eds.).

PRZEMIENIECKI, J.S. (1968), *Theory of Matrix Structural Analysis*, McGraw-Hill.

WASHIZU, K. (1975), *Variational methods in elasticity and plasticity*, Pergamon Press, Oxford.

ZIENKIEWICZ, O.C. (1971), *The finite element method in engineering science*, McGraw-Hill.

Chapter 7

THE PSEUDO-FORCE INFLUENCE METHOD

- A continuum mechanics approach -

7.1 INTRODUCTION

In chapter 3 we derived a pseudo-force procedure for efficient static analyses of framed structures in which local non-linear material behaviour was represented by bar elements. The method was then extended in chapter 4 to include dynamic response. For the case in which mass/dampers were present at only a few discrete points an exact formulation was developed; otherwise the dynamic resistance was approximated using modal techniques while retaining the precise non-linear material influences.

We now probe deeper into the theory behind the pseudo-force method, thereby establishing its connection with the co-rotational finite element method presented in chapter 6. The intent is to extend the pseudo-force concept to problems of (planar) continua in which the strains are infinitesimal but the displacements (rotations) may be arbitrarily large.

7.1.1 The problem

The global equilibrium for a discretised non-linear continuum (with or without dynamic resistance) leads to a system of non-linear equations which may be represented (see equation (6.71)) as

$$\underline{G}(\underline{U}) = \underline{F}_U^{int} - \underline{F}^{ext} = \underline{0} \qquad (N \text{ equations}). \tag{7.1}$$

where $\underline{U}$ represents the nodal displacement freedoms, $\underline{F}_U^{int}$ is the internal resistance of the body and $\underline{F}^{ext}$ is the applied loading which may or may not be a function of $\underline{U}$. Direct linearisation of this was shown to result in an iterative solution procedure of the form

$$\boldsymbol{K}^S \Delta\underline{U} = -\underline{G}_{(k)} \qquad (N \text{ equations}). \tag{7.2a}$$

$$\underline{U}_{(k+1)} = \underline{U}_{(k)} + \Delta\underline{U}. \tag{7.2b}$$

Thus at each iteration, the entire system of N nodal unknowns is solved. For the class of problem having local regions of non-linearity and mass/dampers at only a few discrete points, only a few entries in the generalised stiffness matrix $\boldsymbol{K}^s$ and unbalanced (residual) force $\underline{G}_{(k)}$ are changing at each iteration, and the direct solution procedure is not efficient. We will focus primarily on developing more effective solution methods for this problem class as it lends itself to an exact re-formulation using our pseudo-force procedures. However in order to extend the bounds of the methods developed, we also explore the idea of merging pseudo-force and modal (reduced basis[1]) methods. In this latter procedure, the dynamic resistance and global geometric non-linearity are described approximately while the exact contribution of the resistance of elements undergoing plastic deformations is retained.

The intent is to derive and solve a reduced non-linear system of equations

$$\underline{g}(\underline{x}) = \underline{0} \qquad (n \text{ equations}) \tag{7.3}$$

of dimension $n << N$, which upon linearisation become

$$\overline{\boldsymbol{K}}\,\Delta\underline{x} = -\underline{g}_{(k)} \qquad (n \text{ equations}) \tag{7.4a}$$

$$\underline{x}_{(k+1)} = \underline{x}_{(k)} + \Delta\underline{x}. \tag{7.4b}$$

To arrive at this reduced system, we employ once more the notion of a linear-elastic model acted upon by pseudo-forces representing the inelastic and dynamic resistances.

7.1.2 Element and nodal pseudo-force methods

The inelastic resistance of an element may be represented in the linear-elastic model in two ways. If we apply local pseudo-forces to each individual element independently (as was done for the bar element), we call this an ***element pseudo-force method.*** Unlike a conventional finite element (f.e.) procedure, the pseudo-forces from each element are not summed if the non-linear elements have inter-connecting nodes. The local pseudo-forces are decomposed into ***self-equilibrating load-sets*** multiplied by ***scaling factors.*** From the self-equilibrating load-sets ***influence matrices*** are derived which provide the coupling between the 'non-linear' elements. The unknowns in the reduced system of equations are the scaling factors.

As an alternative, we may apply global pseudo-forces to all nodal freedoms to which non-linear elements are attached (as we discussed briefly at the end of section 4.5.3). In this ***nodal pseudo-force method*** we sum the pseudo-forces acting at common nodal points, treating each

1. In the reduced basis method (see review papers by NOOR, 1981, 1994), an efficient but approximate solution to the general non-linear dynamics problem is sought by using a few mode shapes (basis vectors) to characterise the overall global behaviour. The accuracy and performance of the method then depends crucially on the choice of the basis vectors. This differs from our pseudo-force method where we look for an exact representation of the resistance of those elements undergoing plastic deformations.

nodal freedom separately. Influence matrices are derived by applying unit loads in turn to each global freedom connected to 'non-linear' elements. The unknowns in the reduced system of equations are the global pseudo-forces.

For element pseudo-force methods, the number of unknown pseudo-forces increases in direct proportion to the number of non-linear elements, whereas for the nodal pseudo-force approach the number of unknowns is determined by the connectivity of the non-linear elements. So in general one may say that nodal pseudo-force methods become more effective as the number of non-linear elements with common nodes increases.

For space-framed structures where the non-linear members are modelled as bars or beams, element pseudo-force methods are the most attractive, since non-linear behaviour is governed by only a few members that are either unconnected or whose connectivity is "weak". However for problems of plasticity in continua the plastic zone may cover many elements, resulting in "strong" connectivity, and nodal pseudo-forces schemes are to be preferred. Of course an option is to mix the two schemes, using the nodal procedure in strongly connected areas and the element procedure in weakly connected areas.

Because we make use of influence matrices and pseudo-forces, we refer to the above procedures as the ***Nodal Pseudo-Force Influence Method*** (NPFI-Method) and the ***Element Pseudo-Force Influence Method*** (EPFI-Method).

7.1.3 Literature review of pseudo-force methods

Pseudo-force and related methods have been applied extensively in re-analysis studies of linear-elastic structures. As material non-linearity may be viewed as a continuous modification of the structure's properties, re-analysis of linear-elastic structures is a special case of the non-linear problem. The literature in this field is therefore of some interest as many of the concepts carry over to the non-linear theory. The reader is referred to the excellent reviews on this topic by ARORA (1976) and ABU-KASSIM & TOPPING (1987) which provide a mostly complete summary of the publications up to 1987. Additional information may also be found in chapter 5 of the text of KIRSCH (1981). Below, we give a brief overview of the milestones in the developments of such methods.

Element pseudo-force and related methods

In section 3.3.4, we discussed briefly the heuristic development of the element pseudo-force technique for the re-analysis of linear-elastic structures in which the properties of certain bar elements were to be modified. This heuristic development was traced back to the work of AL-BAKRI (1978) who worked on structural optimisation of linear-elastic space frame towers. However the fundamental principles governing element-based pseudo-force and related methods were expounded much earlier than this and date back to the mid 1950's. From 1956 onwards, Argyris and his co-workers published several articles showing how the response of a modified linear-elastic structure could be obtained without a complete reformulation of the stiffness matrix (ARGYRIS & KELSEY, 1956, 1960, 1961; ARGYRIS, 1964). The approach they favoured was the matrix

force method, which leads naturally to an element-based procedure whereby *initial strains*[1] are introduced into those elements whose material characteristics are to be changed. They also recognised that only a reduced system of equations had to be solved to obtain the unknown initial strains. The first steps were also taken to model material non-linearity in this way (ARGYRIS, 1964).

Other contributions to element-based pseudo-force methods have also been evident and have helped to consolidate the ideas of the procedure. Using the principle of complimentary work, MELOSH & LUIK (1968) re-derived the initial strain technique. This was further elaborated upon by FENVES & ERTAS (1969). More recently, various publications by Holnicki-Szulc, Gierlinski and Mroz (HOLNICKI-SZULC & MROZ, 1985; HOLNICKI-SZULC, 1987, 1989; HOLNICKI-SZULC & GIERLINSKI, 1989, HOLNICKI-SZULC, 1991) have once again highlighted the usefulness of the initial strain concept and shown how it may be applied in various ways to obtain the response of linear-elastic systems under general (non-linear) constraints.

The approach adopted in this work to derive the element-based pseudo-forces differs from that employed in earlier developments in that we strive to ensure a formulation consistent with the non-linear finite element (displacement) method. This ensures that for non-linear problems there is no ambiguity on how to include incremental plasticity or large displacement effects, a difficulty that may arise if one tries to extend heuristically the ideas of linear-elastic re-analysis.

Nodal pseudo-force and related methods

The Woodbury/Householder method (WOODBURY, 1950; HOUSEHOLDER, 1957) provides the inverse of a matrix in terms of an initial matrix and its modification. ARGYRIS *ET AL.* (1971) used this technique to derive a reduced set of equations for re-analysis of linear-elastic structures. This is not a pseudo-force method but, as we will demonstrate below, this ***direct modification procedure*** can be re-cast in pseudo-force form. Indeed the revised form is identical to the pseudo-force method subsequently derived by WANG, PILKEY & PALAZZOLO (1983). This latter method was extended to include non-linear material behaviour by ABU-KASSIM & TOPPING (1987).

Other direct procedures, such as the well-known static condensation method (see for example BATHE, 1982) may also be used to obtain a reduced system of equations. We touched briefly on this procedure earlier in chapter 4, but presently we concentrate our efforts on pseudo-force methods.

Remark

From this review it can be seen that although pseudo-force techniques can be derived in many different ways, there are essentially only two sets of reduced equations - one set for element-based procedures and the other set for procedures that operate on the nodal quantities.

1. For geometrically linear problems, it is well known that pseudo-forces may be generated by initial strains and therefore (as we will show) initial strain methods can be re-posed in pseudo-force form.

7.1.4 Summary of kinematics, constitutive laws and resistance relationships

We now summarise the relationships developed in chapter 6 relating to infinitesimal theory and large displacement theory. These will be used frequently in the remainder of this chapter.

Infinitesimal theory

The relationships for the infinitesimal theory are summarised in Box 7.1. There are a few deviations from the theory presented in chapter 6. Firstly, because the kinematic transformation from displacements to strains is linear, we can write the strain deformation relationship in terms of total deformation (instead of increments of deformation). Secondly, we have split the resistance into two parts. This splitting is purely arbitrary and is one of convenience. Finally, we have dropped the asterisk from the stress and strain terms as there is no need to distinguish co-rotational and infinitesimal measures.

Box 7.1 Relationships for infinitesimal theory

Kinematics: $\underline{u} = S_G \underline{U}; \quad \underline{v} = R_\alpha \underline{u}; \quad \underline{\eta} = A_o \underline{v}$

Strain deformation: $\underline{e} = B\underline{\eta}$

Constitutive law: $\dot{\underline{\sigma}} = (C^E - C^P)\dot{\underline{e}} = C^{EP}\dot{\underline{e}}$

Stresses: $\underline{\sigma} = \underline{\sigma}_E - \underline{\sigma}_{NL}\ ; \quad \underline{\sigma}_E = C^E \underline{e}\ , \quad \underline{\sigma}_{NL} = \int C^P d\underline{e}$

Resistance splitting: $\underline{f}_\eta = \int_{V_e} B^T \underline{\sigma}\, dV = \int_{V_e} B^T (\underline{\sigma}_E - \underline{\sigma}_{NL})\, dV = \underline{f}_\eta^E - \underline{f}_\eta^{NL}$

$$\underline{f}_\eta^E = \left(\int_{V_e} B^T C^E B\, dV \right) \underline{\eta} = k_\eta^E \underline{\eta}$$

$$\underline{f}_\eta^{NL} = \int_{V_e} B^T \underline{\sigma}_{NL}\, dV$$

Large displacement theory

The relationships for the large displacement theory are summarised in Box 7.2. As in the infinitesimal theory, we have split the strain, stress and resistance into two (arbitrary) parts. The first part represents the result that would be obtained if infinitesimal theory (as is used in our linear-elastic analysis software) is used to calculate the deformation increments from the relative displacement increments, while the second part is simply the difference between the true response and this linear-elastic response. Finally, in the kinematic relationships, we have replaced the operator $\tilde{L}$ with $\tilde{L}_o$, which is valid for small strains.

Box 7.2 Relationships for finite rotation theory

Kinematics:

$$\underline{u} = S_G \underline{U}; \qquad \underline{v} = R_\alpha \underline{u}; \qquad \underline{w} = M_o \underline{v}$$

$$\dot{\underline{\beta}} = \begin{bmatrix} \dot{\phi} \\ \dot{\underline{\eta}} \end{bmatrix} = \tilde{L}_o R_\phi \dot{\underline{w}} \qquad \dot{\underline{\beta}}_o = \begin{bmatrix} \dot{\phi}_o \\ \dot{\underline{\eta}}_o \end{bmatrix} = \tilde{L}_o \dot{\underline{w}} \qquad \dot{\underline{\beta}} = \tilde{L}_o \tilde{R}_\phi \tilde{L}_o^{-1} \dot{\underline{\beta}}_o$$

$$\tilde{L}_o = \begin{bmatrix} \tilde{\underline{h}}_o^T \\ \tilde{A}_o \end{bmatrix} \qquad \tilde{L}_o^{-1} = \begin{bmatrix} \tilde{\Omega}_o^T \hat{\underline{X}} & I \end{bmatrix}$$

Strain deformation:

$$\dot{\underline{e}}^* = B\dot{\underline{\eta}} = B\dot{\underline{\eta}}_o + B(\dot{\underline{\eta}} - \dot{\underline{\eta}}_o) = \dot{\underline{e}}_o^* + \dot{\underline{e}}_{NL}^*$$

Constitutive law:

$$\dot{\underline{\sigma}}^* = (C^E - C^P)\dot{\underline{e}}^* = C^E \dot{\underline{e}}_o^* - (C^P \dot{\underline{e}}^* - C^E \dot{\underline{e}}_{NL}^*)$$

Stresses:

$$\underline{\sigma}^* = \underline{\sigma}_{Eo}^* - \underline{\sigma}_{NL}^* \; ; \qquad \underline{\sigma}_{Eo}^* = C^E \underline{e}_o^* \, , \qquad \underline{\sigma}_{NL}^* = \int (C^P d\underline{e}^* - C^E d\underline{e}_{NL}^*)$$

Resistance splitting:

$$\underline{f}_\eta = \int_{V_e} B^T \underline{\sigma}^* \, dV = \underline{f}_\eta^{Eo} - \underline{f}_\eta^{NL}$$

$$\underline{f}_\eta^{Eo} = k_\eta^E \underline{\eta}_o$$

$$\underline{f}_\eta^{NL} = \int_{V_e} B^T \underline{\sigma}_{NL}^* \, dV$$

7.2 MATERIAL PSEUDO-FORCES ACTING ON A SINGLE ELEMENT

The first step in the development is to identify the pseudo-forces acting on the linear-elastic model. This we do for both the geometrically linear and geometrically non-linear problems.

7.2.1 Infinitesimal (geometrically linear) theory

The pseudo-forces can be derived by equating the virtual work of an individual element in the non-linear material model with the same element in an equivalent linear-elastic model (Fig. 7.1). The virtual work for an element in the non-linear model is given by

$$\delta W = \delta \underline{\eta}^T \underline{f}_\eta = \delta \underline{\eta}^T \left(\underline{f}_\eta^E - \underline{f}_\eta^{NL} \right) \tag{7.5}$$

while in the equivalent linear elastic model it is

$$\delta W = \delta \underline{\eta}^T \underline{f}_\eta^E - \delta \underline{v}^T \underline{q}_v^{NL} \, . \tag{7.6}$$

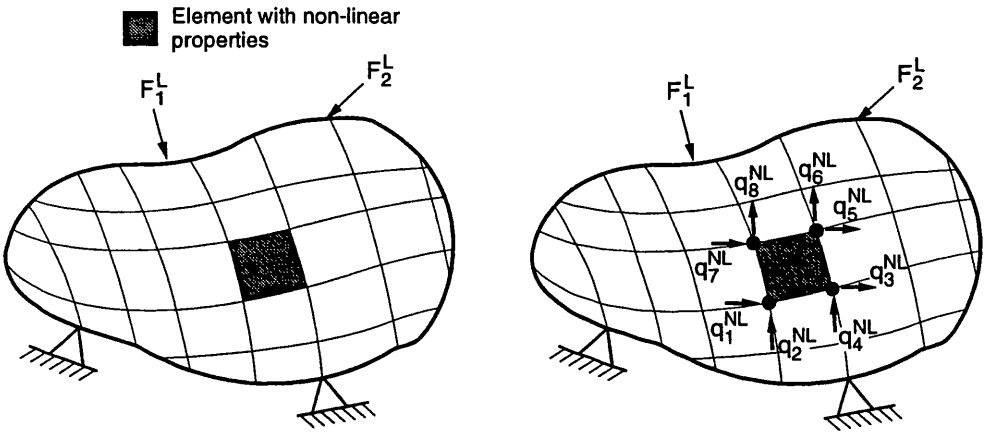

(a) Non-linear material model

(b) Equivalent linear-elastic model with additional pseudo-forces $\underline{q}^{NL}$

Fig. 7.1 Equivalent representation of a non-linear problem

Now, since

$$\underline{\eta} = A_o \underline{v} \tag{7.7}$$

it follows that the two models are identical if and only if local correction or pseudo-forces given by

$$\underline{q}_v^{NL} = A_o^T \underline{f}_\eta^{NL} \tag{7.8}$$

act on the 'non-linear' elements of the equivalent linear-elastic model.

7.2.2 Large displacement (geometrically non-linear) theory

Following the same arguments as above for the infinitesimal theory, and with the aid of the relationships given in Box 7.2, the virtual work in the non-linear model may be written as

$$\delta W = \delta \underline{\eta}^T \underline{f}_\eta = \delta \underline{\eta}^T \left(\underline{f}_\eta^{Eo} - \underline{f}_\eta^{NL} \right). \tag{7.9}$$

Comparing this expression with equation (7.5) of the infinitesimal theory, we observe that an elastic contribution to the element resistance is identified as $\underline{f}_\eta^{Eo}$ and given by

$$\underline{f}_\eta^{Eo} = k_\eta^E \underline{\eta}_o \,. \tag{7.10}$$

This is <u>not</u> the total elastic resistance which would be given by

$$\underline{f}_\eta^{E} = k_\eta^E \underline{\eta} \,. \tag{7.11}$$

We need to make this important distinction because in the equivalent linear-elastic model the deformation-displacement transformation matrix used is A_o and therefore $\underline{\eta}_o$ is calculated from the nodal displacements, not $\underline{\eta}$.

Considering now the equivalent linear-elastic model, the virtual work is

$$\delta W = \delta \underline{\eta}_o^T \underline{f}_\eta^{Eo} - \delta \underline{v}^T \underline{q}_v^{NL} \tag{7.12}$$

and using the kinematic relationships

$$\delta \underline{\eta}_o = A_o \delta \underline{v}, \qquad \delta \underline{\eta} = A_o R_\phi \delta \underline{v} \tag{7.13}$$

we find that the two models are identical if and only if local pseudo-forces given by

$$\underline{q}_v^{NL} = A_o^T \underline{f}_\eta^{Eo} - R_\phi^T A_o^T \underline{f}_\eta \tag{7.14}$$

are applied to the elements in the linear-elastic model.

7.3 GENERAL PRINCIPLES OF PSEUDO-FORCE METHODS

The same general principles govern the development of both nodal and element pseudo-force methods. We begin by separating out a linear-elastic contribution $\underline{F}_U^E$ from the element global resistance such that

$$\underline{F}_U^{int} = \underline{F}_U^E - \underline{F}_U^{NL} . \tag{7.15}$$

The individual contributions can be identified by making use of the virtual work equivalence $\delta \underline{U}^T \underline{F}_U^{int} = \delta \underline{\eta}^T \underline{f}_\eta$ together with the kinematic transformations and other relationships given in Box 7.2. This leads to

$$\underline{F}_U^E = S_G^T R_\alpha^T A_o^T \underline{f}_\eta^{Eo} = \left(S_G^T R_\alpha^T \left[A_o^T k_\eta^E A_o\right] R_\alpha S_G\right) \underline{U} = K^E \underline{U} \tag{7.16a}$$

$$\underline{F}_U^{NL} = S_G^T R_\alpha^T \underline{q}_v^{NL} \tag{7.16b}$$

in which k_η^E is a block diagonal matrix of all linear-elastic element stiffnesses, and from (7.8) and (7.14), $\underline{q}_v^{NL}$ is either

$$\underline{q}_v^{NL} = A_o^T \underline{f}_\eta^{NL} \qquad \text{(infinitesimal theory)} \tag{7.17a}$$

or

$$\underline{q}_v^{NL} = A_o^T \underline{f}_\eta^{Eo} - R_\phi^T A_o^T \underline{f}_\eta \qquad \text{(large displacement theory).} \tag{7.17b}$$

Identifying $\underline{F}^{ext} = \underline{F}^L + \underline{F}^D_U$ as in (6.76), where $\underline{F}^L$ is the applied loading and $\underline{F}^D_U$ is the D'Alembert form of the dynamic resistance, and utilising (7.15) and (7.16a), the global equilibrium equation (7.1) may now be written as

$$\boldsymbol{K}^E \underline{U} = \underline{F}^L + \underline{F}^{NL}_U + \underline{F}^D_U \,. \tag{7.18}$$

This is now in the form of an ***equivalent linear-elastic model*** acted upon by the physical loads $\underline{F}^L$ plus a set of ***material pseudo-forces***, $\underline{F}^{NL}_U$ and ***dynamic pseudo-forces***, $\underline{F}^D_U$. By virtue of (7.16b) we see that the material pseudo-forces $\underline{F}^{NL}_U$ are simply the element pseudo-forces assembled into a global column matrix. This further implies that $\underline{F}^{NL}_U$ has non-zero entries only at nodal freedoms associated with 'non-linear' elements. We also recall from chapter 6 that $\underline{F}^D_U = -(\boldsymbol{M}\ddot{\underline{U}} + \boldsymbol{C}\dot{\underline{U}})$, where $\boldsymbol{M}$ and $\boldsymbol{C}$ are diagonal matrices, and $\underline{F}^D_U$ has non-zero entries only at those nodal freedoms with masses or dampers attached.

Of course the mass and damping matrices could be taken to the left hand side of (7.18) which could then be solved recursively for $\underline{U}$. However for the class of problem under consideration in which $\underline{F}^{NL}_U$ and $\underline{F}^D_U$ have many zero entries, this ***direct initial stiffness*** method would clearly not be a very effective procedure.

We continue by notionally inverting (7.18) (which is never actually done as the solution would be calculated using some form of matrix factorisation, such as the Cholesky method as described in the text of BATHE, 1982), giving

$$\underline{U} = \underline{U}^L + (\boldsymbol{K}^E)^{-1}\left[\underline{F}^{NL}_U + \underline{F}^D_U\right] \tag{7.19}$$

where

$$\underline{U}^L = (\boldsymbol{K}^E)^{-1}\underline{F}^L \tag{7.20}$$

is the solution to the linear-elastic static problem. We also note that (7.19) may be expressed as

$$\underline{U} = \underline{U}^L + \underline{U}^{NL} + \underline{U}^D \,. \tag{7.21}$$

That is the response $\underline{U}$ to the non-linear dynamic problem can be split into three separate components: one for the static loading ($\underline{U}^L$); one for the non-linear material behaviour ($\underline{U}^{NL}$); and another for the dynamic loading ($\underline{U}^D$). This serves to emphasise that linear-superposition is the basis of the pseudo-force approach.

Up to this point, the development of the nodal and element pseudo-force methods is identical. Furthermore, the reduction procedure for the dynamic pseudo-forces also progresses in a similar manner for both methods, as will be explained shortly. The precise details of each procedure will be explained in the remainder of this chapter, but first it may be useful to clarify where we are headed by giving a very brief outline of the methodology.

For the time being we will concentrate on the statics problem as it is in the treatment of the non-linear element resistance that the methods differ. In the nodal pseudo-force method we relate the nodal displacements $\underline{Y}$ of the 'non-linear' elements to the total set of nodal displacements $\underline{U}$ using a boolean matrix $\boldsymbol{Z}_Y$. The total number of entries in $\underline{Y}$ depends on the connectivity of this

'non-linear' element set. In the element pseudo-force method, we keep separate the information for each 'non-linear' element. A transformation matrix $\mathbf{Z}_r$ operating on $\underline{U}$ provides the desired element quantities $\underline{r}$ (usually displacements or deformations). The number of entries in $\underline{r}$ depends directly on the number and types of elements selected. The outcome of each of these transformations on (7.19) is a reduced system of equations. Using the equivalence of virtual work, the global force $\underline{F}_U^{NL}$ is transformed to an equivalent force in each of the reduced systems. The development of both methods for statics problems is outlined in Box 7.3 below.

We remark that in contrast to a standard f.e. procedure, the reduced tangent matrices are full and non-symmetric. However, if we employ an initial stiffness iteration procedure, both $\overline{K}_Y^t$ and $\overline{K}_r^t$ are identity matrices, and no inversion is required. If a modified or full Newton method is preferred, symmetry can be restored by the procedure given in section 3.5.1 (see equation (3.49)). That the reduced tangent matrix is full is interesting. This is a consequence of the influence matrix and it means that each freedom included in the reduced system feels the presence of all others while in a conventional direct finite element procedure, the domain of influence is restricted to those elements that share a common node. This has implications for the efficiency of the pseudo-force method, as discussed in section 7.8.

Box 7.3 Development of Nodal and Element pseudo-force methods for statics

Nodal method		**Element method**
	transformations	
$\underline{Y} = \mathbf{Z}_Y \underline{U}$		$\underline{r} = \mathbf{Z}_r \underline{U}$
$\underline{F}_U^{NL} = \mathbf{Z}_Y^T \underline{F}_Y^{NL}$		$\underline{F}_U^{NL} = \mathbf{Z}_r^T \underline{f}_r^{NL}$
	reduced system	
$\underline{Y} = \underline{Y}^L + \mathbf{Z}_Y (\mathbf{K}^E)^{-1} \mathbf{Z}_Y^T \underline{F}_Y^{NL}$		$\underline{r} = \underline{r}^L + \mathbf{Z}_r (\mathbf{K}^E)^{-1} \mathbf{Z}_r^T \underline{f}_r^{NL}$
	or	
$\underline{Y} = \underline{Y}^L + \mathbf{H}^{YY} \underline{F}_Y^{NL}$		$\underline{r} = \underline{r}^L + \mathbf{D}^{rr} \underline{f}_r^{NL}$
	tangent matrix	
$\overline{K}_Y^t = \mathbf{I} - \mathbf{H}^{YY} \frac{\partial \underline{F}_Y^{NL}}{\partial \underline{Y}}$		$\overline{K}_r^t = \mathbf{I} - \mathbf{D}^{rr} \frac{\partial \underline{f}_r^{NL}}{\partial \underline{r}}$

7.4 THE NODAL PSEUDO-FORCE INFLUENCE METHOD (NPFI-Method)

We begin our general treatment of pseudo-force techniques with the development of the nodal pseudo-force influence method (NPFI-Method).

7.4.1 Infinitesimal theory

In this section, the basic principles of the NPFI-Method are established for problems in which both the displacements and the strains are infinitesimally small while the material properties are non-linear. Both statics and dynamics problems are considered.

The reduced nodal system equations

In the NPFI-Method, the pseudo-forces that represent the element non-linearity and dynamic resistance both depend on some reduced set of displacement freedoms. The displacement freedoms at which mass/dampers are attached are denoted by $\underline{X}$, and those connected to non-linear elements are denoted by $\underline{Y}$. The reduced sets of displacement freedoms and the forces acting on them may be related to the entire set of displacement freedoms and nodal forces by the following mappings

$$\underline{X} = \boldsymbol{Z}_X \underline{U}; \qquad \underline{Y} = \boldsymbol{Z}_Y \underline{U} \tag{7.22a}$$

$$\underline{F}_X^D = \boldsymbol{Z}_X \underline{F}_U^D; \qquad \underline{F}_Y^{NL} = \boldsymbol{Z}_Y \underline{F}_U^{NL} \tag{7.22b}$$

$$\underline{F}_U^D = \boldsymbol{Z}_X^T \underline{F}_X^D; \qquad \underline{F}_U^{NL} = \boldsymbol{Z}_Y^T \underline{F}_Y^{NL} \tag{7.22c}$$

where the last set of equations follow from the equivalence of virtual work. Applying these transformations to (7.19), and denoting by superscript 'L' the response of the linear-elastic static problem due to the applied loading alone, we can write

$$\begin{bmatrix} \underline{X} \\ \underline{Y} \end{bmatrix} = \begin{bmatrix} \underline{X}^L \\ \underline{Y}^L \end{bmatrix} + \begin{bmatrix} \boldsymbol{H}^{XX} & \boldsymbol{H}^{XY} \\ \boldsymbol{H}^{YX} & \boldsymbol{H}^{YY} \end{bmatrix} \begin{bmatrix} \underline{F}_X^D \\ \underline{F}_Y^{NL} \end{bmatrix} \tag{7.23}$$

where we identify $\underline{F}_X^D$ and $\underline{F}_Y^{NL}$ as the dynamic and material ***pseudo-forces***, respectively, and the matrices $\boldsymbol{H}^{AB}$ (A, B being either X or Y) as ***displacement influence matrices*** whose columns are the response $\underline{A}$ for unit loads applied in turn to each degree of freedom in $\underline{B}$ (Fig. 7.2).

Formally, these displacement influence matrices are

$$\begin{aligned} \boldsymbol{H}^{XX} &= \boldsymbol{Z}_X (\boldsymbol{K}^E)^{-1} \boldsymbol{Z}_X^T & \boldsymbol{H}^{XY} &= \boldsymbol{Z}_X (\boldsymbol{K}^E)^{-1} \boldsymbol{Z}_Y^T \\ \boldsymbol{H}^{YX} &= \boldsymbol{Z}_Y (\boldsymbol{K}^E)^{-1} \boldsymbol{Z}_X^T & \boldsymbol{H}^{YY} &= \boldsymbol{Z}_Y (\boldsymbol{K}^E)^{-1} \boldsymbol{Z}_Y^T \end{aligned} \tag{7.24}$$

whereupon we observe that both H^{XX} and H^{YY} are symmetric (since K^E is symmetric), while $H^{XY} = (H^{YX})^T$.

The reduced system equations (7.23) may be solved by the procedures given in chapter 4. Modal techniques can also be employed as noted in section 4.5 - we will return to this topic later in section 7.7. Once the solution for $\underline{X}$ and $\underline{Y}$ has been found, the response of the remaining degrees of freedom may be obtained by the recovery procedure described in section 3.3.3. One should add that it is usually not necessary to recover these 'slave' freedoms at each and every time step. This means that very small time steps can be used to achieve high accuracy in the solution of the reduced system with a much larger time interval being adopted for the recovery process.

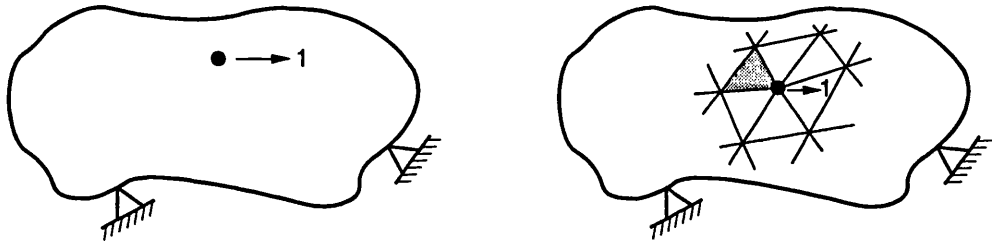

(a) Typical unit load applied to mass point in linear-elastic reference model

(b) Typical unit load applied to nodal freedom of 'non-linear' element or elements

Fig. 7.2 Typical load-sets to determine the influence matrices for the NPFI-Method

Statics and the tangent stiffness matrix

For problems in statics, the system (7.23) reduces to

$$\underline{Y} = \underline{Y}^L + H^{YY}\underline{F}_Y^{NL} \tag{7.25}$$

and this may be solved by any convenient iterative method such as the arc length procedure described in chapter 3.

In a traditional f.e. method based on infinitesimal displacement theory (see section 6.8.2), the tangent matrix is given by

$$K^t = K^E - K^P, \tag{7.26}$$

whereas linearisation of (7.25) leads to a reduced tangent stiffness matrix given by

$$\overline{K}_Y^t = I - H^{YY}\frac{\partial \underline{F}_Y^{NL}}{\partial \underline{Y}} = I - H^{YY}(K_Y^E - K_Y^t) = I - H^{YY}K_Y^P. \tag{7.27}$$

in which

$$K_Y^E = Z_Y K^E Z_Y^T \qquad K_Y^t = Z_Y K^t Z_Y^T \tag{7.28}$$

and we have used the fact that

$$\frac{\partial \underline{F}_U^{NL}}{\partial \underline{Y}} = \frac{\partial \underline{F}_U^{NL}}{\partial \underline{U}} \boldsymbol{Z}_Y^T .$$

It is then apparent that the reduced plasticity matrix $\boldsymbol{K}_Y^P = \boldsymbol{K}_Y^E - \boldsymbol{K}_Y^t$ is given by

$$\boldsymbol{K}_Y^P = \boldsymbol{Z}_Y \boldsymbol{K}^P \boldsymbol{Z}_Y^T = \boldsymbol{T}_Y \boldsymbol{k}_\eta^P \boldsymbol{T}_Y^T ; \qquad \boldsymbol{T}_Y = \boldsymbol{Z}_Y \boldsymbol{S}_G^T \boldsymbol{R}_\alpha^T \boldsymbol{A}_o^T \tag{7.29}$$

where $\boldsymbol{k}_\eta^P$ is a block-diagonal matrix comprising the individual element plasticity matrices as given by (6.54). As may be expected, $\boldsymbol{K}_Y^P$ is simply $\boldsymbol{K}^P$ with the zero rows and columns removed, which corresponds to the assembly of the inelastic stiffness of the non-linear elements only.

Static re-analysis of linear-elastic structures

For problems of static re-analysis the objective is to find the response of a modified linear-elastic structure given the response of the original structure. Clearly this is a special case of the non-linear study. The problem now is to solve

$$(\boldsymbol{K}^E + \Delta \boldsymbol{K})\underline{U} = \underline{F}^L \qquad \text{given} \qquad \underline{U}^L = (\boldsymbol{K}^E)^{-1} \underline{F}^L . \tag{7.30}$$

where $\Delta \boldsymbol{K}$ is sparse. By identifying $\underline{F}_U^{NL} = -\Delta \boldsymbol{K} \underline{U}$ in (7.19), it follows that the reduced system equivalent to (7.25) becomes

$$\underline{Y} = \underline{Y}^L - \boldsymbol{H}^{YY} \Delta \boldsymbol{K}_Y \underline{Y} \tag{7.31}$$

where

$$\Delta \boldsymbol{K}_Y = \boldsymbol{Z}_Y \Delta \boldsymbol{K} \boldsymbol{Z}_Y^T . \tag{7.32}$$

The solution to (7.31) is

$$\underline{Y} = (\boldsymbol{I} + \boldsymbol{H}^{YY} \Delta \boldsymbol{K}_Y)^{-1} \underline{Y}^L . \tag{7.33a}$$

which is in agreement with the pseudo-force solution obtained by WANG, PILKEY & PALAZZOLO (1983). In this form the matrix to be inverted is non-symmetric but (7.33a) may also be written in as

$$\underline{Y} = \boldsymbol{H}^{YY} (\boldsymbol{H}^{YY} + \boldsymbol{H}^{YY} \Delta \boldsymbol{K}_Y \boldsymbol{H}^{YY})^{-1} \underline{Y}^L . \tag{7.33b}$$

where now the matrix to be inverted is symmetric.

Symmetric inversion matrices may also be found by applying the Woodbury/Householder formula (WOODBURY, 1950; HOUSEHOLDER, 1957) to (7.33a). This formula may be written in general form as

$$(M+ABC)^{-1}=\left[I-M^{-1}A\left(B^{-1}+CM^{-1}A\right)^{-1}C\right]M^{-1} \tag{7.34}$$

and selecting

$$M=I,\ ABC=H^{YY}\Delta K_Y I\ , \tag{7.35}$$

we find after some manipulation that

$$\underline{Y}=\left(I-\left[(H^{YY})^{-1}+\Delta K_Y\right]^{-1}\Delta K_Y\right)\underline{Y}^L. \tag{7.36}$$

Interestingly, ARGYRIS *ET AL.* (1971) obtained this solution directly using the Woodbury/Householder formula on the global system (7.30), with $M=K$ and $ABC=\Delta K=Z_Y^T\Delta K_Y Z_Y$. Thus for re-analysis of linear-elastic structures, we conclude that the nodal pseudo-force method proposed by WANG *ET AL.* (1983) is equivalent to the direct modification procedure of ARGYRIS *ET AL.* (1971).

7.4.2 Large displacement theory

We consider now how to include finite rotations - that is geometrically non-linear behaviour. In fact this is rather simple. The number of unknowns in the reduced system does not increase when compared to the infinitesimal theory and the governing system of equations is still represented by (7.23). It is only the composition of the pseudo-forces $\underline{F}_U^{NL}$ that differs as $\underline{q}_v^{NL}$ now depends on finite rotations, as can be seen from (7.17b). The reduced tangent matrix is given by

$$\overline{K}_Y^t=I-H^{YY}\frac{\partial \underline{F}_Y^{NL}}{\partial \underline{Y}}=I-H^{YY}(K_Y^E-K_Y^t) \tag{7.37}$$

where K_Y^E and K_Y^t are given by (7.28). The only difference between this and its geometrically linear counterpart (c.f. eqn. (7.27)) is that $K_Y^E-K_Y^t\neq K_Y^P$ because K_Y^t includes finite rotation terms (see (6.73) for definition of K^t to be used in (7.28) to get K_Y^t).

We conclude that implementation of the large displacement theory into a nodal pseudo-force scheme is rather straightforward.

7.5 THE ELEMENT PSEUDO-FORCE INFLUENCE METHOD (EPFI-Method)

We recall (chapter 3) that to emulate the behaviour of a (geometrically linear) bar element with non-linear material properties, required one set of self-equilibrating pseudo-forces acting along the bar's axis in the linear-elastic reference model. This reflects the fact that only one deformation parameter is required to describe the straining of the bar. For higher order elements we may expect one set of self-equilibrating pseudo-forces for each possible independent deformation mode. Furthermore, from our study on element equilibrium in chapter 6, we anticipate that if large rotations are admitted, the pseudo-forces are composed of two orthogonal load sets.

7.5.1 Infinitesimal theory

We begin with the derivation of the EPFI-Method for geometrically linear problems with material non-linearity. This has been published previously by the writer (STEWART, 1992a). The extension to large rotations is given in the section immediately following.

Pseudo-force decomposition

For infinitesimal displacement theory, the pseudo-forces acting on the linear-elastic reference body were derived previously in equation (7.8) as

$$\underline{q}_v^{NL} = \boldsymbol{A}_o^T \underline{f}_\eta^{NL} . \tag{7.38}$$

Earlier, in chapter 6 , it was established (see eqn. (6.41)) that $\boldsymbol{A}_o^T$ was given by

$$\boldsymbol{A}_o^T = \boldsymbol{S}_o \begin{bmatrix} \boldsymbol{\Gamma}_o \\ \boldsymbol{I} \end{bmatrix} \tag{7.39}$$

where the sorting matrix $\boldsymbol{S}_o$ is only a book-keeping exercise to re-order the degrees of freedom. Considering now a single element, the columns of $\boldsymbol{\Gamma}_o$ are the reaction forces at freedoms that are restrained to render the element statically determinate when unit loads (the columns of $\boldsymbol{I}$) are applied in turn to each of the deformation freedoms. Thus for each element we have

$$\boldsymbol{A}_o^T = \begin{bmatrix} \underline{a}_1 & \underline{a}_2 & \cdots & \underline{a}_m \end{bmatrix} \tag{7.40}$$

where each $\underline{a}_i$ represents a ***self-equilibrating load-set*** (whose column entries sum to zero) derived by applying unit loads in turn to each deformation degree of freedom (d.o.f.) of the statically restrained element. The number, m, of independent self-equilibrating load-sets is equal to the number of unknown deformation freedoms of the element ($m = 1$ for bar element).

Now from (7.38) and (7.40), it is apparent that the element pseudo-forces may be expressed as

$$\underline{q}_v^{NL} = \boldsymbol{A}_o^T \underline{f}_\eta^{NL} = \underline{a}_1 f_1^{NL} + \underline{a}_2 f_2^{NL} + \cdots \underline{a}_m f_m^{NL} = \underline{q}_1^{NL} + \underline{q}_2^{NL} + \cdots \underline{q}_m^{NL} . \tag{7.41}$$

Thus the element pseudo-forces $\underline{q}_v^{NL}$ may be represented as a linear combination of constant ***self-equilibrating load-sets*** $\underline{a}_i$ and associated unknown ***scaling factors*** f_i^{NL}. Importantly, for a given element the scaling factors $\underline{f}_i^{NL}$ depend only on that element's deformation (history). That is

$$\underline{f}_i^{NL} = \underline{f}_i^{NL}(\underline{\eta}_i) = \int_{V_e} \boldsymbol{B}^T \underline{\sigma}_{NL} \, dV . \tag{7.42}$$

where this integral form was presented in Box 7.1.

The total number of self-equilibrating load sets for a model with J non-linear elements is

$$M = \sum_{j=1}^{J} m_j \tag{7.43}$$

with m_j being the number of independent deformations for non-linear element j. Note that m_j may differ for each element type.

The pseudo-force decomposition is one of the key steps in the development of the EPFI-Method. It is depicted in Fig. 7.3 for both triangular and bar elements (note the similarity between this figure and Fig. 6.8).

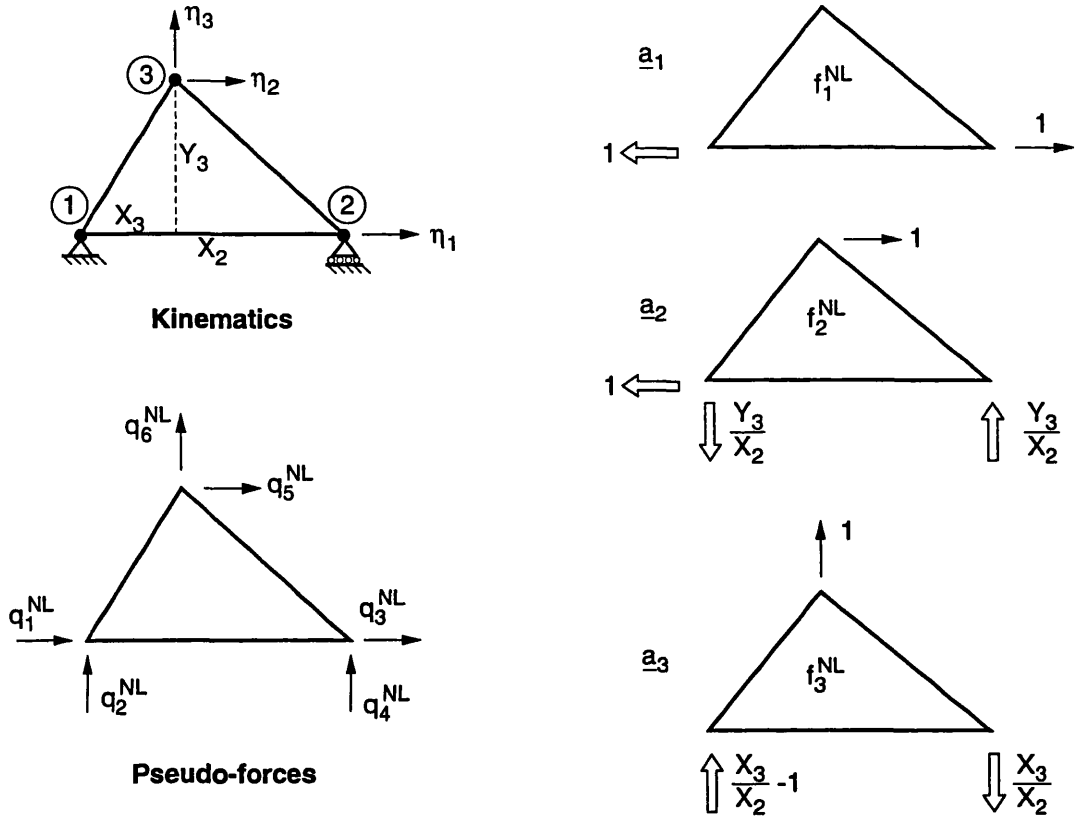

(a) Triangular element

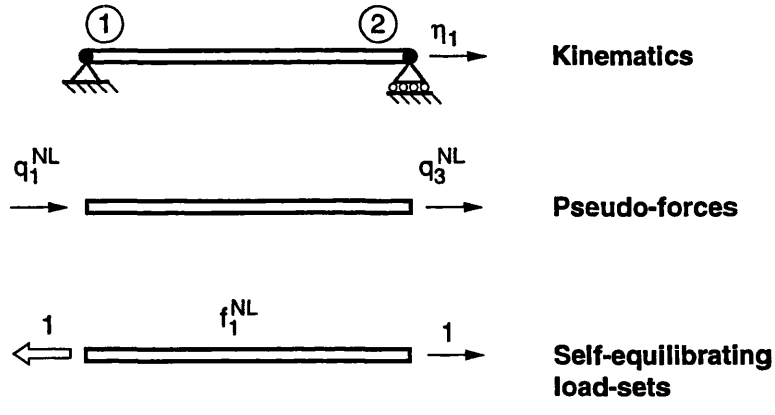

(b) Bar element

Fig. 7.3 Pseudo-force decomposition for triangular and bar elements

For the bar element this provides

$$A_o^T = \underline{a}_1 = \begin{bmatrix} -1 \\ 0 \\ 1 \\ 0 \end{bmatrix}; \quad \underline{q}_v^{NL} = \begin{bmatrix} -1 \\ 0 \\ 1 \\ 0 \end{bmatrix} f_1^{NL} . \tag{7.44a}$$

and we observe that $\underline{q}_v^{NL}$ is in agreement with equation (3.1), while for the triangle with $a_o = Y_3 / X_2$ and $b_o = X_3 / X_2$ we have

$$A_o^T = [\underline{a}_1 \quad \underline{a}_2 \quad \underline{a}_3] = \begin{bmatrix} -1 & -1 & 0 \\ 0 & -a_o & b_o - 1 \\ 1 & 0 & 0 \\ 0 & a_o & -b_o \\ 0 & 1 & 0 \\ 0 & 0 & 1 \end{bmatrix}; \quad \underline{q}_v^{NL} = \begin{bmatrix} -1 & -1 & 0 \\ 0 & -a_o & b_o - 1 \\ 1 & 0 & 0 \\ 0 & a_o & -b_o \\ 0 & 1 & 0 \\ 0 & 0 & 1 \end{bmatrix} \begin{bmatrix} f_1^{NL} \\ f_2^{NL} \\ f_3^{NL} \end{bmatrix} \tag{7.44b}$$

which is in agreement with (6.39). For both element types we indeed observe that the columns $\underline{a}_i$ sum to zero.

The pseudo-force decomposition is similar to the 'natural technique' employed by ARGYRIS *ET AL.* (1979) and the 'mode-amplitude' method used by ROBINSON (1985) for stress-based finite elements.

Influence matrices and the reduced system

In the general non-linear dynamic problem, two types of pseudo-forces are present in the equivalent linear-elastic model (recall Fig. 4.1). Each 'non-linear' element has a set of local material pseudo-forces $\underline{q}_v^{NL}$ (with scaling factors $\underline{f}_\eta^{NL}$) acting at its nodal points, while dynamic pseudo-forces $\underline{F}_U^D$ act at the mass/damper freedoms. The coupling between these forces is achieved through elastic influence matrices.

We consider first the response of the linear-elastic model when load-sets $\underline{a}_i$, corresponding to unit values of the material pseudo-force multipliers, are applied in turn (Fig. 7.4a). For each load-set applied, the deformation of the 'non-linear' elements provides a column of the ***deformation influence matrix*** $D^{\eta\eta}$, while the displacements at the mass/damper freedoms provides a column of the ***displacement influence matrix*** $H^{X\eta}$. Similarly, applying unit loads in turn to each of the mass/damper freedoms (Fig. 7.4b) provides the columns of the ***displacement influence matrix*** H^{XX} and ***deformation influence matrix*** $D^{\eta X}$.

The influence matrices and the governing reduced system of non-linear equations will now be derived formally.

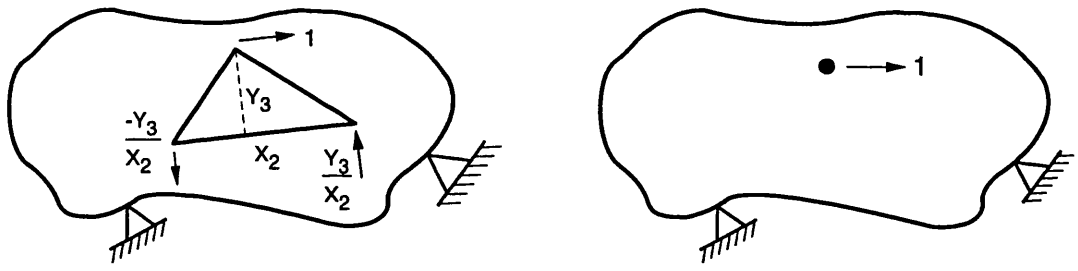

(a) Typical self-equilibrating load-set applied to 'non-linear' element in linear-elastic reference model

(b) Typical unit load applied to mass point in linear-elastic reference model

Fig. 7.4 Typical load-sets to determine the influence matrices for the EPFI-Method

Using the kinematic relationships in Box 7.1, the deformations of the entire set of 'non-linear' elements may be written as

$$\underline{\eta} = Z_\eta \underline{U} \qquad Z_\eta = A_o R_\alpha S_G \tag{7.45}$$

where Z_η is a constant matrix, the subscript η merely indicating that this matrix provides the kinematic transformation between the deformations and the nodal displacements. Also, by the equivalence of virtual work in any reference system,

$$\underline{F}_U^{NL} = Z_\eta^T \underline{f}_\eta^{NL} \,. \tag{7.46}$$

Now, applying the transformations (7.45) and (7.46) to (7.19), and letting $\underline{\eta}$ denote the deformations in the non-linear elements only (that is Z_η represents only a sub-set of all the element transformations), the equivalent of the reduced system of equations (7.23) is

$$\begin{bmatrix} \underline{X} \\ \underline{\eta} \end{bmatrix} = \begin{bmatrix} \underline{X}^L \\ \underline{\eta}^L \end{bmatrix} + \begin{bmatrix} H^{XX} & H^{X\eta} \\ D^{\eta X} & D^{\eta\eta} \end{bmatrix} \begin{bmatrix} \underline{F}_X^D \\ \underline{f}_\eta^{NL} \end{bmatrix} \tag{7.47}$$

where

$$\begin{aligned} H^{XX} &= Z_X (K^E)^{-1} Z_X^T \qquad H^{X\eta} = Z_X (K^E)^{-1} Z_\eta^T \\ D^{\eta X} &= Z_\eta (K^E)^{-1} Z_X^T \qquad D^{\eta\eta} = Z_\eta (K^E)^{-1} Z_\eta^T . \end{aligned} \tag{7.48}$$

and the superscript 'L' denotes responses in the linear-elastic static problem due to the applied loading alone. These equations are of the same form as those derived earlier in chapter 4 (ref. eqn. (4.3c)). We observe that both H^{XX} and $D^{\eta\eta}$ are symmetric, while $H^{X\eta} = (D^{\eta X})^T$.

Since each column of Z_X^T has only a single non-zero unit entry that corresponds to the location of a mass/damper freedom, it is clear that the columns of H^{XX} and $D^{\eta X}$ provide the response to unit load-cases applied to these freedoms in turn. Furthermore, since

$$D^{\eta\eta} = Z_\eta (K^E)^{-1} Z_\eta^T = \left\{ Z_\eta (K^E)^{-1} S_G^T R_\alpha^T \right\} A_o^T$$

$$= \left\{ Z_\eta (K^E)^{-1} S_G^T R_\alpha^T \right\} \left[\underline{a}_1 \quad \underline{a}_2 \quad \cdots \quad \underline{a}_M \right] \tag{7.49}$$

it is confirmed that the column entries of $D^{\eta\eta}$ (which has dimension $M \times M$) are indeed the deformations in all non-linear elements for each self-equilibrating load-set $\underline{a}_i$ applied in turn. It immediately follows from (7.48) that the columns of $H^{X\eta}$ are the displacements at the mass/damper freedoms when each $\underline{a}_i$ is applied.

Statics and the tangent stiffness matrix

For problems in statics, the reduced system (7.47) becomes

$$\underline{\eta} = \underline{\eta}^L + D^{\eta\eta} \underline{f}_\eta^{NL} \tag{7.50}$$

and this may be solved by the arc-length procedure described in section 3.4, employing either the tangent matrix, the initial stiffness matrix, or some other convenient stiffness matrix.

The reduced tangent stiffness matrix associated with (7.50) is given by

$$\overline{K}_\eta^t = I - D^{\eta\eta} \frac{\partial \underline{f}_\eta^{NL}}{\partial \underline{\eta}} = I - D^{\eta\eta} k_\eta^P \,. \tag{7.51a}$$

The matrix k_η^P is diagonal for the bar element, but in general it is block diagonal. $\overline{K}_\eta^t$ is non-symmetric but this poses no difficulty as (7.51a) may be written as

$$\overline{K}_\eta^t = (D^{\eta\eta} - D^{\eta\eta} k_\eta^P D^{\eta\eta})(D^{\eta\eta})^{-1} \tag{7.51b}$$

and all terms are now symmetric. For initial stiffness iterations, $\overline{K}_\eta^t$ is simply the identity matrix, I.

7.5.2 The infinitesimal EPFI-Method and Initial Strain formulations

Material non-linearity can also be simulated in a linear-elastic model using initial deformations (or strains). The presence of initial (lack-of-fit) deformations $\underline{\eta}_I$ in a linear-elastic model with total deformations $\underline{\eta}$ leads to element forces given by

$$\underline{f}_\eta = k_\eta^E (\underline{\eta} - \underline{\eta}_I) \,. \tag{7.52}$$

The element forces in the non-linear material model can be expressed (see Box 7.1) as

$$\underline{f}_\eta = \underline{f}_\eta^E - \underline{f}_\eta^{NL} = k_\eta^E \underline{\eta} - \underline{f}_\eta^{NL} \tag{7.53}$$

and it is apparent that to simulate material non-linearity the value of initial deformation required in the linear-elastic model is given by

$$\underline{\eta}_I = (k_\eta^E)^{-1} \underline{f}_\eta^{NL} . \tag{7.54}$$

Figure 7.5 illustrates the initial deformation concept for the bar element. It is clear from this figure that η_I is in fact equivalent to the total plastic strain.

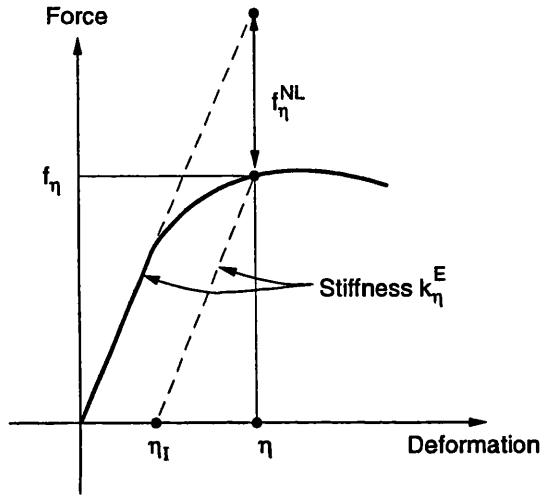

Fig. 7.5 The equivalence of initial deformations η_I and pseudo-forces f_η^{NL} for a bar element

Thus we conclude that for infinitesimal theory the terms "pseudo-force", and "initial deformation (strain)" are effectively synonymous.

With the aid of (7.52) and (7.54), the system (7.50) can be now be expressed in three alternative forms

$$\text{(1a)} \quad \underline{\eta} = \underline{\eta}^L + D^{\eta\eta} \underline{f}_\eta^{NL} \qquad \text{(pseudo-force)} \tag{7.55a}$$

$$\text{(2a)} \quad \underline{f}_\eta = \underline{f}_\eta^L + S\underline{\eta}_I \qquad \text{(initial strain)} \tag{7.55b}$$

$$\text{(3a)} \quad \underline{\eta} = \underline{\eta}^L + V\underline{\eta}_I \qquad \text{(initial strain)} \tag{7.55c}$$

in which

$$\underline{\eta}_I = (k_\eta^E)^{-1} \underline{f}_\eta^{NL} \qquad \underline{f}_\eta = k_\eta^E \underline{\eta} - \underline{f}_\eta^{NL} \qquad \underline{f}_\eta^L = k_\eta^E \underline{\eta}^L$$

$$S = k_\eta^E (V - I) \qquad V = D^{\eta\eta} k_\eta^E . \tag{7.56}$$

In the case of re-analysis of linear-elastic structures, in which the initial elastic element stiffness k_η^E becomes $\tilde{k}_\eta^E$ after modifying the material properties, the pseudo-force scaling factors and the initial strains are given respectively by

$$\underline{f}_\eta^{NL} = -\Delta k_\eta^E \underline{\eta} \qquad \text{and} \qquad \underline{\eta}_I = -(k_\eta^E)^{-1} \Delta k_\eta^E \underline{\eta} = \left[(\tilde{k}_\eta^E)^{-1} - (k_\eta^E)^{-1}\right] \underline{f}_\eta . \tag{7.57}$$

where

$$\Delta k_\eta^E = \tilde{k}_\eta^E - k_\eta^E . \tag{7.58}$$

If these expression are substituted into equations (7.55), the solution of the modified problem can be found as

(1b) $\underline{\eta} = (I + D^{\eta\eta} \Delta k_\eta^E)^{-1} \underline{\eta}^L$ (pseudo-force) (7.59a)

(2b) $\underline{f}_\eta = \left(I + S\left[(k_\eta^E)^{-1} - (\tilde{k}_\eta^E)^{-1}\right]\right)^{-1} \underline{f}_\eta^L$ (initial strain) (7.59b)

(3b) $\underline{\eta} = \left[I + V(k_\eta^E)^{-1} \Delta k_\eta^E\right]^{-1} \underline{\eta}^L$ (initial strain) (7.59c)

Method (2) corresponds to the re-analysis procedure developed by ARGYRIS & KELSEY (1956, 1960, 1961) and MELOSH & LUIK (1968) using the matrix force method. Evidently, as has been demonstrated, it can equally be derived from the principle of virtual displacements. The force influence matrix S, as given by (7.56), is symmetric.

Method (3) corresponds to HOLNICKI-SZULC & GIERLINSKI'S ***Virtual Distortion Method*** (VDM). The term 'virtual' is used by these authors in the sense of 'fictitious' or 'pseudo' and is not to be confused with virtual work. The VDM approach has been employed to determine the response of modified linear-elastic structures under certain conditions of (non-linear) constraint (HOLNICKI-SZULC & MROZ, 1985; HOLNICKI-SZULC, 1987, 1989; HOLNICKI-SZULC, 1991). Recently, HOLNICKI-SZULC & GIERLINSKI (1989) have used equilibrium constraints in the VDM procedure to obtain the behaviour of skeletal frames comprising non-linear bar and beam elements. A particularly innovative idea pursued by Gierlinski was to use the VDM principle for efficient probabilistic structural modelling (GIERLINSKI, 1992).

The deformation influence matrix V in the VDM approach corresponds to unit (lack-of-fit) distortions applied in turn to each member's deformation freedoms. It is generally non-symmetric. However if we multiply (7.55c) through by k_η^E we get

$$\hat{\underline{f}}_\eta = \underline{f}_\eta^L + P \underline{\eta}_I \tag{7.60}$$

where $\hat{\underline{f}}_\eta = k_\eta^E \underline{\eta}$ is a fictitious force (which may be interpreted as the force that would exist in the linear-elastic structure at deformation $\underline{\eta}$), and $P = k_\eta^E V$ is a symmetric force influence matrix.

We conclude that for infinitesimal displacement problems, all pseudo-force or initial strain formulations should result in a similar set of reduced equations. Indeed the distinction between

the methods as such is not important. What is important is that the deformations produced by the pseudo-forces or initial strains, acting together with the physical loading, do in fact represent the correct solution to the non-linear problem under consideration. For re-analysis of linear-elastic structures, the correct pseudo-forces or initial strains can often be arrived at by heuristic arguments. However for general non-linear continuum mechanics problems, it is advisable to follow a more rigorous derivation based on fundamental concepts such as the principle of virtual work as proposed herein.

7.5.3 Large displacement theory

We consider now how to include finite rotations in small strain statics problems. The extension to dynamics is straightforward, following the principles established previously in section 7.4.1 and will not be repeated.

Reduced system - absolute and relative local displacements

We begin as shown in Box 7.3 by extracting information relevant to the non-linear elements from the global displacements $\underline{U}$. Denoting the local element displacements as $\underline{v}$, the kinematic transformation linking $\underline{v}$ and $\underline{U}$ is

$$\underline{v} = \mathbf{Z}_v \underline{U} \qquad \mathbf{Z}_v = \mathbf{R}_\alpha \mathbf{S}_G \tag{7.61}$$

where it is understood that $\mathbf{Z}_v$ includes only those transformation matrices associated with the non-linear elements. Multiplying the global equilibrium equation (7.19) through by $\mathbf{Z}_v$ and with

$$\underline{F}_U^{NL} = \mathbf{Z}_v^T \underline{q}_v^{NL} \ , \tag{7.62}$$

where $\underline{q}_v^{NL}$ is given by (7.17b), we easily arrive at

$$\underline{v} = \underline{v}^L + \mathbf{D}^{vv} \underline{q}_v^{NL} \tag{7.63}$$

in which

$$\mathbf{D}^{vv} = \mathbf{Z}_v (\mathbf{K}^E)^{-1} \mathbf{Z}_v^T \ . \tag{7.64}$$

The columns of the influence matrix $\mathbf{D}^{vv}$ are the displacements at the nodal freedoms of the 'non-linear' elements for local unit loads applied in turn to each of these freedoms. Although rather simple, unfortunately it is not efficient to work with this system as it contains two surplus freedoms per element (not three surplus freedoms as would be the case in the infinitesimal theory since we now need an additional equation to calculate the rotations). We can remove these two surplus freedoms by using the relative displacements $\underline{w}$ instead of the absolute displacements $\underline{v}$. This is achieved using the kinematic transformation $\underline{w} = \mathbf{M}_0 \underline{v}$ (see Box 7.2). The equivalence of virtual work then provides

$$\underline{q}_v^{NL} = \boldsymbol{M}_o^T \underline{q}_w^{NL} \qquad \text{with} \qquad \underline{q}_w^{NL} = \tilde{\boldsymbol{A}}_o^T \underline{f}_\eta^{Eo} - \tilde{\boldsymbol{R}}_\phi^T \tilde{\boldsymbol{A}}_o^T \underline{f}_\eta \tag{7.65}$$

and equation (7.63) becomes

$$\underline{w} = \underline{w}^L + \boldsymbol{D}^{ww} \underline{q}_w^{NL} , \tag{7.66}$$

where

$$\boldsymbol{D}^{ww} = \boldsymbol{M}_o \boldsymbol{D}^{vv} \boldsymbol{M}_o^T . \tag{7.67}$$

The columns of the ***relative displacement influence matrix*** $\boldsymbol{D}^{ww}$ are obtained by applying pairs of local unit loads in turn to the element freedoms of each 'non-linear' element. If we consider the element to be fully restrained at node 1, then for each pair of unit forces, one force acts on an unrestrained freedom and the other is the reaction force at node 1. This is shown in Fig. 7.6. For an element with p nodes, $2(p - 1)$ unit load-sets are required.

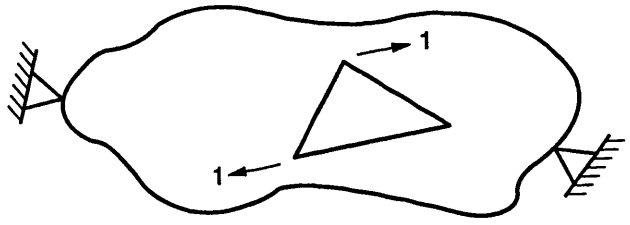

Note: only one load-set shown, total of 4 to be applied for triangular element.

Fig. 7.6 Generating the influence matrix $\boldsymbol{D}^{ww}$

Reduced tangent stiffness matrix

Linearisation of (7.66) and employing the stiffness relationships derived in section 6.7 together with the kinematic relationships summarised in Box 7.2 provides the reduced tangent matrix for the relative displacement formulation as

$$\bar{\boldsymbol{K}}_w^t = \boldsymbol{I} - \boldsymbol{D}^{ww} \frac{\partial \underline{q}_w^{NL}}{\partial \underline{w}} = \boldsymbol{I} - \boldsymbol{D}^{ww} \left(\boldsymbol{k}_w^{Eo} - \boldsymbol{k}_w^t \right) \tag{7.68}$$

where,

$$\boldsymbol{k}_w^{Eo} = \tilde{\boldsymbol{A}}_o^T \boldsymbol{k}_\eta^E \tilde{\boldsymbol{A}}_o \; ; \qquad \boldsymbol{k}_w^t = \tilde{\boldsymbol{R}}_\phi^T (\tilde{\boldsymbol{A}}_o^T \boldsymbol{k}_\eta^t \tilde{\boldsymbol{A}}_o + \tilde{\boldsymbol{H}}_o \tilde{\boldsymbol{k}}_{\phi\phi}^\sigma \tilde{\boldsymbol{H}}_o^T) \tilde{\boldsymbol{R}}_\phi \tag{7.69}$$

and

$$\tilde{\boldsymbol{k}}_{\phi\phi}^\sigma = \begin{bmatrix} k_{\phi_1} & & & \\ & k_{\phi_2} & & \boldsymbol{O} \\ \boldsymbol{O} & & \ddots & \\ & & & k_{\phi_M} \end{bmatrix} ; \quad k_{\phi_i} = (\hat{\underline{X}}^T \tilde{\boldsymbol{A}}_o^T \underline{f}_\eta)_i \; ; \quad \tilde{\boldsymbol{H}}_o^T = \begin{bmatrix} \tilde{\underline{h}}_{o_1}^T & & & \\ & \tilde{\underline{h}}_{o_2}^T & & \boldsymbol{O} \\ \boldsymbol{O} & & \ddots & \\ & & & \tilde{\underline{h}}_{o_M}^T \end{bmatrix} . \tag{7.70}$$

We recall from chapter 6 that $\underline{\hat{X}}_i$ refers to the local Lagrangian (initial) co-ordinates of the element.

This provides the most compact and straightforward formulation of the element pseudo-force method for finite rotations. However it is not very revealing. In particular we cannot easily compare this form with the infinitesimal theory which involved a deformation influence matrix $\boldsymbol{D}^{\eta\eta}$. To get this insight, it is necessary to formulate the problem in terms of generalised displacements - that is deformations and rotations.

Reduced system - generalised displacements

The transformation to a generalised displacement formulation is achieved in two stages. Firstly we multiply (7.66) through by $\tilde{\boldsymbol{L}}_o$. This provides a system of equations in $\underline{\beta}_o$. The entries in $\underline{\beta}_o$ are stored element by element as

$$\underline{\beta}_o^T = \left[(\phi_o \ \underline{\eta}_o^T)_1 \ \ (\phi_o \ \underline{\eta}_o^T)_2 \ \ \cdots \ \ (\phi_o \ \underline{\eta}_o^T)_M\right]. \tag{7.71}$$

However it will prove more convenient to group the rotations and deformations and store these as

$$\underline{\mu}_o^T = \left[\phi_{o_1} \phi_{o_2} \cdots \phi_{o_M} \ \underline{\eta}_{o_1}^T \underline{\eta}_{o_2}^T \cdots \underline{\eta}_{o_M}^T\right] = \left[\underline{\phi}_o \ \ \underline{\eta}_o^T\right] \tag{7.72}$$

and similarly for $\underline{\beta}$. We achieve this by using a re-ordering operator $\boldsymbol{S}_\mu$ such that

$$\underline{\mu}_o = \boldsymbol{S}_\mu \underline{\beta}_o \qquad \underline{\mu} = \boldsymbol{S}_\mu \underline{\beta} \qquad \boldsymbol{S}_\mu \boldsymbol{S}_\mu^T = \boldsymbol{I}\,. \tag{7.73}$$

Therefore (7.66) becomes

$$\underline{\mu}_o = \underline{\mu}_o^L + \boldsymbol{S}_\mu \tilde{\boldsymbol{L}}_o \boldsymbol{D}^{ww} \underline{q}_w^{NL}\,. \tag{7.74a}$$

Using the fact that $\boldsymbol{M}_o^T \underline{q}_w^{NL} = \underline{q}_v^{NL}$ (see (7.65)), $\boldsymbol{D}^{ww} = \boldsymbol{M}_o \boldsymbol{D}^{vv} \boldsymbol{M}_o^T$ (see (7.67)), and $\tilde{\boldsymbol{L}}_o \boldsymbol{M}_o = \boldsymbol{L}$ (see (6.22)), equation (7.74) may be written as

$$\underline{\mu}_o = \underline{\mu}_o^L + \boldsymbol{S}_\mu \boldsymbol{L}_o \boldsymbol{D}^{vv} \underline{q}_v^{NL}\,. \tag{7.74b}$$

We progress further by using the expansion $\boldsymbol{R}_\phi = \boldsymbol{\Phi}_c + \boldsymbol{\Phi}_s \boldsymbol{\Omega}_o$ which was introduced in chapter 6, where we recall that $\boldsymbol{\Phi}_c$ is a diagonal matrix of cosines and $\boldsymbol{\Phi}_s$ is a diagonal matrix of sines. The pseudo-forces given by (7.17b) may then be expressed as

$$\underline{q}_v^{NL} = \boldsymbol{A}_o^T\left(\underline{f}_\eta^{Eo} - \boldsymbol{\Phi}_c \underline{f}_\eta\right) - \boldsymbol{\Omega}_o^T \boldsymbol{A}_o^T\left(\boldsymbol{\Phi}_s \underline{f}_\eta\right) \tag{7.75}$$

where we have used the fact that $\boldsymbol{\Phi}_c \boldsymbol{A}_o^T \equiv \boldsymbol{A}_o^T \boldsymbol{\Phi}_c$ (and similarly for $\boldsymbol{\Phi}_s$).

In the infinitesimal theory, we found that each column $\underline{a}_i$ of A_o^T corresponds to a self-equilibrating force set. Furthermore, in section 6.5.3 it was established that the columns of $\Omega_o^T A_o^T$ (let these be $\underline{b}_i$) represent the same self-equilibrating load-sets rotated anti-clockwise through 90 degrees. We can therefore interpret the terms in brackets in equation (7.75) as scaling factors for these basic load-sets. This is shown in Fig. 7.7 for a structure in which the non-linear member characteristics are represented by bar elements. We observe that if the axial force f_η in the bar is negative, the orthogonal force-set is de-stabilising, since the force $f_2^{NL} = -f_\eta \sin\phi$ then acts in the direction of the rotation.

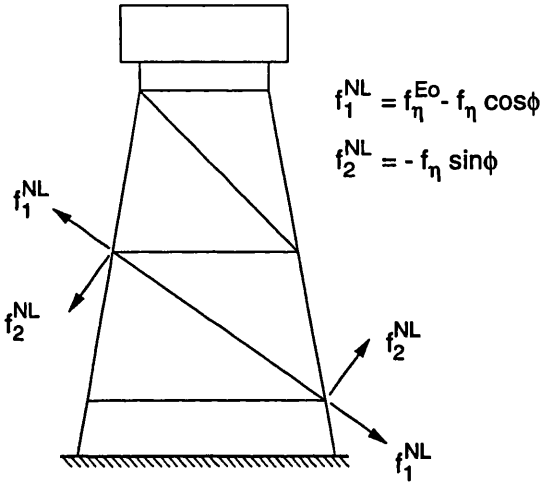

Fig. 7.7 Pseudo-forces associated with a bar element (including large displacement effects) acting on linear-elastic reference model

Now with (7.75) and since

$$S_\mu L_o = \begin{bmatrix} H_o^T \\ A_o \end{bmatrix} \tag{7.76}$$

we can write (7.74b) as

$$\begin{bmatrix} \underline{\phi}_o \\ \underline{\eta}_o \end{bmatrix} = \begin{bmatrix} \underline{\phi}^L \\ \underline{\eta}^L \end{bmatrix} + \begin{bmatrix} D^{\phi\phi} & D^{\phi\eta} \\ D^{\eta\phi} & D^{\eta\eta} \end{bmatrix} \begin{bmatrix} -\Phi_s \underline{f}_\eta \\ \underline{f}_\eta^{Eo} - \Phi_c \underline{f}_\eta \end{bmatrix} \tag{7.77}$$

which may also be expressed as

$$\underline{\mu}_o = \underline{\mu}_o^L + D^{\mu\mu} \underline{f}_\mu^{NL} \,. \tag{7.78}$$

From the representation (7.77) it is now apparent that in addition to $\boldsymbol{D}^{\eta\eta}$, which is common to both the infinitesimal and finite rotation theory, we now have a further three influence matrices. The total influence matrix $\boldsymbol{D}^{\mu\mu}$ in (7.78) comprises four sub-matrices that are given by

$$\begin{aligned} \boldsymbol{D}^{\phi\phi} &= \boldsymbol{H}_o^T \boldsymbol{D}^{vv} \boldsymbol{\Omega}_o^T \boldsymbol{A}_o^T ; \quad \boldsymbol{D}^{\phi\eta} = \boldsymbol{H}_o^T \boldsymbol{D}^{vv} \boldsymbol{A}_o^T \\ \boldsymbol{D}^{\eta\phi} &= \boldsymbol{A}_o \boldsymbol{D}^{vv} \boldsymbol{\Omega}_o^T \boldsymbol{A}_o^T ; \quad \boldsymbol{D}^{\eta\eta} = \boldsymbol{A}_o \boldsymbol{D}^{vv} \boldsymbol{A}_o^T \end{aligned} \tag{7.79}$$

and since

$$\boldsymbol{A}_o^T = \left[\underline{a}_1 \;\; \underline{a}_2 \;\; \cdots \;\; \underline{a}_M\right] \quad \text{and} \quad \boldsymbol{\Omega}_o^T \boldsymbol{A}_o^T = \left[\underline{b}_1 \;\; \underline{b}_2 \;\; \cdots \;\; \underline{b}_M\right], \tag{7.80}$$

where $\underline{a}_i$ is a self-equilibrating load-set and $\underline{b}_i = \boldsymbol{\Omega}_o^T \underline{a}_i$ is orthogonal to $\underline{a}_i$, it follows that the influence matrices are the response of the linear-elastic model when each $\underline{a}_i$ and $\underline{b}_i$ are applied in turn. Thus

- $\boldsymbol{D}^{\eta\eta}$ is a symmetric matrix of element deformations whose columns are generated by each self-equilibrating load-set $\underline{a}_i$;
- $\boldsymbol{D}^{\eta\phi}$ is a non-symmetric matrix of element deformations whose columns are generated by the rotated load-set $\underline{b}_i$;
- $\boldsymbol{D}^{\phi\eta}$ is a non-symmetric matrix of element rotations whose columns are generated by each self-equilibrating load-set $\underline{a}_i$;
- $\boldsymbol{D}^{\phi\phi}$ is a non-symmetric matrix of element rotations whose columns are generated by the rotated load-set $\underline{b}_i$;

Comparing this formulation with that of the relative displacement approach, we observe that in the present case, an element with p nodes (and $2p$-3 deformation modes) contributes $4p$-6 load-sets to the influence matrix determination, whereas for the relative displacement method only $2p$-2 are employed. Therefore although the number of unknowns in the reduced system is the same in both cases, with the exception of the bar element additional load-sets are required to develop the influence matrix if generalised displacements are used in preference to relative displacements. This is in contrast to the infinitesimal theory where the number of unknowns (and load-sets) is always one fewer when generalised deformations rather than relative displacements are employed.

Reduced tangent stiffness matrix

We could form the reduced tangent matrix from (7.77), but to enable comparison with the finite element matrices developed in chapter 6 we instead linearise (7.74a). Taking the derivative with respect to $\underline{\mu}$ provides

$$\overline{\boldsymbol{K}}_{\mu}^{t} = \frac{\partial \underline{\mu}_o}{\partial \underline{\mu}} - \boldsymbol{S}_{\mu} \tilde{\boldsymbol{L}}_o \boldsymbol{D}^{ww} \frac{\partial \underline{q}_w^{NL}}{\partial \underline{w}} \frac{\partial \underline{w}}{\partial \underline{\mu}} . \tag{7.81}$$

From the relationships in Box 7.2 we have

$$\frac{\partial \underline{\mu}}{\partial \underline{\mu}} = S_\mu \frac{\partial \underline{\beta}}{\partial \underline{\beta}} S_\mu^T = S_\mu \left[\tilde{L}_o \tilde{R}_\phi^T \tilde{L}_o^{-1} \right] S_\mu^T \; ; \qquad \frac{\partial w}{\partial \underline{\mu}} = \tilde{L}_o^{-1} \frac{\partial \underline{\beta}}{\partial \underline{\beta}} S_\mu^T = \tilde{R}_\phi^T \tilde{L}_o^{-1} S_\mu^T \tag{7.82}$$

and therefore equation (7.81) may also be expressed as

$$\bar{K}_\mu^t = S_\mu \, \tilde{L}_o \, \bar{K}_w^t \, \tilde{R}_\phi^T \, \tilde{L}_o^{-1} \, S_\mu^T \tag{7.83}$$

where $\bar{K}_w^t$ is given by (7.68). Now, for an individual element, it can be demonstrated that one of the columns of $\tilde{\Omega}_o^T \tilde{A}_o^T$ is always equal to $\tilde{\underline{h}}_o$ and it therefore follows that for the complete set of non-linear elements we may write the geometric stiffness contribution to k_w (see eqn. (7.69)) as

$$\tilde{H}_o \tilde{k}_{\phi\phi}^\sigma \tilde{H}_o^T = \tilde{\Omega}_o^T \tilde{A}_o^T S_h^T \tilde{k}_{\phi\phi}^\sigma S_h \tilde{A}_o \tilde{\Omega}_o \tag{7.84}$$

in which S_h^T simply sets the columns of $\tilde{\Omega}_o^T \tilde{A}_o^T$ that are not of interest to zero. Making use of (7.84) in the description of $\bar{K}_w^t$, employing the relationships of Box 7.2 and introducing the decomposition of $\tilde{R}_\phi$ given by (6.6), we arrive, after some algebraic manipulation of (7.83), at

$$\bar{K}_\mu^t = \left\{ \begin{bmatrix} \tilde{H}_o^T \\ \tilde{A}_o \end{bmatrix} \tilde{R}_\phi^T - \begin{bmatrix} D^{\phi\phi} & D^{\phi\eta} \\ D^{\eta\phi} & D^{\eta\eta} \end{bmatrix} \begin{bmatrix} -(S_h^T \tilde{k}_{\phi\phi}^\sigma S_h \tilde{A}_o \tilde{\Omega}_o \Phi_c + k_\eta^t \tilde{A}_o \Phi_s) \\ k_\eta^P \tilde{A}_o \Phi_c + (k_\eta^E - S_h^T \tilde{k}_{\phi\phi}^\sigma S_h) \tilde{A}_o \tilde{\Omega}_o^T \Phi_s \end{bmatrix} \right\} \tilde{L}_o^{-1} S_\mu^T \, . \tag{7.85a}$$

which for small rotations reduces to

$$\bar{K}_\mu^t = \left\{ \begin{bmatrix} \tilde{H}_o^T \\ \tilde{A}_o \end{bmatrix} - \begin{bmatrix} D^{\phi\phi} & D^{\phi\eta} \\ D^{\eta\phi} & D^{\eta\eta} \end{bmatrix} \begin{bmatrix} -S_h^T \tilde{k}_{\phi\phi}^\sigma S_h \tilde{A}_o \tilde{\Omega}_o \\ k_\eta^P \tilde{A}_o \end{bmatrix} \right\} \tilde{L}_o^{-1} S_\mu^T \, . \tag{7.85b}$$

Buckling

Buckling occurs when the determinant of $\bar{K}^t$ is zero. Let us verify (7.68) and (7.85b) for the buckling load of a simple linear-elastic bar of length l_o and axial stiffness k_a supported by a horizontal spring of stiffness k_s, as shown in Fig. 7.8.

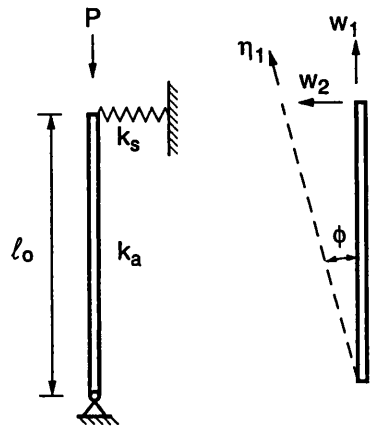

Fig. 7.8 Buckling of a restrained linear-elastic bar

The basic geometrical data for this problem are:

$$\tilde{A}_o = [1 \quad 0] \qquad \tilde{\Omega}_o = \begin{bmatrix} 0 & 1 \\ -1 & 0 \end{bmatrix} \qquad S_h = \frac{1}{l_o}\begin{bmatrix} 1 & 0 \\ 0 & 1 \end{bmatrix} \qquad \underline{\hat{X}}^T = [l_o \quad 0]$$

$$\underline{\tilde{h}}_o^T = [0 \quad 1/l_o] \qquad \tilde{k}_{\phi\phi}^{\sigma} = [k_\phi] = \left[\underline{\hat{X}}^T \tilde{A}_o^T \underline{f}_\eta\right] = -[Pl_o] \qquad \Phi_c = I \qquad \Phi_s = 0$$

relative displacement formulation

$$D^{ww} = \begin{bmatrix} 1/k_a & 0 \\ 0 & 1/k_s \end{bmatrix}$$

$$k_w^{Eo} - k_w^t = -k_\phi \underline{\tilde{h}}_o \underline{\tilde{h}}_o^T = \frac{P}{l_o}\begin{bmatrix} 0 & 0 \\ 0 & 1 \end{bmatrix}$$

$$\bar{K}_w^t = \begin{bmatrix} 1 & 0 \\ 0 & 1 \end{bmatrix} - \frac{P}{l_o}\begin{bmatrix} 0 & 0 \\ 0 & 1/k_s \end{bmatrix}$$

generalised displacement formulation

$$D^{\phi\phi} = [1/(k_s l_o)] \quad D^{\eta\phi} = D^{\phi\eta} = [0]$$

$$D^{\eta\eta} = [1/k_a] \quad k_\eta^P = 0$$

$$\bar{K}_\mu^t = \left\{\begin{bmatrix} 0 & 1/l_o \\ 1 & 0 \end{bmatrix} - \begin{bmatrix} 0 & P/(k_s l_o^2) \\ 0 & 0 \end{bmatrix}\right\} \tilde{L}_o^{-1} S_\mu^T .$$

In both cases, the determinant is zero when

$$P_{crit} = k_s l_o$$

which is the well known buckling load for this problem.

Initial strains and finite rotation theory

Unlike the infinitesimal theory, it is not possible to interpret the pseudo-forces given by (7.17b) solely as initial deformations. This is obvious if one considers once more the bar element shown in Fig. 7.7. Initial deformations can only be introduced along its length, giving rise to an initial axial force. However to account for finite rotations, an additional force-set normal to the bar axis is also required which cannot be generated by any initial deformation field. Thus one may argue that the pseudo-force formulation is general whereas the initial stress and initial strain formulations are limited to geometrically linear problems.

7.6 A SUGGESTED SOLUTION PROCEDURE

We complete this section by providing a modified Newton iterative solution procedure for one load increment of the generalised (large displacement) element pseudo-force method for statics problems (see Box 7.4). The solution algorithm for the infinitesimal theory then follows directly simply by setting $\tilde{R}_\phi = I$, $\Phi_c = I$, $\Phi_s = 0$ and disregarding the equations that relate to the rotations. This procedure would normally be augmented by a generalised constraint equation to provide an arc-length control algorithm as described in chapter 3.

Box 7.4 Element pseudo-force solution scheme for statics problems

Set starting values: $\underline{\mu}_{o(i)} = \underline{\mu}_o$; $\underline{\mu}_{(i)} = \underline{\mu}$; $\underline{f}^{NL}_{\mu(i)} = \underline{f}^{NL}_{\mu}$, etc.

Increment external 'load': $\underline{\mu}^L_o = \underline{\mu}^L_{o(i)} + D\underline{\mu}^L_o$

Set iteration counter: $k = i$

Do until converged

residual vector: $-\underline{g}_{(k)} = \underline{\mu}^L_o + (\boldsymbol{D}^{\mu\mu}\underline{f}^{NL}_{\mu} - \underline{\mu}_o)_{(k)}$

incremental 'disp.': $\Delta\underline{\mu} = -\left[\overline{\boldsymbol{K}}_{\mu(j)}\right]^{-1}\underline{g}_{(k)}$; $j \le k$

$\underline{\mu}_{(k+1)} = \underline{\mu}_{(k)} + \Delta\underline{\mu}$

$$\underline{\mu}_{o(k+1)} = \underline{\mu}_{o(i)} + \int_{\underline{\mu}_{(i)}}^{\underline{\mu}_{(k+1)}} \boldsymbol{S}_{\mu}\,\tilde{\boldsymbol{L}}_o\,\tilde{\boldsymbol{R}}^T_{\phi}\tilde{\boldsymbol{L}}_o^{-1}\boldsymbol{S}^T_{\mu}\,d\underline{\mu}$$

total 'disp.' change: $D\underline{\mu} = \underline{\mu}_{(k+1)} - \underline{\mu}_{(i)}$

$D\underline{\mu}_o = \underline{\mu}_{o(k+1)} - \underline{\mu}_{o(i)}$

total strain inc.: $D\underline{e}^* = \boldsymbol{B}\,D\underline{\eta}$

stress recovery: $$\underline{\sigma}^*_{(k+1)} = \underline{\sigma}^*_{(i)} + \int_{\underline{e}^*_{(i)}}^{\underline{e}^*_{(i)}+D\underline{e}^*} \boldsymbol{C}^{EP}\,d\underline{e}^*$$

internal force: $\underline{f}_{\eta(k+1)} = \int_{\Omega} \boldsymbol{B}^T\underline{\sigma}^*_{(k+1)}\,dV$

$\underline{f}^{Eo}_{\eta\,(k+1)} = k^E_{\eta}(\underline{\eta}_{o(i)} + D\underline{\eta}_o)$

$$\underline{f}^{NL}_{\mu(k+1)} = \begin{bmatrix} -\Phi_s\underline{f}_{\eta} \\ \underline{f}^{Eo}_{\eta} - \Phi_c\underline{f}_{\eta} \end{bmatrix}_{(k+1)}$$

next iteration: $k = k+1$

End do

Update strains etc.: $\underline{e}^* = \underline{e}^* + D\underline{e}^*$; $\underline{\mu}_o = \underline{\mu}_o + D\underline{\mu}_o$; $\underline{\mu} = \underline{\mu} + D\underline{\mu}$

Iteration count: $i = k$

Computationally similar steps would be involved in implementing any of the other pseudo-force procedures discussed in this chapter. The matrix $\overline{K}_{(j)}$ is any tangent stiffness along the solution path; in particular the initial stiffness procedure has $\overline{K}_{(o)} = I$. The solution procedure proposed is path independent with the stress recovery based on the total increments of strain as measured from the last converged solution point (see discussion in section 3.4.3 and section 6.6). For non-linear dynamics problems the approach follows that given in section 4.3.

7.7 EXTENDING THE DOMAIN OF APPLICABILITY OF THE PFI-METHOD USING REDUCED BASIS METHODS

The above formulation of both nodal and element based pseudo-force methods are limited in application to the class of non-linear dynamic problem in which the material and geometric non-linearities are limited to a few elements, and the mass/dampers are located at a few nodal points. For some applications such as the static collapse behaviour of braced offshore frames it is usually adequate (as was demonstrated by example in chapter 5) to ignore the global effects of geometric non-linearity. Also, for the dynamic analysis of these frames, only a few mass points need be considered because most of the mass is concentrated at the top of the structure. However in some problems, especially concerning continua, it may be desirable or indeed necessary to include global geometric non-linearity and to take account of mass/damping distributed over the body. We now explore how to extend our (dynamic) EPFI-Method for such problems - the enhancement of the NPFI-Method would follow similar procedures.

We consider problems in which the geometric non-linearity of the elements that do not deform into the plastic range is rather 'weak'. By this we imply that elastic buckling does not dominate the response behaviour. The reason for this restriction is to enable the geometric non-linearity to be treated in an approximate way. So, the objective is to include in our reduced system analysis in an approximate way, the influence of globally induced second order geometrical effects as well as distributed dynamic resistance. The problem under consideration may be specified as having

- an arbitrary number of mass points
- weak geometric non-linearity in an arbitrary number of elements
- plasticity (with possibly strong geometric non-linearity) in a few elements

In section 4.5.4, we saw that problems with many masses/dampers could be dealt with by mixing so-called reduced basis techniques (see NOOR, 1981, 1994 for review) with the EPFI-Method. The procedure involved approximating the global dynamic response with the lowest mode shapes (i.e. the reduced basis) of the linear-elastic problem to obtain the inertia and damping forces. These were then identified as pseudo-forces acting on the linear-elastic reference model, and the EPFI-Method was used to reduce the system to the non-linear element deformation freedoms. An extension to this method that looks attractive is to evaluate both the dynamic resistance and the 'background' non-linear geometric contribution using the reduced basis while employing the EPFI-Method for those elements that deform plastically .

The idea is to write the equilibrium equation (7.18) as

$$K^E \underline{U} = \underline{F}^L + \underline{F}_U^{NL} + \underline{F}_U^{\Delta} + \underline{F}_U^D \tag{7.86}$$

in which $\underline{F}_U^{NL}$ contains both material and geometrical non-linear effects for those elements that strain in the plastic domain, while $\underline{F}_U^{\Delta}$ represents the geometrical non-linear effect of the remaining elements. Now, let us employ the reduced basis $\underline{\xi}$, such that

$$\underline{U}^* = \Phi_r \underline{\xi}\,, \qquad \Phi_r = \left[\underline{\phi}_1 \;\; \underline{\phi}_2 \;\; \cdots \;\; \underline{\phi}_r\right] \tag{7.87}$$

where $\underline{U}^*$ is an approximation to $\underline{U}$ and the columns $\underline{\phi}_i$ are taken to be the r lowest free vibration modes of the linear-elastic system. These are obtained by solving the eigen-value problem

$$(K^E - \omega_i^2 M)\underline{\phi}_i = \underline{0} \qquad i = 1, r \tag{7.88}$$

where ω_i is the circular frequency associated with eigen-mode $\underline{\phi}_i$, M is the mass matrix (which need not be diagonal) and K^E is the linear-elastic stiffness matrix of the reference model. Equation (7.86) is now reduced in two separate ways. The first reduction procedure uses the modal technique to develop a set of dynamic equations in the unknowns $\underline{\xi}$. The second procedure employs the EPFI-Method and yields a set of equations in the unknowns $\underline{w}$ associated with the plastically deforming elements. These transformations result in

$$I_r \ddot{\underline{\xi}} + C_r \dot{\underline{\xi}} + \Omega_r^2 \underline{\xi} = \Phi_r^T \left[\underline{F}^L + \underline{F}_{\xi}^{\Delta} + Z_w^T \underline{q}_w^{NL}\right] \tag{7.89a}$$

$$\underline{w} = \underline{w}^L + D^{ww} \underline{q}_w^{NL} + Z_w (K^E)^{-1} \left[\underline{F}_{\xi}^{\Delta} + \underline{F}_{\xi}^{D}\right] \tag{7.89b}$$

where

$$I_r = \Phi_r^T M \Phi_r \qquad C_r = \Phi_r^T C \Phi_r \qquad \Omega_r^2 = \Phi_r^T K^E \Phi_r\,. \tag{7.90}$$

The matrix C_r is a diagonal damping matrix (assuming Rayleigh damping), Ω_r^2 is a diagonal matrix whose entries ω_i^2 are the squares of the circular natural frequencies, and the notation for forces is $\underline{F}_U(\underline{U}^*) \equiv \underline{F}_U(\Phi_r \underline{\xi}) \equiv \underline{F}_{\xi}$. The kinematic transformation matrix is identified by $Z_w = M_o Z_v$, where Z_v is given by (7.61) and M_o is identified in Box 7.2.

Although the reduced system (7.89a) and (7.89b) can now be solved, $\underline{F}_{\xi}^{\Delta}$ is a non-linear function of $\underline{\xi}$ and must be evaluated at each iteration. This non-trivial computation makes the method rather inefficient. To get around this, we invoke the assumptions of weak geometric non-linearity and small rotations, and write

$$\underline{F}_{\xi}^{\Delta} \cong \tilde{\underline{F}}_{\xi}^{\Delta} + \tilde{K}^{\sigma} \Phi_r (\underline{\xi} - \tilde{\underline{\xi}}) \tag{7.91}$$

where $\tilde{K}^{\sigma}$ is the global initial stress stiffness matrix (of the elements that do not strain into the plastic regime) and $\tilde{\underline{\xi}}$ is any previous value of $\underline{\xi}$ on the solution curve. Inserting this into (7.89a) and (7.89b) we find

$$I_r \ddot{\underline{\xi}} + C_r \dot{\underline{\xi}} + (\Omega_r^2 - \tilde{K}_r^{\sigma})\underline{\xi} = \underline{f}_r^L + \underline{f}_r^{\Delta} + H^{\xi w}\, \underline{q}_w^{NL} - \tilde{K}_r^{\sigma}\tilde{\underline{\xi}} \tag{7.92a}$$

$$\underline{w} = \underline{w}^L + \underline{w}^{\Delta} + D^{ww}\underline{q}_w^{NL} + D^{w\sigma}(\underline{\xi} - \tilde{\underline{\xi}}) - (D^{wM}\ddot{\underline{\xi}} + D^{wC}\dot{\underline{\xi}}) \tag{7.92b}$$

in which the new terms introduced are given by

$$\underline{w}^{\Delta} = Z_w (K^E)^{-1} \tilde{\underline{F}}_{\xi}^{\Delta} \qquad \underline{f}_r^{\Delta} = \Phi_r^T \tilde{\underline{F}}_{\xi}^{\Delta} \qquad \tilde{K}_r^{\sigma} = \Phi_r^T \tilde{K}^{\sigma} \Phi_r \qquad H^{\xi w} = \Phi_r^T Z_w^T$$
$$D^{w\sigma} = Z_w (K^E)^{-1} \tilde{K}^{\sigma} \Phi_r \qquad D^{wM} = Z_w (K^E)^{-1} M \Phi_r \qquad D^{wC} = Z_w (K^E)^{-1} C \Phi_r \tag{7.92c}$$

where we may define

- $H^{\xi w}$ as the generalised displacement influence matrix;
- $D^{w\sigma}$ as the geometric relative displacement influence matrix;
- D^{wM} as the modal mass relative displacement influence matrix; and
- D^{wC} as the modal damping relative displacement influence matrix.

At each iteration the solution progresses by first solving (7.92a) for $\underline{\xi}$, $\dot{\underline{\xi}}$ and $\ddot{\underline{\xi}}$. These are then input into (7.92b) which is solved for the local pseudo-forces $\underline{q}_w^{NL}$. Since the geometric non-linearity is presumed weak, the geometric force approximation (7.91) need only be updated infrequently.

In this procedure, we used the linear vibration modes as our reduced basis. The assumption is that these adequately represent the global behaviour. Other bases may be equally (or perhaps more) suitable - see NOOR (1994). For problems in statics, one could use the linear buckling modes as the basis vectors. However, it might be just as well to also use the dynamic modes for static analysis and simply ignore the velocity and acceleration resistance in the solution of (7.92a).

This idea of combining a reduced basis technique with either the EPFI-Method or the NPFI-Method seems worthwhile to pursue in more detail as it opens up the possibility of tackling a much wider variety of problems using unconventional solution strategies.

7.8 EFFICIENCY AND EFFECTIVENESS OF PSEUDO-FORCE METHODS

In chapters 3 & 4 we developed a simulation system that enabled us to obtain the non-linear (dynamic) response of structures with non-linear bar elements using a linear-elastic structural analysis program without modification. The influence matrices and linear elastic response for the non-linear elements were extracted manually by applying separately the actual loading and unit load-cases. There were three main attractions to this approach. Firstly, it provides an engineer with a non-linear (dynamic) capability that he otherwise would not have; secondly, the system is portable and can interface to any linear-elastic program; and thirdly, the linear-elastic program does not need to be modified. From this perspective the pseudo-force method is very effective.

Also, it is apparent from the practical examples considered in chapter 5, that for a limited number of non-linear bar elements the solution of the reduced system is extremely fast.

For plasticity problems in continua the manual extraction of the influence matrices is clearly not possible. Even for beam elements, the additional pseudo-forces required to account for the interaction between non-linear bending moment and axial force may become problematic. Therefore the effectiveness of the manual interface procedure certainly diminishes with increasing element complexity (and is more prone to human error). An alternative would be to develop a control macro that sets up the unit load-case input data, runs the linear-elastic program and extracts the relevant information. Another possibility is to implement the pseudo-force method inside either a linear or non-linear f.e. program, although this requires access to program source code.

With this last option, the question of numerical efficiency must be addressed. If we were to implement a pseudo-force procedure into an f.e. code, we would need to know when it is more efficient than other methods and when it is not. Clearly the efficiency must be related to the number of unknowns in the reduced system.

In a conventional direct solution algorithm in which the global tangent stiffness is formulated at each iteration, the bulk of the computation time is dominated by the Cholesky decomposition of the matrix and requires order Nb^2 operations, where N is the number of degrees of freedom and b is the half bandwidth - see KAVLIE & POWELL (1971). In the pseudo-force method most of the computational time is consumed by the calculation of the influence matrix. This takes approximately Nbn operations, n being the number of unit load sets (for either the element based or nodal based methods). However each subsequent analysis of the reduced system (using tangent stiffness reformulations) involves only order n^3 operations. Once the influence matrix has been determined, the overhead involved at each solution step in the pseudo-force method compared to complete re-formulation is small provided $n^3 << Nb^2$.

Thus the pseudo-force approach will offer considerable advantages over direct solution procedures for problems in which the reduced system remains unaltered and must be solved several times. Examples on space-framed structures where large efficiency gains are apparent are:

(a) *Static collapse and cyclic response* - the response is controlled by a few elements and the reduced system must be solved frequently to trace the solution curve.

(b) *Probabilistic structural analysis* - this can involve several hundred static collapse analyses and pseudo-force principles are ideally suited to this problem class (GIERLINSKI, 1992).

(c) *Non-linear dynamic collapse* - the reduced system as opposed to the full system is solved every time step (STEWART, 1992b).

Pseudo-force methods are not always an attractive option, however. For example, for one single re-analysis of a linear-elastic structure, the pseudo-force method becomes less effective since the computational time is governed by the influence matrix assembly. In this case n must be much smaller than b (which is a very restrictive requirement) for the pseudo-force method to compete with a reformulation of the entire stiffness matrix. That is pseudo-force methods are generally not numerically efficient if the structure is modified once only. This is true generally of all procedures for static re-analysis, as has also been pointed out by KAVLIE & POWELL (1971).

7.9 REFERENCES

ABU-KASSIM, A.M., AND TOPPING, B.H.V. (1985), "The theorems of structural variation for linear and non-linear finite element analysis", *Civil-COMP. 85, Second Int. Conf. on Civil & Struct. Eng. Comp. (U.K.).*, pp159-171.

ABU-KASSIM, A.M., AND TOPPING, B.H.V. (1987), "Static re-analysis: a review", *J. Struct. Eng.*, ASCE, **113**, pp1029-1045.

AL-BAKRI, M.A.E. (1977), *Optimum design of transmission towers*, PhD thesis, Univ. of Surrey.

ARGYRIS, J.H., AND KELSEY, S. (1956), "The matrix force method of structural analysis and some new applications", Ministry of Supply, *Aeronautical Research Council Reports & Memoranda*, No. 3034, UK.

ARGYRIS, J.H., AND KELSEY, S. (1960), "Initial strains in the matrix force method of structural analysis", *Jrnl. of Royal Aero. Soc.*, **64**, pp493-495.

ARGYRIS, J.H., AND KELSEY, S. (1961), "The validity of the initial strain concept", *Jrnl. of Royal Aero. Soc.*, **65**, pp129-138.

ARGYRIS, J.H. (1964), "Recent advances in matrix methods of structural analysis", *Progress in Aeronautical Sciences*, **4**, (Küchemann & Sterne Eds.), Pergamon Press.

ARGYRIS, J.H., BRONLUND, O.E., AND ROY, J.R. (1971), "A direct modification procedure for the displacement method", *AIAA Journal*, **9**(9), pp1861-1864.

ARGYRIS, J., BALMER, H., ST. DOLTSINIS, J., DUNNE, P.C., HASSE, H., KLEIBER, M., MALEJANNAKIS, G.A., MLEJNEK, H.P., MÜLLER, M., AND SCHARPF, D.W. (1979), "Finite element method - the natural approach", *Comp. Meth. App. Mech. & Eng.*, **17/18**, pp1-106.

ARORA, J.S. (1976), "Survey of structural re-analysis techniques", *ASCE J. Struct. Division*, **112**, pp783-788.

BATHE, K.J. (1982), *Finite element procedures in engineering analysis*, Prentice-Hall, New Jersey.

FENVES, S.J, AND ERTAS, R. (1969) "Multiple configuration analysis of structures", *ASCE J. Struct. Division*, **95**, **ST7**, pp1586-1589.

GIERLINSKI, J.T. (1992), "Reliability analysis of offshore structures RASOS", *Proc. 6th Int. Conf. Offshore Structs.*, BOSS '92, London, UK.

HOLNICKI-SZULC, J., AND MROZ, Z. (1985), "Active control of stresses and deflections of elastic structures by means of imposed distortions", *Proc. 2nd Int. Syp. Struct.Control*, Univ. of Waterloo, Ontario.

HOLNICKI-SZULC, J. (1987), "Degradation of elastic structures simulated by initial distortions", *Mech. of Struct. & Machines*, **15**, pp1-15.

HOLNICKI-SZULC, J. (1989), "Optimal structural remodelling - simulation by virtual distortions", *Comm. App. Num. Meth.* **5**, pp289-298.

HOLNICKI-SZULC, J. AND GIERLINSKI, J.T. (1989), "Structural modifications simulated by virtual distortions", *Int. J. of Num. methods in Eng.*, **28**, pp645-666.

HOLNICKI-SZULC, J. (1991), *Virtual Distortion Method*, Lecture notes in engineering, **65**, (C.A. Brebbia & S.A. Orszag, Eds.), Springer-Verlag.

HOUSEHOLDER, A.S. (1957), "A survey of some closed methods for inverting matrices", *SIAM J.*, **5**(**1**), 155-169.

KAVLIE, D., AND POWELL, G.H. (1971), "Efficient re-analysis of modified structures", *ASCE J. Struct. Division*, **97**, **ST1**, pp377-392.

KIRSCH, U. (1981), *Optimum structural design*, (ch. 5 - re-analysis methods), McGraw-Hill.

MELOSH, R.J., AND LUIK, R. (1968), "Multiple configuration analysis of structures", *ASCE J. Struct. Division*, **ST11**, pp2581-2596.

NOOR, A.K. (1981), "Recent advances in reduction methods for non-linear problems", *Computers & Structs.*, **13**, 31-44.

NOOR, A.K. (1994), "Recent advances and applications of reduction methods", *Appl. Mech. Rev.*, **47**(5), 125-146.

ROBINSON, J. (1985), "The mode-amplitude technique and hierarchical stress elements - a simplified and natural approach", *Int. J. for Num. Meth. in Eng.*, **21**, pp487-507.

STEWART, G. (1992a), "Nonlinear structural dynamics by the pseudo-force influence method - Part I: Theoretical considerations ", *Intl. Offshore and Polar Engineering Conf.* (ISOPE), Vol. I, San Francisco, USA.

STEWART, G. (1992b), "Nonlinear structural dynamics by the pseudo-force influence method - Part II: Application to offshore platform collapse", *Intl. Offshore and Polar Engineering Conf.* (ISOPE), Vol. I, San Francisco, USA.

WANG, B.P., PILKEY, W.D., AND PALAZZOLO, A.B. (1983), "Re-analysis, modal synthesis and dynamic design", in *State-of-the-art finite element technology*, ch. 8, pp225-295, A. Noor & W. Pilkey (eds.), ASME, New York.

WOODBURY, M. (1950), "Inverting modified matrices", *Memorandum Report 42, S.R.G.*, Princeton, N.J.

Appendix A

BUCKLING AND LOCAL BUCKLING OF TUBULAR COLUMNS

A1 Buckling strength of tubular columns

For a perfectly straight linear-elastic column of area A, Euler derived the buckling load as:

$$P_{cr} = \pi^2 EA/(kl/r)^2. \tag{A1}$$

in which kl/r is the slenderness of the member (of length l and radius of gyration r) and E is Young's modulus. The parameter k is the effective length factor and is selected to reflect the boundary conditions (k=0.5 for both ends restrained against rotation; k=1.0 for both ends free to rotate). The influence of material non-linearity was considered by Engesser in 1889 (CHEN & ATSUTA, 1976). His *tangent modulus theory* gives the buckling load (non-dimensionalised by the yield load, P_y) as

$$\frac{P_{cr}}{P_y} = \frac{E_t}{E}\frac{1}{\chi^2}; \quad \chi = \frac{1}{\pi}\sqrt{\frac{\sigma_y}{E}}\frac{kl}{r} \tag{A2}$$

where E_t is the tangent modulus (the slope of the material uni-axial stress/strain curve),σ_y is the yield stress, and χ is the reduced slenderness (CHEN & HAN, 1985).

Most structural steels do not harden appreciably after yielding, behaving essentially as elastic/perfectly-plastic. For a material of this type, according to (A2) a column free of residual stresses would buckle at the lower of the Euler load or the plastic squash load, P_y (upper curve in Fig. A1). Real columns do have residual stresses and these reduce the buckling load (BEEDLE & TALL, 1960). CHEN & ROSS (1977, 1978), measured the actual axial residual stresses in fabricated cold-rolled-and-welded tubulars typically found in offshore jacket structures and found the maximum compressive longitudinal residual stress σ_R to be about $0.3\sigma_y$. If a small stub were to be removed from the column and subjected to axial compression, the proportional limit stress would be given by $\sigma_p = \sigma_y - \sigma_R$, and the effective tangent modulus beyond this stress would be reduced (POPOV & BLACK, 1981). A revised buckling strength can be predicted by the tangent modulus theory by assuming, say, that beyond the proportional limit the tangent modulus is a linear function of stress:

$$\frac{E_t}{E} = 1 - \frac{\sigma - \sigma_p}{\sigma_y - \sigma_p} \quad \sigma \geq \sigma_p \,. \tag{A3}$$

The normalised buckling load then becomes

$$\frac{P_{cr}}{P_y} = \frac{1}{1+(1-\sigma_p/\sigma_y)\chi^2} \qquad \chi \le \sqrt{\sigma_y/\sigma_p} \tag{A4}$$

which falls under the classification of a Rankine-Gordon formula (CHEN & ATSUTA, 1976). At $\chi = \chi_c = \sqrt{\sigma_y/\sigma_p}$, the tangent buckling stress is equal to the Euler buckling stress and beyond χ_c the Euler curve is used. Using a residual stress of $0.3\sigma_y$ provides the Rankine-Gordon buckling prediction curve shown in Fig. A1.

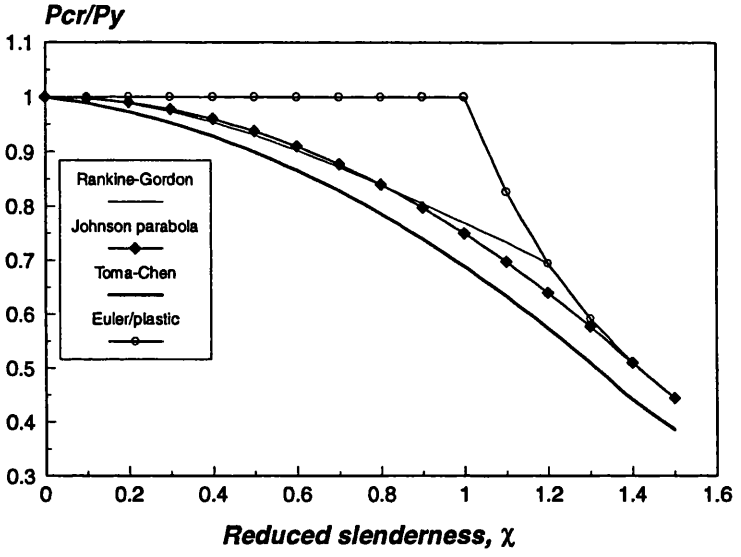

Fig. A1 Buckling curves for columns

An alternative form of equation (A3) is the so-called Ostenfeld-Bleich quadratic relationship (JOHNSON, 1966) given by

$$\frac{E_t}{E} = \frac{\sigma(\sigma-\sigma_p)}{\sigma_p(\sigma_y-\sigma_p)} \qquad \sigma \ge \sigma_p \tag{A5}$$

leading to

$$\frac{P_{cr}}{P_y} = 1-\frac{\sigma_p}{\sigma_y}\left(1-\frac{\sigma_p}{\sigma_y}\right)\chi^2 \qquad \chi \le \sqrt{\sigma_y/\sigma_p}\ . \tag{A6}$$

When $\sigma_p/\sigma_y = 0.5$, the buckling resistance given by (A6) has a minimum value given by

$$P_{cr}/P_y = 1-\chi^2/4. \tag{A7}$$

This corresponds to the *Johnson parabola* proposed in the Column Research Council's guides (JOHNSON, 1966, 1976) for rolled sections and which has been adopted by the AISC building code.

API has also incorporated this equation into its recommended practice for design of offshore structures.

Until now, it has been assumed that the column is initially geometrically perfect. However, most real columns have some out-of-straightness (o-o-s) and out-of-roundness (o-o-r), as well as residual stresses. As a result of the out-of-straightness the column now carries bending moment as well as axial forces and is typically referred to as a beam-column. On the basis of numerical computations that employed realistic residual stresses and imperfections on the limit of acceptability (0.1% o-o-s, and 1% o-o-r), TOMA & CHEN (1979) have proposed the following buckling curve:

$$\begin{aligned} P_{cr}/P_y &= 1-0.091\chi-0.22\chi^2\,; \quad \chi<\sqrt{2} \\ &= 0.015+0.834/\chi^2\,; \quad \chi\geq\sqrt{2} \end{aligned} \tag{A8}$$

which lies somewhat below Johnson's parabola (see Fig. A1). Although the Johnson parabola lies just below the available test data on fabricated tubular columns (ten tests by CHEN & ROSS, 1977, and six by BOUKAMP, 1975), the limited amount of data may not be fully representative, particularly with respect to geometrical imperfections. Because the Toma & Chen curve explicitly accounts for these imperfections (and all other important aspects) it should provide a particularly robust measure of the characteristic buckling strength.

A2 Local Buckling

On the basis of the experimental data of SHERMAN (1980) and STEPHENS *ET AL.* (1983), API-RP2A advises that members having $D/t < 10340/\sigma_y$ (stress in MPa) have high rotational capacity and are unlikely to be susceptible to local buckling. The column buckling experiments of SMITH *ET AL.* (1979), which are summarised in Table A1, support the API conclusions.

Table A1: Data from Smith, Kirkwood & Swan

D/t	σ_y	$\frac{(D/t)\sigma_y}{10340}$	local buckling?
29	250	0.70	no
45	220	0.96	no
60	250	1.45	yes
85	490	4.03	yes

Monotonic deformations

For monotonic deformations, lower bound estimates of the onset of local buckling have been derived. On the basis of data from KOROL (1978) and SHERMAN (1983), the following formula was proposed by SOHOL & CHEN (1987):

$$\varepsilon_{cr}/\varepsilon_y = 4.1-500t/D+22500(t/D)^2 \tag{A9}$$

where ε_y is the yield strain and ε_{cr} is the local axial strain beyond which a local buckle would initiate.

To use (A9) requires knowledge of the local strains in the hinge. As an alternative, MARSHALL *ET AL.* (1977) integrated the curvature over a hinge length determined from experimental data, and gave lower and upper estimates of the critical plastic hinge rotations. If we use their lower bound estimate of critical curvature and the best estimate of hinge length, a reasonable estimate of the critical plastic hinge rotation is given by:

$$\theta_{cr}^{p} = 800(t/D)^3. \tag{A10}$$

This can also be related to the energy dissipation in the member.

Table A2 gives the critical strains and rotations based on (A9) and (A10) for D/t ratios typical of offshore structures.

Table A2: Critical strains and rotations vs D/t ratio

D/t	30	40	50	60
$\varepsilon_{cr}/\varepsilon_y$	12.4	5.7	3.1	2.0
θ_{cr}^{p} (deg.)	1.7	0.74	0.37	0.21

Alternating plasticity

Experimental studies on cyclic behaviour (SHERMAN, 1980; GRANLI, - - -; ZAYAS *ET AL.*, 1982; POPOV & BLACK, 1981) show that opening and closing of plastic hinges can lead to cyclic local buckling. This causes the member capacity to rapidly degrade and the very high local strains that develop in the wrinkled wall soon lead to fracture induced through low cycle fatigue. The prediction of local buckling under alternating plasticity is not straightforward. In the absence of a better criterion, MARSHALL *ET AL.* (1977) suggest that local buckling will occur when the cumulative plastic strain or rotation exceeds the monotonic critical values (given by equations such as (A9) and (A10)).

A3 References

References given in this appendix may be found at the end of chapter 2.

Appendix B

THE DEVELOPMENT OF A PLASTIC HINGE BEAM-COLUMN MODEL

B1 A generalised Shanley model

To study the behaviour of a simply supported beam-column, SHANLEY (1947) suggested that the column be represented by two rigid elements connected by deformable non-linear axial springs. In the model developed below we also employ two rigid elements but instead of springs use deformable hinges at midspan and at the ends. This generalisation of Shanley's concept leads to a very simple but adequate model to describe the monotonic load-shortening curve of a tubular beam-column .

The basic element is a rigid link of length $l/2$ with a zero length deformable hinge at each end. The column is formed by joining two elements together (Fig. B1). Each hinge has an elastic axial stiffness of $k_a = 4AE/l$ (giving an overall axial stiffness of AE/l) and a rotational elastic stiffness of k_θ (giving an effective rotational elastic spring stiffness at the centre of $k_\theta/2$). An axial end load P and a constant transverse load of intensity q per unit length act on the column producing a central rotation θ measured anti-clockwise from the vertical. It is required to calculate the load-shortening response.

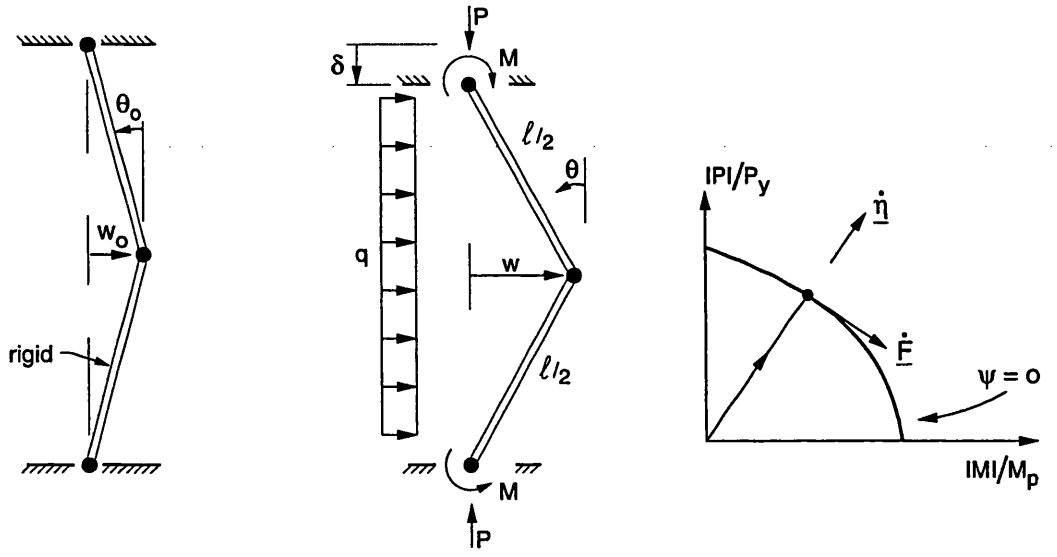

(a) Initial configuration *(b) Deformation under load (3 plastic hinges)* *(c) Hinge constraint*

Fig. B1 Generalised Shanley beam-column model

Equilibrium

Neglecting terms of order θ^2 compared with unity, and with M being the bending moment in the hinge, equilibrium of the column satisfies

$$P\theta l/2+ql^2/16=2M=2k_\theta\theta^e \tag{B1}$$

where θ^e is the elastic component of the rotation θ, and q is the applied lateral load intensity (Fig. B1b). In incremental form, this provides

$$(\dot{P}\theta+P\dot{\theta})l/2=2\dot{M}=2k_\theta\dot{\theta}^e\ . \tag{B2}$$

Rotational spring stiffness and elastic response

The rotational spring stiffness k_θ is selected such that the elastic buckling load of the column is equal to the Euler value. In the elastic range, $\dot{\theta}=\dot{\theta}^e$, and since buckling occurs when $\dot{P}=0$, it follows from the incremental equilibrium equation (B2) that

$$k_\theta = P_E l/4\ . \tag{B3}$$

If the effective length of the column is known, the Euler load P_E can be established from (A1). The selection of an appropriate effective length is discussed in section 2.4.3. It is easily verified that the rotation in the elastic range can be expressed as

$$\theta=(\theta_o+\frac{ql}{8P_E})\frac{1}{1-P/P_E} \tag{B4}$$

where θ_o is the initial rotation.

Yield surface

The axial force and moment capacity of the hinge are constrained to lie on a non-hardening yield surface $\Psi=0$ which, for a thin walled tubular cross section (see for example CHEN & HAN, 1985) of diameter D, wall thickness t, and yield stress σ_y, is given by

$$\Psi=\frac{M}{M_p}-\cos\left(\frac{\pi}{2}\frac{P}{P_y}\right)=0\ ;\quad M_p=D^2t\sigma_y,\quad P_y=\pi D\ t\sigma_y \tag{B5}$$

where M_p is the fully plastic moment and P_y is the squash load. From this follows the incremental relationship

$$\dot{\Psi}=\frac{\partial\Psi}{\partial M}\dot{M}+\frac{\partial\Psi}{\partial P}\dot{P}=0 \tag{B6}$$

which is equivalent to

$$\dot{M}=-h\dot{P}\ ;\quad h=\frac{\partial\Psi/\partial P}{\partial\Psi/\partial M}=\frac{\pi}{2}\frac{M_p}{P_y}\sin\left(\frac{\pi}{2}\frac{P}{P_y}\right). \tag{B7}$$

Initial imperfection

We now consider how to ensure that the inelastic buckling strength matches the Toma-Chen load P_{TC}. An initial midspan imperfection $w_o = \theta_o l/2$ is selected such that in the absence of lateral loading the force resultants just reach the yield surface at the axial load P_{TC}. From (B1), (B4) and (B5), the initial imperfection is calculated as

$$\frac{w_o}{l} = \frac{2M_p}{P_E}\left(\frac{P_E}{P_{TC}} - 1\right)\cos\left(\frac{\pi}{2}\frac{P_{TC}}{P_y}\right). \tag{B8}$$

Kinematics

The central rotation of the column measured anti-clockwise from the vertical is

$$\theta = \theta_o + \theta^e + \theta^p \tag{B9}$$

where θ^e is the elastic rotation and θ^p is the plastic rotation. The total shortening of the column is then given by

$$\delta = 4(\delta^e + \delta^p) + 2\delta^g \tag{B10}$$

where δ^e ($= Pl/4AE$) and δ^p are respectively the elastic and plastic shortening in one hinge, and δ^g is the geometric shortening per element. The incremental plastic shortening in the hinge is determined from the associated flow rule which implies normality of the plastic increment with the yield surface (see HILL, 1950, for example), as shown in Fig. B1. This provides the relationship between the axial and rotational increments of plastic deformation

$$\dot{\delta}^p = h\,\dot{\theta}^p \tag{B11}$$

where h is given by (B7). It is easily verified that since the increment of loading is $\dot{\underline{F}} = [\dot{P}, \dot{M}]^T = \dot{P}[1, -h]^T$ and the increment of deformation is $\dot{\underline{\eta}} = [\dot{\delta}^p, \dot{\theta}^p]^T = \dot{\delta}^p[1, 1/h]^T$, the normality requirement $\dot{\underline{F}}\,\dot{\underline{\eta}}^T = 0$ is satisfied.

B2 Solution algorithm

The solution procedure for the plastic hinge beam-column model is given in Box B1. This can easily be implemented into a spread-sheet, making it very straightforward to generate the load-shortening curve for members of any given geometry.

Box B1: Solution algorithm for plastic hinge beam-column model

Step (a): Elastic range

Increment rotation and calculate axial deformation

$$\theta_i^e = \theta_{i-1}^e + \dot{\theta}^e \; ; \qquad \theta_i = \theta_{i-1} + \dot{\theta}^e$$

$$\delta^e = Pl/4AE \; ; \qquad \delta_i^g = \cos\theta_o - \cos\theta_i$$

$$\delta_i = 4\delta_i^e + 2\delta_i^g$$

Recover forces

$$P_i = (P_E\theta_i^e - \frac{ql}{8})/\theta_i \; ; \qquad M_i = k_\theta \theta_i^e$$

If on yield surface, goto step (b); otherwise return to step (a).

Step (b): Plastic range

Increment total rotation

$$\theta_i = \theta_{i-1} + \dot{\theta}$$

Calculate new loading

$$\dot{P} = -P_{i-1}\left[\theta_i + \frac{4}{l}h_{i-1}\right]^{-1}\dot{\theta} \qquad \text{(follows from (B2) and (B7))}$$

$$P_i = P_{i-1} + \dot{P} \; ; \qquad M_i = M_p \cos\left(\frac{\pi}{2}\frac{P_i}{P_y}\right)$$

Calculate elastic and plastic rotation increments

$$\dot{\theta}^e = (M_i - M_{i-1})/k_\theta \; ; \qquad \dot{\theta}^p = \dot{\theta} - \dot{\theta}^e \; ;$$

Calculate axial incremental and total deformation

$$\dot{\delta}^p = h_i\dot{\theta}^p \; ;$$

$$\delta_i^p = \dot{\delta}_{i-1}^p + \dot{\delta}^p \; ; \qquad \delta^e = Pl/4AE \; ; \qquad \delta_i^g = \cos\theta_o - \cos\theta_i$$

$$\delta_i = 4(\delta_i^e + \delta_i^p) + 2\delta_i^g \; .$$

B3 References

References given in this appendix may be found at the end of chapter 2.

Appendix C

SOLUTION OF SYSTEMS OF EQUATIONS BY THE GENERALISED NEWTON METHOD

C1 Newton's procedure

We can write a system of equilibrium equations in the general form

$$\underline{g}(\underline{x}) = \underline{F}^{int} - \underline{F}^{ext} = \underline{0} \tag{C1}$$

where $\underline{g}$ may be identified as the components of the ***residual*** vector; $\underline{F}^{int}$ as the components of the internal force or resistance vector; $\underline{F}^{ext}$ as the components of the applied loading vector, and $\underline{x}$ as the unknowns. Many methods may be used to solve this system of nonlinear equations. A useful review of some of the common procedures is given by ODEN (1972). A popular and powerful technique is the family of Newton methods. These employ a first order Taylor expansion about configuration $\underline{x}_{(k)}$ to give an estimate of the correction $\Delta\underline{x}$ required to satisfy equilibrium. That is if $\underline{g}(\underline{x}_{(k)} + \Delta\underline{x}) = \underline{0}$, then the first order expansion yields

$$\underline{g}_{(k)} + \left[\frac{\partial \underline{g}}{\partial \underline{x}}\right]_{(j)} \Delta\underline{x} = \underline{0} \quad ; \; j \le k \tag{C2}$$

from which we obtain the generalised Newton scheme:

$$\Delta\underline{x} = -\left[\frac{\partial \underline{g}}{\partial \underline{x}}\right]^{-1}_{(j)} \underline{g}_{(k)} \; ; \quad \underline{x}_{(k+1)} = \underline{x}_{(k)} + \Delta\underline{x} \tag{C3}$$

where the iteration counter starts at 1 and gives the total number of iterations required to reach the current step. We may identify

$$\boldsymbol{K}_{(j)} = \left[\frac{\partial \underline{g}}{\partial \underline{x}}\right]_{(j)} \tag{C4}$$

as a generalised 'stiffness' or iteration matrix. It is noted that <u>any</u> iteration matrix can be employed. The only requirement is that convergence (to the desired solution point) be attained.

C2 References

References given in this appendix may be found at the end of chapter 3.

Appendix D

THE EQUIVALENCE OF VARIOUS CONSTITUTIVE MODELS FOR SMALL STRAINS

D1 Introduction

We stated in chapter 6 that the co-rotational approach was particularly attractive for problems concerned with large displacements (but small strains), because within the co-rotating frame the usual infinitesimal relationships may be used directly. There are alternative ways of developing constitutive models and it may be wondered how the various approaches are related to one another, and if indeed they produce the same results for the small strain problems in which our interest lies.

In this appendix we set out the co-rotational model in some more detail and then compare it with more abstract formulations.

D2 Special notation

A distinction is made between vectors and vector components and tensors and tensor components. Both vectors ($\vec{a}$) and tensors ($\underline{\underline{A}}$) are quantities that are independent of co-ordinate systems. Once a suitable coordinate system (or basis) has been selected, the components of the vector or tensor may be defined with respect to this basis. Changing the basis changes the components. So, for example,

$$\vec{v} = v_i \vec{e}_i \tag{D1}$$

represents a vector $\vec{v}$ having components v_i with respect to the unit base vectors $\vec{e}_i$, and

$$\underline{\underline{T}} = T_{ij} \vec{e}_i \otimes \vec{e}_j \tag{D2}$$

represents a second order tensor $\underline{\underline{T}}$ having components T_{ij} with respect to the base vectors $\vec{e}_i$. The symbol $\otimes$ represents the dyadic product. Einstein summation convention is used. So (D1) implies

$$\vec{v} = v_i \vec{e}_i = v_1 \vec{e}_1 + v_2 \vec{e}_2 \ . \tag{D3}$$

The outer (dyadic) product of the two vectors $\vec{a}$ and $\vec{b}$ is written

$$\vec{a} \otimes \vec{b} = a_i b_j \vec{e}_i \otimes \vec{e}_j . \tag{D4}$$

The single dot product $\underline{\underline{A}} \cdot \underline{\underline{B}}$ corresponds to a summation over one index of each tensors' components, whereas the double dot product $\underline{\underline{A}} : \underline{\underline{B}}$ corresponds to a summation over two indices. For example, for the two second order tensors

$$\underline{\underline{A}} = a_{ij}\, \vec{e}_i \otimes \vec{e}_j \qquad \underline{\underline{B}} = b_{ij}\, \vec{e}_i \otimes \vec{e}_j \tag{D5}$$

the dot products result in

$$\underline{\underline{A}} \cdot \underline{\underline{B}} = a_{ij} b_{jk}\, \vec{e}_i \otimes \vec{e}_k \qquad \underline{\underline{A}} : \underline{\underline{B}} = a_{ij} b_{ij} \; . \tag{D6}$$

Further details on tensors may be found in the text of MALVERN (1969).

D3 Objectivity of stress and strain tensors

Clearly, rigid body motions should not affect the form of a constitutive relationship. That is the stress rate and strain rate tensors should both be zero under rigid body motions. Such a property is called objectivity (HUGHES, 1984; MALVERN, 1969). The Cauchy stress rate tensor is not objective. This can be demonstrated by expressing the Cauchy tensor components in a fixed reference system whose base vectors $\vec{e}_i$ do not change in time (Fig. D1a). Thus

$$\underline{\underline{\sigma}} = \sigma_{ij}\, \vec{e}_i \otimes \vec{e}_j \qquad \text{implies} \qquad \dot{\underline{\underline{\sigma}}} = \dot{\sigma}_{ij}\, \vec{e}_i \otimes \vec{e}_j \; , \tag{D7}$$

and since the Cauchy stress components σ_{ij} change under rigid body motion, $\dot{\sigma}_{ij}$ does not vanish. Therefore $\dot{\underline{\underline{\sigma}}}$ is not an objective measure of stress rate and a constitutive relationship involving $\dot{\underline{\underline{\sigma}}}$ is inappropriate.

Below we discuss some of the commonly used objective stress and strain tensors and their associated constitutive relationships.

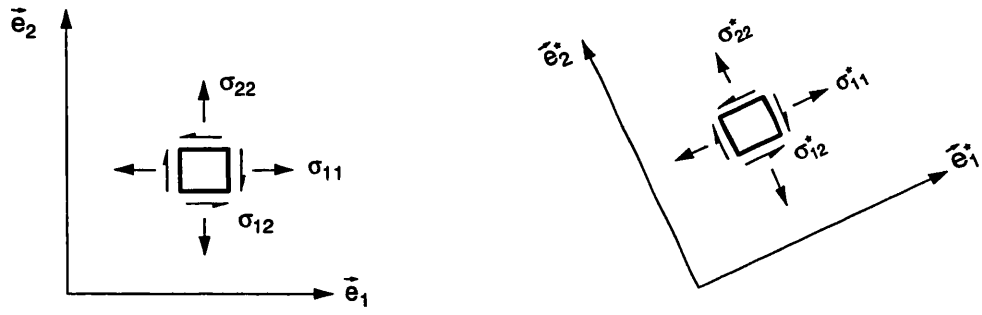

(a) Fixed base vectors *(b) Co-rotating base vectors*

Fig. D1 Components of the Cauchy stress tensor w.r.t. fixed and co-rotating base vectors

D4 A constitutive law in the co-rotating reference system

Co-rotational formulations are motivated as follows. We express the Cauchy stress tensor as

$$\underline{\underline{\sigma}} = \sigma^*_{ij}\, \vec{e}_i^{\,*} \otimes \vec{e}_j^{\,*} \tag{D8}$$

where σ^*_{ij} are the components with respect to a basis $\vec{e}_i^{\,*}$ that co-rotates with the material (Fig. D1b). Now since the components σ^*_{ij}, which are those that would be recorded by an observer moving with the material, do not change under rigid body motion, this suggests that we define a new rate tensor as

$$\dot{\underline{\underline{\sigma}}}^c \overset{def}{=} \dot{\sigma}^*_{ij}\, \vec{e}_i^{\,*} \otimes \vec{e}_j^{\,*}. \tag{D9}$$

This is called the co-rotational Cauchy stress rate tensor and it is clearly objective.

Similarly, for small strains, the objective co-rotational infinitesimal strain rate tensor may be defined as

$$\dot{\underline{\underline{e}}}^c \overset{def}{=} \dot{e}^*_{ij}\, \vec{e}_i^{\,*} \otimes \vec{e}_j^{\,*}, \quad \text{with} \quad \dot{e}^*_{ij} = \frac{1}{2}\left(\frac{\partial \dot{u}^*_i}{\partial X^*_j} + \frac{\partial \dot{u}^*_j}{\partial X^*_i} \right) \tag{D10}$$

where the displacements $\underline{u}^*$ are measured with respect to a co-rotating reference body with co-ordinates $\underline{X}^*$ (see Fig. 6.10).

Writing the co-rotational constitutive tensor of elasto-plastic moduli as

$$\underline{\underline{\underline{\underline{C}}}}^c = C^*_{ijkl}\, \vec{e}_i^{\,*} \otimes \vec{e}_j^{\,*} \otimes \vec{e}_k^{\,*} \otimes \vec{e}_l^{\,*}, \tag{D11}$$

a valid and physically appealing constitutive law is then given by

$$\dot{\underline{\underline{\sigma}}}^c = \underline{\underline{\underline{\underline{C}}}}^c : \dot{\underline{\underline{e}}}^c \quad \Rightarrow \quad \dot{\sigma}^*_{ij} = C^*_{ijkl}\, \dot{e}^*_{kl}. \tag{D12}$$

This states that if one adopts a reference frame that is rotating with the material, the usual Cauchy stress, infinitesimal strain and material constants as used in an infinitesimal displacement theory can be directly employed.

The co-rotational constitutive model is therefore very simple and has a clear physical interpretation. Some of the other models proposed for large displacement problems, although equivalent, are more abstract in their formulation and consequently their physical background is more obscure. Two such formulations are now discussed.

D5 Constitutive laws in the fixed reference frame

The co-rotational formulation is only one of the many that have been proposed for large displacement problems. Often a fixed reference frame is used and the following constitutive models employed:

Rate of Second Piola Kirchoff stress and Green-Lagrange strain tensors

$$\dot{S}_{ij} = \tilde{C}_{ijkl}\dot{E}_{kl} \tag{D13}$$

where

$\dot{S}_{ij}$ is the rate of change of the Piola-Kirchoff stress

$\dot{E}_{ij}$ is the rate of change of Green-Lagrange strain

This type of constitutive model is widely adopted (see, for example, WASHIZU, 1975; HIBBITT *ET AL.*, 1970; and BATHE, 1982).

Jaumann rate of Cauchy stress and deformation gradient tensors

$$\overset{\nabla}{\sigma}_{ij} = C^{J}_{ijkl}\, d_{kl} \tag{D14}$$

where

d_{ij} are the components of the deformation gradient tensor; and

$\overset{\nabla}{\sigma}_{ij}$ is the Jaumann rate of Cauchy stress.

The Jaumann form of constitutive model is has been employed by several researchers, including HUGHES (1984), and NEEDLEMAN & TVERGAARD (1984).

The question arises how these stress and strain measures are related to one another and how to select the components of the material property tensor to ensure equivalence of the constitutive models for small strain.

Rate of Second Piola Kirchoff stress and Green-Lagrange strain tensors

We first take a look at the constitutive equations that are appropriate if the Second Piola Kirchoff stress rate and Green-Lagrange strain rate tensors are employed. The Second Piola Kirchoff stress tensor is defined as

$$\underline{\underline{S}} \overset{def}{=} \det(\underline{\underline{F}})\,\underline{\underline{F}}^{-1}\cdot\underline{\underline{\sigma}}\cdot\underline{\underline{F}}^{-T} = S_{ij}\,\vec{e}_i \otimes \vec{e}_j \tag{D15}$$

in which the deformation gradient tensor $\underline{\underline{F}}$, maps the material line segment $d\vec{X}$ in the undeformed configuration to $d\vec{x}$ in the deformed configuration.

That is

$$d\vec{x} = \underline{\underline{F}} \cdot d\vec{X}$$
$$\underline{\underline{F}} = F_{ij}\,\vec{e}_i \otimes \vec{e}_j\,; \quad F_{ij} = \frac{\partial x_i}{\partial X_j}\,. \tag{D16}$$

The tensor $\underline{\underline{F}}$ can be uniquely decomposed such that

$$\underline{\underline{F}} = \underline{\underline{R}} \cdot \underline{\underline{U}} \tag{D17}$$

where $\underline{\underline{R}}$ is an orthogonal rotation tensor and $\underline{\underline{U}}$ is the symmetric stretch tensor. For small strains, $\underline{\underline{F}} \approx \underline{\underline{R}}$ and $\underline{\underline{S}} = \underline{\underline{R}}^T \cdot \underline{\underline{\sigma}} \cdot \underline{\underline{R}}$, from which it is apparent that

$$S_{ij} = R_{mi} R_{nj} \sigma_{mn} = \sigma^*_{ij}. \tag{D18}$$

So, for small strains, the components of the Second Piola Kirchoff stress tensor with respect to a fixed reference frame are identical to those of the Cauchy stress tensor in a co-rotating frame. This result is well known (see, for example, CHRISFIELD, 1991).

The rate form of (D15) for small strains is simply

$$\dot{\underline{\underline{S}}} = \dot{S}_{ij}\,\vec{e}_i \otimes \vec{e}_j = \dot{\sigma}^*_{ij}\,\vec{e}_i \otimes \vec{e}_j \tag{D19}$$

and since $\dot{\sigma}^*_{ij}$ is zero for rigid body motion, $\dot{\underline{\underline{S}}}$ is objective. We also observe that

$$\dot{S}_{ij} = \dot{\sigma}^*_{ij}. \tag{D20}$$

Thus, when the strains are small, the components the Second Piola Kirchoff stress rate tensor in a fixed reference frame are identical to those of the co-rotational Cauchy stress rate tensor with respect to the co-rotational frame.

The objective strain rate measure conjugate to $\dot{\underline{\underline{S}}}$ is the rate of Green-Lagrange strain, $\dot{\underline{\underline{E}}}$ defined as

$$\dot{\underline{\underline{E}}} = \underline{\underline{F}}^T \cdot \underline{\underline{d}} \cdot \underline{\underline{F}} = \dot{E}_{ij}\,\vec{e}_i \otimes \vec{e}_j \tag{D21}$$

where the components of $\dot{\underline{\underline{E}}}$ and $\underline{\underline{d}}$ with respect to the fixed base vectors are

$$d_{ij} = \frac{1}{2}\left(\frac{\partial \dot{u}_i}{\partial x_j} + \frac{\partial \dot{u}_j}{\partial x_i}\right) \tag{D22}$$

$$\dot{E}_{ij} = \frac{1}{2}\left(\frac{\partial \dot{u}_i}{\partial X_j} + \frac{\partial \dot{u}_j}{\partial X_i} + \frac{\partial \dot{u}_k}{\partial X_i}\frac{\partial u_k}{\partial X_j} + \frac{\partial u_l}{\partial X_i}\frac{\partial \dot{u}_l}{\partial X_j}\right) \tag{D23}$$

For small strains $\dot{\underline{\underline{E}}} = \underline{\underline{R}}^T \cdot \underline{\underline{d}} \cdot \underline{\underline{R}}$, from which it is apparent that

$$\dot{E}_{ij} = R_{mi} R_{nj} d_{mn} = d^*_{ij} = \dot{e}^*_{ij} \tag{D24}$$

which confirms that $\dot{\underline{\underline{E}}}$ is objective since $\dot{e}^*_{ij}$ is zero for rigid body motion.

Furthermore, we can now state that when the strains are small, the components of the Green-Lagrange strain rate tensor in a fixed reference frame are identical to those of the co-rotational infinitesimal strain rate tensor with respect to the co-rotational frame.

Now let the constitutive law be formulated as

$$\dot{\underline{\underline{S}}} = \tilde{\underline{\underline{C}}} : \dot{\underline{\underline{E}}} \quad \Rightarrow \quad \dot{S}_{ij} = \tilde{C}_{ijkl} \dot{E}_{kl} \,. \tag{D25}$$

From (D20), (D24) and (D12) it follows immediately that $\tilde{C}_{ijkl} = C^*_{ijkl}$. So for small strains, using the Second Piola Kirchoff stress rate and Green-Lagrange strain rate tensor components on the fixed basis is exactly equivalent to using the co-rotational stress and strain rate tensor components on the co-rotating basis, and the same material properties should be used in both cases. However the tensors themselves are not the same (since when the components are equal the base vectors differ).

Jaumann rate of Cauchy stress and deformation gradient tensors

Finally, we examine the constitutive model used with the so-called Jaumann rate of Cauchy stress. We begin by differentiating the relationship $\underline{\underline{S}} = \underline{\underline{R}}^T \cdot \underline{\underline{\sigma}} \cdot \underline{\underline{R}}$ (valid for small strain strains) which gives

$$\dot{\underline{\underline{S}}} = \underline{\underline{R}}^T \cdot \overset{\nabla}{\underline{\underline{\sigma}}} \cdot \underline{\underline{R}} = \dot{S}_{ij} \vec{e}_i \otimes \vec{e}_j = \dot{\sigma}^*_{ij} \vec{e}_i \otimes \vec{e}_j \tag{D26}$$

where $\overset{\nabla}{\underline{\underline{\sigma}}}$ is an objective tensor called the Jaumann rate of Cauchy stress and is defined as

$$\overset{\nabla}{\underline{\underline{\sigma}}} \overset{def}{=} \dot{\underline{\underline{\sigma}}} - \underline{\underline{\Omega}}\,\underline{\underline{\sigma}} + \underline{\underline{\sigma}}\,\underline{\underline{\Omega}}; \qquad \underline{\underline{\Omega}} = \dot{\underline{\underline{R}}}\,\underline{\underline{R}}^T. \tag{D27}$$

For small strains, this is also equivalent to the Green-Nagdi rate of Cauchy stress (HUGHES, 1984). Re-arranging (D26) provides

$$\overset{\nabla}{\underline{\underline{\sigma}}} = \dot{\sigma}^*_{ij} \underline{\underline{R}} \cdot \vec{e}_i \otimes \vec{e}_j \cdot \underline{\underline{R}}^T = \dot{\sigma}^*_{ij} \vec{e}^*_i \otimes \vec{e}^*_j = \dot{\underline{\underline{\sigma}}}^c \tag{D28}$$

That is for small strains, the Jaumann and Green-Nagdi rates of Cauchy's stress tensor are identical to the co-rotational stress rate tensor. Furthermore, by (D24),

$$\underline{\underline{d}} = \dot{\underline{\underline{e}}}^c \tag{D29}$$

and it follows that

$$\dot{\underline{\underline{\sigma}}}^{c} = \underline{\underline{C}}^{c} : \dot{\underline{\underline{e}}}^{c} \quad \equiv \quad \overset{\nabla}{\underline{\underline{\sigma}}} = \underline{\underline{C}}^{J} : \underline{\underline{d}} \qquad \text{if} \qquad \underline{\underline{C}}^{J} = \underline{\underline{C}}^{c} . \tag{D30}$$

With respect to the fixed basis we have

$$\overset{\nabla}{\sigma}_{ij} = C^{J}_{ijkl} d_{kl} \tag{D31}$$

where d_{kl} is defined in (D22) and

$$\sigma_{ij} = \dot{\sigma}_{ij} - \Omega_{ik}\sigma_{kj} + \sigma_{il}\Omega_{lj} \qquad \text{with} \qquad C^{J}_{ijkl} = R_{mi}R_{nj}R_{pk}R_{ql}C^{*}_{ijkl} . \tag{D32}$$

This shows that the components of the material property tensor must be rotated back to the fixed basis unless the material is isotropic in which case $C^{J}_{ijkl} = C^{*}_{ijkl}$.

Thus the equivalence of commonly used constitutive laws has been demonstrated in the small strain regime. The recent text by CHRISFIELD (1991) provides a good overview of these concepts for bar and beam elements.

D6 References

References given in this appendix may be found at the end of chapter 6.